

# **Photocatalytically Active and Optically Transparent Titanium Dioxide Thin Films Prepared by Ion Assisted Physical Vapor Deposition**

Von der Naturwissenschaftlichen Fakultät  
der Gottfried Wilhelm Leibniz Universität Hannover

zur Erlangung des Grades

**DOKTOR DER NATURWISSENSCHAFTEN**

**Dr. rer. nat.**

genehmigte Dissertation

von

**Dipl.-Chem. Redouan Boughaled El Lakhmissi**

geboren am 26.03.1972 in Tissouka, Marokko

**2013**

Referent: Prof. Dr. Michael Wark

Korreferent: Prof. Dr. Detlev Ristau

Tag der Promotion: 15.07.2013



## Erklärung

Hiermit erkläre ich, dass ich die vorliegende Dissertation "**Photocatalytically Active and Optically Transparent Titanium Dioxide Thin Films Prepared by Ion Assisted Physical Vapor Deposition**" als Mitarbeiter des Laser Zentrums Hannover e.V. und Doktorand in der Gottfried Wilhelm Leibniz Universität Hannover selbständig verfasst und alle benutzten Hilfsmittel sowie evtl. zur Hilfeleistung herangezogenen Institutionen vollständig angegeben habe.

Die Dissertation wurde nicht schon als Diplom- oder ähnliche Prüfungsarbeit verwendet.

Hannover, 10 Mai 2013

Dipl.-Chem. Redouan Boughaled El Lakhmissi



## Acknowledgement

I would like to take this opportunity to pay my heartiest thanks to my mentor **Prof. Dr. Michael Wark** for his guidance and valuable advice. He always encouraged and motivated me to learn more and more about the subject.

I am grateful to **Prof. Dr. Detlev Ristau** for giving me the opportunity to work at Laser Zentrum Hannover e.V. and also for his invaluable help and encouragement, without which I would not have been able to do this research.

I am also thankful to **Dr. Henrik Ehlers** for his support and guidance on all academic questions I came across during my research work at the Process Development Group, which works under his expert leadership.

The above named three persons were my source of inspiration for undertaking this Ph.D.

I had the pleasure of entering into the world of photocatalysis few years ago under the matchless expertise of **Prof. Dr. Detlef Bahnemann**, and his help, support and agreement to chair the thesis defense has been invaluable.

In Laser Zentrum Hannover e.V., I enjoyed working within Prof. Dr. Detlev Ristau's team and I wish to thank the entire team in his department, especially my colleagues in the Process Development Group for the helpful discussions, Dr. Nils Beermann, Sebastian Schlichting, Carsten Schmitz and Andreas Tewes. I also wish to express here my great appreciation for the co-workers in the department of Thin Film Technology, especially Istvan Balasa, Dr. Stefan Günster, Lars Jensen, Dr. Marco Jupé, and Puja Kadkhoda for the useful discussions. My additional thanks go out to Rainer Gebauer for the accomplishment of the SEM pictures.

In particular, I am grateful to Dr. Oliver Merka of Leibniz Universität Hannover, and Prof. Dr. Thorsten Gesing and Dr. Lars Robben of Bremen Universität for their help and support with the XRD measurements. I also extend my gratitude to Prof. Dr. U. Bartuch of Göttingen Universität for the use of AFM testing, Dr. Anna-Maria Welsch and Prof. Dr. Harald Behrens of Leibniz Universität Hannover for their investigations into the Raman data, and Dr. Iris Trick of Fraunhofer-Institut für Grenzflächen- und Bioverfahrenstechnik IGB Stuttgart for conducting the anti-bacterial tests.

For financial assistance I am thankful to the German Federal Ministry of Education and Research (BMBF) for the 'photokat' project (FKZ: 01 RI 0637H, DLR, Bonn) and the German Federal Ministry of Economics and Technology for the 'Future Scales' project (VP2186405MK9).

On a personal level, I take this opportunity to thank my family and friends for their encouragement, understanding and love.

## Kurzzusammenfassung

Die Herstellung von selbstreinigenden Oberflächen mit guten optischen Eigenschaften und hoher photokatalytischer Effizienz steht seit einigen Jahren im Fokus von Forschung und Industrie. Für einen breiteren Einsatz dieser Technologie muss die photokatalytische Effizienz und optische Qualität erheblich gesteigert werden. Ziel dieser Forschungsarbeit ist es, die Beschichtungstechnologie- und Materialien hinsichtlich dieser beiden Parameter für transparente Schichten zu optimieren. Diese Aufgabe erfordert eine standardisierte Analyse der hergestellten Oberflächen und die Entwicklung einer Methode zur Messung des damit korrelierten photokatalytischen Effekts. Der Schwerpunkt liegt auf der Verwendung der physikalischen Gasphasenabscheidungstechnologie (englisch: physical vapor deposition, kurz PVD) zur Herstellung dünner Filme. Diese umfasst sowohl den Einsatz ionengestützter Beschichtungsprozesse (englisch: Ion Assisted Deposition, kurz IAD) als auch konventioneller thermischer Verdampfungsverfahren.

Der Fokus dieser Arbeit liegt auf der erstgenannten Methode. Zu diesem Zweck wurden die Plasma-Quelle Leybold APSpro und die Ionenquelle Denton CC-105 eingesetzt. Dabei wurden die wesentlichen Parameter für die Herstellung von transparenten photokatalytischen Titandioxidschichten untersucht. Unterschiedliche Entladungsströme, Spannungsgrößen und Gasflusswerte wurden in der Ionen-Quelle verwendet. Es wurden drei verschiedene Beschichtungsanlagen eingesetzt: die SYRUSpro 1100 von Leybold im Zusammenspiel mit der Ionenquelle APSpro sowie die BAK 760 und BAK 640 der Firma Balzers zusammen mit der Ionenquelle CC-105 bzw. CC-104. Es wurden solche Beschichtungsparameter ausgewählt, die typischerweise für die Herstellung von  $\text{TiO}_2$ -Beschichtungen mit guten optischen Eigenschaften verwendet werden.

Es wurde ein Vergleich zum Wirkungsgrad der Photokatalyse zwischen den  $\text{TiO}_2$ -Beschichtungen durchgeführt. Die Ergebnisse zeigen, dass  $\text{TiO}_2$ -Filme aus der IAD-Anwendung mit der Quelle Denton CC-105 die größte Photoaktivität und auch einem superhydrophilen Effekt besitzen. Darüber hinaus zeigen die IAD Proben eine antimikrobielle Aktivität gegenüber Test-Mikroorganismen. Eine weitere wichtige Betrachtung ist die Untersuchung des Einflusses der Beschichtungstemperatur, Verdampfungsrate und weiterer Beschichtungsparameter der Ionenquelle auf die optischen Eigenschaften der  $\text{TiO}_2$ -Filme mit dem Ziel, diese zu optimieren. In dieser Studie wurde die bedeutende Rolle der spezifischen Oberflächeneigenschaften von Photokatalysatoren aufgezeigt. Durch den Einsatz verschiedener Techniken zur Charakterisierung war es möglich, die Mikrostruktur von IAD- Schichten mit Anatas- und Rutil- Strukturen zu beobachten.

Zusammenfassend lässt sich feststellen, dass mit dem IAD-Verfahren hergestellte  $\text{TiO}_2$ -Beschichtungen durch UV-Bestrahlung und sichtbares Licht nicht nur einen Selbstreinigungseffekt zeigen, sondern auch eine antimikrobielle Wirkung entfalten. Diese Eigenschaften machen  $\text{TiO}_2$  Filme zu einem idealen Kandidaten für verschiedene Anwendungen in der Präzisionsoptik wie z.B. für Brillen und bei Laborgeräten wie Präzisionswaagen.

**Schlagwörter:** *Ionengestützte Prozesse, Photokatalytisch aktive dünne Schichten, Titandioxid, PVD*



## Abstract

It has been an ambition of both researchers and industries for the past many years to produce self-cleaning surfaces that have a good optical quality and photocatalytic efficiency, particularly with regard to a broader application. It is anticipated that the research described in this thesis will help to realize this aspiration by optimizing coating technologies and materials as well as to introduce standardized methods for surface analysis and the correlated photocatalytic efficiency.

The primary focus of this thesis is to produce thin films using physical vapor deposition technologies (PVD), which involves the investigation of ion assisted deposition (IAD) and conventional thermal evaporation methods. To address this focus, the different operational parameters of two plasma ion-sources, one from Leybold (APSprö) and another from Denton (CC-105), were studied, as the operational parameters are essential in the production of transparent photocatalytic titanium dioxide ( $\text{TiO}_2$ ) thin films. The discharge current, voltage and gas flow were also varied in the ion-sources to ascertain the optimal parameters. Three coating machines were used in this research: SYRUSpro 1100 from Leybold was used with the ion-source APSpro, BAK 760 from Balzers with the ion-source CC-105, and BAK 640, also from Balzers, with CC-104. The selected deposition parameters for all three processes were those that are typically used to produce  $\text{TiO}_2$  coatings with suitable optical properties.

During the research, a comparison was made between the photonic efficiencies for the photocatalytic degradation of the dye methylene blue of differently processed  $\text{TiO}_2$  coatings. The processes compared were that of IAD using CC-105, IAD using APSpro, the conventional PVD process, and commercially available photocatalytic active  $\text{TiO}_2$  glass. These comparisons showed that  $\text{TiO}_2$  films processed with IAD using the CC-105 source exhibited the highest photodecomposition rate and super-hydrophilicity effect, with the samples as well demonstrating antimicrobial activity towards test microorganisms. Another notable consideration in the production of  $\text{TiO}_2$  films is the correlation of its optical properties with the deposition temperature, evaporation rate, and various other deposition parameters of the ion-source. All of these were evaluated to find the optimal result.

This research greatly isolated the significant role that the surface properties of the photocatalyst  $\text{TiO}_2$  play when coated using the IAD process, which has not previously been identified to such a degree. Additionally identified was the complicated relationship between anatase and rutile thin films, which has an important impact on the photocatalytic effect.

The conclusion of this research is that  $\text{TiO}_2$  films produced using the IAD method have not only a self-cleaning ability, but also an antimicrobial effect both under UV illumination. As a result of these properties, PVD prepared  $\text{TiO}_2$  films are a distinct candidate for use in different applications involving precision optics, such as in spectacles, window glass, laboratory equipment, for example scales, and many more.

**Keywords:** *Ion Assisted deposition, Photocatalytically active thin films, Titanium dioxide, PVD*





# Table of Contents

ERKLÄRUNG.....	III
ACKNOWLEDGEMENT.....	V
KURZZUSAMMENFASSUNG .....	VII
ABSTRACT.....	IX
TABLE OF CONTENTS .....	1
<b>1. INTRODUCTION .....</b>	<b>5</b>
1.1 MOTIVATION .....	5
1.2 RESEARCH STRATEGY .....	7
1.2.1 Photocatalysis.....	7
1.2.2 Ion and Plasma Assisted Process Concepts.....	7
1.3 OVERVIEW OF THESIS.....	8
<b>2. BASICS .....</b>	<b>11</b>
2.1 PHOTOCATALYSIS.....	11
2.1.1 Photocatalytic process.....	13
2.1.2 Coated TiO <sub>2</sub> as a Photocatalyst and Microstructure Influence .....	16
2.1.3 Industrial Application of TiO <sub>2</sub> Photocatalyst.....	20
2.1.4 Visible Light and TiO <sub>2</sub> Doping.....	25
2.1.5 Methylene Blue as a Photodegradation Model .....	27
2.1.6 Anti-Bacterial and Self-Cleaning Effect.....	28
2.2 PRODUCTION PROCESSES OF TiO <sub>2</sub> THIN FILMS.....	30
2.2.1 Conventional Physical Vapor Deposition without IAD .....	31
2.2.2 Sputter Physical Vapor Deposition.....	31
2.2.3 Physical Vapor Deposition with IAD.....	34
2.2.4 Crystallinity of Thin Films by Different Coating Methods .....	40
2.2.5 Correlation: Deposition method, photoactivity, microstructure, antibacterial ability.....	42
2.3 SUMMARY.....	42
<b>3. EXPERIMENTAL SET-UP .....</b>	<b>45</b>
3.1 SYNTHESIS OF THIN FILM LAYERS .....	45
3.1.1 Materials and Methods .....	45
3.1.2 Pretreatment Procedures.....	46

3.1.3	<i>Thermal Evaporation PVD</i> .....	46
3.1.4	<i>Ion Assisted Deposition</i> .....	46
3.1.5	<i>XTC Thin Film Deposition Controller and Broadband Monitoring Platform</i> .....	50
3.1.6	<i>Coating Parameters</i> .....	51
3.2	OPTICAL QUALITY OF THIN FILM LAYERS.....	53
3.2.1	<i>Fast Scattering Tests</i> .....	53
3.2.2	<i>Absorbance and Transmission Measurements</i> .....	54
3.3	SURFACE ANALYSIS OF THIN FILM LAYERS.....	54
3.3.1	<i>Scanning Electron Microscopy (SEM)</i> .....	54
3.3.2	<i>Transmission Electron Microscopy (TEM)</i> .....	54
3.3.3	<i>Elemental Analysis (EDX)</i> .....	55
3.3.4	<i>X-ray Diffraction (XRD)</i> .....	55
3.3.5	<i>Atomic Force Microscopy (AFM)</i> .....	56
3.3.6	<i>Water Droplet Contact Angle Measurement (CAM)</i> .....	56
3.3.7	<i>Raman Spectroscopy</i> .....	58
3.4	ANTI-BACTERIAL PROPERTIES.....	58
	<b>4. OPTIMIZATION OF PHOTOCATALYTIC ACTIVITY MEASUREMENTS</b> .....	<b>59</b>
4.1	CALCULATION OF PHOTONIC EFFICIENCIES.....	59
4.2	DEVELOPMENT OF A PHOTOCATALYTIC MEASUREMENT SYSTEM.....	61
4.3	PHOTONIC EFFICIENCY EVALUATION IN ACCORDANCE WITH ISO AND DIN STANDARDS.....	67
	<b>5. RESULTS OF PHOTOCATALYTIC ACTIVITY OF DIFFERENT PVD PROCESSES</b> .....	<b>69</b>
5.1	COMPARATIVE ANALYSIS OF DIFFERENT COATING PROCESSES USING METHYLENE BLUE DEGRADATION.....	69
5.1.1	<i>Influence of the Coating Processes</i> .....	70
5.1.2	<i>Influence of Gas Flow</i> .....	73
5.1.3	<i>Influence of Discharge Bias</i> .....	74
5.1.4	<i>Influence of Temperature</i> .....	76
5.1.5	<i>Influence of Thickness</i> .....	78
5.2	COMPARATIVE ANALYSIS OF DIFFERENT COATING PROCESSES USING OTHER DYES: INTERLABORATORY TESTS.....	79
5.2.1.	<i>Stearic acid and luminescent dye tests, (Fraunhofer Institute IST, Braunschweig)</i> .....	80
5.2.2.	<i>Photocatalytic surfaces based on a solid state luminescent dye</i> .....	81
5.2.3.	<i>Photocatalytic performances using 'Reduction of NOx' and Acetaldehyde</i> .....	82
5.3	PHOTOCATALYTIC DISINFECTION AND MICROBIOLOGICAL ANALYSIS.....	84
	<b>6. STRUCTURE AND SURFACE PROPERTIES OF PVD TITANIA THIN FILMS</b> .....	<b>89</b>
6.1	INVESTIGATION OF XRD CRYSTAL ANALYSIS.....	89
6.2	TEM AND DS EXAMINATION.....	91
6.3	MODIFICATION OF SURFACE MORPHOLOGY.....	92

6.3.1	<i>Energy-Dispersive X-ray Spectroscopy Chemical Analysis</i> .....	92
6.3.2	<i>SEM Analysis</i> .....	96
6.3.3	<i>Scanning Probe Microscopy by Means of AFM</i> .....	98
6.3.4	<i>Influence of the Process Parameters on Hydrophilicity</i> .....	106
6.3.5	<i>Industrial application</i> .....	108
6.4	DURABILITY TESTS: MECHANICAL AND ENVIRONMENTAL STABILITY OF TiO <sub>2</sub> LAYERS.....	110
6.4.1	<i>Layer Adhesion Test</i> .....	110
6.4.2	<i>Moderate Abrasion</i> .....	111
6.4.3	<i>Severe Abrasion Resistance Test</i> .....	112
6.4.4	<i>Solubility Test</i> .....	114
6.4.5	<i>Experiments with Polymers</i> .....	114
	<b>7. OPTICAL PROPERTIES OF IAD PHOTOCATALYTIC THIN FILMS</b> .....	<b>119</b>
7.1	DEPOSITION AND ANNEALING TEMPERATURE INFLUENCE.....	119
7.1.1	<i>Optical Properties of TiO<sub>2</sub> Thin Films</i> .....	119
7.1.2	<i>Morphology of IAD Optics</i> .....	126
7.2	OXYGEN FLOW INFLUENCE.....	129
7.2.1	<i>Optical Properties of the TiO<sub>2</sub> Thin Films</i> .....	130
7.2.2	<i>Morphology of IAD Optics</i> .....	133
7.3	THICKNESS INFLUENCE.....	134
7.4	CORRELATION BETWEEN REFRACTIVE INDICES AT 500 AND 1064 NM AND THE DIFFERENT COATING PARAMETERS 138	
7.5	SCATTERING TESTS CORRELATING TO IAD PARAMETERS.....	140
7.6	CHAPTER CONCLUSIONS.....	143
	<b>8. CORRELATION BETWEEN PHOTOCATALYTIC ACTIVITY, CRYSTAL MICROSTRUCTURE AND MORPHOLOGY OF IAD TRANSPARENT TITANIA THIN FILMS</b> .....	<b>145</b>
8.1	CORRELATION BETWEEN GRAIN SIZE, PHOTONIC EFFICIENCY AND HYDROPHILICITY WITH ION-SOURCE CURRENT AS A VARIABLE.....	146
8.2	EFFECT OF THE COATING PARAMETERS ON MICROSTRUCTURE AND PHOTOCATALYTIC ACTIVITY.....	155
	<b>9. FUTURE RESEARCH AND UTILITY</b> .....	<b>165</b>
9.1	PHOTOCATALYTIC TRANSPARENT THIN FILMS UNDER VISIBLE LIGHT.....	165
9.1.1	<i>Optical Properties</i> .....	166
9.1.2	<i>Photocatalytic Properties</i> .....	167
9.1.3	<i>SEM Microstructure and Grain Size Determination</i> .....	168
9.2	COATING POTENTIAL ON LABORATORY EQUIPMENT (SCALES).....	171
	<b>10. GENERAL CONCLUSIONS</b> .....	<b>173</b>

<b>11. REFERENCES .....</b>	<b>177</b>
<b>12. APPENDIX .....</b>	<b>195</b>
12.1 ADDITIONAL INFORMATION .....	195
12.1.1 <i>Additional Text</i> .....	195
12.1.2 <i>Additional Figures</i> .....	198
12.1.3 <i>Additional Tables</i> .....	204
12.2 SYMBOLS AND ABBREVIATIONS .....	205
12.3 TABLE OF FIGURES.....	206
12.4 TABLES.....	206
12.5 SCIENTIFIC PUBLICATIONS.....	208
12.5.1 <i>Journal publications</i> .....	208
12.5.2 <i>Papers in Progress</i> .....	208
12.5.3 <i>Conference Talks</i> .....	208
12.5.4 <i>Seminar Talks</i> .....	209
12.5.5 <i>Press Release</i> .....	209
12.5.6 <i>Final Project Reports</i> .....	209
12.5.7 <i>Conference Posters</i> .....	210
12.6 CURRICULUM VITAE.....	211

## 1. Introduction

### 1.1 Motivation

The focus of this research is to produce photocatalytic oxide layers and layer systems that show a high optical transparency and photoactivity by using ion assisted evaporation process with an additional emphasis on supplementary characteristics such as, super-hydrophilicity and antibacterial functions. A combination of photoactivity, super-hydrophilicity and an antibacterial effect enables these layered surfaces to decompose and eliminate organic and biologic waste compounds by using ultra violet (UV) or visible light, all while retaining its 'environmentally friendly' characteristics. The TiO<sub>2</sub> layers used in this research were deposited using the physical vapor deposition (PVD) method and further improved by the ion assisted deposition (IAD) process. This was done in order to improve the previously mentioned characteristics.

The combination of these TiO<sub>2</sub> films having effective optical properties and a self-cleaning ability is a significant and highly recommended aspect when considering the production of thin films. It is much anticipated that both of these characteristics together will be greatly beneficial for technology application and future research<sup>[1-4]</sup>. As a result of the attention that this issue has gained, researchers have frequently proposed physical and chemical mechanisms to offer an explanation of the self-cleaning quality<sup>[5-7]</sup>.

TiO<sub>2</sub>, owing to its pronounced photoactive properties, is deemed to be a good choice in the oxidation-reduction process. The photocatalytic effect, which can be explained by the absorption of UV quanta from the sunlight and the formation of holes and electrons, which react with the substances on the surface, is the mechanism that forms intermediate products that aid in the destruction of organic compounds. The exact correlation between the morphology of coated films and the self-cleaning effect using complex parameters of ion assisted deposition was previously not well understood. This research has successfully endeavored to resolve this, allowing for the development of thin films that can be used in multiple applications, such as high index materials and precision optics.

To understand the different levels of photocatalytic activity and the parameters affecting it, thin films prepared under defined conditions have to be studied. The coating parameters have a direct impact on thin film properties like crystallinity, surface morphology and hydrophilicity. Besides generally important quantities of PVD-processes, such as, substrate temperature or pressure, the main objective of this research is to control the layer characteristics by the ion-source features. To quantify their influence, a careful characterization of the resulting thin films by appropriate

analytical techniques is crucial. The aim should be to find a suitable explanation for those apparent correlations. By doing so, it is possible to facilitate the production and use of laminated structures by creating a dense layer of atoms.

From a more technical perspective this thesis is a pursuit to generate titania films that exhibit a hydrophilic property and also enable high photocatalytic activity. This has led to an analysis of different types of transparent mineral glasses and to a smaller degree plastic, so that their optical quality can be enhanced.

In regards to commercial and industrial uses of this research, there is a high possibility for its application and much market potential for the plasma and ion assisted evaporation procedures. Not only do these procedures offer the ability to integrate with existing industrial implementation processes, but they also provide (1) adaptability of the process parameters for photocatalytically efficient high optical quality layers and layer systems, and (2) achievable suitability for different substrates and evaporation systems.

Owing to rapid developments in the fields of nanotechnology, precision mechanics, thin film technology, and novel materials, a more precise knowledge of the surface characteristics and the quality control after processing is a vital challenge. Treatments that provide a self-cleaning ability to surfaces are both economically and commercially significant. This also makes the surfaces environmentally friendly by reducing the need for consumption of cleaning chemicals. Because of these characteristics, self-cleaning surfaces be applied in many fields, such as industry, traffic, construction, and have an immense worth in all the fields which employ them. They can, for example, save the time spent by workers on the cleaning of surfaces, while also maintaining a satisfactory standard of hygiene. Self-cleaning surfaces can also be applied to different transparent plastics which have good optical quality.

The ultimate objective of this research is to design a process for transparent TiO<sub>2</sub> films of high photocatalytic activity by surface modification. One of the auxiliary objectives to accomplish this primary was to correlate different thin film deposition process concepts, which may include electron-beam vaporization techniques or the use of various ion-sources, with the process of photocatalysis. These electron-beam vaporization techniques can produce, by selecting appropriate parameters such as substrate temperature or coating rate, dense layers that can effectively improve reproducibility of layer morphology. The water contact angle is used to evaluate the surface wettability and the reinforcement of the hydrophilicity by surface morphology, which corresponds to the self-cleaning effect.

## 1.2 Research Strategy

### 1.2.1 Photocatalysis

The term ‘photocatalysis’ refers to the process of photon-driven catalysis. In essence, the photocatalytic reactions, which include organic substrate degradation, occur on the contact surface and break down organic waste compounds by irradiation of light. This then allows the organic dirt to be easily washed away, making the photocatalysis process environmentally friendly and very easy to maintain<sup>[8-21]</sup>.

To aid in the photocatalysis process a TiO<sub>2</sub> semiconductor was used. It is well known to be the preeminent metal oxide for this purpose, and therefore has been the subject of many prior academic and industrial studies<sup>[22-28]</sup>. It also is a widely-used high refractive-index material in optical thin films due to its preferable band gap properties<sup>[29-33]</sup> and is well suited in the production of coatings that are transparent in a broad spectral range<sup>[34-35]</sup>, all of which make it the most promising of the known photocatalytic materials<sup>[36, 37]</sup>.

### 1.2.2 Ion and Plasma Assisted Process Concepts

The main focus of this research was the implementation of IAD processes due to their many advantages compared to other deposition processes. The fact that IAD can be quickly and efficiently implemented to existing deposition systems, when used with ion-source equipment, gives this process one of its many advantages. This efficiency results directly in a lowering of both cost and time<sup>[38, 39]</sup>. The level of flexibility and control offered by the ion-beam techniques is an advantage to both processes when compared to other gas-discharge procedures.

Another important aspect of the research was the optimization of these ion assisted processes, especially in regard to the production of TiO<sub>2</sub> layers that are photocatalytically efficient under UV-irradiation. Ideally, the layers should have enough mechanical hardness, adequate optical and microstructure properties when tested against adverse chemical effects. Innovation in the optimization of photocatalytical processes was needed to achieve these properties. This has several central issues. Two of which are the mechanism of demineralization and the definition of promising coating parameters. Varying process concepts have been proposed using Denton’s CC-105 ion-source<sup>[40-43]</sup>, which was chosen as a result of its ability to generate inert and reactive gas ions of different energy levels. This ion-source was compared against Leybold’s APSpro<sup>[44]</sup>, as together; they both represent state-of-the-art complete coating set-up technology and are used in today’s precision optics<sup>[45,46]</sup>. Generally, the ion-sources provide a great range of application where functional layering is required<sup>[47-53]</sup>.

The project management schedule followed in order to realize the previously described objectives was strictly adhered to, and is classified in three groups: First is the ‘management of process parameters’ group in which the coating parameters are defined. Next is the ‘coating and characterization’ stage in which the samples are coated using the defined parameters and then analyzed. The final stage is for ‘innovation and employment’ where applications are sought for the processes based upon the gathered results.

### **1.3 Overview of thesis**

The research work for this thesis was done in accordance with the following schedule:

First and foremost is the basis of this research:

- Production of PVD thin films with and without ion-source and comparison between different deposition processes and parameters.

Following this is a managed and continuous work process in the ensuing steps:

- Rough parameterizing of ion assisted evaporating on the basis of thin layers from oxidic coating materials, predominantly TiO<sub>2</sub>.
- Studies for subsequent pretreatment methods, such as cleaning steps and a plasma etching setup, and treatment techniques in the coating plant such as influence of temperature.
- Innovation and employment of an on-line measurement system for demineralization of methylene blue.
- Evaluation of the elementary characteristics of hydrophilic and antimicrobial layers.
- Influence of the process parameters on the fundamental optical characteristics of monolayers.
- Study of microstructure and adapted parameterizing of the photocatalytic performance.
- Realization of the appropriate anatase phase, balancing in relation to the optical quality losses and homogeneity of titania layers.
- Correlation between microstructure and functional properties of titania films.
- Extension of the research area to visible light range photocatalytical activation.
- Industrial application.

The subsequent chapters in this thesis all focus on different issues. Chapter 2 first contains a thorough review of the existing research in the field of photocatalysis and coating processes for an overview of the current state of research. Chapter 3 describes the PVD processes employed in the experiments carried out for this research, while Chapter 4 gives the methods used to calculate



photonic efficiency of films, which includes the purposely developed system and software. Details of a two-path laser measurement system that is used to determine the kinetic performance of the TiO<sub>2</sub> catalyst under well-defined light illumination conditions are also provided in Chapter 4 and the results from this mechanism studies are discussed in Chapter 5. Chapters 6 and 7 present the structure, surface, and optical properties of titania thin films. In Chapter 8, correlations based upon the analysis and the experimental results are drawn, and conclusions are described. Inferences on how to optimize the functional properties of thin films under visible light are given in Chapter 9. This Chapter is also dedicated to possible future research in the field of photocatalysis, and discusses new and innovative uses of thin films. Succinct conclusions of all the chapters can be found at the end of the thesis. A bibliography can be found in Chapter 11.

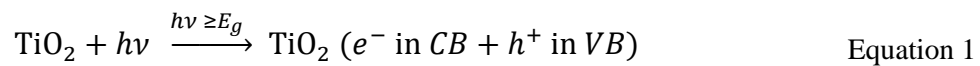


## 2. Basics

This chapter concentrates on a general overview of relevant research aspects carried out. These relevant topics are photocatalysis, TiO<sub>2</sub> as a photocatalyst, crystal modification of TiO<sub>2</sub>, visible light and doping TiO<sub>2</sub>, methylene blue as a degradation model, anti-bacterial and self-cleaning effects, and deposition processing of titania thin films. Other related research discussed includes correlations between various factors influencing crystal structure, surface morphology, and self-cleaning and optical quality.

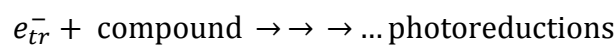
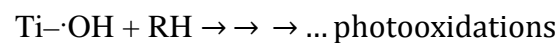
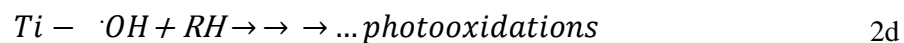
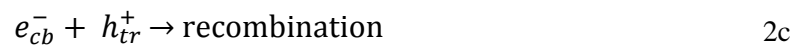
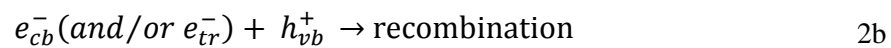
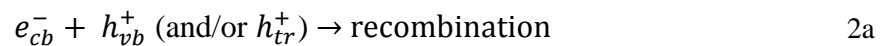
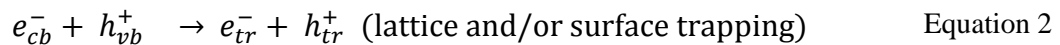
### 2.1 Photocatalysis

The basis of the photocatalytic reaction studied in this research is the fact that TiO<sub>2</sub> has a wide band gap of 3.2 eV and will generate electron/hole ( $e^-/h^+$ ) pairs when illuminated (Equation 1).



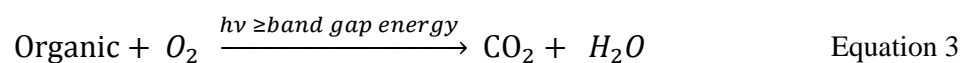
where  $E_g$  is the semiconductor band gap energy.

The valence band (VB) potential has enough positive charge to generate hydroxyl radicals ( $\cdot\text{OH}$ ) on the surface of the thin films, and the conduction band (CB) potential has enough negative charge to form superoxide radicals ( $\text{O}_2^-$ )<sup>[54-56]</sup>. The role of photoexcited titania particulates then is to act as pools of electrons and holes which can be used in some multielectron transfer processes (Eq. 2a to 2d)<sup>[19,57]</sup>. Therefore:



where  $e_{tr}^-$  is a trapped electron, for example as  $\text{Ti}^{3+}$ , and  $h_{tr}^+$  is a trapped hole denoted here as a surface bound OH radical, i.e. as  $\text{Ti} - \cdot\text{OH}$ <sup>[58]</sup>. The hydroxyl radical is a powerful oxidizing agent

and the organic pollutants that are present at or near the surface of the semiconductor are normally oxidated to  $\text{CO}_2$ . This process can be given as such:



The outcome of the separated electron and hole upon excitation can follow several pathways. Figure 1 illustrates some of the de-excitation pathways for the electrons and holes.

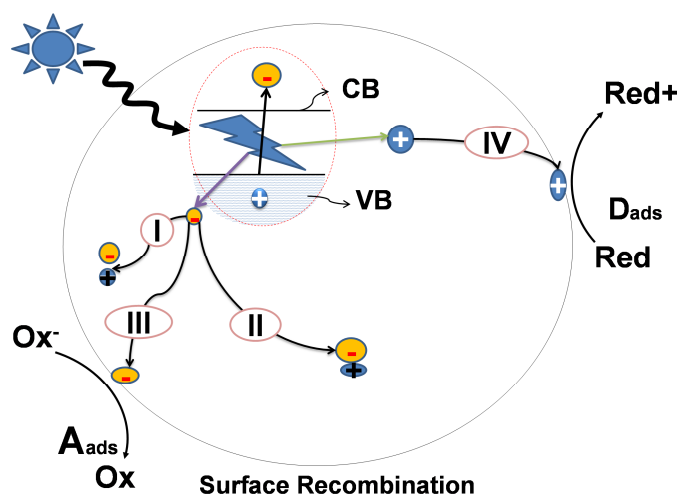


Figure 1. The Photocatalytic Mechanism occurring in four steps. I and II: absorption of photon energy greater than the band gap energy of material and generation of photoexcited electron-hole pairs in the bulk. III: Reduction of acceptor (A). IV: Oxidation of Donor (D) <sup>[59]</sup>.

To expand, Pathway I corresponds to the volume of the semiconductor particle and Pathway II to the surface, both showing the recombination of the separated electron and hole. The photoinduced electron transfer to adsorbed inorganic or organic forms to the solvent consequences from migration of electrons and holes to the semiconductor surface <sup>[60]</sup>. The efficiency of the electron transfer process is greater if the species are pre-adsorbed on the surface <sup>[59]</sup>.

Pathway III shows that on the surface the semiconductor can donate electrons to reduce an electron acceptor, which is oxygen in an aerated solution.

Pathway IV then exhibits that a hole can migrate to the surface where an electron from a donor species can combine with the surface hole resulting in an oxidization of the donor species.

The positions of the band edges for the conduction and valence bands and the redox potential levels of the adsorbate species determine the probability and rate of the charge transfer processes for electrons and holes. The valence band hole can either be trapped at intrinsic oxygen sites or

can influence organic species present in the solution. To give an example, with methylene blue decolorization, photogenerated holes  $h^+$  firstly induce the formation of the dye radical cation  $MB^{\bullet+}$  which is converted to  $MBOO^{\bullet+}$  by  $O_2$  [61]. Conversely, later in the degradation process the peroxy radical additionally reacts further to thionine and inorganic acids and  $CO_2$  is lastly formed after a series of photocatalytic reaction steps via the intermediates aniline, 4-nitroaniline and acetic acid.

### 2.1.1 Photocatalytic process

The mechanism of Photocatalysis with  $TiO_2$  is provided in full in the Chapter 4, but a summary is given below.

Numerous metal oxide and sulfide semiconductors have band edge positions outside the reduction potential of  $O_2/O_2^{\cdot-}$  and  $\cdot OH/H_2O$ . They cover  $TiO_2$  ( $E_{bg}= 3.0\sim 3.2$  eV),  $SrTiO_3$  ( $E_{bg} = 3.2$  eV),  $ZnO$  ( $E_{bg} = 3.2$  eV), and  $CdS$  ( $E_{bg} = 2.5$  eV) (Figure 2). Yet, among these semiconductors,  $TiO_2$  has proven to be most inexpensive and suitable for widespread environmental applications. It is chemically and biologically inert. Compared with other semiconductors,  $TiO_2$  is stable with respect to photo-corrosions and can be used over prolonged periods.

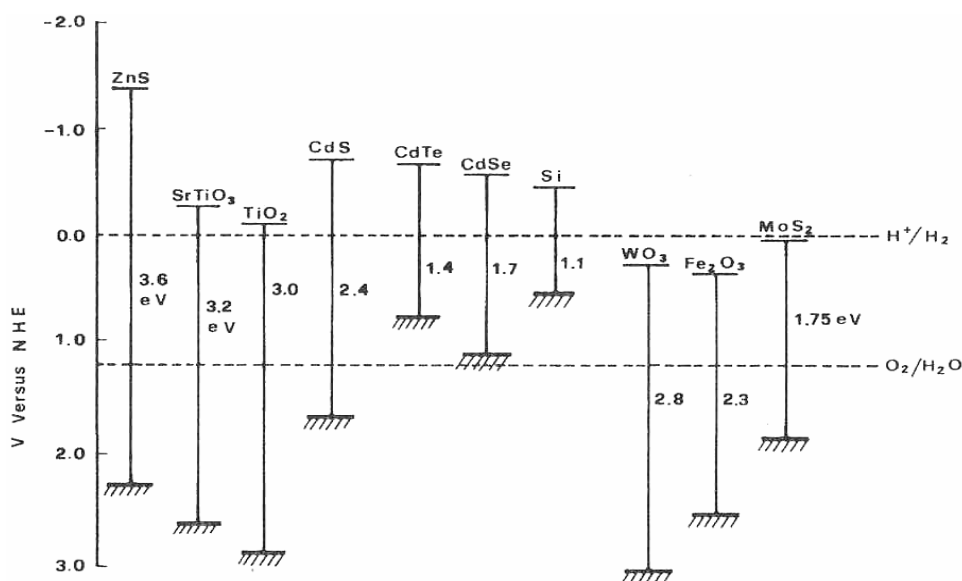


Figure 2. Band edge positions of selected semiconductors (e.g.  $TiO_2$ : 3.0) in contact with an aqueous electrolyte [29]. The bottom of the valence band is indicated by the hatched lines, and the position of the  $H^+/H_2$  and  $O_2/H_2O$  redox couples, important for water splitting, are also specified.

$TiO_2$  has a wide band gap and generates electron/hole ( $e^-/h^+$ ) pairs when illuminated. The redox potential of the  $H_2O/\cdot OH$  couple (-2.8 eV) lies within its band energy, so that it can be used for water splitting [29].

There has been a large quantity of literature concerning the mechanism of the photocatalytic effect since the discovery of the electrolysis of water on TiO<sub>2</sub> electrodes by Fujishima and Honda in 1972<sup>[1]</sup>. After this, the potential application of titania as the most efficient photocatalyst has been the driving force behind the development of ‘easy-to-clean’ surfaces exhibiting photocatalytic degradation of organic pollutants (Figure 3)<sup>[60,62]</sup>.

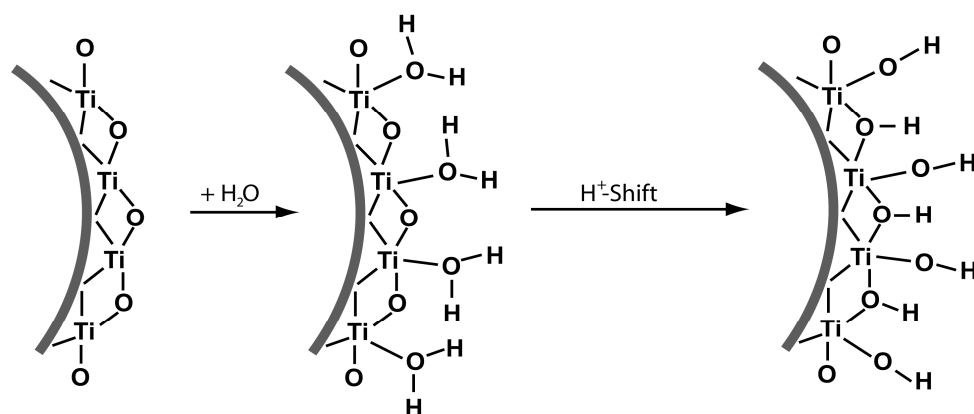


Figure 3. Mechanism explaining the addition of H<sub>2</sub>O and proton H<sup>+</sup> Shift on the titania surface<sup>[60]</sup>.

The hydroxyl radical is a powerful oxidizing agent and organic pollutants are present at or near the surface of TiO<sub>2</sub>, resulting in their complete oxidation to CO<sub>2</sub><sup>[2, 63, 64]</sup>. In heterogeneous photocatalysis systems, photoactive properties of adsorbate molecules and catalyst substrates determine the chemical transformation<sup>[60, 65-67]</sup>. For inert oxide substrates, it is between the adsorbate molecules where electron transfer takes place. The function of the catalyst is only to be a platform for efficient molecular interaction<sup>[68]</sup>. Photoactivity of catalysts is influenced by various factors, namely morphology, crystalline quality, particle size, size distribution, phase composition, porosity, density of hydroxyl groups, band gap and surface area<sup>[69]</sup>.

TiO<sub>2</sub>, as the most well-known photocatalyst, has a proven ability of catalyzing decomposition of dye under light, and in the presence of oxygen. Since there are many other authors who report the same, just as an example of the experiments conducted in 2007 by Faisal et al.<sup>[66]</sup>, Dulay et al.<sup>[70]</sup>, Hurum et al.<sup>[71]</sup>. It was found that Degussa P25 has a higher photocatalytic activity than other TiO<sub>2</sub> powders. Optimum photocatalytic efficiencies are exhibited at pH 10 and pH 4.6. At alkaline pH, this efficiency is attributed to hydroxyl radicals forming on the TiO<sub>2</sub> surface more efficiently with increasing concentration of hydroxide ions.

Research shows that it is very important to adapt the light source (the type of lamp used, type of filter and/or reflector and/or diffuser used; intensity of radiation, spectrum of the incident radiation), oxygen amount, whether dissolved in the solution scavenges the electron generated, preventing the recombination of electrons and holes, pH conditions depending on the kind of defined pollutant parameters to achieve high degradation rates. As seen in the literature, phenol

conversions were found to be more important for acid than for basic media, Okamoto et al., (1985)<sup>[72]</sup> and Serpone et al., (1996)<sup>[58]</sup> have reported that pH 3 was the optimum for the photocatalytic decomposition of phenol. This photocatalytic degradation was complete after 5 hours<sup>[2, 60, 73, 74]</sup>.

A new approach was suggested in 2003 by Hurum<sup>[71]</sup> in that they used the electron paramagnetic resonance (EPR) to characterize the behavior of the excited electrons. They reported that the electrons are first changed from rutile CB to localize states (traps) having their energy level in the anatase band gap, then to anatase particle surface. This model requires that the rutile phase, as well as the anatase phase, is present, which can be valid for e.g. P25. This application can be related to prepared IAD titania films if both phases are present. Additionally, as rutile is active under close to visible light, it is able to absorb more photons that contribute to an increase in global efficiency. Figure 4 elucidates the two different approaches: the original theory and Hurum's approach. At any rate, it seems clear that the strength of Degussa P25 is the contact between rutile and anatase that allows charges separation at the interface of the two titania phases. The aim these two new approaches is to understand the requirement of anatase and rutile contacts for the prepared IAD titania films.

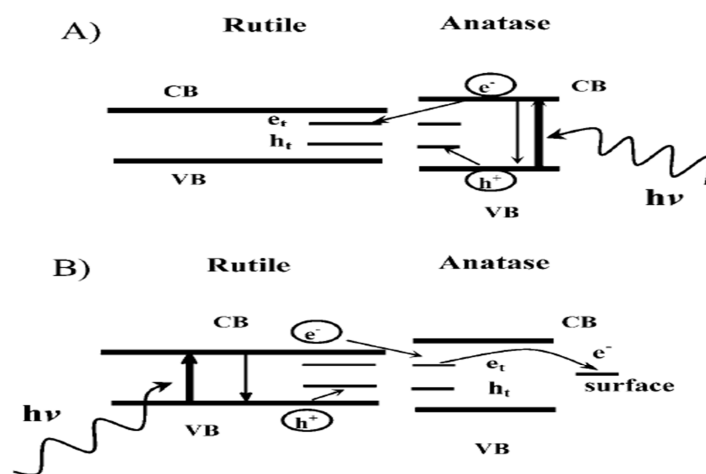


Figure 4. Approaches to characterize the behavior of the excited electrons. (A) The P25 activity model showing charge separation on rutile and anatase performances as an electron sink (previously proposed prior to 2003)<sup>[58, 75]</sup>. (B) Proposed rutile antenna model and following charge separation (proposed by Hurum on 2003)<sup>[71]</sup>.

## 2.1.2 Coated TiO<sub>2</sub> as a Photocatalyst and Microstructure Influence

### (a) Surface Structure of TiO<sub>2</sub>

Nanoparticle-based Titania photocatalytic gradient coatings can be deposited on various substrates, including plastics<sup>[68,76,77]</sup>. In order to obtain a better UV light trapping ability, Japanese researchers Nuida, Kanai, Hashimoto, Watanabe, and Ohsaki designed a TiO<sub>2</sub> deposited Al mirror with a self-cleaning ability<sup>[63,69]</sup>. The surface prepared in their research showed improved photocatalytic efficiency, from 1.2 to 1.4 times more efficient, and a hydrophilicity rate that was 3.3 times improved as compared with single TiO<sub>2</sub> layered glass of the same thickness<sup>[78]</sup>.

Hashimoto, et al<sup>[22]</sup> have shown that the surface structure of TiO<sub>2</sub> changes after UV irradiation, forming a metastable state. However, they have not yet obtained a definition of this state which could be caused by an increase in the number of hydroxyl (OH) groups on the TiO<sub>2</sub> surface. They proposed a mechanism for the highly hydrophilic conversion under UV light illumination, as shown in Figure 5.

To give further details, the photogenerated holes produced in the bulk of TiO<sub>2</sub> diffuse to the surface and are trapped at lattice oxygen sites.

Most trapped holes are consumed to react with the adsorbed organics directly, or adsorbed water, producing OH radicals. However, a small portion of the trapped hole may react with TiO<sub>2</sub> itself, breaking the bond between the lattice titanium and oxygen ions by the coordination of water molecules at the titanium site. The coordinated water molecules release a proton for charge compensation, and then a new OH group forms, leading to the increase in the number of OH groups at the surface. It is considered that the singly coordinated new OH groups produced by UV light irradiation are thermodynamically less stable compared to the initial doubly coordinated OH groups. Therefore, the surface energy of the TiO<sub>2</sub> surface covered with the thermodynamically less stable OH groups is higher than that of the TiO<sub>2</sub> surface covered with the initial OH groups. Because a water droplet is substantially larger than the hydrophilic (or hydrophobic) domains, as shown in Figure 5, it instantaneously spreads completely on such a surface, thereby resembling a two-dimensional capillary phenomenon<sup>[79]</sup>.



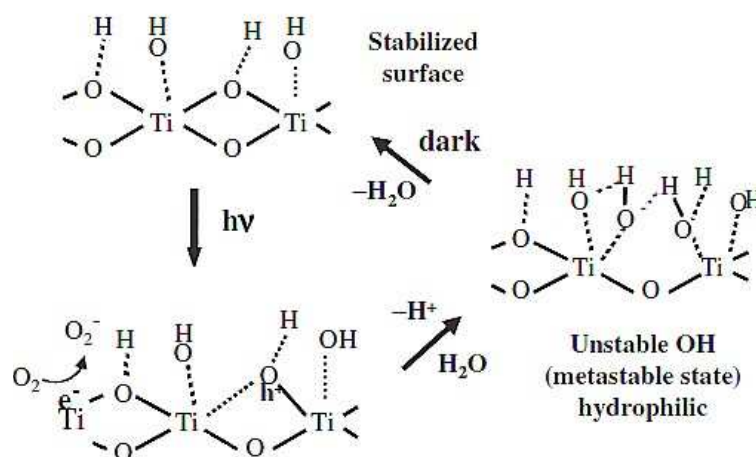


Figure 5. Schematic illustrations of reversible changes in amount of hydroxyl groups on  $\text{TiO}_2$  film under UV light irradiation and in the dark<sup>[79]</sup>.

Following is a quick citation example of the literature, as the focus of the work has already been defined for thin films. Shape, size and the crystalline phase of  $\text{TiO}_2$  nanomaterials can be determined. The morphology of  $\text{TiO}_2$  transforms, from particle to rod-like and bowknot-like, when the pH of a solution increases, and the crystalline phase changes from anatase to brookite. The diameter of the nanoparticles reduces with an increase in the acidity in the system, with the smallest being 7 nm, exhibiting a higher surface area and photocatalytic efficiency for the degradation of phenol<sup>[80]</sup>.

When compared made by conventional PVD thin films, mesoporous  $\text{TiO}_2$  thin films could be more photocatalytic, mainly due to a higher active surface area<sup>[81-86]</sup>. The highest photocatalytic activity and the slowest conversion rate, hydrophobic and hydrophilic state, have been observed in mesoporous thin films calcined at 400 °C, when the films are composed of both anatase and rutile phases<sup>[81]</sup>. In this case, the equilibrium adsorption of methylene blue on the film relates to  $0.575 \times 10^{14} \text{ mol/cm}^2$ . For example, the surface area engaged by a molecule MB was calculated to be approximately  $0.615 \text{ nm}^2$ ; the monolayer on an area of  $1 \text{ cm}^2$  contains  $1.63 \times 10^{14}$  molecules. The limiting of MB relates to 53.4% of monolayer coverage, which is a result of this calculation. Otherwise, the effects of calcination temperature on BET surface areas are 69.9, 10.5, and 2.7 for 500, 700, and 900 °C, respectively<sup>[87]</sup>.

It has been further demonstrated in other studies that mesoporous  $\text{TiO}_2$  can be successfully synthesized with a sol-gel method, and 450 °C calcined sample was approx. 2  $\mu\text{m}$ , surface area:  $212 \text{ m}^2\text{g}^{-1}$ , pore size: 6.2 nm, and crystal size: 8.2 nm<sup>[88]</sup>. Mesoporous  $\text{TiO}_2$  films were used in other studies as the template matrices, with the mesoporosity defined as narrow pore size distributions and synthesis through sol-gel technique.

Films deposited on ITO-coated glass considerably differ in their porosity characteristic to those prepared on glass slides; their porous system displays a bimodal pore size distribution. This results from the shape of the adsorption isotherms, as adsorption and, especially, desorption branches show two regions of steep increase and decrease in the quantity of adsorbed Kr<sup>[89]</sup>. As a mesoporous film comprises of anatase pore walls and voids filled with air, such an index of refraction, is an effective value corresponding to a porosity of 37% for mesoporous layer. This is only slightly larger than that revealed from the Kr adsorption experiment (30%)<sup>[81]</sup>.

There are limited consistent studies investigating the effect of the thin film microstructure on the photocatalytic activity. The film crystallinity is usually the main topic of interest, with the grain structure and porosity being commonly ignored, which is surprising as the film porosity especially influences the active surface area, in turn having a strong effect on the photocatalytic activity. There are previous studies that to show that the film microstructure is strongly related to the photocatalytic activity of the TiO<sub>2</sub> thin films<sup>[90, 91]</sup>. The thin film surface area can be increased by increasing the porosity. The dimensions and the nature of the organic substance to be broken down are important for obtaining the minimum pore size. The thickness of the thin film, especially for high porosity, is also important due to the depth of the pores and the increased active film surface area<sup>[92, 93]</sup>.

The environmental stability and the precise desired quality of optical IAD coatings are in large part limited by the film microstructure porosity, more than the porosity. The reason for this is in IAD thin films on transparent glass, the primordial effect is the microstructure.

One focus of this thesis is to ascertain two points. One being whether the titania microstructure beneficially enhances the transfer of photo-generated electrons from the anatase phase to the rutile phase. The other is the reduction of the electron-hole combination rate in anatase resulting in an enhanced activity. The increase of photoactivity and hydrophilicity can be deduced by specific high surface areas, mesoporous structures, sufficient surface hydroxyl content and the degree of surface roughness<sup>[87]</sup>. The question is whether IAD samples should or should not be mesoporous, and using which coating parameters.

The mesoporous phenomena discussed here was used as a comparison to the IAD samples. The benefits of mesoporous thin films are not usable in the degradation of a solid adsorbed layer as their activity remains low. However, but such films can be of good use when initiating photocatalytic degradation processes in the gaseous phase<sup>[94]</sup>. TiO<sub>2</sub> films prepared using r.f. magnetron sputtering in O<sub>2</sub>/Ar mixture on cold temperature; 50 °C to 60 °C, silicate glass substrate show a growth of anatase and rutile phases.

Deposition processes modeling has advanced by now defining design rules and spacing to avoid porosity to influence the optical quality. Fractions depend on pre-treatment parameters in these cases; with an increase in the total pressure leading to a rutile phase showing a tendency to convert to anatase. XRD measurements of these films show a dependence of morphology on the thickness of the thin films in that once the thickness exceeds 65 nm, the amorphous structure converts to anatase phase, with some trace of rutile phase. Pure anatase phase is achieved with a thickness of 185 nm, and shows the best photocatalytic activity. Experiments show that a correlation exists between photocatalytic activity and anatase phase and size of anatase grains <sup>[95]</sup>.

### (b) Microstructure of TiO<sub>2</sub>

TiO<sub>2</sub> has 11 allotropic forms: anatase, rutile, brookite, TiO<sub>2</sub>-B ‘bronze’ and seven high pressure phases of TiO<sub>2</sub>. These latter phases do not occur in nature and they are synthesized by high pressure treatment of anatase or rutile <sup>[18]</sup>.

Anatase is used in most research regarding photocatalysis <sup>[8, 28, 60, 96]</sup>, mainly due to its more thoroughly characterized aspects when compared to rutile (such as electronic behavior and bulk structural). This high usage is mainly a result of the preparation methods used in that it is, for example, easier to generate anatase than rutile at temperatures below 600 °C. It is only possible to obtain rutile above 800 °C, the transition temperature to the thermodynamically most stable phase rutile <sup>[28]</sup>.

Many publications describe the benefits of certain coating of the structure and optical coating of thin films <sup>[97-100]</sup>. TiO<sub>2</sub> crystallizes depending on, for example, the titanium precursor and the applied temperature in the well-known phases: anatase, rutile, and brookite. The anatase phase is regarded as being the most suitable for photocatalysts, especially the {001} facet <sup>[97]</sup>, while the rutile phase is used for optical and electronic purposes due to its high dielectric constant and high refractive index.

The following Figure 6, shows that all arrangements are a build-up of TiO<sub>6</sub> octahedra forming a three-dimensional network, a regular assembly of long parallel chains and a regular assembly of somewhat staggered chains with anatase, rutile and brookite, respectively.

Table 1 shows the crystal parameters of the different TiO<sub>2</sub> forms.

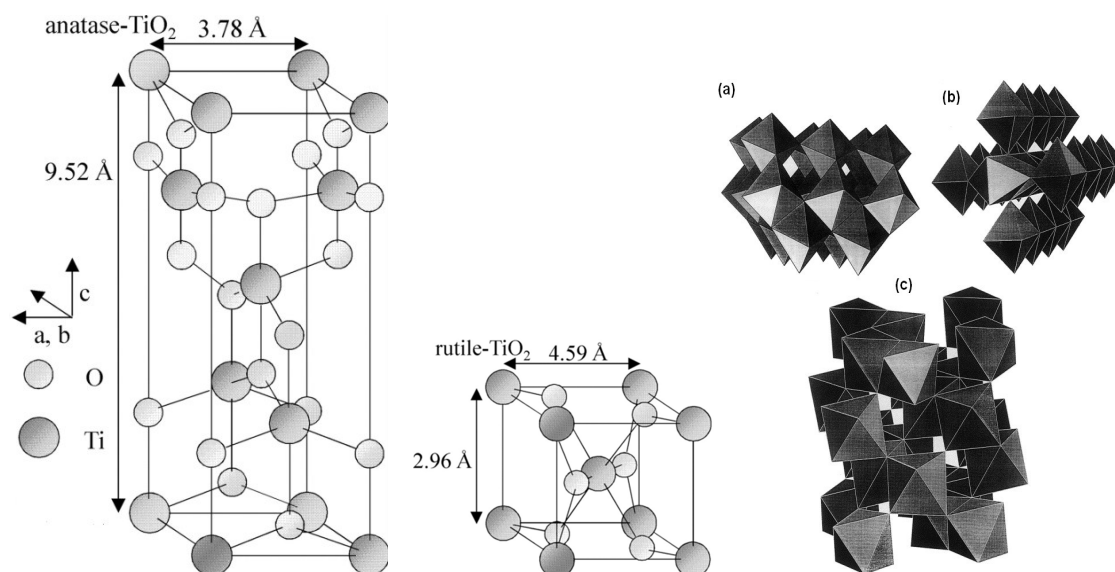


Figure 6. Crystal Structures of Titanium Oxide. Fragments from the crystalline arrangements of (a) anatase, (b) rutile and (c) brookite <sup>[101]</sup>.

Table 1. Cell parameters and density of TiO<sub>2</sub> forms,  $\rho_s$  is the selection density <sup>[102]</sup>

Form	a (Å)	b (Å)	c (Å)	$\beta$ (°)	$\rho_s$ (cm <sup>3</sup> .g <sup>-1</sup> )	Space group
Rutile	4.594	4.594	2.9586	90	4.25	P42/mnm
Anatase	3.777	3.777	9.501	90	3.92	I41/amd
Brookite	12.163	3.735	6.513	107.29	3.76	C2/m

### 2.1.3 Industrial Application of TiO<sub>2</sub> Photocatalyst

The role of nanotechnology in the production of photocatalytic, super-hydrophilicity and transparent thin films is pivotal, and multiple uses of surfaces deposited with thin films make this subject essentially interdisciplinary.

The possibility to photocatalytically improve the hydrophilicity of TiO<sub>2</sub> surfaces has been researched since 1995 and substantial amounts of research have been conducted on the morphology and structure of thin films, photochemistry, practical applications and the ways to improve photocatalytic characteristics (Figure 7) <sup>[2, 66, 79, 103]</sup>.

Development in this field of TiO<sub>2</sub> photocatalysis is still ongoing, yet Hashimoto and Fujishima believe that its rapid advancement over a ten-year span serves as one of the best examples of how scientific knowledge can develop and produce a new industry.

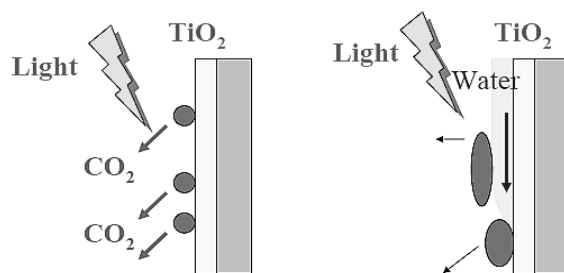


Figure 7. Hydrophilicity effect on photocatalysis. Left: Gradually-adsorbed dust degradation by strong oxidation. Right: Removal of a large quantity of dust via pouring water, thereby using the super-hydrophilicity effect.

The photocatalytic activity of TiO<sub>2</sub> is biased by numerous features, including film thickness, surface area, degree of crystallinity and crystallite size. The microstructure and porosity of the thin films can expand the surface area. The thickness of the thin film is important. For high crystallinity it is advantageous and alluring to minimize the number of grain boundaries, such as to increase the grain size. This is in opposition to the desire to increase the surface area, such that a typical grain size range of approximately 10-20 nm is deemed an optimum compromise between these two concerns. Anatase is reported to be the most photoactive phase of the three most common TiO<sub>2</sub> crystalline phases, making this is one of the reasons why most studies labor with crystalline anatase thin films. Anatase is also the crystal phase which forms most easily for small grain sizes and at the processing conditions is commonly used. Crystalline thin films for many techniques can only be achieved when heated during or after coating, thereby limiting the substrate material choice and making most polymers not applicable.

Additionally, uptake of sodium or other detrimental contaminants from the substrate must be avoided<sup>[3, 77]</sup>. TiO<sub>2</sub> films are usable in various commonly-known commercial products, such as medical equipment, or mirrors used in automobiles and windows<sup>[12, 79, 104]</sup>. Researchers have struggled to determine optimal parameters, such as light intensity or reactor set-up, for the utilization of TiO<sub>2</sub> in the deposition of thin films<sup>[8, 11, 81, 105]</sup>.

A good amount of work has already been done in the field of photocatalysis in the last 2 decades, most of which shows that deposition methods and the use of TiO<sub>2</sub> coatings are not limited in their scope to the sophisticated industrialized economies. As an example, it has been proposed that it is worth researching the uses of solar photocatalysis to detoxify water contaminated with pesticides, which can be useful for an agrarian society<sup>[106]</sup>. Other research has concluded that it is possible to develop easy-to-use methods that can then be employed in urban and semi-urban areas of developing countries for the degradation of contaminants<sup>[107]</sup>. TiO<sub>2</sub>, along with solar energy, is more useful for disinfecting water than solar energy alone, and as a catalyst it ensures safe usage that is both suitable and reusable. Many vigorous attempts have been made to explain this 'easy to

clean' phenomenon by analyzing it from various aspects <sup>[2, 79, 108]</sup>. Outside during the daytime, there are typically several hundred milli-Watts per square centimeter of UV light even in the shade, which is low from the overall vantage point of energy density. However, this is huge when compared to molecules adsorbed on the surface as this amount approximates to  $10^{15}$  of photons/cm<sup>2</sup> per second. It should however be noted it is only when the number of incident photons is greater than that of molecules gathering on the surface per unit time that this function is effective. Put simply, this is not an effective function when the flux of photons is insufficient compared to that of the organic substances <sup>[22, 79]</sup>.

Research completed using TiO<sub>2</sub> on coliform proves that this decreases the concentration of coliform in under 10 minutes, and also prevents their regrowth after photocatalytic disinfection <sup>[109]</sup>. Recent research shows that there is an environmental possibility of making photocatalytic water treatment technology more commercially viable for industrial application via the use of TiO<sub>2</sub>-Kaolin <sup>[110]</sup>. Another useful application of TiO<sub>2</sub> in the field of environmental sciences is the complete mineralization of toxic organic pollutants. Photocatalysis provides a clean, attractive, low-temperature, non-energy intensive approach to dealing with pollutants in water and wastewater, which has caused it to be a focus for the environmental sciences, with the role of TiO<sub>2</sub> in the destruction of pesticides researched by Shankar et al. (2004) <sup>[111]</sup> as an example. This expressed research shows that TiO<sub>2</sub> enhances the photocatalytic degradation of monocrotophos MCP which is a widely used and extremely toxic organophosphate insecticide, making TiO<sub>2</sub> even more commercially viable. For the complete mineralization of MCP, TiO<sub>2</sub> takes 540 minutes and less than 420 minutes when supported by H $\beta$  zeolite. Resulting from increased adsorption of MCP, H $\beta$  supported TiO<sub>2</sub> is more active towards degradation than other catalysts, and therefore optimum loading of TiO<sub>2</sub> on zeolite surface alone can improve the degradation rate. TiO<sub>2</sub>/H $\beta$  zeolite has been discovered to be the best in synthesis activity of isomer 5. Organic reactions on solid supports have garnered much attention of late as a result of the advantages these catalysts possess, such as their environmentally friendly nature, acidic properties, the high purity of the products, shape-selectivity <sup>[112, 113]</sup>, their easy work-up <sup>[114]</sup>, and their recyclability and cutback in waste production <sup>[115]</sup>. H $\beta$  zeolite also shows higher photonic efficiency in degradation and mineralization <sup>[111]</sup>.

Another advantage of TiO<sub>2</sub> is in its industrial application to reduce the air pollution (Figure 8 left). Research recently completed in the U.S. to determine the abrasion and wear resistance properties of TiO<sub>2</sub> and its impact on the environment shows that the wearing of the samples with 5% TiO<sub>2</sub> provided a small decrease in the coating NO removal efficiency of 26.9%. However, the sample-wearing with 3% TiO<sub>2</sub> gave a slightly improved NO removal efficiency of 18.0% <sup>[111]</sup>. EDX analysis confirms that during intensive utilization, the relative concentration of Ti on the

specimens did not substantially change, as compared to the original samples. The dependence of the NO removal efficiency on humidity, coating composition, and flow rate has to be further investigated to evaluate the potential of releasing nanoparticles into the environment prior to validation of technological efficiency<sup>[116]</sup>.

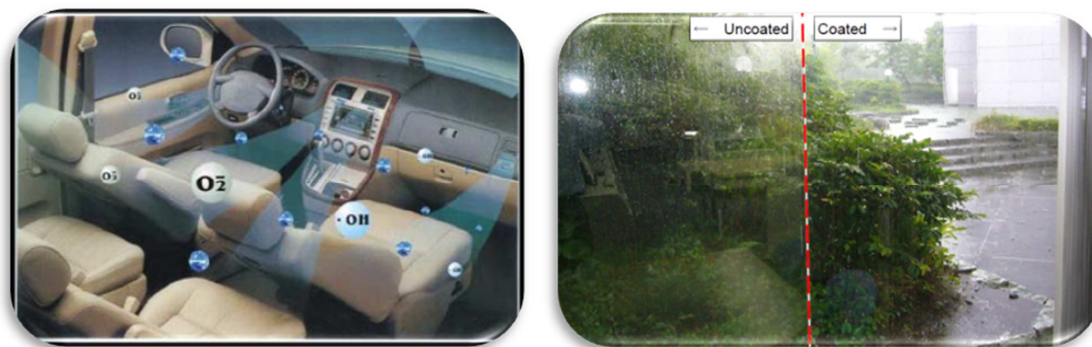


Figure 8. Examples of industrial application of titania photocatalyst. Left: air purification in automobile industry. Right: glass quality in windows industry<sup>[117]</sup>.

While general industrial use is both possible and useful, an important utility of TiO<sub>2</sub> layers or multi-layers is in the optical industry (Figure 8 right) if a high optical transparency can be preserved. Dense TiO<sub>2</sub> thin films can be deposited using different processes, such as sputtering and IAD<sup>[118]</sup>. Research has been carried out to improve optical quality of thin films which, in technical terms, depends on their refractive index. One of these studies by Gracia *et al*<sup>[119]</sup> in 2006 on a variable refractive index prepared using ion-beam and plasma enhancement confirms that the porosity decreases the value of  $n$ . This correlation has been noted specifically with thin films prepared with Plasma-Enhanced Chemical Vapor Deposition (PECVD) involving high amounts of Ti. Films prepared with Ion-beam Induced Chemical Vapor Deposition (IBICVD) show the opposite results, hence leading to the conclusion that the presence of Ti affects the ‘polarizability’ of ions and optical properties of thin films. This method might be worthwhile in quantifying optical ultrathin films, for example 10 nm, where it is difficult to determine  $n$  via other optical methods<sup>[120]</sup>. This paper shows that there is a linear correlation between the Auger parameter in mixed oxides and the electronic polarizability gained from the refractive index through the Lorentz-Lorenz relationship. Additionally, due to economic and technical disadvantages, the CVD process is no longer productive in the coating of the most well-known commercial photocatalytic glass product, Pilkington Activ™<sup>[121]</sup>.

Corrosion current density and the corrosion rate of multilayers on the basis of titanium were found through examination of the potentiodynamic polarization curves<sup>[122]</sup>. The corrosion current density for the TiN+multiTiAlSiN+TiN coatings coated by PVD process is 0.36  $\mu\text{A}/\text{cm}^2$  and TiC+Ti(C,N)+Al<sub>2</sub>O<sub>3</sub>+TiN deposited by CVD procedure is 0.21  $\mu\text{A}/\text{cm}^2$ , which attests to good

anticorrosion properties of the PVD methods. Resulting from the use of the multilayered deposition in the PVD procedure, these good properties are associated with better options of corrosion prevention. The successive deposition of coating layers can neutralize failures, such as crevices, pores or columnar structure occurring in the event of the single layer put down in the deposition process. In this way, the corrosion agents' path is longer or blocked.

Concurrent to these studies, it was found that coatings deposited by PVD and CVD methods display high corrosion resistance. The best results were obtained for the coatings deposited through the PVD process<sup>[3]</sup>. The obtained results are the basis for the optimization of resistance of the PVD and CVD coatings deposited onto the substrate. The influence of PVD-IAD methods has been studied in this thesis to understand the hardness of the surface<sup>[123]</sup>.

Pilkington Activ<sup>TM</sup> glass is presently widely known to be produced by the CVD method, or by the PVD, and demineralization tests conducted on anatase Pilkington Activ<sup>TM</sup> using Reactive Black 5 and Acid Blue 9 in air-solid system exhibit average agglomerate with a particle-size of 95 nm in diameter. Characterization results show faster decolorization of Acid Blue 9 under solar irradiation as compared with laboratory photoreactor experiments conducted for 8 hours of UV exposure, but in both cases there was still no difference in the number of incident photons reaching the surface. Chin and Ollis<sup>[121]</sup>, concluded that the demineralization curve exhibited the pseudo-first order initial rate constant. Anatase was the only phase revealed. The colored dye formed a colored intermediate and experiments under sunlight exposure on the Active<sup>TM</sup> glass decolorized AB9 faster than the laboratory photoreactor experiments after 480 min of UV, and then finally turned to a colorless product. It is hypothesized that the additional UV-B photons in this light spectrum and the higher outdoor water vapor density account for the differences between the sunlight versus the black light-blue activity.

It can be understood from the previously mentioned literature that TiO<sub>2</sub> thin films can be deposited with a variety of wet chemical and vapor deposition based techniques, the most popular being sol-gel, chemical vapor deposition (CVD), and a physical vapor deposition (PVD) procedure, magnetron sputtering. Other than the deposition technique used, it is necessary to control the deposition parameters in order to produce thin films that realize the basic high surface area and good crystallinity requirements. There are many techniques in which heating during or after deposition is the only way to gain crystalline thin films<sup>[30, 54, 55, 124, 125]</sup>.

The problem of the constantly increasing air pollution affecting urban areas has recently driven researchers to take advantage of photocatalytic characteristics to reduce the toxic substances contaminating the atmosphere. Italcementi was the first industrial group to patent photocatalytic cementations materials (Figure 9).





Figure 9. The photocatalytic effect in urban areas<sup>[126]</sup>. (1) CO, VOC (Benzene, Toluene, etc.), Methyl Mercaptan (gas), Organic chlorinated compounds, Polycondensed aromatic compounds, Acetaldehyde, Formaldehyde. (2) NO<sub>x</sub>, SO<sub>x</sub>, NH<sub>3</sub> (gas).

#### 2.1.4 Visible Light and TiO<sub>2</sub> Doping

Previous research involving the photocatalytic rate expression has observed that the photocatalytic activity is enhanced by addition of silver<sup>[127]</sup>. To an extent, exposure to UV light after calcination of Ag-TiO<sub>2</sub> treated films can improve photocatalytic activity. This is due to the structure modification of doped titania. The detailed investigation on the XRD patterns of the silver-doped TiO<sub>2</sub> powders demonstrated that the doping of metal ions with less oxidative states than IV produced the deficiency of O vacancies in TiO<sub>2</sub>. Research on the oxidation of methylene blue shows that aqueous solutions can photosensitize the process with the help of dissolved oxygen, while experiments conducted prove that there is a correlation between titania films of different thickness and the rate of reduction of an ink film, which is simpler to use and acts faster than dye solutions<sup>[79, 128]</sup>.

TiO<sub>2</sub> thin films with the ability to work under visible light ( $\lambda > 450$  nm) can be deposited with the help of IAD and metal ion-implantation. Molecular calculation of such prepared thin films show that for making TiO<sub>2</sub> films capable of absorbing visible light it is beneficial to modify TiO<sub>2</sub> to be able to absorb this light. Thin films prepared with this method can cause effective degradation of water and air diluted toxic compounds under visible light<sup>[129]</sup>.

XRD measurements of TiO<sub>2</sub>-Ag composite thin films reveal that pore-less films show the anatase phase TiO<sub>2</sub> and porous films show a mixture of anatase and rutile TiO<sub>2</sub> phases<sup>[78, 130, 131]</sup>. Photocatalytic activity in such thin films can be improved by making porous structure or by introducing active elemental Ag. In the experiments conducted in this area, medium sized PS200-

Ag composite films were observed to have the best photocatalytic activity. This was concluded on the basis of the fact that methylene blue was demineralized completely after the films were exposed to UV for 7 hours<sup>[132]</sup>. Self-degradation of methylene blue under UV and physical adsorption pure TiO<sub>2</sub>, PS-TiO<sub>2</sub>, PSTiO<sub>2</sub>-1% Ag, and PS-TiO<sub>2</sub>-5% Ag thin films exhibited 43%, 68%, 72%, and 69% degradation, respectively<sup>[133]</sup>. This co-doping might increase photocatalytic activity on degradation of methylene blue under visible light irradiation. The experiments show that interfacial charge transfer on films is the main factor in photocatalytic reaction<sup>[134]</sup>.

In regards to Ag, also used for IAD doping of TiO<sub>2</sub> thin films in this research, their electrons become excited and transform to adsorbed oxygen with the formation of O<sub>2</sub> when irradiated with the light of their Plasmon resonance wavelength. The Ag nanoparticles are subsequently oxidized by O<sup>2-</sup> to colorless Ag<sup>+</sup> ions<sup>[135, 136]</sup>. These Ag<sup>+</sup> ions are reduced in the presence of TiO<sub>2</sub> by the excited electrons, and Ag nanoparticles are reformed. Therefore, recombination of the electron and hole prior to the superoxide activation step is a limiting factor of the photocatalytic reaction<sup>[137]</sup>. Silver has been shown to have a beneficial influence on the photoactivity of nanocrystalline semiconductor photocatalysts<sup>[138, 139]</sup>. It has been reported that the combination of semiconductor substrate and metal cluster give improved photocatalytic activity through trapping the photoinduced charge carriers and thereby improving the charge transfer processes<sup>[140-142]</sup>.

Doping with Ag is especially advantageous for industrial use. A comparison of undoped and Ag-doped TiO<sub>2</sub> thin films with separate doping concentrations and different annealing temperatures shows that the films heated at 100 °C held kinetics equal to that of low methylene blue degradation. In contrast to this, the Ag-doped samples annealed at 500 °C showed enhanced photocatalytic activity, which can be attributed to a charge separation mechanism which hinders the recombination of photogenerated pairs, and also to Ag, which helps increase the TiO<sub>2</sub> dispersion<sup>[143, 144]</sup>. There are papers on the suppression of photocatalytic activity beyond the optimum loading level as a result of separated phases of the oxides of the dopants<sup>[145]</sup>, the reduction of the active sites on photocatalyst<sup>[146]</sup>, the increase of electron-hole pair recombination at the doping sites<sup>[147]</sup> and at the oxygen vacancies<sup>[148, 149]</sup>. Each TiO<sub>2</sub> type had its own optimum loading level, which was dependent on the agglomeration behavior, dispersion and coverage of the Ag on each TiO<sub>2</sub> type. This behavior affected the photogenerated charge separation, the number of reaction sites and the photon flux. Small particles tend to have high, while large particles tend to have low Ag contents as optimum loading levels.

The idea from this literature research is to conclusively prove this result for IAD samples and to try to gain a first impression of the capacity of enhancing the photocatalytic performance in visible light using this doped titania.

### 2.1.5 Methylene Blue as a Photodegradation Model

It is unfortunate that there is no standard procedure or reference sample for measuring the photocatalytic activity of TiO<sub>2</sub> thin films, meaning that it is difficult to compare results between laboratories or different measurement setups. In 1999, Mills and Wang concluded that in photodegradation processes, photobleaching of MB, initiated by TiO<sub>2</sub>, in aqueous solution is considered to be ambiguous and is not favored by scientists<sup>[61]</sup>. However, these conclusions were challenged and disproved later. For instance, in the last few years, certain authors proved that TiO<sub>2</sub> and other surfaces react with MB to calculate the photocatalytic activity what needs to be taken care of are the standard parameters and avoidance of materials with low absorbing capability<sup>[123, 150]</sup>. Using the experimental set-up of an initial MB concentration of 10 μmol/l, irradiation intensities below 5 W/m<sup>2</sup> have been calculated for substrates comprising quantum efficiencies greater than ζ = 0.09% for colloidal TiO<sub>2</sub> prepared via controlled hydrolysis<sup>[151]</sup>. To calculate the photonic efficiency of transparent thin films, successful attempts have been made for developing automated experimental systems by in-situ measurement of demineralization of methylene blue<sup>[152, 153]</sup>. Yet, methylene blue is an effective photosensitizer, as they possess triplet states of appropriate energies for sensitization of oxygen. Triplet energy ET is equal to 32 (kcal mol<sup>-1</sup>)<sup>[154]</sup>. Methylene blue is a phenothiazinium dye with a strong absorbance in the range of 550 - 700 nm, and a significant quantum yield (φΔ = 0.52)<sup>[155]</sup>.

Using the same principle as described, and with quantifying the measurement data as a goal, a software algorithm was developed based on LabVIEW (developed by National Instruments) with the intention of speeding up the evaluation of the photocatalytic process information. This created measurement system is appropriate as being compliant with the German Institute for Standardization (DIN) 52980 standard and by using the demineralization method as a basis, it calculates the photonic efficiencies of the coated samples.

As has been previously mentioned in this chapter, with methylene blue degradation, as an example, photogenerated holes h<sup>+</sup> at first induce the formation of the dye radical cation MB<sup>\*+</sup> which, is converted to MBOO<sup>\*+</sup> by O<sub>2</sub>. The photobleaching of MB, provoked by TiO<sub>2</sub>, in aqueous solution is shown by Mills<sup>[61]</sup> to be a rather ambiguous system. As expected, the TiO<sub>2</sub>-sensitized photobleaching of MB is not reversible in an oxygen-saturated aqueous solution as the MB reaction was a result of an oxidative process. However, leucomethylene blue (LMB) is initially generated in an acidified solution, using the photobleaching process in an oxygen-saturated solution. This situation is due to LMB reacting very slowly with oxygen to form MB when under acidic conditions. Although continued irradiation eventually leads to the complete mineralization of the dye, the initial observed photobleaching of the dye is not by necessity a result of the dye oxidation, especially if the reaction is done under conditions favorable to LMB formation.

Subsequently, the favorable conditions are generally discussed and brought into accordance with the standardization of photocatalytic effect using methylene blue. This will be generally used for PVD-IAD samples. The overall degradation of methylene blue ( $C_{16}H_{18}N_3SCl$ ) with oxygen is summarized in the following equation:

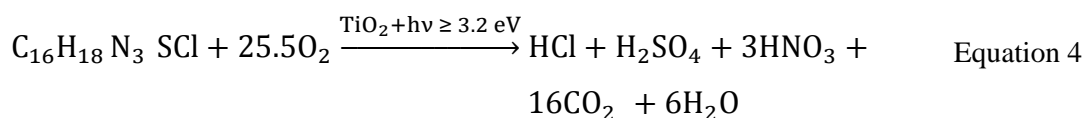


Figure 10 describes the formation of the reduced and colorless form of methylene blue, leucomethylene blue, which represents a good indicator for the start of the photocatalytic reaction. Since the discoloration can be easily observed by UV-Vis spectroscopy or photometry, it was used in this study to evaluate the photocatalytic activity of  $TiO_2$  films prepared with different synthesis parameters.

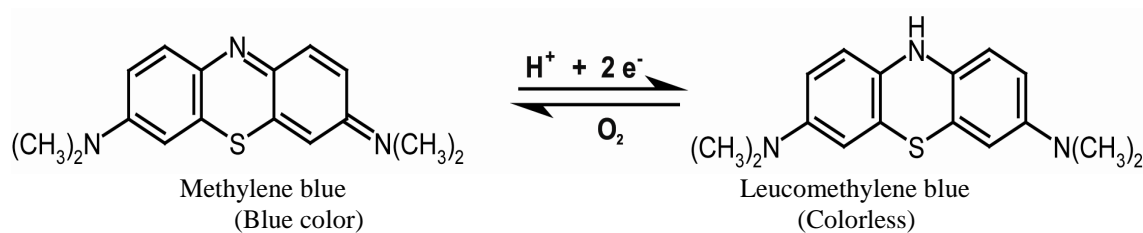


Figure 10. Photobleaching of methylene blue.

A methylene blue solution manufactured by Carl Roth GmbH was used at a concentration of  $10\ \mu\text{mol/l}$ . Methylene blue solution possesses benzoide and chinoide ring systems.

Methylene blue was chosen as the best way to demonstrate the photocatalytic activity and calculate the photonic efficiency. The objective of the methylene blue study was to correlate the use of different ion deposition process parameters in order to produce  $TiO_2$  films of different packing densities to the resulting photocatalytic properties, thus obtaining materials for self-cleaning optical components.

### 2.1.6 Anti-Bacterial and Self-Cleaning Effect

Nanocomposite materials can be very advantageous for making thin films anti-microbial. This can be especially helpful on surfaces that cannot be sterilized by using high temperature. Nanoparticles are environmentally friendly and highly economical in industrial processes, and they produce highly stable thin films. Hygienic properties make thin films produced with nanoparticles an ideal choice for being used on medical equipment <sup>[156]</sup>.

In experiments done on antibacterial membranes using apatite, Ag, AgBr and TiO<sub>2</sub> show that their employment for this purpose gives very suitable results, which are attributed to the synergetic action of these four components and the unique porous structure and high surface area of nanofibrous membrane. Each component in this antibacterial membrane provides a different function: the hydroxyapatite captures bacteria by acting as the adsorption material; the Ag nanoparticles act as the release-active antibacterial agent; the AgBr nanoparticles act as the visible sensitive and release-active antibacterial agent; and the TiO<sub>2</sub> acts as the UV sensitive antibacterial material and substrate <sup>[131, 157]</sup>.

Especially, when experimented with *E. coli*, it was discovered that addition of electro-spun membrane can substantially improve anti-bacterial effect on *Escherichia coli* as compared to the use of these very components in powder form. Permanence of anti-bacterial activity of these membranes is another noticeable feature <sup>[158]</sup>.

It is also possible to give self-cleaning ability to the thin films, which further enhances their practical anti-bacterial use. For example, polyvinyl difluoride (PVDF) membranes containing TiO<sub>2</sub> have a better antifouling and self-cleaning ability as compared with simple PVDF membranes <sup>[7]</sup>. Also, photoacoustic technique analysis shows that sol-gel TiO<sub>2</sub> films have a good ability to eliminate micro-organisms which contaminate river water <sup>[105]</sup>.

To understand the antimicrobial effect, some research has been done on stainless steel substrates AISI 304. The results show that with a growth rate of 5 nm/h, columnar-grained TiO<sub>2</sub> thin films of anatase phase structure can be produced by magnetron sputtering. For the anatase phase, if oxygen supply is increased with the pressure of 0.5 Pa and the deposition time is extended to 30 minutes or more, the resulting thin films can have the maximum photocatalytic activity and antimicrobial activity. Hence, it is the anatase phase which determines the level of photocatalytic activity and consequently the antimicrobial activity. The tests from which these conclusions were drawn were carried out on *Staphylococcus aureus* and *Escherichia coli* <sup>[159]</sup>.

Another possibility is to produce thin films with antimicrobial and photocatalytic properties that can work under the UV light of domestic fluorescent lights. Successful experiments have been conducted for this on indoor paints, using nano ZnO coatings, in which these coatings proved to be more photocatalytic and antimicrobial than nano TiO<sub>2</sub> <sup>[160]</sup>.

Due to their possible antimicrobial application, photocatalytic titanium dioxide films have been researched over many years <sup>[133, 134]</sup>. A methylene blue solution has been used to test the photocatalytic activity of the deposited titania films, and antimicrobial effect analyzed by way of the '*sarcinia lutea*' standard. A gram-positive bacterial strain, such as *Sarcinia lutea*, was used for

this test for coated and uncoated samples. The cells were cultivated under optimal conditions. The cell number was established by cultivation (Rodac-Agar plates) and measuring colony-forming units and the samples were also examined in a dark environment as a reference <sup>[129, 132]</sup>.

## 2.2 Production Processes of TiO<sub>2</sub> Thin Films

In the production of TiO<sub>2</sub> thin films, there are different deposition processes that can be selected from (Figure 11). The two main categories are ‘Transformation’ and ‘Separate’. Under ‘Transformation’ there are two possible ways to carry out deposition, i.e. through thermal oxidation or doping implantation diffusion. The processes falling under the head of ‘Separate’ can be further sub-divided in three categories, that of ‘Chemical Vapor Deposition’ (CVD), ‘Physical Vapor Deposition’ (PVD), and ‘others’ such as spin-on and sol-gel methods. CVD is done using the conventional method, Plasma Enhanced Chemical Vapor Deposition (PECVD), Metal-organic Chemical Vapor Deposition (MOCVD) and Plasma Impulse Chemical Vapor Deposition. PVD is carried out in three different ways <sup>[161, 162]</sup>. Firstly by evaporation of coating materials caused at high temperatures using conventional and ion-assistance, secondly by sputtering, which involves the process of ion-beam sputtering (IBS) and direct current (DC), alternating current (AC) and magnetron, and lastly with pulsed laser. This pulsed laser method is not discussed in this chapter as has two disadvantages; being technically and economically unfeasible. An example of this unfeasibility is its debris generation, its rapid decline of the coating flux with distance from the source and the difficulty in attaining films on large area substrates <sup>[163]</sup>.

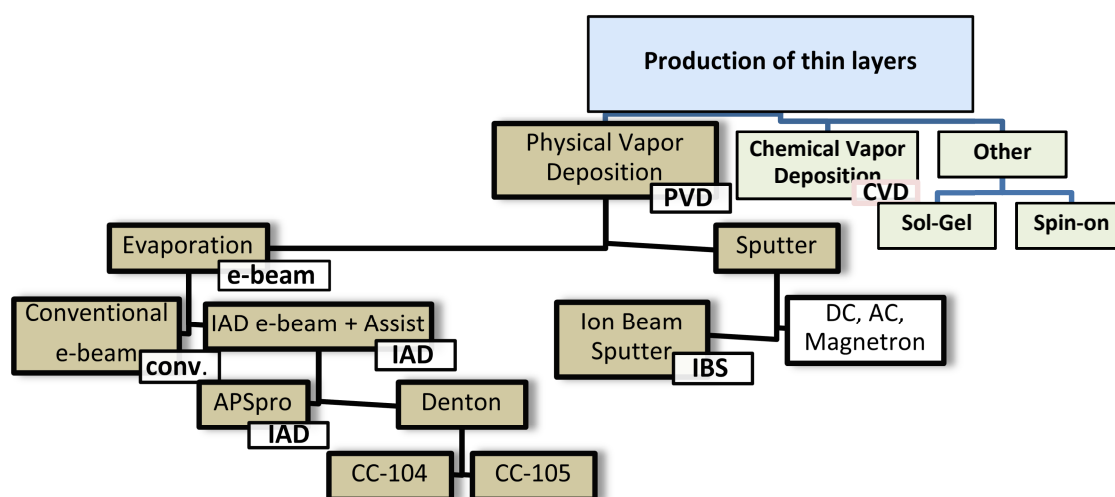


Figure 11. Different deposition processes <sup>[164]</sup>. There are different mechanisms to prepare thin films, but in the frame of this work conventional and IAD techniques are investigated. The brown-shaded cells show the processes used in this research.

### 2.2.1 Conventional Physical Vapor Deposition without IAD

The conventional physical vapor deposition, including electron beam evaporation has several advantages. The main advantage of PVD is the smooth coating that is provides of the thin layers while also achieving good adhesion to the substrate. Another advantage provided is the ability to control the process conditions to generate crystalline thin films without external substrate heating, while substrate self-heating can occur during the coating process<sup>[3, 165]</sup>. However, there are still some disadvantages with this process. These include a complex technical vacuum procedure, a slow deposition rate, essential and difficult ion cleaning, and not suitable for rebuilds. It also has the disadvantage of being expensive. The first process investigated in this thesis is the ‘conventional method’, which is an e-beam PVD process without the implementation of an ion-source (Figure 12).

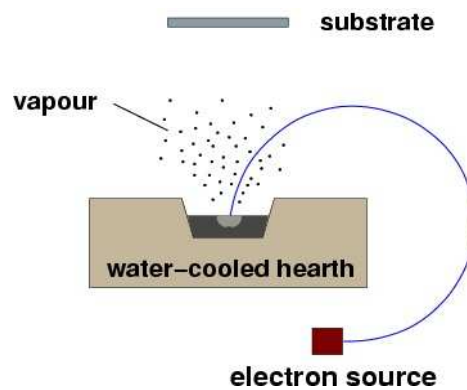


Figure 12. Electron beam in a PVD process<sup>[166]</sup>.

### 2.2.2 Sputter Physical Vapor Deposition

PVD falls under the category of ‘Separate’ processes. It includes various vacuum deposition methods. PVD involves high temperatures and plasma sputter bombardment<sup>[167, 168]</sup>. The term PVD was used for the first time in 1966 by Powell, Oxley and Blocher Jr. (1966) in their book ‘Vapor Deposition’<sup>[169]</sup>. Various types of PVD are sputter deposition, pulsed laser deposition, cathodic arc deposition and electron-beam physical vapor deposition. Significant features of electron-beam PVD include relatively high deposition rates, columnar and polycrystalline microstructure which can be improved by manipulating the process parameters, low contamination, superior thermal efficiency and dense coating<sup>[170]</sup>. Literature relating to these three types has been discussed in the following paragraphs.

Magnetron reactive sputtering, which is another type of ‘sputter deposition’ (Figure 13), is used for depositing thin films on laboratory equipment. This is one of the most popular processes of depositing thin films and ensures a high degree of precision. It has been successfully tested for

deposition on microscope glass slides with the help of magnetron reactive sputtering method<sup>[163]</sup>. Thin film doping with Sn after IAD deposition reduces the band gap, and therefore results in a stronger absorption capacity and photocatalytic activity than conventional TiO<sub>2</sub> deposited thin films. This signifies the usefulness of ion implementation on TiO<sub>2</sub> thin films<sup>[171]</sup>. In the deposition processes, if an RF bias voltage is applied to a substrate it can enhance the ion bombard effect and the mobility of as-deposited atom by dc reactive magnetron sputtering<sup>[172]</sup>.

In recent years, pulse magnetron sputtering (Figure 13) has been used for fabrication of multi-functional high reflective and anti-reflective layers<sup>[173]</sup>. For high reflective stacks, a deposition temperature of 150 °C can be used, which is suitable for polymer materials. Anti-reflective methods are appropriate for glass substrates. Exposure to UV-A light leads to a super-hydrophilic behavior and easy-to-clean quality of the thin films<sup>[174]</sup>.

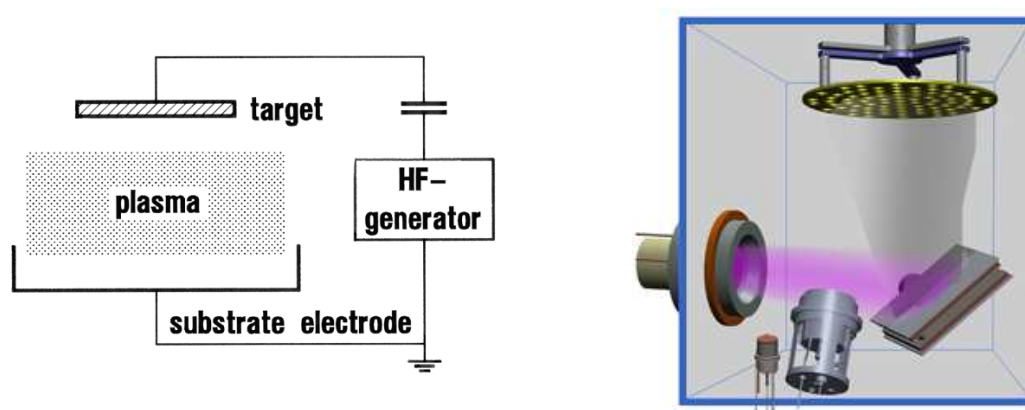


Figure 13. Sputter deposition principles. Plasma loads positively on 'plasma potential', target electrode (to block capacitor) charges up negatively to ion and electron current in balance. Right: IBS illustration<sup>[175]</sup>.

The research done on the deposition processes has provided evidence of the influence of sputtering pressure on photocatalytic activity, band gap and adhesion strength. The samples prepared using this sputtering method consists of the anatase phase and the particle size reduces to nanometer scale. Better photocatalytic activity and stronger adhesion has been found in the experiments carried out at 2 Pa pressure in comparison to ambient pressure. At this pressure the TiO<sub>2</sub> thin films exhibit a decrease in photocatalytic activity and blue shift of absorption edges in the UV region, suggested by some authors to be possibly due to the quantum size effect<sup>[174]</sup>. One example of a PVD process is to use reactive radio frequency magnetron sputtering. Yamagishia et al.<sup>[176]</sup> showed that this deposition process, with a total pressure up to 3 Pa, can be successfully applied to create an anatase polycrystalline structure. Also, the photocatalytic activity in such cases acts proportionately to total pressure during deposition. Dependence has correlation with transport processes of high-energy particles between the target and the substrate. Bombardment of



high-energy particles on the growing film surface can cause poor photocatalytic activity of films deposited at a lower pressure of 1 Pa <sup>[125]</sup>.

The goal of this PVD comparison is to give a concise reference and description of the processes, methods, and equipment essential for the deposition of technologically and multi-functionally titania films. There are two expanded applications, the first of which being a more basic understanding of discharge magnetron sputter materials. The second is the ability to compare it with the PVD- IAD of devices that contain these materials. The differences between the processes benefit the understanding of both physical and chemical reactions; these overlapping processes are sputtering and IAD. The principal parameters are that the layer growth could be fundamentally influenced by the choice of the deposition rate, substrate temperature, and plasma parameters. The impingement of the dense layer coated with extra ion energy conducts to adjust the layer structure in a reproducible broad range. The crystal modification of TiO<sub>2</sub> using an IAD process, in contrast to magnetron sputter, has a high degree of anatase content and thus enable a high photocatalytic activity.

By using pulse magnetron sputtering (PMS) deposition, also involving activated plasma, it is possible to deposit crystalline layers with anatase or rutile phase <sup>[125]</sup>. In comparison with layers containing only rutile phase, better photoinduced super-hydrophilicity is found in TiO<sub>2</sub> layers which have significant amounts of anatase phase. However, there is evidence that PMS or the plasma-activated deposition method does not make much difference to the properties of deposited layers. PMS is also useful for uniformity in layer thickness, without affecting the photocatalytic activity. The PMS method can be used for deposition on polycarbonate and polyethylene terephthalate surfaces as it also works with low-substrate temperature, thus adding to the utility of thin films for a large number of products <sup>[177]</sup>. In the recent past, experiments have been conducted for depositing transparent TiO<sub>2</sub> layers with the help of pulsed laser deposition using a metallic Ti target and ambient O<sub>2</sub> gas at 400 °C <sup>[178]</sup>. The results of these experiments have shown that pressure of O<sub>2</sub> as an oxidizing agent affects optical and photocatalytic properties of thin films; with 15 Pa pressure of O<sub>2</sub>, it is possible to have TiO<sub>2</sub> film with good optical transmittance of 200 to 800 nm wavelength.

The as-deposited film structure of TiO<sub>2</sub> films prepared using another form of sputtering, radio-frequency magnetron sputtering, shows crystalline anatase-type TiO<sub>2</sub>. In such cases the O-H bond of the surface increases proportionally with the Ar ion-beam irradiation time. Due to oxygen vacancies, the photo-induced hydrophilicity of Ar ion-beam treated TiO<sub>2</sub> films is enhanced. Studies conducted in this area show that Ar ion-beam irradiation improves photo-induced hydrophilicity under weak UV-illumination (e.g. indoors) <sup>[179]</sup>. The refractive index improves if TiO<sub>2</sub> is deposited with ion assistance, thereby employing oxygen ions in energy range of 100-

500 eV and current densities of  $100 \text{ pA.cm}^{-2}$ . Other enhanced characteristics include the refractive index and the extinction coefficient. The optical band gap is also strictly dependent on the energy of the used ions. The refractive index of thin films slightly increases when thin films are annealed after deposition at  $500 \text{ }^\circ\text{C}$ , without having any impact on extinction coefficient. Such films also exhibit a monophasic anatase structure<sup>[180]</sup>. This optical and microstructural limitation is considered to be a disadvantage of magnetron sputtering, so a comparison with IAD is significant throughout this thesis.

Conforming to these studies, there is an obvious improvement in the optical and photocatalytic properties of thin films generated with ion-source, which has been studied in this thesis. Hence, there is a potential for further enhancement and a need for the determination of the impact of an ion-source on a surface morphology and microstructure. With the aim of clarifying this impact, the ejection of surface atoms from an electrode surface by momentum transfer from bombarding ions to surface atoms was studied. Sputtering is clearly an etching procedure and is therefore used for surface cleaning and pattern delineation. This method is also used for film deposition that is akin to evaporative deposition due to its production of a vapor of electrode material.

The increase of the refractive index  $n$  with rising oxygen current density demonstrates that ion-bombardment during deposition changes the growth of film columnar microstructure, which then results in film densification; however, the porosity of the microstructure of the film greatly limits the environmental stability of optical coatings.

Due to the impact on the electrical and thermo-mechanical properties of the film, it is clearly vital to largely understand its microstructure. To reproduce the microstructure of the layer, it is important to first take into account the mechanisms causing this development. Once the film has gained enough surface mobility and is allowed to continue to grow, the constituent of the film endeavor to reduce their free energy. One way to achieve this reduction is a decline in the curvature of the titania surface. The instability determined by geometry is one way in which the mechanism can influence the film microstructure. This effect is described in detail in subsequent chapters.

### **2.2.3 Physical Vapor Deposition with IAD**

In general, there are two measures that are the most common for the application of the ion-source to the coating of the thin film. One of these measures, IBS, is directing ions at a sputtered target from the source, and the sputtered material is coated as a thin film. The second measure, IAD, directs ions from the source at the coated substrate.

The word ‘assisted’ in Ion Assisted Deposition refers to the coating plant and not to the reactive gas, hence the reason that IBS does not use this word even though it operates with Argon as a reactive gas. Providing the thin film adatoms on the substrate with increased energy, and thus mobility, before nucleation is the aim of both of these procedures, which will then cause the above mentioned modifications in film’s properties to follow. The concurrent use of two or more ion-sources can provide both IBS and IAD.

As compared with the above mentioned PVD and conventional deposition methods, the use of ion assisted electron-beam evaporation has proven to be very helpful in deposition of  $\text{TiO}_2$  thin films of functional properties, most importantly, the optical coating quality<sup>[181]</sup>. It is the uniformity, density and texture of the thin films that determine their optical performance<sup>[4, 41]</sup>. A good starting approximation of the refractive index profile is calculable with deposition rates recorded with a quartz crystal monitor during deposition for layers. Basically, the refractive index profile is the distribution of refractive indices of materials within an optical fiber. In research conducted in 2006, an in-situ broadband monitor system was developed and integrated into a Leybold SYRUS machine (Figure 14), which could monitor different layer systems, namely classical multilayer designs (e.g. filter), composite layers (e.g. mixture layers for rugate-filters) and metal island layers<sup>[182]</sup>.

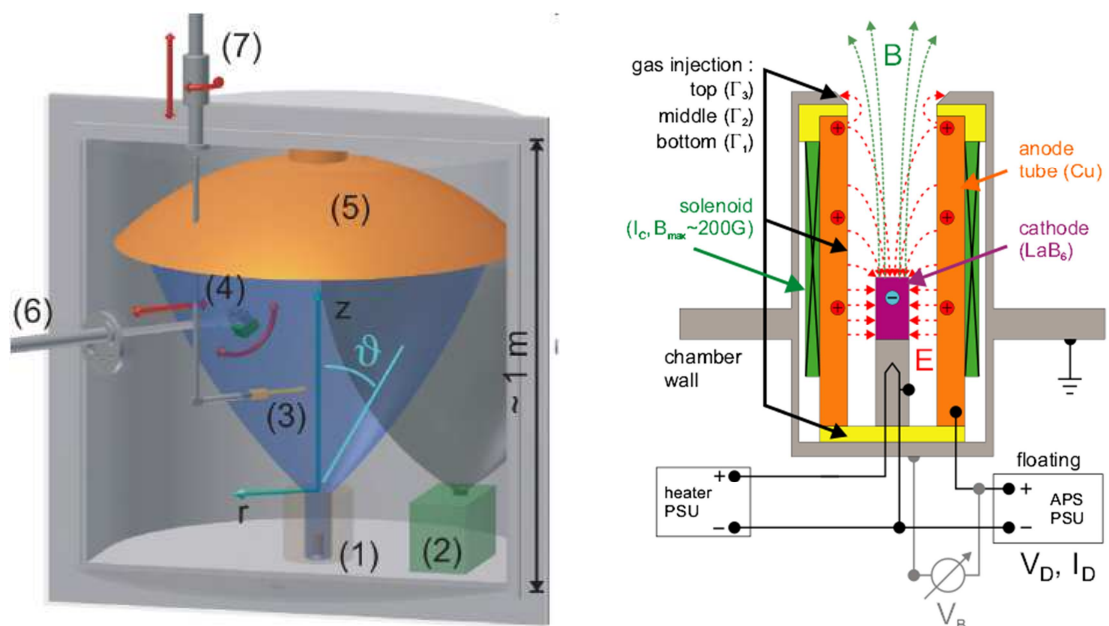


Figure 14. Assembly of the APS. Left: IAD chamber with different systems: (1) APS, (2) electron beam evaporator, (3) Langmuir probe (LP), (4) retarding field energy analyzer (REFA). LP and REFA are placed to cover wide ranges in the horizontal and vertical directions. (5) Substrate holder, (6) horizontal manipulator, (7) vertical manipulator. Right: The cylindrical dc-glow discharge with an auxiliary axial magnetic field. A solenoid is coiled up around the anode. Gas flow rates at different locations ( $\Gamma_1$ ,  $\Gamma_2$ , and  $\Gamma_3$ ).  $I_D$ : discharge current and  $V_D$ : discharge voltage<sup>[183]</sup>.

The definition of Snell's law is the relationship between the angles of incidence and refraction, when referring to light or other waves transiting through a boundary between two different isotropic media, for example, water and glass. Refraction of light at the interface between two media of different refractive indices, with  $n_2 > n_1$  is shown in Figure 15, left. As the velocity is lower in the second medium ( $v_2 < v_1$ ), the angle of refraction  $\theta_2$  is less than the angle of incidence  $\theta_1$ ; this is to say that the ray in the higher-index medium is closer to the normal.

$$\frac{\sin \theta_1}{\sin \theta_2} = \frac{v_1}{v_2} = \frac{n_2}{n_1} \quad \text{Equation 5}$$

with each  $\theta$  as the angle measured from the normal of the boundary,  $v$  as the velocity of light in the respective medium and  $n$  as the refractive index of the respective medium.

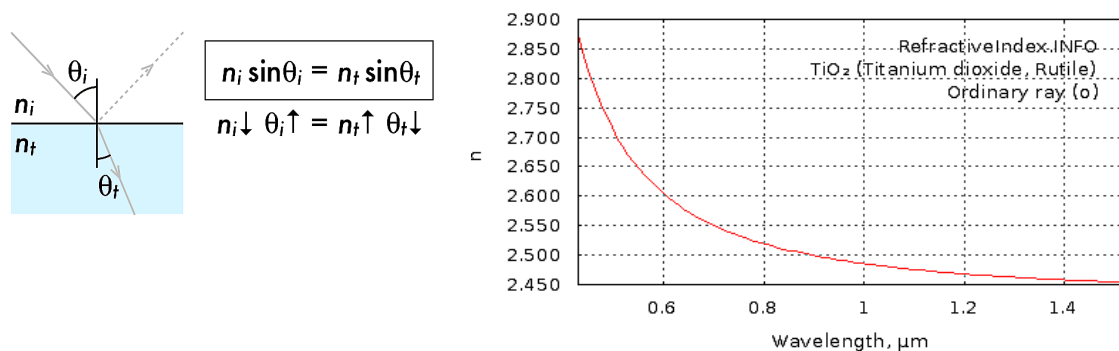


Figure 15. Basic Law of refraction and dispersion curve of titania. Left: Snell's law of refraction<sup>[184]</sup>. Right: Example of a dispersion curve of TiO<sub>2</sub> Rutile<sup>[185]</sup>.

Figure 15 (right) shows the frequency dependence on the wavenumber for dispersive waves. This is usually created by first using a dispersion relation to obtain frequency/wavenumbers pairs and then plotting them. Particularly convenient for the advancement of the refractive index in the wavelength range from the UV through the visible to the IR area (to 2.3  $\mu\text{m}$ ) is the classical dispersion theory derived Sellmeier Equation (Equation 6), which permits the description of this refractive index advancement over the total transmission region with one set of data and also allows for the calculation of precise intermediate values.

The Sellmeier formula is an empirical relationship between the refractive index and the wavelength for a transparent instrument, and is used to establish the dispersion of light in this medium. This is defined by the following equation:

$$n^2(\lambda) = 1 + \frac{B_1 \cdot \lambda^2}{\lambda^2 - C_1} + \frac{B_2 \cdot \lambda^2}{\lambda^2 - C_2} \quad \text{Equation 6}$$

where  $n$  is the refractive index,  $\lambda$  is the wavelength, and  $B$  and  $C$  are experimentally determined *Sellmeier coefficients*.

The degree of the opacity of a substance layer to light rays is termed Optical Density <sup>[186]</sup>. Layer absorbance is the substance layer's capability to absorb radiation that is mathematically expressed as the negative common logarithm of transmittance. Wavelength and temperature can be used to alter the refractive indices of the glasses, with the temperature coefficient of refractive index being the term for the relationship of the refractive index variation to temperature change <sup>[35, 38]</sup>.

#### (a) Influence of IAD on the Structure and Optical Quality

Yang (2007) concluded that an increased deposition temperature enhances the structure and optical properties of thin films. To be precise, if the deposition process is carried out at 300 °C followed by annealing at 450 °C, the films show a refractive index of 2.29 at 550 nm wavelength. In some research, higher transparency was obtained at a deposition temperature of 300 °C, with an allowed band gap of 3.81-3.92 eV <sup>[52]</sup>. Research conducted using cathode vacuum arc ion plating with ion-beam assistance shows that TiO<sub>2</sub> films deposited using this method displayed a phase transition from amorphous to anatase polycrystalline structure with a (101) preferential orientation at the annealing temperature of 500 °C for 1 hour under a normal environment. Experiments have shown a shift in absorption edges of thin films from 325 nm to 340 nm as the ion-beam current was reduced to half, i.e. to 160 mA. The introduction of ion-beam also improves the photocatalytic activity of films significantly, especially under irradiation with visible light <sup>[187]</sup>. It has been found from other analytical results of IAD prepared thin films that a decrease in working pressure and substrate temperature results in an increase in the refractive index of the films. An increase in the annealing temperature proportionally increases the surface roughness, and a decrease in annealing temperature helps to increase the refractive index <sup>[188-190]</sup>.

#### (b) Ability of IAD to be combined with Argon

Another way of depositing TiO<sub>2</sub> thin films is through Ar<sup>+</sup>-IAD method. With the help of this method, thin films of uniform cross-sectional structures can be deposited if the ion-current densities are maintained between 0 and 5  $\mu\text{A}\cdot\text{cm}^{-2}$ , regardless of the surface type. If the process is carried out at higher temperatures, it causes roughness on the surface. Without the use of ion bombardment, the films obtained exhibit an amorphous structure <sup>[191]</sup>.

### (c) Ability of IAD to Use Carbon and Noble Elements for Doping

Carbon can also be used for doping of  $\text{TiO}_2$ . The results of experiments done with CO and  $\text{CO}_2$  in ion assisted electron-beam evaporation show that carbon enhances the photocatalytic properties of thin films. Using this method, the films are also annealed at 500 °C for 8 hours to increase titania crystallinity. Thus, in terms of photocatalytic activity, super-hydrophilicity, degradation of methylene blue and reduction of silver ions, a shift in the absorption in the spectrum of visible range was obtained with annealed carbon doped  $\text{TiO}_2$  anatase film that was doped with carbon content of 1.25 wt% <sup>[192]</sup>.

Noble metals such as gold, silver, platinum and iridium have also been tested for doping with  $\text{TiO}_2$  with an improvement in the charge separation in terms of photocatalytic efficiency in both UV and visible light. Better photocatalytic degradation, both under UV and visible light, and in comparison with simple  $\text{TiO}_2$  thin films an increase in efficiencies of MO photo-degradation from 2.43 to 4.1 times, can be achieved when Pt/ $\text{TiO}_2$  films were dipped in 0.01 and 0.001M  $\text{H}_2\text{PtCl}_6$  solution <sup>[193]</sup>. Noble metals can be used, in nanoparticles, in deposition of  $\text{TiO}_2$  films with the help of electron-beam irradiation. Their impact on the photocatalytic activity of thin films largely depends on the solution used <sup>[194]</sup>. Additionally, the introduction of nitrogen introduced new occupied orbitals in between the valence band, that are comprised primarily of O-2p orbitals, and conduction band which are comprised primarily of Ti-3d orbitals (Figure 16).

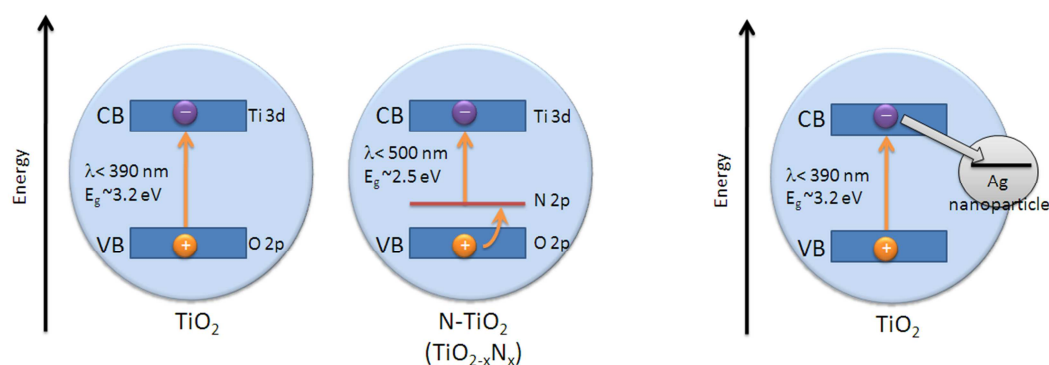


Figure 16. Left: N-doping as explained by Asahi <sup>[195]</sup>. Doping with nitrogen results in a mid-band gap energy level which reduces the energy gap required for charge separation. Right: Incorporation of silver nanoparticles facilitates longer charge separation by trapping photogenerated electrons <sup>[196, 197]</sup>.

### (d) Ability of IAD to Coat Using Different Substrates

Experiments conducted using IAD on porous Teflon sheets (PTS) show that  $\text{TiO}_2/\text{PTS}$  can be a good choice for waterproof materials because of its water repellent and self-cleaning properties.

Water-repellent properties induced by PTS and the self-cleaning properties induced by TiO<sub>2</sub> photocatalyst were observed during these experiments <sup>[188]</sup>.

Apart from plain glass or plastic, experiments have been conducted on Si (100) for deposition of thin films. For Si (100), substrate deposition is carried out with O<sub>2</sub> cluster ion-beam assistance. Substrate temperature of 200 °C produces amorphous films, whereas temperature of 300 °C produces films which contain both rutile and anatase. The refractive index of films and photocatalytic decomposition of methylene blue by UV-irradiation increases with an increase in substrate temperature. The contact angle of substrates to water decreases to 10 by UV-irradiation for 30 min, however, in case of TiO<sub>2</sub> bulk in rutile structure it remains at the initial value of 75 degrees. At atomic level the surface of films remains smooth. The experiments show higher photocatalytic characteristics in anatase <sup>[198]</sup>.

As a summary, the Ion-Beam Sputtering (IBS) process, which is considered the most competitive method to IAD, requires that an existing system be altered to its specific use, or an altogether new system may be needed, both of which constitute much more of an investment in resources. The IAD process is also advantageous because of its scalability, easily creating large and small surfaces, and especially beneficial owing to its ability to adjust deposition parameters in just the one method, thus making the properties of the films highly controllable. The IBS procedure does not have the scale range of IAD as it has a limited supply in sizes of ion-sources. While there are many technical benefits to IAD techniques, there are also economic advantages.

A good way of creating oxidizing species, which in turn cause higher surface energy, on polymer is by chemical treatment using strong oxidizing agents. A high hydrophilicity of the treated substrates allows deposition of uniform layer on them. The treatment does not cause any further roughness on the polymer surface. The layers remain uniform and adherent if dip coating method is used. The TiO<sub>2</sub> nanoparticles on the films can be stabilized electrostatically, even in the absence of a surfactant. The photocatalytic efficiency of layers depends on thickness of layers because it provides more active surface area. The coating also improves mechanical properties of thin films, increases hardness of substrate by 2.5 times and improves its scratch resistance by 6.4 times <sup>[199]</sup>.

Other authors found that TiO<sub>2</sub>, when used on 300 nm pyrex glass tube, showed signs of fracture due to different thermal coefficients of over-layer and the substrate during calcination. Other factors are contraction and stress during drying. The films also show highly porous surface morphology of anatase particles. TiO<sub>2</sub> immobilized pyrex glass tube can be used as a photocatalytic reactor which, from the point of view of practical use, can avoid filtration of suspended TiO<sub>2</sub> powder <sup>[6]</sup>.

Dissimilar to these past studies, the influence of ion-source current in IAD has not been well analyzed in the literature and has been used in this thesis to understand the ability to coat substrates other than glass, with an enhanced PVD procedure.

#### **2.2.4 Crystallinity of Thin Films by Different Coating Methods**

Before presenting the crystallinity of the titania prepared using IAD, an overview of the influence of the deposition methods on the microstructure, such as magnetron sputtering and atomic layer deposition, is presented here.

##### **(a) TiO<sub>2</sub> Deposited by Magnetron Sputtering**

There are many publications that describe magnetron sputtering; below are only two selective examples of this technology so as to compare against the IAD procedure. In experiments done using reactive pulse magnetron sputtering on float glass, no significant photocatalytic activity was observed for 100 nm thick TiO<sub>2</sub> layers at low total pressures. Possible reasons for this could be the smooth surface and nanocrystalline microstructure, as well as the crystallographic orientation, which has the ability to affect adsorption<sup>[200]</sup>.

The deposition parameters of the DC sputtering process determine the structural characteristics of films in the anatase and rutile phases. Films deposited at 16 mTorr contain more intrinsic and structural defects which could be the main cause of the higher photocatalytic activity in the photodegradation of organic molecules. The band gap energy changes on different substrates, such as glass and FTO, and could increase with an increase in pressure<sup>[80]</sup>.

The application of direct current pulse magnetron sputtering system at room temperature can be helpful in deposition of highly photocatalytically active TiO<sub>2</sub> thin films. Deposition parameters have pivotal importance in this process as they affect the target yield and kinetic energy of Ti particles. If the working pressure is increased, up to 1.4 Pa, it transforms the structure from amorphous to anatase phase and the resulting annealed thin films can have excellent photocatalytic efficiency<sup>[201]</sup>.

Much research has established that the deposition temperature range of 500-600 °C leads to growth with a particle size average of 50 nm, while a temperature range of 750 to 800 °C causes the films to grow along (211) the crystallinity orientation. The films with a random anatase structure exhibit higher photo-degradation efficiency and lower band gap energy as compared with (211) oriented growth structure<sup>[131]</sup>. In order to optimize the processing parameters, tests have been conducted to evaluate the effect of sputtering power on photocatalytic activity of deposited TiO<sub>2</sub> thin films. The method is regarded as very effective due to the as-deposited films prepared with sputtering power of 200 W exhibiting a crystalline structure of anatase phase.



When the sputtering power is changed, it in turn changes the crystallinity and surface morphology; the films prepared with these parameters show the highest photocatalytic efficiency<sup>[199]</sup>. Concurrent to these studies, the influence of ion-source current in IAD has been analyzed in this thesis to understand the modification of crystallinity and surface morphology.

### **(b) TiO<sub>2</sub> Deposited with IAD**

In the IAD process, 300 °C is taken as the transition temperature for the transformation from amorphous to anatase phase during annealing, and 500 °C from amorphous and anatase to rutile phase. This increase in the annealing temperature also increases the refractive index, transmittance percentage and the band gap energy. The highest transparency level can be secured at an annealing temperature of 400 °C, and the highest refractive index, that of 2.62, and the band gap energy, 3.26 eV, can be achieved at 500 °C with the anatase phase. The thin films start developing defects if they are annealed at 700 °C to form rutile phase<sup>[202]</sup>. The aim of using IAD is the possibility of obtaining titania films with refractive index higher than 2.40 (550 nm) at a deposition temperature lower than 350 °C. This is challenged in Chapter 5 to 8.

### **(c) TiO<sub>2</sub> Crystallinity on Different Substrates**

The choice of the substrate materials is another issue that needs to be considered as it must be well-suited to the deposition conditions in order to stay inert and undamaged during the deposition process. It is also important for the substrate to be resistant to the crystallization temperature of the thin film and not cause contamination<sup>[91, 203]</sup>. A notable example of this are polymer substrates such as Poly(methyl methacrylate) (PMMA) and Polycarbonates (PC), as they have a relatively low temperature resistance (typically 150 °C) and are made inadequate due to the out-gassing of, for example, water. Avoiding contamination of the TiO<sub>2</sub> thin film by inward diffusion of Na<sup>+</sup> or other ions, as mentioned in Chapter 6, from the substrate is also necessary<sup>[77, 204]</sup>.

It has been revealed by earlier studies that there is a strong reliance of the photocatalytic activities of annealed TiO<sub>2</sub> thin films on the substrate type used<sup>[92]</sup>. The influence of a soda-lime glass substrate on the photocatalytic activity of heat treated TiO<sub>2</sub> films has also been explored by other authors<sup>[92, 205]</sup>.

SiO<sub>2</sub> or TiO<sub>2</sub> buffer layers improve the bending resistance of thin films, but SiO<sub>2</sub> has an improved resistance due to its stronger adhesion ability. Both TiO<sub>2</sub> and SiO<sub>2</sub> improve crystallinity of ITO films and the surface properties of polyethylene terephthalate (PET)<sup>[206]</sup>.

### 2.2.5 Correlation: Deposition method, photoactivity, microstructure, antibacterial ability

Research done on the microstructure of polycrystalline and epitaxial TiO<sub>2</sub> thin films with anatase and rutile structure reveals fine crystallinity and compact structure of films prepared with r.f. magnetron sputtering. Single- and polycrystalline films show 10% higher optical band gap as compared to the bulk, thus is due to the strain of lattice deformation. For single-crystalline and polycrystalline anatase and rutile TiO<sub>2</sub> thin films bactericidal abilities can be evaluated by exterminating *Escherichia coli*, using film stick method under UV. The two kinds of films show similar bactericidal efficiencies.

To provide a correlational study, one of the simple methods for quantitative measurement of photocatalytic activity is the utilization of evaporated layers of stearic acid. Thin films of stearic acid have good homogeneity and can be decomposed on a photocatalytic surface under UV-illumination. Experiments show that an activity of a much higher factor than commercial glass can be obtained with modified PVD technique, i.e. a factor 100 higher than a commercial glass. The highest stearic acid deposition rate proved via experiments is 3 nm/min at 0.66 mW/cm<sup>2</sup> (366 nm) <sup>[207]</sup>. As per the experiments conducted by L. Wanga <sup>[208]</sup>, films with high refractive index ( $n \sim 2.60$  at 1.4  $\mu\text{m}$ ) and low extinction coefficient can be deposited at low substrate temperature i.e. 150 °C, and with some assistance. These films were observed to be homogeneous and insensitive to moisture and, depending on evaporation conditions, different growth morphologies and phase transformation were also found. Crystallinity, and with that the refractive index, can also be improved with substrate temperature of 250 °C. With reference to optical properties, fused silica substrates show discouraging results <sup>[163]</sup>.

## 2.3 Summary

To give a quick general overview of the literature reviewed in this Chapter (2. Basic), it can be summarized as follows.

- ✓ The literature reviewed above shows that the functional properties of thin films, such as photocatalysis, super-hydrophilicity and transparency, make this subject essentially wide-ranging. Due to suitability of TiO<sub>2</sub> thin films for different purposes, they have different applications in different fields.
- ✓ In environmental sciences, TiO<sub>2</sub> can be used with clean, attractive, low-temperature and non-energy intensive methods for removing pollutants from water, and even wastewater. TiO<sub>2</sub> under solar energy is more effective at disinfecting water than solar energy alone. It can also be applied to pavements for reducing air pollution. TiO<sub>2</sub>'s hygienic

characteristics make it a very good choice for depositing thin films on medical equipment. In the optical industry,  $\text{TiO}_2$  is extensively utilized for deposition because its refractive index has a direct correlation with the presence of Ti on thin films. At present, Pilkington Activ™ is the most widely produced commercial photocatalytic glass. Demineralization tests conducted on Pilkington Activ™ show that it has an anatase phase and can demineralize dyes such as methylene blue, which has lately been used in research as a good degradation model for determination of photonic efficiency<sup>[75, 209]</sup>. The basic factors which determine photonic efficiency include photodecomposition parameters, such as light illumination, reactor set-up, reaction time and type, amount of catalyst utilized and concentration of substrates.

- ✓ This chapter focuses on presenting the titania microstructure as it is also helpful for the enhancing the transfer of photo-generated electrons from the anatase phase to the rutile phase for the IAD procedure. A second focus is on how the increase of photoactivity and hydrophilicity can be determined by specific grain size annealed morphology, sufficient surface hydroxyl content and the degree of surface roughness. The optimum of microstructure using PVD-IAD is resulting by high deposition rates, which produce columnar and polycrystalline titania. This can be improved by manipulating the process parameters, low contamination, superior thermal efficiency, and dense coating. Intended for high crystallinity it is remarkable to increase the grain size. This is opposing to the desire to increase the surface area, so that typically a grain size range of about 10-20 nm is considered an optimum compromise between these two issues.
- ✓ Corresponding to the literature studies, the basic mechanisms contributing to the change of the microstructure and surface properties, resulting from the transfer of ion energy, has been taken in consideration. The preparation of transparent photocatalytic active PVD-IAD layers, the mechanism selection of dense molecules for optic characterization, has been focused on. This contribution has been analyzed in this thesis to understand the momentum transfer, if its leads to an increase in the mobility of the adatoms, enabling them on the basis of the energy corresponding.
- ✓ To apply all of the results gathered within the literature, the PVD method with ion-beam sputtering or ion assisted deposition were operated as two parallel classifications. IAD is a commonly employed method for the deposition of thin films with a high degree of precision. It is utilized for fabrication of multi-functional high reflective and anti-reflective layer stacks. On being exposed to UV-A light, thin films show super-hydrophilic behavior. Additionally, the films show the anatase phase and the particle size

reduces to a few nanometers and correlate with each other. The refractive index of thin films slightly increases when thin films are annealed after deposition at 500 °C. For improving the control of the deposition process, in 2006 an in-situ broadband monitor system (BBM) was developed and integrated into the Leybold Optic SYRUS machine. At low total pressures, thin TiO<sub>2</sub> layers do not show significant photocatalytic activity. Band gap energy varies on different substrates, such as glass and can increase with an increase in pressure. In case of single-crystalline, polycrystalline anatase and rutile TiO<sub>2</sub> thin films, bactericidal abilities can be evaluated by exterminating *Escherichia coli* using film stick method under UV-illumination. PVD gives optical qualities to thin films such as good starting approximation of the refractive index profile which is calculable with deposition rates. By decreasing the working pressure and increasing the deposition rate and substrate temperature, the refractive index of films can be increased. Higher transparency in thin films can be obtained if the deposition temperature is increased from 50 to 300 °C. If the thin films are annealed at 700 °C for the rutile phase, they start developing defects and deformities. Films produced with IAD are homogeneous and also insensitive to moisture, depending on evaporation conditions. Also, such films exhibit different growth morphologies and phase transformations.

This chapter discusses relevant information regarding TiO<sub>2</sub> thin film deposition for photocatalytic applications, and also uses a comparative study of the PVD deposition methods to summarize the current knowledge of photocatalytic performances. As most studies on transparent PVD thin films do not thoroughly discuss the effect that microstructure has on photocatalytic activity, a comparative microstructure analysis using various deposition methods was conducted. During this review it was seen that previous research in this field has found that the microstructure of the thin films can enlarge the surface area and that maintaining a small grain size is important in determining the inward diffusion of the organic substance and outward diffusion of reaction products.

Unfortunately, a difficulty arose in the comparison of the published values using different measurement setups as there is established no standard procedure or reference sample for the evaluation of TiO<sub>2</sub> thin films' photocatalytic activity. It is the main author's impression that this issue is an important one for the future. For this research, an automated measurement system was developed for PVD photocatalytic activity. In addition, the aforementioned optical properties are used as a reference to qualify the IAD optic samples produced by Denton CC-105. Addressing the gaps of understanding identified in the literature is one of the objectives of this thesis.

### 3. Experimental Set-Up

The following chapter contains a description of the techniques and equipment used in the research of deposition of thin films. The deposited films were characterized for their photoactivity, hydrophilicity, optical quality coating and microstructure, and before starting the deposition process, specific coating materials and pretreatment processes were first chosen. The process was carried out with and without ion-source assistance, and also with varied gas flow, temperature, thickness, and annealing methods. The optical quality of the films, especially transmission, reflection, scattering and band gap, was established, and for the surface analysis, the following commonly known techniques were employed: scanning electron microscopy (SEM), atomic force microscopy (AFM), tunnel electron microscopy (TEM), X-ray diffraction (XRD), elemental analysis (EDX), water droplet measurement and Raman spectroscopy. Lastly, the deposited films were tested for anti-bacterial properties with the application of negative bacterium, such as *Sarcinia lutea*.

#### 3.1 Synthesis of Thin Film Layers

##### 3.1.1 Materials and Methods

###### (a) Coating Materials

Different commercially available coating materials were tested for this research, including TiO<sub>2</sub>, SiO<sub>2</sub>, Ag, and Au. TiO<sub>2</sub> was obtained from Merck KGaA, SiO<sub>2</sub> from COTEC GmbH, and Ag, and Au from Evonik Degussa GmbH. All the materials were used in the form in which they were originally received.

###### (b) Selection of Substrates

Different types of glass substrates were used in the research, such as Borosilicate glass, D263 (Menzel) glass, and Quartz glass SUPRASIL<sup>®</sup> 2 (Suprasil), which is a high purity synthetic fused silica grade, manufactured by Heraeus using flame hydrolysis. Borosilicate glass, with very low iron content, is utilized as the cover glass in microscopy for biological, medical and optical research work, and has refractive indices of 1.456 at 656.3 nm, 1.458 at 587.6 nm, 1.466 at 435.8 nm, and 1.508 at 248 nm, respectively. Borosilicate glass is without absorption in the visible range of the spectrum, but the excellent optics properties make this glass an ideal material for experiments in fluorescence microscopy. High purity quartz glasses are utilized for UV and deep UV applications with superior quality in this range. Suprasil presents the highest purity and has a high content of OH<sup>-</sup> groups of around 400 ppm. Isopropanol and acetone were applied to

clean these glasses and plasma-jet etching techniques were used to create suitable preconditions for production of layers.

### **3.1.2 Pretreatment Procedures**

Before the coating process, special focus was given to suitable techniques which may be employed for chemical processes or lacquer finish of the substrates. Pre-treatment process of films is done by manual chemical pre-conditioning, automated processing and plasma etching. Manual processing involves use of acetone, isopropanol, or both. Automated cleaning involves the treatment of substrate in 3 stages. In the actual experiment, first the substrate was dipped in ultrasonic distilled water, and then in Alkali metal salts, produced by Cleaning Technology SA, Switzerland. Next, the substrate was dipped in a solution of Deconex liquids, containing 150 ml D12PA, 37.5 ml D12PA and 112.5 ml of HT19, produced by Borer Chemie AG, and then finally, in distilled water. Drying was carried out at 80 °C, and pre-conditioning was accomplished using plasma-jet etching methods in the materials, which can improve the adhesive strength of the layers. In this plasma-jet etching process, the surface is bombarded by the Denton CC-105 ion-source and during the process, which lasted for approximately 10 minutes, the ion-source current was maintained between 1 A and 5 A and the voltage was kept within the range of 200 to 250 V (more details in Info Appendix 1).

### **3.1.3 Thermal Evaporation PVD**

For the process of thermal evaporation, conventional methods for physical vapor deposition (PVD) were applied in the experiments. For this purpose, a high vacuum evaporation plant BAK 760 was used. The standard diffusion pump used in BAK 760 has high stability, even in ultra-high vacuum (UHV), with no pressure fluctuations <sup>[163]</sup>.

### **3.1.4 Ion Assisted Deposition**

Other than conventional thermal evaporation methods, which provide particles in the gas phase with low kinetic energy, the ion assisted deposition (IAD) process was used in the experiments. In accordance with high kinetic energy, ion assisted coating processes usually lead to a substantially increased optical and mechanical quality of the films, yet ion assisted deposition enables improved microstructure with significant product advantages <sup>[98, 99, 210]</sup>. Along with IAD methods, conventional PVD methods were also studied with deposited TiO<sub>2</sub> thin films. For these coating processes, Balzers BAK 760 plant, mentioned above, and a SYRUSpro 1100 machine were used. The Denton CC-105 was the ion-source used in the Balzers equipment. SYRUSpro 1100 was operated with the ion-source Advanced Plasma Source Professional (APSprö). SYRUSpro 1100 and APSPro can only be employed in a complete installation system.

The above coating plants were equipped with e-beam evaporators, a diffusion pump for BAK 760, a Cryo pump for SYRUSpro 1100 machine, and online UV/Vis spectrometers which record the spectra of the growing layers <sup>[211]</sup>. Many deposition processes were tried during the course of this research, the first process being a conventional thermal deposition concept which involves the use of oxygen as the reactive gas. This was carried out using BAK 760 without an ion-source. The second deposition process was based on the APSpro plasma source used in the SYRUSpro 1100, and in this process, argon and oxygen were used as reactive gases. In the final process, BAK 760 was again used, but this time with Denton CC-105 as the ion-source and oxygen as the reactive gas. The ion-source Denton CC-105 was specifically used only in the third process to determine the impact of ion-source on coatings.

The two coating plants used for deposition, the SYRUSpro 1100 and Balzers BAK 760, mentioned above, are shown in the pictures of Figure 17. Balzers BAK 760 which was frequently used during the course of this research, with a 10 KW electron-beam set using CC-105 source with crucible drive, shutter, high voltage, E-gun controller and filament supply.



Figure 17. Thermal e-beam coating plants. Left: SYRUSpro 1100 with Advanced Plasma Source. Right: Balzers BAK 760 with Denton CC-105.

Denton CC-105 is equipped with typical cathode-anode device apparatus, and a tungsten filament which works as a neutralizer. The ion-source was operated with pure oxygen at different discharge current ranges, with typical discharge currents ranged between 1 and 5 A, and the discharge voltage regulated between 150 V and 300 V by varying the oxygen flow with values between 10 to 50 standard cubic centimeters. The Denton ion-source can be used to generate ions

with energy values of up to 300 eV and can also replace the conventional low energy glow discharge system employed in order to clean substrates prior to coating. The value of the neutralizer voltage was maintained in the area of 10 V, which resulted in filament currents between 25 and 30 A. For SYRUSpro 1100, used in conjunction with the plasma source APSpro, the following deposition parameters were altered: The substrate temperature was varied between cold and 300 °C, the voltage between 60 and 160 V, the reactive gas flow for oxygen between 30 and 50 sccm, the flow for argon between 2 and 10 sccm, and finally, the coating thickness between 200 and 1000 nm <sup>[123]</sup>.

To determine the influences of the selected parameters, tests were conducted on the energy spectrum of the ions emitted by the source. Appropriate cleaning procedures, including UV-irradiation cleaning, mechanical ultrasound and manual cleaning, were applied to the substrates before starting the deposition processes, and different substrates were heated at different temperatures, between cold (50 to 60 °C) and 350 °C, prior to deposition. The geometrical arrangement, the distance between the ion-source and the substrates, was in the range of 30 cm to 70 cm, with deposition rates between 0.15 nm/s for TiO<sub>2</sub> and 0.35 nm/s for SiO<sub>2</sub>, respectively. Thin films with a thickness between 50 nm and 1000 nm were produced on quartz and glass substrates.

There are certain other parameters which can have an impact on TiO<sub>2</sub> films. In the conducted experiments, glass substrate was subjected to a pretreatment process, explained above, and after, the thickness of TiO<sub>2</sub> films was measured during the deposition process using a quartz crystal monitor named XTC Thin Film Deposition Controller, manufactured by INFICON (see. 3.1.5). The following diagrams show the important parts of the experiment apparatus.

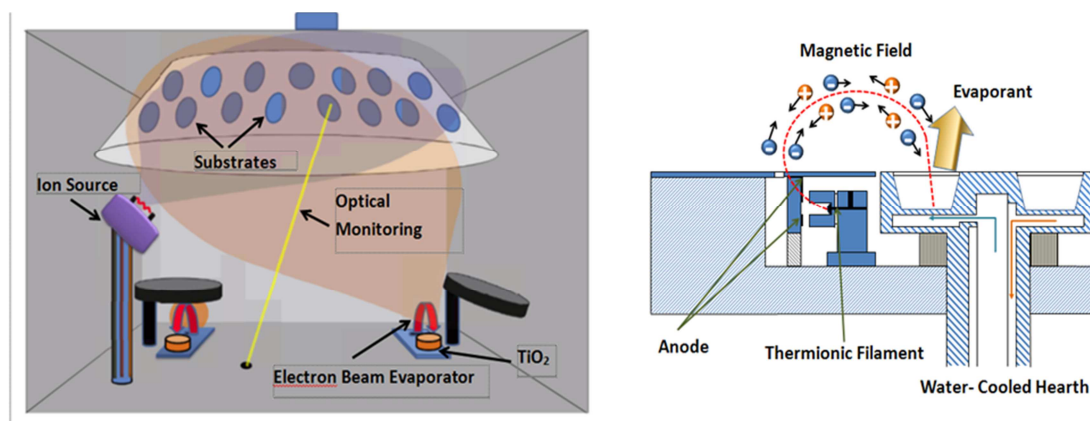


Figure 18. Evaporation coating system. Left: Balzers vacuum chamber. Right: Electron-beam evaporation bloc <sup>[212]</sup>.



The optical substrate of this process is situated in a rotated support, and the shutter controls evaporation of titanium in the vacuum chamber as illustrated in Figure 18 (left). Electron-beam evaporation is shown in Figure 18(right), and the Denton CC-105 ion-source parameters are listed in Table 2.

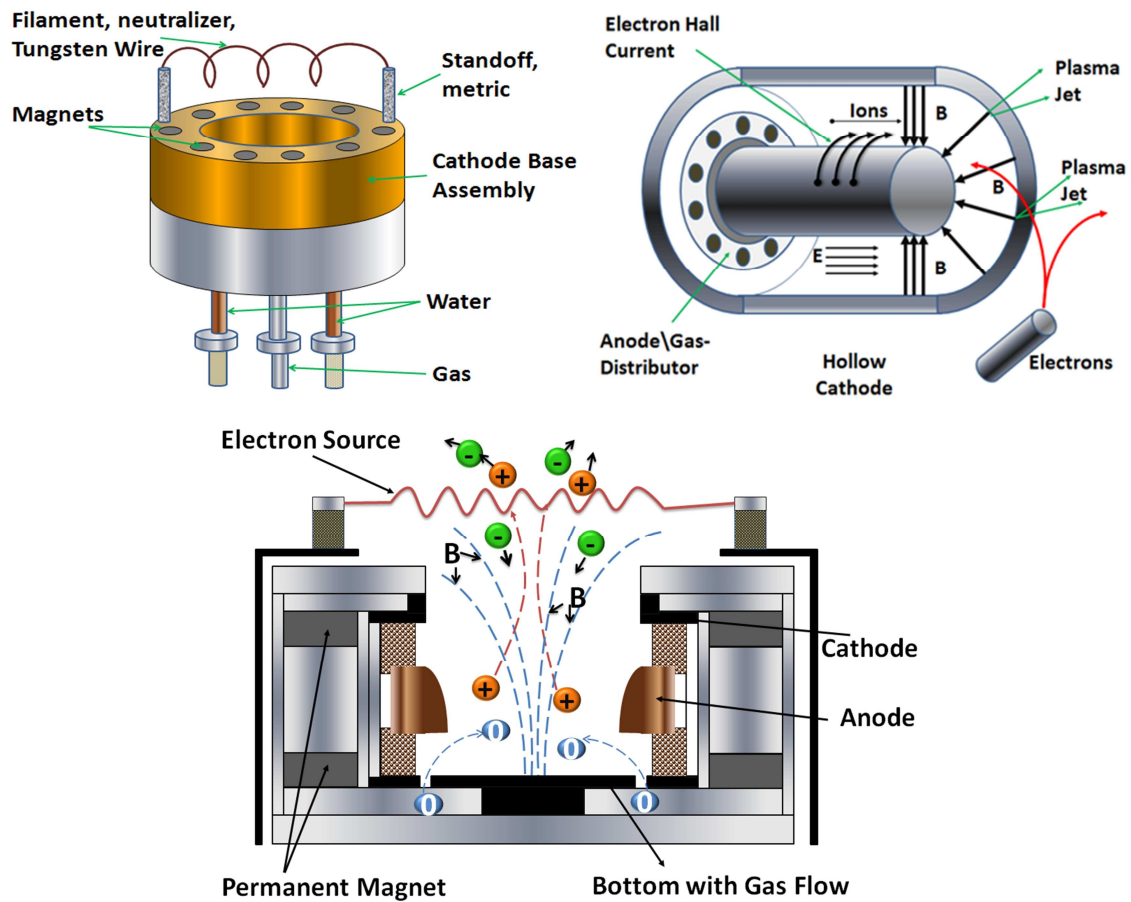


Figure 19. Principal parts of the ion-source. Left top: Tungsten filament, magnets, and gas and water cooling systems. Right top: Magnet field in the plasma jet, hollow cathode with electron hall current and anode/gas-distributor. Bottom: Acceleration of ions towards the substrate holder in the magnetic field <sup>[213]</sup>.

Both the vacuum chamber and the Denton CC-105 ion-source are shown in Figure 19. The Denton CC-105 ion-source was originally named End- Hall. It is a cylindrical source with an anode at its base for the gas supply, and it internally emits electrically heated electrons while maintaining discharge levels between its cathode and anode. The combination of the electric and magnetic fields in the ion-source produce an accelerated flow of ions in the form of plasma jet <sup>[161, 214]</sup>. In the ion assisted deposition processes, the End- Hall ion-source is filled with highly purified, oxygen or argon gas, over 99 % pure. The plasma source consists of an oxygen flow as a reactive gas, added through a ring placed at the top of the anode tube.

During the coating processes, different sets of parameters were used as follows: the materials used for thermal evaporation included titanium, silicon, silver, and aluminium, and for the coating plant, voltage was kept at 8 kV and the current at 0.4 A. The pressure of the oxygen in the vacuum chamber during the processes was kept at  $3 \times 10^{-4}$  mbar constantly, the heating was maintained between 50 and 350 °C, and for the neutralizer setup, the voltage was at 10 V and the current between 27 to 30 amperes (Info Appendix 2).

The above parameters for the coating process have been collected and summarized in the Table 2. All details can be found in Table Appendix 1.

Table 2. Technical data of the coating process from Balzers BAK760 using CC-105.

Plant & Coating Process Properties							
Voltage		8 kV		Current		0.35 A	
Calotte Heater (Process temperature)		Cold - 350 °C		O <sub>2</sub> Valve Control Unit		3 x 10 <sup>-4</sup> mbar	
High Vacuum		0.001 mbar		Coating Thickness		10 - 1500 nm	
Coating Rate	SiO <sub>2</sub>	0.35 nm/s		Plasma Etching	O <sub>2</sub> gas	20 - 40 sccm*	
	TiO <sub>2</sub>	0.15 nm/s			Heater	Cold - 350 °C	
					Time	5 to 30 min	

Ion-Source Properties							
Neutralizer Wire		Tungsten		O <sub>2</sub> Ion- Source Flow		20 - 40 sccm*	
Neutralizer Power	Voltage	9 - 13 V		Ion-Source Process	Discharge Voltage	180 - 280 V	
	Current	22 - 30 A			Discharge Current	1 - 5 A	

\*[1sccm= 0.01646 mbar·l/s].

### 3.1.5 XTC Thin Film Deposition Controller and Broadband Monitoring Platform

The process of deposition was controlled with the help of XTC Thin film Deposition Controller as this device has the ability to accurately control deposition rate and thickness. Advantages of XTC include its capacity to check even the smallest value of thickness, along with the fact that it can process numerous films simultaneously. Its parameters were first defined in order to control the deposition process and the deposition parameters were then entered in XTC, an explanation of which is given below.

To give more detailed information in deposition technique using XTC, the main factor was the Rise Time, which defines the length of the rise. Soak Power represented the start of the melting point of the source material. After the deposit state, it may be necessary to reduce the source's power to zero, a rule of the XTC program stage 'Idle Ramp', which helps maintain the appropriate level of voltage power. The three main information points entered in the deposition parameters were the deposition rate, shutter delay states, and final thickness, and these principle parameter were entered into the Sensor as the 'tooling' factor. This factor corrects for the geometrical differences between the sensor and the substrate because the flow of material from a deposition is not uniform, it is necessary to account for the different amount of material flow onto the sensor compared to the mentioned substrate. It applies to primary crystal and is represented by the following equation:

$$\text{Tooling} = t_{f_{in}} \cdot \left( \frac{t_{f_{sub.}}}{t_{f_{cry.}}} \right) \quad \text{Equation 7}$$

where  $t_{f_{in}}$  = initial tooling factor,  $t_{f_{sub.}}$  = actual thickness at the substrate and  $t_{f_{cry.}}$  = thickness on the crystal (more details in Info Appendix 3).

As an alternative, using the in situ measurement system at the Laser Zentrum Hannover e.V., Broadband monitoring was elaborated, redesigned and implemented, which allowed continuous recording of transmission spectra in the vacuum directly on the coated substrates. The monitoring device can detect the completion of the coating design.

### 3.1.6 Coating Parameters

Different deposition processes have been investigated, and generally, all necessary parameters, as mentioned in the Table 2, were kept within a certain range: for the vacuum chamber; high vacuum between 8 - 10 kV, emission at approximately 0.3 - 0.5 A, O<sub>2</sub> gas at 3 x 10<sup>-4</sup> mbar, temperature from 50 to 350 °C. The temperature values presented a fluctuation of ±10 °C due to the technical set-up. For the ion-source; neutralizer potential ( $U$ ) between 8 and 15 V, neutralizer current ( $I$ ) between 25 and 33 A, ion-source discharge voltage ( $U$ ) between 180 and 280 V, ion-source discharge current ( $I$ ) from 1 to 5 A, flow of oxygen as a reactive gas between 20 and 40 sccm. For the coating process, the deposition rate was held at 0.15 nm/s and the film thickness between 10 to 1000 nm.

The essential parameters were varied within the ranges mentioned in Table 2 in order to study the influence of each of the individual coating factors. The gas flow of ion-source was varied in different processes for analyzing its impact on deposition. The process factors were the potential

( $U$ ) and current ( $I$ ) of electron-beam evaporator, the oxygen ( $O_2$ ) added in vacuum chamber, the substrate temperature ( $T$ ) in the vacuum chamber, the filament neutralizer potential ( $U$ ) and its current ( $I$ ), and the potential ( $U$ ) and current ( $I$ ) of the ion-source itself. In addition to these, the coating rate ( $r$ ) and thickness ( $d$ ) were also kept constant.

There are many reasons that some parameters are constant and others are varied. The operation of the ion-source CC-105 with a neutralizer regulation mode leads to an improved stability over a longer duration. When an ion-source is driven by a discharge current between 1 and 5 V, the discharge voltages range from 185 to 260 V, consequently meaning that maintaining the discharge power supply parameters at a constant is not an absolute guarantee for a constant ion energy distribution<sup>[211]</sup>. The layer properties depend on this ion energy distribution, the reason being that parameters such as discharge voltage, current, gas flow and temperature are varied. In contrast to this, due to the technical reason of the stability duration of the ion-source and its ion energy distribution, other parameters such as coating plant technical data, are mostly fixed according to the evaporation performance, which leads to homogeneous layers and low absorption values for IAD processes.

Expected to APS processes, the oxygen is added with the help of the ion-source through channels where a high gas flow, ranging from 20 to 50 sccm, is used for its ionization. DC voltage is used for this purpose and is applied between the body of the source LaB<sub>6</sub> cathode and the cylindrical ring anode. The ions are propelled towards the substrate with the help of a magnet and their momentum is transferred to the condensing film molecules, which enhances the surface mobility of the substrate and packing density. A tungsten filament, shown in Figure 19, was also used in this process, acting as a neutralizer.

Thin films were deposited using the following six PVD processes:

- Conventional method without any ion-assistance (Process I).
- Ion Beam Sputtering technology (Process II).
- Thermal e-beam evaporation method with SYRUSpro 1100 coating plant using argon and/or oxygen as reactive gas and assisted by Advanced Plasma Source (APS) (Process III).
- Thermal e-beam evaporation method with Denton CC-104 using Balzers BAK 640 (Process IV). The Denton CC-104 differs technically to CC-105 in diameter, ion discharge current and voltage.
- Thermal e-beam evaporation with Denton CC-105 using Balzers BAK 760 (Process V).
- Optimized Thermal e-beam evaporation method with Denton CC-105 using Balzers BAK 760 at high temperature coupled with annealing (Process VI).

In some cases, the deposited films were annealed with temperature, rate, and time all used as variable factors. The temperature was varied in the range of 200 to 550 °C, and the films were analyzed first after 4 hours, and later after 24 hours. The first group of films was annealed at 450 °C for 4 hours and then re-annealed at 400 °C for 7.5 hours. The second group of samples was annealed at a lower temperature of 250 °C for 8 hours. The aim of this procedure was to observe the influence of different conditions of annealing in the structure, optical properties and photocatalytic performance of the TiO<sub>2</sub> films.

## 3.2 Optical Quality of Thin Film Layers

### 3.2.1 Fast Scattering Tests

To evaluate the optical quality of titania thin films, optical scatter measurements are an important factor in all production steps. One specific method of optical scattering is the Total Scattering (TS) method, which evaluates the roughness of the layer. Another specialized method invented at LZH is Fast TS<sup>[215]</sup>, which controls the defects on the sample surface and imperfections in the bulk of the components.

These procedures are based on a two-dimensional TS mapping for routine characterizations of optical samples. Forward and backward TS scans can be performed in a few minutes, making them highly efficient. The beam radius can be adjusted from 35 to 750 μm. Micron particle produced by electron beam lithography are investigated. The lateral resolution to distinguish between two neighbor scatter centers is less than 50 microns. Integration of the scattering in a defined angle range, from 2 to 85°, in the forward or backward path is obtained through TS measurements (Figure 20). A sign as to the quality of the illuminated region can be gathered from the TS value, which can also be used to qualify roughness<sup>[215]</sup>.

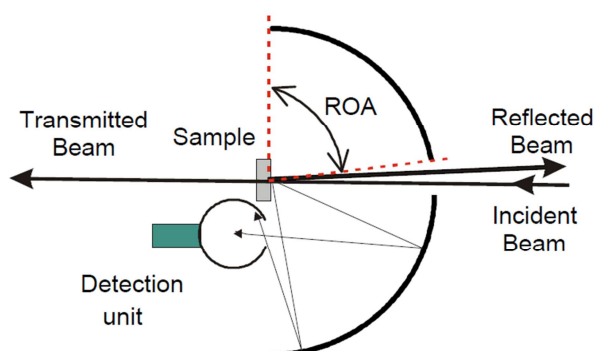


Figure 20 Total backscattering measurement using a Coblenz hemisphere in accordance with ISO/DIS 13696. 'Range of acceptance angle' is depicted by ROA.

### **3.2.2 Absorbance and Transmission Measurements**

To measure the layer transmission spectrum, LAMBDA 1050 and 950 Spectrophotometers, manufactured by PerkinElmer, were used for the analysis of the coated thin films characteristics. With these spectrophotometers, the performance of UV/Vis/NIR was obtained for wavelengths between 175 nm and 2000 nm. The most important parts of these spectrometers are Deuterium and Tungsten Halogen Light Sources, Double Holographic Grating Monochromators, Common Beam Mask, Common Beam Depolarizer, Chopper and Sample and Reference Beam Attenuators<sup>[216]</sup>. The measured spectra were used to calculate the band gap and refractive index of thin films.

## **3.3 Surface Analysis of Thin Film Layers**

The objective of the surface analysis was to examine adhesion strength, chemical activity, contaminants and interaction between the substrates and layers. It involves the examination of the layer composition of photocatalytic films. An optimal way to understand the outer layer and its functionality is by generating elemental maps of the coated surface.

### **3.3.1 Scanning Electron Microscopy (SEM)**

Scanning Electron Microscope (SEM) was selected to analyze the morphological texture of photo-catalytic thin films. SEM's deep field allows for a number of samples to be suitably focused at the same time while also producing suitable resolution images of the thin films, to as low as 5 nm<sup>[217]</sup>. Due to this high magnification, large depth of focus, great resolution, and overall ease of sample observation, SEM was selected to analyze the external morphology (texture), chemical composition, and crystalline structure of photocatalytic thin films<sup>[218]</sup>. Scanning and image formation processes were carried out using 'FEI Quinta 400 Fas' with a resolution of 1 nm, manufactured by EDAX Inc., and 'CamScan S2' at 5 nm resolution, manufactured by NORAN Instruments Inc. Accelerated electrons in SEM carried significant amounts of kinetic energy dissipated in the form of a variety of signals, which included secondary electrons, backscattered electrons, diffracted backscattered electrons and photons. Secondary electrons and backscattered electrons are very useful for revealing the morphology and topography of the surfaces, and also in illustrating the contrasts in composition in multiphase surfaces, for this research the TiO<sub>2</sub> coated films<sup>[216-218]</sup>.

### **3.3.2 Transmission Electron Microscopy (TEM)**

The transparent thin films were further characterized in this research by transmission electron microscopy (TEM). SEM causes electrons to bounce or scatter upon impact so as to scan the surface of the sample. By contrast, TEM directs an electron beam through the sample to process

it. SEM images provide accurate three-dimensional representations, whereas TEM pictures are two-dimensional and may require interpretation. However, TEM is more advantageous in terms of resolution and magnification than compared to SEM.

Since electrons have a much smaller wavelength than photons, it minimalizes the problem of diffraction barrier and enables higher resolution imagery. By driving electrons towards the specimen and detecting the ones transmitted through it, it is possible to note the densities of thin films, as well as the diffraction information where structures, such as crystals, are positioned in an organized fashion. The advantages of TEM, especially when it is used for thin films, include provision of information on crystalline structures and density maps, and, theoretically, the possibility of a subatomic resolution. For this research, TEM was conducted at the Institute of Physical Chemistry, Gottfried Wilhelm Leibniz University, Hanover by Dr. I. Bannat and was used on thin films, prepared by ultrasonic dispersion in ethanol and fixation on a copper supported carbon film<sup>[123]</sup>. Powders scratched from thin films were analyzed with Jeol JEM-2100F field-emission instrument at 200 kV with an ultra-high resolution pole piece that provides a point-resolution higher than 0.19 nm. The Gatan imaging filter (GIF 2001) used in the microscope enabled enhancement of the dynamics in the selected area electron diffraction (SEAD) pattern by elastic filtering, with a bandwidth of 15 eV.

### 3.3.3 *Elemental Analysis (EDX)*

Energy-dispersive X-ray spectroscopy (EDX) analysis of thin films is used to identify elemental composition of a sample. In this research EDX was carried out using equipment manufactured by EDAX Inc. and NORAN Instruments Inc. EDX analysis was part of the same series of experiments that included the previously discussed SEM. The EDX equipment comprises of a beam source, a pulse processor, an X-ray detector and an analyzer, and is installed with SEM for elemental analysis.

### 3.3.4 *X-ray Diffraction (XRD)*

XRD is a non-destructive technique used to identify crystalline phases and preferred orientations<sup>[219]</sup>. The X-ray diffraction carried out at the Institute of Physical Chemistry of Gottfried Wilhelm Leibniz University, Hannover was investigated in this research by Dr. L. Robben and Dr. O. Merka with a Philips X'pert diffractometer at room temperature in the range of  $0.8$  to  $10^\circ 2\theta$ , using Cu  $K\alpha$  radiation ( $\lambda = 1.5406 \text{ \AA}$ ). The X-ray diffraction was performed in grazing incidence using a small (incident) angle of  $0.5^\circ$ . The measurements were performed in a  $2\theta$  range of  $20^\circ$  to  $60^\circ$  on a Bruker D8 Advance equipped with a  $0.4^\circ$  soller slit on the detector side.

X-ray diffraction data for the ‘Rietveld phase analysis’ was recorded on a Bruker D4 Endeavor diffractometer with reflection geometry, a secondary Ni filter, and Cu  $K\alpha_{1,2}$  radiation, which was done in order to identify the crystalline phases and orientation of the thin film samples. The process was conducted at the Institute of Mineralogy of Gottfried Wilhelm Leibniz University, Hannover. Four thousand data points were collected using a step width of  $0.02^\circ$  in the  $2\theta$  from  $5$  to  $80^\circ$  with 1 second measurement time per step and the TOPAS 4.2 (Bruker AXS) software was used in the analysis of these, using the Rietveld method. The parameters optimized during the process of refinement included scale factors, two background parameters, and zero point error and sample heights. So that a calculation profile shapes could be made, a fundamental parameter approach was implemented and done on the basis of standard instrumental parameters with varying average crystal size (integral breadth) of the reflections. In all phases, lattice parameters and crystallite size were refined. The source of structural data for the known phases was ICSD database. The references of the data are as follows: rutile [62679], anatase [9854]<sup>[220]</sup>.

### 3.3.5 Atomic Force Microscopy (AFM)

An atomic force microscope (AFM) has a precise nanometer resolution which helps in inspecting insulators and controlling the atomic force for coated thin films. It has the ability to measure mechanical responses and also allows manipulation of individual atoms in atom-by-atom mechanical assembly. AFM used during the course of research for this thesis uses the Contact-Modus and Non-Contact-Modus.

### 3.3.6 Water Droplet Contact Angle Measurement (CAM)

The angle measurement of the water droplet was the primary tool used to measure the hydrophilicity of the surfaces. When drawing a tangent line from the droplet to the solid surface where the droplet touches it, the contact angle is the angle between the tangent line and the solid surface<sup>[221]</sup>. This technique is extremely surface sensitive, with the ability to detect properties on a monolayer. The following Figure 21 shows the different wetting possibilities.



Figure 21. Different contact angle possibilities. Left: ( $> 90^\circ$ ) poor wetting, center: ( $25^\circ$ ) good wetting, and right: ( $< 5^\circ$ ) complete wetting.



OCA 20 manufactured by Data Physics Instruments GmbH was used for measuring CAM during the course of research for this thesis. The hydrophilic property of the TiO<sub>2</sub> coated thin films was evaluated by measuring the contact angle of a water droplet on the films under ambient conditions in air atmosphere. CAM was carried out using the Sessile-Drop method. For this, three droplets of de-ionized water were placed on a sample at an equal distance of 2 cm, with one drop in the center and two on each of its sides. Drop volumes were 5  $\mu$ l and the deposition rate was 1  $\mu$ l/s. This experiment was repeated three times, with the average value of the experiments taken as the measured value of a sample.

The experimental error of the measurements was calculated at  $\pm 2^\circ$ . CAM was applied four times, twice on the right and twice on the left, as per Figure 22, for the titania samples directly after coating and after annealing to test the hydrophilicity of the thin films.

Measurement is restarted in six steps, the first being (1) drop orientation determination, followed by (2) setup instrument and then (3) adjust camera angle calibration to determine the surface's vertical position and record it as baseline. The fourth step is to (4) capture an image and obtain the baseline at the correct level and store and reuse Baseline, and after that is the (5) fluid loading. The final step is (6) drop dispense.

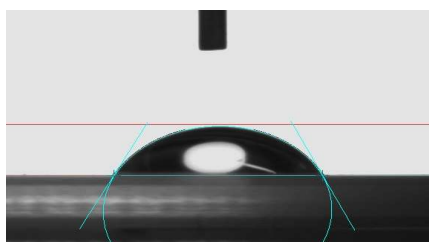


Figure 22. Picture of Contact Angle Measurement gained using the Drop Shape Method. The measured drop is symmetrical around a midway vertical axis. Viscosity or inertia plays a role in shape establishment, as the drop is not in motion. There is no significant difference between the right side ( $62.7^\circ$ ) and the left side ( $62.4^\circ$ ).

#### (a) CAM of As-Deposited Samples

The water contact angle of the deposited samples was studied under different conditions, the first of which being under initial settings, normal room temperature. Next, the samples were subjected to UV light with an intensity of 1.1  $\text{mW}/\text{cm}^2$ , and the contact angle was measured after both 22 hours and 67 hours. Once finished, the three samples were then placed in the dark for 22 hours, 44 hours and 116 hours respectively.

## (b) CAM of As-Annealed Coated Thin Films

The effect of annealing on hydrophilic properties of different thickness was examined at an initial stage and after 67 hours of UV light, with Suprasil used as the substrate. Experiments were carried out under different substrate temperatures, ranging between 50 to 250 °C.

### 3.3.7 Raman Spectroscopy

Raman spectra were collected using a Bruker Senterra Raman spectrometer at room temperature. It is equipped with an Olympus BX series with the FlexFocus™ system for confocal depth profiling and a set of objectives with long and short working distances. The 532 nm line of a combined Ne/laser was chosen as the excitation source. A laser power of 20 mW was used, with an acquisition time of 15 s and 7 repetitions. The Raman spectra are presented in the range from 90 to 1550  $\text{cm}^{-1}$  with a resolution of  $\sim 3 \text{ cm}^{-1}$ , and have an automatic fluorescence rejection via the SERDS (Shifted Excitation Raman Difference Spectroscopy) method. All spectra have been baseline corrected, as well as for Bose-Einstein condensation<sup>[222]</sup> and subsequently, for the purpose of easier comparison, all spectra have been integrated and normalized to 1. The signal contribution from the substrate glass has been collected for each sample, subsequently scaled and removed from the individual titania spectra, leaving the Raman signal purely of the deposited  $\text{TiO}_2$  phase.

## 3.4 Anti-Bacterial Properties

The anti-bacterial properties of  $\text{TiO}_2$  coated thin films make them very useful for various consumer products and, most importantly, in the fields of medical, sanitation and foodstuff. By employing plasma-technical process in deposition, the concept can be used in more durable consumer products requiring disinfecting characteristics.

To analyze anti-bacterial properties, tests were conducted by Dr. I. Trick at the Fraunhofer Institute for Interfacial Engineering and Biotechnology (IGB), Stuttgart. At IGB, Gram-positive bacterial strain, such as *Sarcina lutea*, was used. The cells were cultivated under optimal conditions. The coating experimental set-parameters for microbiological evaluation of *Sarcina Lutea* used as a Gram-positive bacterium are summarized in Table 6). The evaluation of the cell number, which was determined in the experiments, is shown in the photographic form (see Figure 41). The cell number was determined by cultivation (Rodac-Agar plates) and identifying colony-forming units. A cell number  $2.9 \times 10^6$  cells sample was chosen and distributed homogeneously on the surfaces. As a reference, a few samples were examined also in the dark environment.

## 4. Optimization of Photocatalytic Activity Measurements

Titania photocatalytic measurements have been thoroughly studied by photochemists in the last 20 years [8, 108, 223, 224]. These studies have taken into consideration the dependencies of degraded substances, pH-values, catalysts (manufacturer, doping, size of nanoparticles, concentration, etc.), and light exposure. Degussa P25, Sachtleben Hombikat, etc. can achieve efficiencies of a few percent depending on which preparation method is selected. Possible test substances that have 'simpler' molecules than methylene blue in an aqueous system, namely isopropanol, dichloroacetic acid, 4-chlorophenol, methanol, oxalic acid and formic acid, were discussed. Standardization efforts photocatalytic measurements are still in the early stages. Overall, however, the majority of researchers have their greatest experience with methylene blue.

This chapter presents the development of a measurement system for the simultaneous determination of photocatalytic activity for up to 8 rotated coated samples in an aqueous medium, which is also fully automatized online using the C++ programming language and the LabVIEW (National Instruments) system platform software.

### 4.1 Calculation of Photonic Efficiencies

The demineralization process was performed with a solution of 10  $\mu\text{mol/l}$  concentration, with the initial concentration measured with the help of spectral photometers.

The Langmuir-Hinshelwood law, broadly used in liquid- and gas-phase photocatalysis, is the expression that the rate of photomineralization of organic substrates via oxygen sensitized on titania surfaces follows, although with slight alterations [225-227]. A pseudo-first-order Langmuir-Hinshelwood model, as developed by Al-Ekabi and Serpone [62], was used to determine the kinetics of the photo-degradation and to quantify the photocatalytic activities as shown in Equation 8:

$$r = \frac{-dC}{dt} = \frac{k_r \cdot K \cdot C_0}{1 + K \cdot C_0} \quad \text{Equation 8}$$

where  $r$  is the rate of decoloration of the methylene blue,  $C$  is the actual concentration and  $C_0$  is the initial concentration.  $K$  represents the equilibrium constant for adsorption of the organic substrate on the photocatalyst, and  $k_r$  reflects the limiting rate of reaction at maximum coverage under the experimental conditions. The integrated form of Equation 8 is:

$$\ln\left(\frac{C_0}{C}\right) + K(C_0 - C) = k_\gamma \cdot K \cdot t \quad \text{Equation 9}$$

where  $t$  is the process time. At low initial concentration of the organic substrate, the second term in Equation 7 becomes smaller in comparison to the first term. Hence, omitting this term, the final form is shown in the following Equation 10:

$$\ln\left(\frac{C_0}{C}\right) = k' \cdot t \quad \text{Equation 10}$$

where  $k'$  is the apparent rate constant of the photodecomposition ( $s^{-1}$ ).  $k'$  is considered to be equal to the term  $(k_\gamma \cdot K)$ . The  $k'$  values can be obtained from the slopes of the straight line plots of  $\ln(C_0/C)$  against irradiation time  $t$  by the method of least squares, and the rates of dye degradation were calculated by multiplying the rate constants with the appropriate initial dye concentration. The  $k'$  values can be equivalent to the  $K \cdot t$  term due to the experimental calibration.

From the light used for illumination  $\lambda$ , the intensity of light  $I$ , was measured with a photodiode already calibrated and integrated to the measurement system. The speed of light in vacuum  $c$  and the Planck constant  $h$ , the photonic fluxes  $J_0$  is calculated, shown in Equation 11:

$$J_0[m^{-2}s^{-1}] = \frac{\lambda \cdot I}{c \cdot h} \quad \text{Equation 11}$$

Finally, the photonic efficiencies for the photocatalysis with the different films are calculated using the following Equation 12:

$$\xi = \frac{C_0 \cdot k' \cdot V \cdot N_A}{A \cdot J_0} \quad \text{Equation 12}$$

where  $V$  is the cuvette volume of test methylene blue in accordance with the (DIN) 52980 standard,  $N_A$  the Avogadro number and  $A$  the illuminated film area. Determined for an assumed photoactive surface and an initial MB volume and concentration, irradiances below a specific maximum irradiance will yield zero-order kinetic behavior of the system. The initial concentration  $c = 10 \mu\text{mol} / \text{l}$  corresponds to 3.56 mg/l.

The exhibition of saturation behavior, where the perceived rate constant drops with the increase of initial organic pollutant, is typical for the degradation rate of organic substrates. There are three

aspects that could account for this performance<sup>[28]</sup>. (1) As the surface layer of the solid photocatalyst is where the main steps in the photocatalytic process happen, reaction favoring associates with a high adsorption capacity. Because most of the reactions follow the Langmuir-Hinshelwood equation, this means that at a high initial concentration all catalytic sites are occupied.

The catalyst surface concentration is not affected by additional increasing the concentration, which could result in a reduction in the perceived first-order rate constant. (2) The production and movement of photogenerated electron-hole pairs and their reaction with organic compounds happen in series, and thus every stage could turn out to determine the rate for the overall procedure. The latter dominates the process at low concentrations; hence the degradation rate has a linear increase with concentration.

Conversely, the former will become the principle stage at high temperatures, resulting in the degradation rate increasing slowly with concentration. If certain illumination intensity is provided, it is even possible to gain a constant degradation rate as a function of concentration. (3) The rate constant of parent compounds are also affected by any intermediates produced during the photocatalytic process. A higher concentration of adsorbed intermediates can be gathered from higher initial concentration, thereby affecting the total rate.

## 4.2 Development of a Photocatalytic Measurement System

In order to determine the photocatalytic properties of produced titania films, a photocatalysis measurement process was developed. Quartz cuvettes were used as containers for methylene blue during the demineralization experiments. The cuvettes were cleaned with a Hellmanex II (Helma, Germany) solution under ultrasound before being filled with methylene blue.

The titania film samples were immersed in a methylene blue (MB) solution being dissolved in distilled water with an initial concentration of 10  $\mu\text{mol/L}$ , at approximately pH 7 at room temperature. This is illustrated in Figure 23.

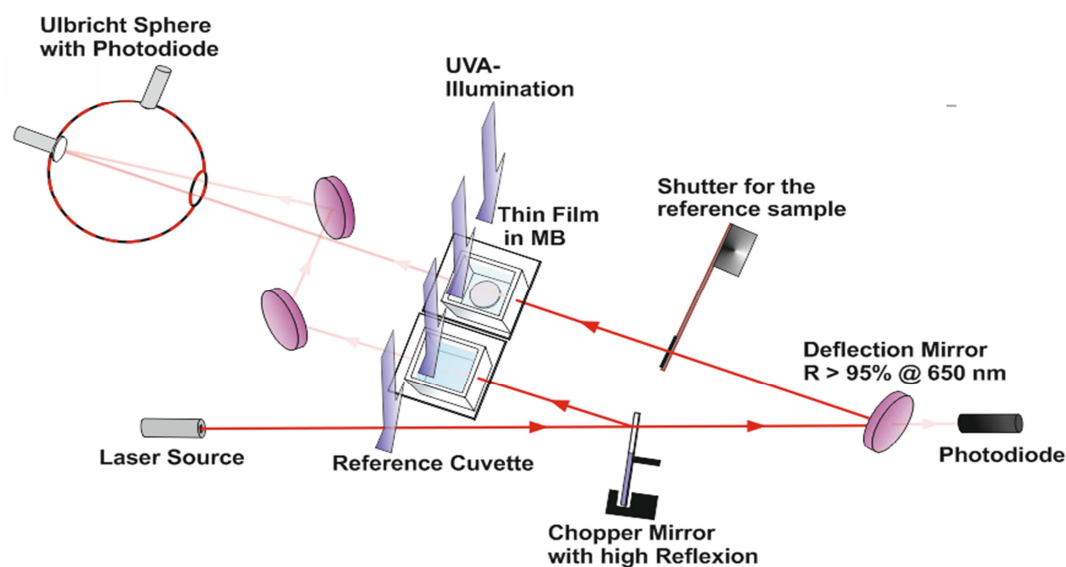


Figure 23. Experimental set-up of the online measurement of the photocatalytic degradation of methylene blue <sup>[123]</sup>.

MB Cuvette containing the concentration of the test solution was kept for 24 hours in the dark to ensure that adsorption equilibrium has been reached. One volume of the solution was brought into contact with the TiO<sub>2</sub> films in one cuvette, and a second amount in a different cuvette was utilized as a reference. Thin films were deposited in a round surface with a diameter of 25 mm. The cuvettes were also covered with quartz glass lids during the photo-degradation test. A commercial TL 10 Philips Lamp emitting in the UV-A region of 350 to 400 nm was used to illuminate the films for 24 hours at room temperature (Figure 24, left), and the lamp was turned on 30 minutes before the start of the degradation experiment to achieve a stable emission spectrum as shown in Figure 24, right. It was observed that the absorbance of the TiO<sub>2</sub> films was at its maximum when approximately 1 mW/cm<sup>2</sup> UV-light was adjusted.

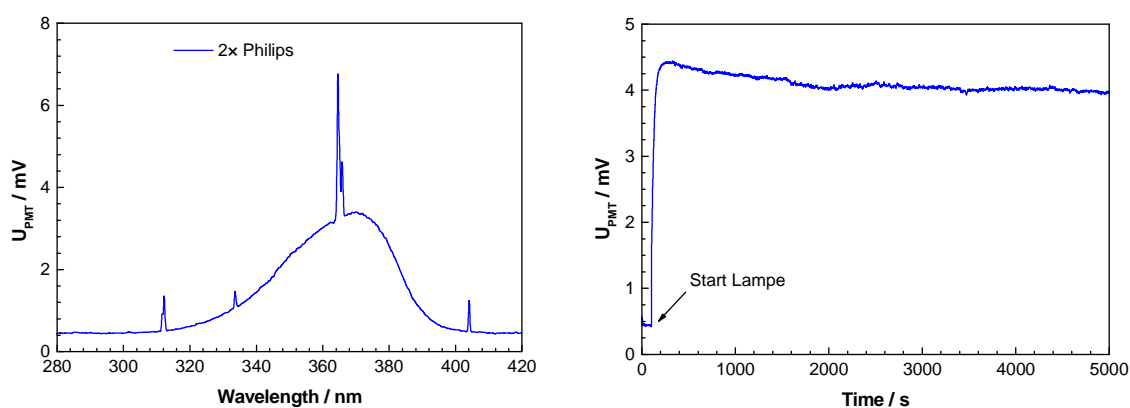


Figure 24. The emission spectrum of the UV-Lamp used. Left: Variation of light power versus wavelength. Right: Irradiation stability of the lamp needed to reach its full power ( $\lambda_{\max}$ : 366 nm).

To measure the optical attenuation induced by methylene blue in the cuvettes, a laser source was employed, and the output power of this laser source was controlled by a photodiode mounted behind a deflection mirror for the measurement radiation. A rotating chopper mirror was used to switch the measurement beam between (1) the reference channel passing the cuvette containing MB with an uncoated substrate and (2) the measurement channel passing the MB cuvette with the immersed sample. The beams from these two channels were steered into an Ulbricht sphere with a photo multiplier tube. Using this configuration, the AC-amplitude of the signal from the photomultiplier tube corresponds to the difference in the optical attenuation between the reference and the measurement channel, determined by comparing the coated sample with the reference sample. In order to quantify the measurement data, a software algorithm was created on the basis of the programming package LabVIEW with the aim of speeding up the recording and evaluation of photocatalytic process information<sup>[123]</sup>. This measurement process is approved as being compliant with the German Institute for Standardization (DIN) 52980 standard, and on the basis of this demineralization method, the photonic efficiencies of the coated samples are calculated.

The development of the measurement system came in two steps. Firstly, the possibility to measure only one coated sample parallel to the reference one (Figure 23). In this case, a shutter was necessary to alternate between the optical ways through the booth cuvettes. Reference measurements were carried out simultaneously with a second channel by using a blind cover in the solution. The second step was the development of this procedure into an automated system for up to 8 separate samples, and also with the online measurement of photonic efficiency (Figure 28).

Reference MB solution measurements without a coated sample should show ‘phantom-photoactivity’ due to, primarily, scattered UV-radiation or adsorption of MB to the sample or the cuvette surface. An example of this is shown in Figure Appendix I, (blue line).

In order to take photocatalytic measurements of the thin films, they were placed under an Actinic BL TL 20 Watt lamp with pre-illumination conditions at the same level for 15 hours. A long-wave UV-A radiation was emitted in the 350- 400 nm range, and the ratio UV-B/ UV-A was less than 0.1 % (UV-B between 280 to 315 nm). Figure 24 shows the measured emission spectrum for the lamp and the time needed for the stability of irradiation.

The reaction temperature was kept at an ambient level using a cooling system placed between the light source and the reactor. The pH of the reaction suspension was not adjusted (pH free = 6.7~7.2). The suspended catalyst in the aqueous system was oxygenated continuously by the ambient air.

Prior to the photonic efficiency tests, a calibration procedure was performed by varying the concentration of the methylene blue solutions, using 0, 2, 4, 6, 8, and 10  $\mu\text{mol/l}$ , and an absorption wavelength  $\lambda = 664 \text{ nm}$  was chosen, as at 664 nm the transmission spectrum shows a minimum (Figure 25). The calibration graph used for further mathematical fittings is shown in Figure 26. A saturation effect was observed for high concentrations of methylene blue.

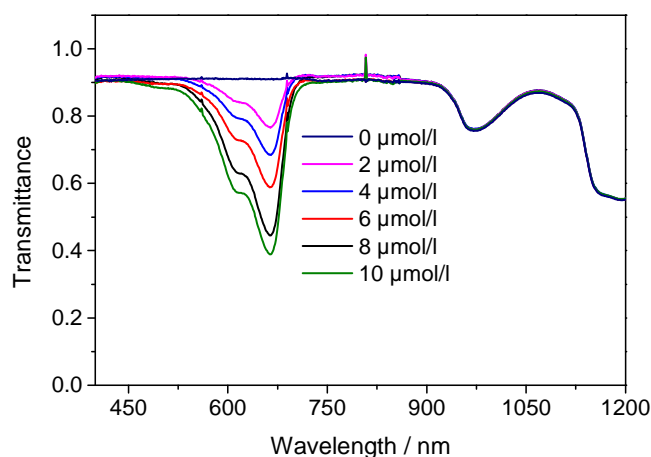


Figure 25. Transmission Spectra of methylene blue cuvettes using 0, 2, 4, 6, 8, and 10  $\mu\text{mol/l}$ .

The experimental calibration curve with different concentrations of methylene blue, shown in Figure 26, was necessary to start the online measurements of the photodegradation of methylene blue under UV illumination. Useful process development was not possible without an accompanying characterization, so a precise automated measuring procedure was specifically made to determine the photocatalytic activity.

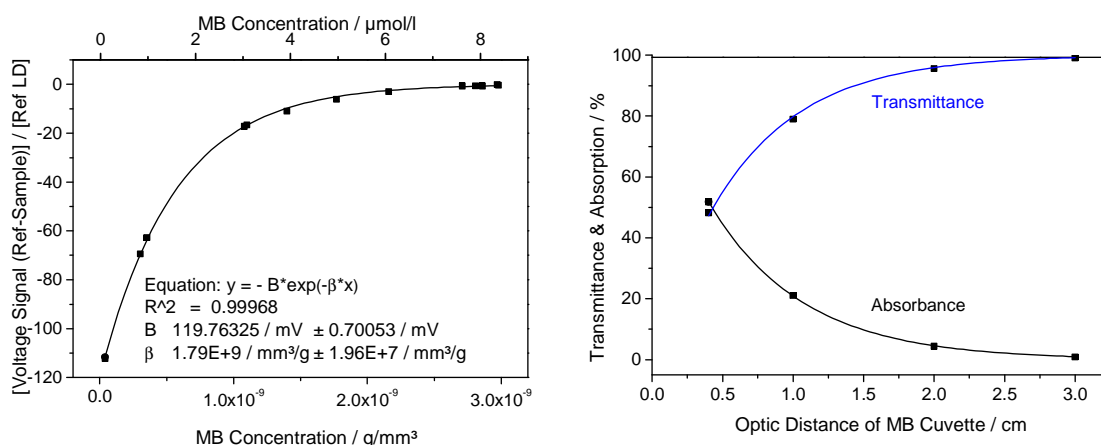


Figure 26. Experimental calibration curves. Left: Concentration dependent transmittance of methylene blue solutions at 664 nm employed for experimental calibration of the online photodegradation measurement system. Right: Influence of optical distance of MB cuvette on the transmission. This system was optimized as shown in Figure 28.



Precision in photocatalytic measurements can be achieved by optimizing the performance of measuring instruments. To achieve an optimal wavelength distribution of allocated radiation photodiodes, Ulbricht sphere, Optical Chopper, detectors and laser calibration procedure were adjusted. The C++ programming language and LabVIEW system design platform software were used to create data analysis software named 'PhoCat' with a LZH License. The goal of this procedure was to achieve the appropriate adjustment of the technical setups for a high reproducibility of photocatalytic activity tests. An inter-laboratory test comparing the coated samples from different external research partners could further optimize the development of photocatalysis processes. The impact of parameters, such as coating rate, temperature, source parameter and substrate pretreatment, on photocatalytic activity was analyzed in the processes above, and this analysis served as the basis for further enhancement of the coating parameters. Based on a total of 288 data points collected from the tests carried out, an empirical correlation equation was developed to express the reactant residue with respect to the UVA irradiance of  $1 \text{ mW/cm}^2$ . A rotation system was created to perform two tasks, to simultaneously measure 8 cuvettes and to also measure through the quartz cuvette as illustrated in Figure 27.

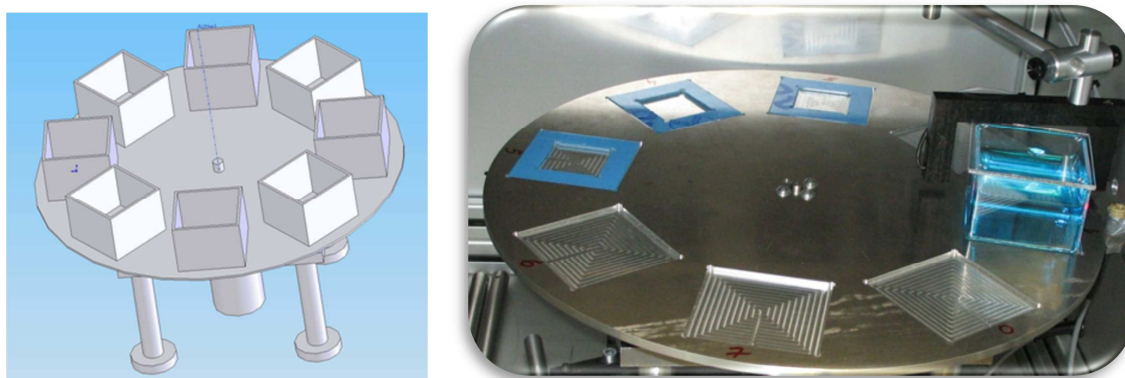


Figure 27. Illustration of the method developed to measure 8 cuvettes for their geometrical thin film surface coatings.

Identical approaches were taken to the test procedures, where the samples were first cleaned and then conditioned according to the DIN 52980 standard. The  $10 \mu\text{mol/l}$  concentration of methylene blue solution used was set in accordance with the same DIN standard, and after completion of the coating process, the cleaning process was repeated with distilled water. The treated samples were examined as per the 'underwater method' rather than the drop method. The coated glass surfaces treated with methylene blue were standard glass substrates that were either spherical, with a diameter of 25 mm, or squared, with 50x50 mm dimensions. The samples were dipped in methylene blue for 24 hours and were analyzed using online measuring software. A light irradiation procedure was used for all samples, with Philips TL10 as the source of irradiation, and a maximum wavelength of 370 nm (350 - 400 nm) was used. These steps were repeated 3 times to

ensure accuracy of the results. The temperature in the chamber was kept under constant check, never being allowed higher than 40 °C, and was measured with the help of a computer linked to the main apparatus. The cuvettes used in the process were covered with quartz glass to examine UV permeability.

The existing automated measurement system, as can be seen in Figure 28, was created to be able to work within the experimental conditions previously mentioned.

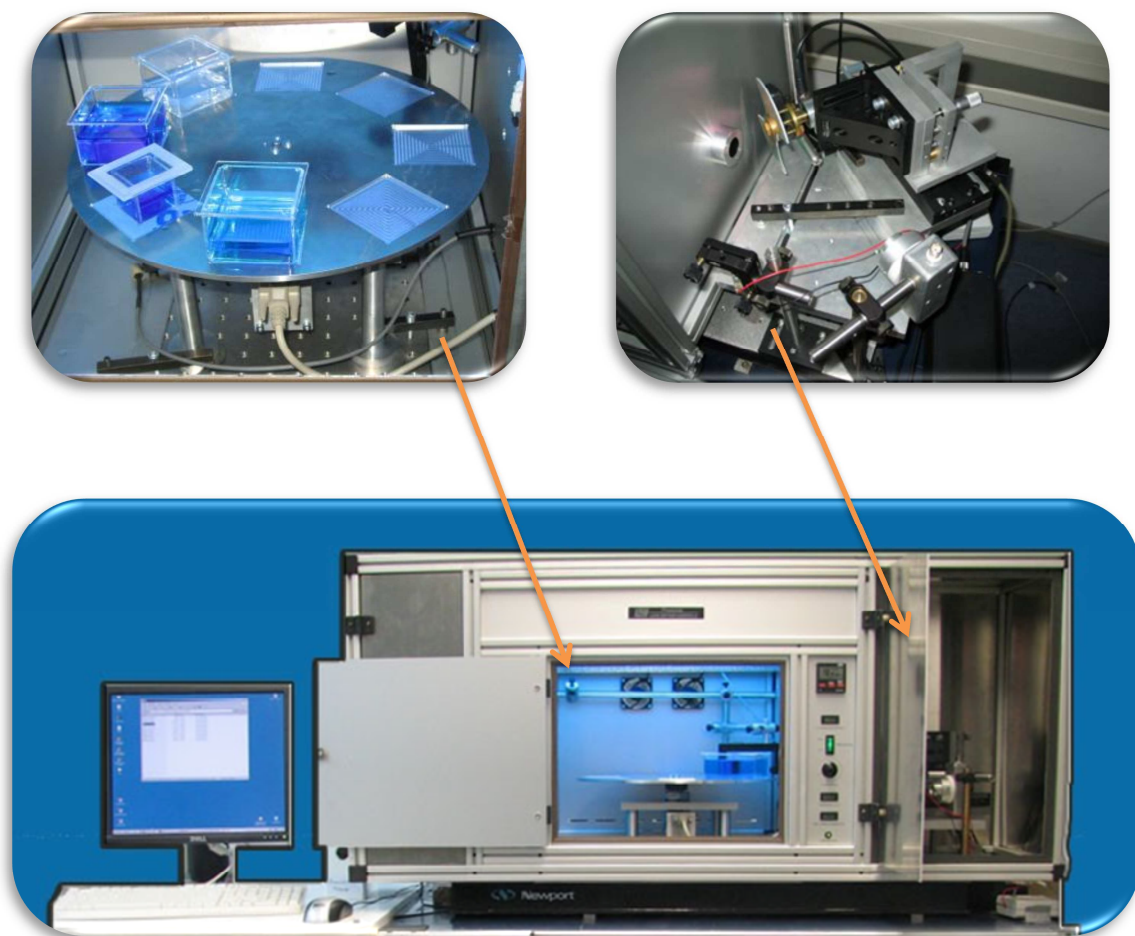


Figure 28. Illustration of the automated measuring system used to determine the photocatalytic activity of thin films. Top left: A rotation plate that can hold up to 8 quartz cuvettes at once. Top right: A laser source and optical Chopper as laser beam components. Bottom: Overall picture of the created apparatus with program package to compute the measurements.

A visualization of the C++ program used to determine the photocatalytic activity is illustrated in Figure Appendix I. A set of calibration curves, such as the transmission values in UV and visible range for different concentrations of methylene blue, were provided to characterize the photocatalytic activity (see Figure 29).

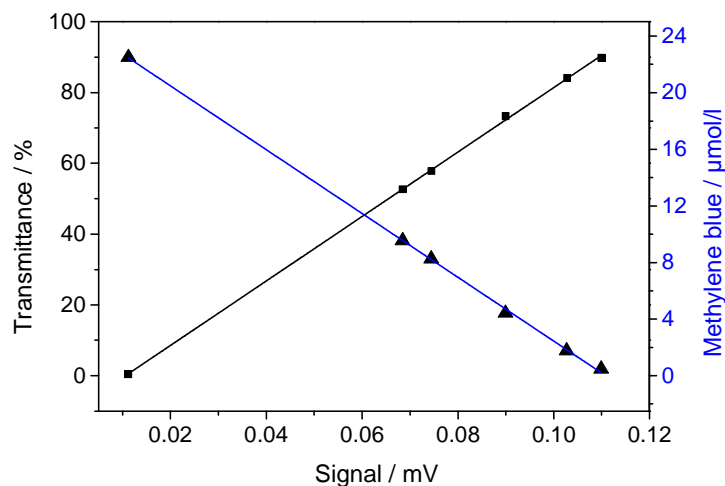


Figure 29. Calibration curves examples used to compute the measurements. Graph of methylene blue solutions, with a transmission dip of 664 nm wavelength.

Finally, the calculation of the photonic efficiency was performed on the data collected through the variation of the solution's concentration. The calculation created to perform this is found in Figure Appendix II.

### 4.3 Photonic Efficiency Evaluation in accordance with ISO and DIN Standards

Different characterization tests carried out at the LZH facility, in accordance with DIN 52980 standard, were used to determine the photocatalytic activity (Info Appendix 4). Table 3 shows a comparison of demineralization methods used by LZH Center, based on methylene blue, and by Fraunhofer IST Institute, based on stearic acid.

A total of five samples were used for a comparative analysis out of which three were Pilkington Activ™ samples used as reference and two were prepared at LZH using IAD process. This comparison depicts the existence of an appropriate correlation between the two demineralization methods.

The following measurement system allows reproducibility and has the ability to take online measurements of many samples at once. This eliminates possible errors which may occur in the normal process of taking a small part of sample for parallel transmission measurement. Another important advantage of this system is that it provides an internal characterization method which can correlate with other instruments and methods described in Chapter 3.

Table 3. Comparison of the photonic efficiencies between stearic acid (IST) and methylene blue (LZH)

Sample ID	Demineralized Molecule $10^{11}$ [J/cm <sup>2</sup> s]	Photonic efficiency % (IST)	Photonic efficiency % (LZH)
Pilk Activ 1	2.491	0.007	0.008
Pilk Activ 2	2.684	0.008	-
Pilk Activ 3	2.629	0.007	0.009
IAD Process V	19.61	0.055	0.061
IAD ProcessV, after annealing	22.25	0.063	0.069

## 5. Results of Photocatalytic Activity of Different PVD Processes

This chapter contains a compilation of the results obtained regarding the different process variants in the PVD processes for optimization of photocatalytic activity. This compilation is to serve as a broad summary of the correlation details, and thus will not list every correlation between every different parameter.

The PVD photonic efficiency is very small, often to the order of 0.01%. This affects not only the dyes but all excited photocatalytic reactions. The small amount of these dyes can be easily covered through parasitic mechanisms. Therefore, strict attention to the reliability of the 'zero measurement', necessary as an active reference sample with consistent preconditions in dark, light source, and initial concentration, has to be considered<sup>[81, 228]</sup>. To classify the activity obtained through the comparison to other films in the literature, here are some examples. Other results are already discussed in Chapter 2, Basics. Using the experimental set-up of an initial MB concentration of 10  $\mu\text{mol/l}$ , irradiation intensities of below 5  $\text{W/m}^2$  have been calculated for substrates comprising quantum efficiencies greater than  $\zeta = 0.09\%$  for colloidal  $\text{TiO}_2$  prepared by controlled hydrolysis of  $\text{TiCl}_4$ <sup>[151]</sup>. The photocatalytic activity of  $\text{TiO}_2$  films is determined also by the affinity of its surface towards the reactants and solvents. With tailored surface properties, even such compounds can be photocatalytically reacted, to exhibit a practically negligible reaction rate if a standard  $\text{TiO}_2$  photocatalyst is used. Mesoporous films of  $\text{TiO}_2$  have been shown to be efficient photocatalysts, particularly for the degradation of dyes, yet their photocatalytic efficiency strongly depends on the respective degradation mechanism. In this experiment, the photonic efficiency of Pilkington Activ<sup>TM</sup> was 0.0236<sup>[81]</sup>.

Pilkington Glass Activ<sup>TM</sup> represents a possible suitable successor to P25  $\text{TiO}_2$ , especially as a benchmark photocatalyst film for comparing other photocatalyst or self-cleaning films<sup>[121, 209, 229]</sup>.

### 5.1 Comparative Analysis of Different Coating Processes Using Methylene Blue Degradation

The coating parameters discussed in this thesis are classified under the following six PVD processes (Table 4):

Table 4. Parameterization of processes

Process	Nr.	Platform	Ion-Source	Gas
5 comparative PVD methods				
conventional e-beam without ion-source	Process I	BAK 760	Without	O <sub>2</sub>
Ion Beam Sputtering	Process II	IBS		Ar, O <sub>2</sub>
Thermal e-beam evaporation	Process III	SYRUSpro 1100	APSPRO	Ar, O <sub>2</sub>
	Process IV	BAK 640	Denton CC-104	O <sub>2</sub>
	Process V	BAK 760	Denton CC-105	O <sub>2</sub>
Optimized PVD method				
Thermal e-beam evaporation, developed at high temperature	Process V,	BAK 760	Denton CC-105	O <sub>2</sub>

To analyze the IAD parameter dependence of the photocatalytic activity, the processes were repeatedly compared to the preparation of the photocatalytic layers.

Illustrations 30 to 34 (pp. 71-77), shown in the sub-chapters below, depict the impact on the layers of the substantial coating parameters, which includes the ion-source, gas flow, discharge bias, and the process temperature and thickness. A comparison of the methylene blue degradation on the coated surfaces prepared with these different parameters is presented with uncoated glass as the reference sample.

### 5.1.1 Influence of the Coating Processes

The initiate comparative study was established for conventional (Process I), IBS (Process II), and thermal e-beam evaporation with (Process III). Conventional thermal evaporation methods (Process I) are used to clarify the influence that an absence of ion-assistance has, such as for the demineralization of methylene blue without operating any ion-source. More recently, ion-beam sputtered oxides have been found to exhibit optical properties which are superior to those of films of the same material deposited using thermal e-beam evaporation<sup>[163, 179]</sup>. These larger differences indicate a larger value of refractive index  $n$  for the ion assisted coating.

In distinction to this, the Advanced Plasma Source (APS, Leybold) generates argon plasma. The oxygen for activated reactive evaporation processes is fed into this plasma over the aperture of the source by a special nozzle system. The major parameter controlling the energy of the ions impinging on the substrate is the bias voltage of the source. Due to the possibly influence on the photocatalytic performance, a check is required (see 5.1.3).

The process concept considered throughout is based upon the gridless end-hall ion-source Denton CC-105. A broad ion beam is transported through this source and can be operated with pure oxygen for the reactive coating of oxide compounds. Typical operation conditions consist of a discharge current of 3.0 A, resulting in a discharge voltage of approximately 220 V at a chamber pressure of  $3 \times 10^{-4}$  mbar, and a constant oxygen flow rate of 25 sccm through the discharge region. To initiate the ionization of the feed gas and to neutralize the ion beam, a voltage of approximately 10.5 V is applied to a tungsten filament (diameter: 0.635 mm, length: 13 cm) which is installed at the outlet of the source. The operation parameters selected greatly influences the mean ion energy and the energy distribution. Generally speaking, the maximum is found at approximately 50 - 60% of the discharge voltage.

The degradation of MB over 20 hours (Figure 30) showed that  $\text{TiO}_2$  under UV-illumination is able to mineralize the organic compound dissolved in water and, consequently, water purification can be proposed as a technological application. The figure revealed that the photocatalytic activity curve, gained via the SYRUSpro 1100 using APS source at 250 °C on thin films of 300 nm with a Bias equals to 70 V, contains larger differences in diminution of MB concentration extreme than the curve for the conventional e-beam evaporated coating and little faster than the IBS technology samples.

In this deposition process, Pilkington Activ™, the commercial photocatalytic glass, was used as a reference. The photocatalytic activity level of commercially available materials used in roofing tiles, window glass and ceramic plates is usually at a very low level. The photonic efficiencies of these substrates fall within the range of 0.05 %; from 2000 UV photons one releases a straight reaction. There is a certain amount of loss in energy that can be attributed to the fact that charge carriers are produced deep inside the titania layer and must then be transported to the surface.

The above evaluation of the different processes of methylene blue demineralization is shown in Figure 30, with the uncoated piece of glass as the reference sample. The process shown was carried out with BAK 760, using Denton CC-105 as the ion-source and oxygen as the reactive gas, using the parameters 250 °C, 0.15 nm/s, ~500 nm, and it shows the highest photoactivity level. The photocatalytic efficiency of the examined samples lies between 0.0170% (IBS) and 0.0559% (IAD-CC 105).

The rate of demineralization of methylene blue over 24 hours and the variation of the ratio of  $\ln(C/C_0)$  versus time were determined. The corresponding plots of the data are presented in the Figure 30.

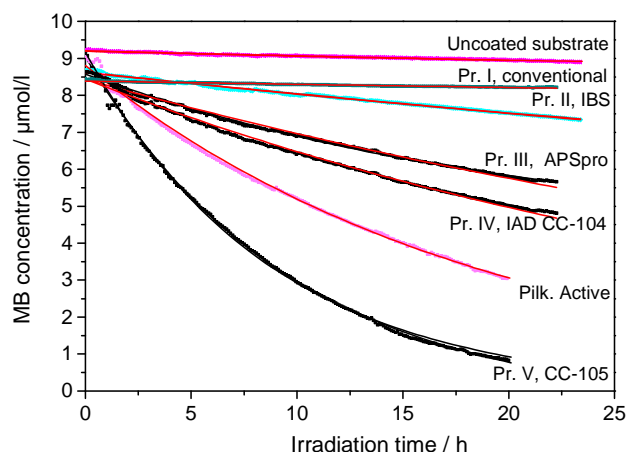


Figure 30. Investigated coating concepts in comparison. Influence on the demineralization process of conventional (thickness: 300 nm, T: 200 °C), IBS (thickness: 300 nm, 200 °C, gas: O<sub>2</sub> and Ar) APSpro (thickness: 300 nm, 200 °C, gas: O<sub>2</sub> and Ar), IAD with CC-104 (thickness: 300 nm, T: 200 °C, O<sub>2</sub>: 20 sccm), commercial glass, and the developed IAD with CC-105 (3.5 A, thickness: 300 nm, 250 °C, 25 sccm).

The films prepared using BAK 760 exhibited a photodecomposition rate of methylene blue that was 1.8 times higher than commercially available products with a self-cleaning ability, and 36 times higher when compared to uncoated substrates. These results are a consequence of the different technical parameters of the processes. Leybold SYRUSpro 1100, as the depositing apparatus, emits ions. Denton CC-105, as an ion-source, has the ability to generate reactive gas ions as a deposition parameter, while APS Pro can create ion streams with defined energy values in eV range. Denton CC-105 gives enhanced results in terms of photoactivity that are simply not achievable through conventional thermal processes, even with the use of high substrate temperature.

All coatings show properties superior to the conventional electron beam evaporated coating. Depending on the desired application, a dense microstructure can be obtained by an adjustment of the parameters of the ion assistance. Although there has been significant progress in the ion-sources processes, mainly II, III and V, the coating quality when using APSpro, Denton CC-104 and CC-105 still differs. The subsequent experiment offers far-reaching opportunities for controlling the photoactivity variations. There are many properties proposed for the mentioned PVD processes, including layer composition control, dense coatings, high substrate temperature, low contamination and high deposition rates<sup>[39, 123, 210, 211]</sup>. Retarding Field Analyzer (RFA), named also 'Faraday Cup' being determined by the potential of the magnetic field, the discharge ion current, and the gas flow, reveals the 'integral' energy distribution of ions emitting from the ion-source. The RFA is a maneuver for measuring the current in a beam of charged particles. In its most basic form, the RFA comprises of a conducting metallic chamber or cup that intercepts a particle beam. An electrical load is attached which conducts the current to a measuring



instrument <sup>[230]</sup>. The number of ions or electrons hitting the cup can be determined by measuring the current. This concept is depicted as follows.

$$P_{\text{cup}} = \int \frac{dI_{\text{cup}}}{dU_{\text{ret}}} U_{\text{ret}} dU_{\text{ret}} \quad \text{Equation 13}$$

where  $I_{\text{cup}}$  is the current and  $U_{\text{ret}}$  is the potential.

The energy distribution level of ions as the discharge voltage, maintained for APSpro, CC-104 and CC-105, holds a practical importance in that it influences the adsorption level of atoms, thereby also affecting the morphology of the thin films. Figure 31, displays the results gained from the influence of the different ion-sources on the methylene blue demineralization rate <sup>[123]</sup>. Based on a total of 288 measured data an empirical correlation equation has been developed to express the reactant residue. The values compiled in Figure 31 demonstrate that the photonic efficiency for the IAD at 300 °C is by a factor of almost two or more higher than for the APS and conventional processes. Furthermore, also the coatings obtained after IAD with the CC-105 source on cold substrates are much less photoactive than that on the hot substrate indicating that the substrate temperature has a crucial influence.

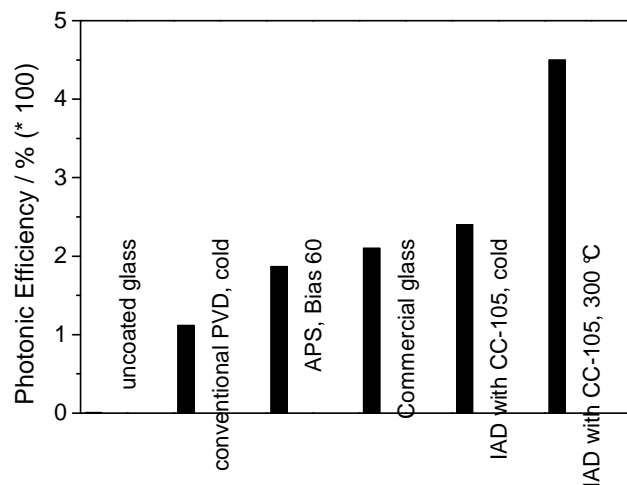


Figure 31. Photonic efficiencies obtained for TiO<sub>2</sub> coatings processed with IAD cold and at 300 °C, IAD with APS Bias 60 and conventional cold PVD process compared with that of a commercial photoactive TiO<sub>2</sub> glass.

### 5.1.2 Influence of Gas Flow

Electron beam evaporation techniques have been studied with varying TiO<sub>2</sub> deposition processes. Using a powerful electron beam, the source material, chiefly TiO<sub>2</sub>, a sub-oxide <sup>[231, 232]</sup> or Ti-metal <sup>[233]</sup>, is heated with an oxygen partial pressure below 3 x 10<sup>-4</sup> mbar. A low chamber pressure

is needed when using a standard setup. In order to prevent scattering of the evaporated particles and the oxidation of the electron gun with a standard setup, a low chamber pressure is required, although it is possible to use higher pressures in the deposition chamber if the electron gun is differentially pumped. The evaporation rate is fixed at 0.15 nm/s.

Results of the influence of reactive gas flow are presented in Figure 33 only for the case that the CC-105 was operated at discharge current kept constant at 2.5 A.

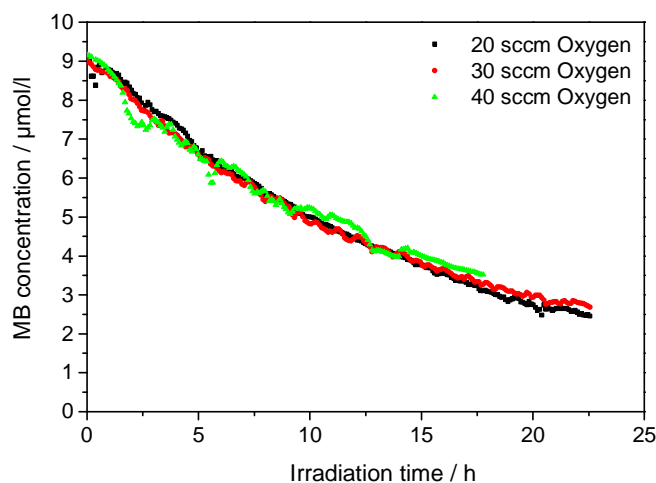


Figure 32. Influence of the oxygen flow, for the IAD process with CC-105 (2.5 A, 150 °C, 300 nm).

Generally, the production of oxide layer materials can be achieved through the use of oxygen as a reactive gas, so that layers can be produced with extremely low absorbance<sup>[234]</sup>. The layer photoactivity after the use of a reactive gas in the range of 30 ( $\pm 10$ ) sccm cannot be greatly changed in the course of a coating process.

From the Retarding Field Analyzer measurement (RFA) measurement, the previous result cannot be related only on the energy distribution of the separated ions of the oxygen. In anticipation of the investigation of three-dimensional emission characteristics, it should be mentioned here that the distribution of low-energy ions is less directed than the height of the energy content<sup>[235]</sup>.

Through a change in the ion-source current values, it is possible to increase the ion energy transfer, then leading to an additional effect on the condensation of the layer and possibly a change in the microstructure. The precise influence of this ion dose on the variation of MB concentration under UV is thoroughly studied in the next few chapters.

### 5.1.3 Influence of Discharge Bias

According to the research reports on CC-105 on the last years<sup>[211, 213, 235]</sup>, the correlation between the discharge voltage and the peak position of the ion energy distribution is not clearly defined in

the regulation mode with constant discharge current and gas flow. As a consequence, keeping the discharge power supply parameters constant is no absolute guarantee for a constant ion energy distribution.

During Deposition Process III, in which SYRUSpro 1100 and APSpro were used, a bias of 60 volts resulted in good photoactivity of the films, which was revealed by measuring the level of methylene blue demineralization. Photoactivity then gradually decreased when the bias voltage was increased from 60 to 130 V. Both the energy distribution of the ions and the spatial distribution of the ion-current density were dependent on the high level of stability of the ion-source parameter. The influence of bias voltage on the demineralization, changed depending on which ion-source was employed for the process. The ion-source works under strong magnetic fields, thus showing a correlation between the magnetic field and conductivity, which then in turn will affect the bias. Using two different magnetic fields,  $B$  and  $B_0$ , it is possible to create a potential difference in which the following equations can be seen:

$$\Delta V_p = \frac{k \cdot T_e}{e} \ln \left( \frac{B}{B_0} \right) \quad \text{Equation 14}$$

where  $\Delta V_p$  is the potential difference in plasma,  $k$  is the Boltzmann constant,  $T_e$  is the electron temperature, and  $e$  is the elementary charge. A varying bias expresses a change of potential  $V_p$ , and during the ion-source working, the field  $B_0$  become denser than  $B$ .

The ion energy of ions hitting the cathode largely associates with this bias. Practically, the bias applied to the substrate governs the energy of ions arriving at the surface of the growing film. A sheath is formed between substrate and plasma because of this bias, causing the potential difference between plasma potential and surface potential to drop.

The discharge current range is in agreement with the mentioned information, and this current allows for the controlling of the ion flux during coating. This effect interferes with changes in the shape of the plasma, from which the ions are extracted. The potential difference in plasma helps to analyze the ion energy measurements which directly correspond to the ion energy distribution.

As can be seen above, the APS ion-source, with different bias values, affects both the potential created and the ions distribution. Consequently, the range of the discharge current influences the absorption of Ti atoms on the surface, which then affects photocatalytic characteristics. Figure 33 shows the influence of the discharge current on the decomposition of methylene blue.

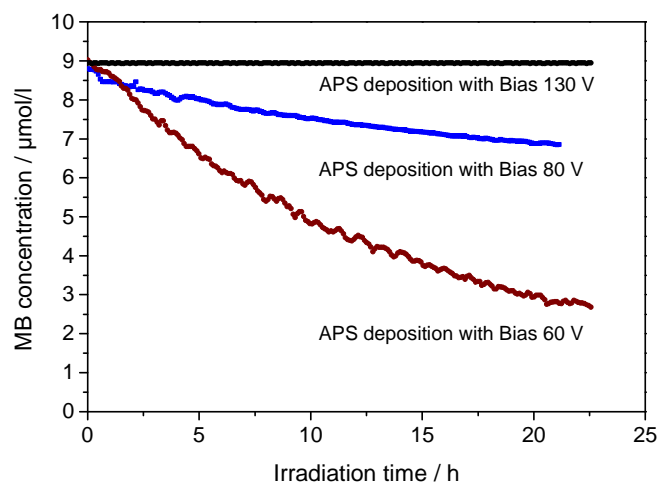


Figure 33. Bias voltage when coating with SYRUSpro 1100 at 250 °C on thin films of 300 nm. A higher voltage reduces the demineralization of methylene blue.

The power changing across corresponding to the bias voltage is non-neutral, comprising predominantly of the thermal and structural equilibrium. The bias voltage of the body of the source is the main parameter controlling the energy of the ions impacting on the substrate. A bias voltage of 0 V characterizes the conventional e-beam PVD process without ion assistance. Additionally, the increase of potential variation for the APSpro ion-source cannot be conforming to the mentioned structural equilibrium needed.

The titania layers are optically and morphologically adequate with an APS bias voltage of only 60 V, being, for example, stress free <sup>[211]</sup>, whereas higher bias voltages cause compressive film stress and a low refractive index, such as at 80 or 130 V.

#### 5.1.4 Influence of Temperature

A comparison of the deposition process carried out using different ion-sources at different coating temperatures shows that Balzers BAK 760, at 200 °C and using Denton CC-105, achieves a comparatively faster decolorization, resulting in an almost colorless solution. This was compared to SYRUSpro 1100 with APRpro at 50 and 200 °C and Balzers BAK 760 with Denton CC-105 at 50 °C, where the methylene blue concentration was only reduced to half, from 10 μmol/l to 5 μmol/l (Figure 34).

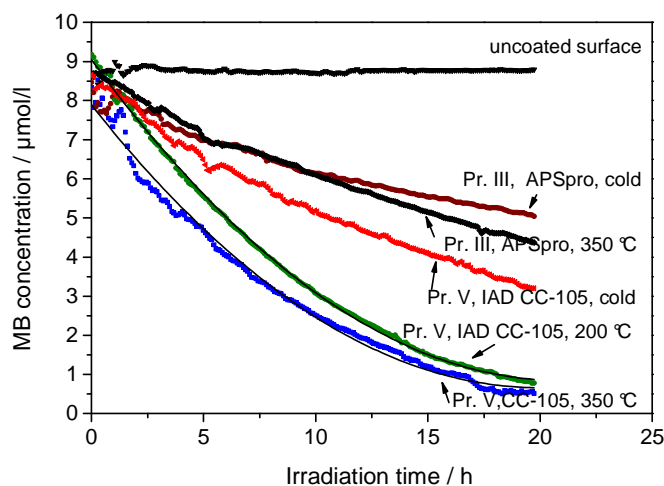


Figure 34. Influence of the Substrate temperature. A comparison of heated (200 and 350 °C) and unheated (60 °C) processes on the demineralization of methylene blue over 20 hours.

Minor variations in temperature are known to not greatly disturb the photocatalytic oxidation rate<sup>[19]</sup>. This reliance, albeit low, on temperature by the degradation rate can be seen by the low activation energy (a few kJ/mol) as contrasted to normal thermal reactions. It is possible that the organics' photodegradation is managed by hydroxyl radical reactions as the activation energies are similar to that of hydroxyl radical formation<sup>[236]</sup>. The interfacial electron transfer speed to oxygen could be capable of controlling the effect that temperature has on the oxidation rate<sup>[237]</sup>. The swift desorption at higher temperatures of both substrates and intermediates from the catalyst, on the other hand, is likely another factor in this process, which could lead to a greater effective surface area for the reaction. At this step of the process, the rate-limiter is desorption at lower temperatures<sup>[238]</sup>. While only relatively small alterations (0.04 eV) have been discovered in relative positions of the Fermi level of titania powders at temperatures between 21 to 75 eV, an increase in temperature results in the observation of improved interfacial electron-transfer kinetics<sup>[239]</sup>.

The rate of decrease is significant in the case of titania films coated at higher temperatures. This increase of photocatalytic activity can be related to the surface morphology, crystal structure and the enhanced photo-response of titania films as shown in Chapter 2 (2.2.3, 2.2.4 and 2.2.5) reviewing the current literature. Thin films coated at 200 and 300 °C had a higher surface roughness, which lead to an increase in the effective surface area and thus improved the activity, as shown in Chapter 7 and Chapter 8. In this case, the grain boundaries are reduced and a less recombination losses of electron hole pairs are generated due to UV-illumination.

### 5.1.5 Influence of Thickness

Figure 35 exhibits that the photocatalytic activity has a relationship with the coating thickness, so that photoactivity is low when the coating thickness is between 15 nm and 150 nm, but increases gradually between 200 nm and 550 nm. Beyond 600 nm coating thickness, photoactivity remains almost constant.

The effect of the coating thickness, from 15 to 1000 nm, on the photocatalytic activity of IAD films has not been previously reported in the literature. For other deposition methods, this critical effect relates to a limited diffusion length of the charge and a cumulative light absorption with increasing film thickness as tested by H. Tada et al.<sup>[93]</sup>. They reported that the critical film thickness was ca. 100 to 150 nm and so deduced a charge carrier diffusion length of approximately 300 nm. The effect of film thickness generally indicates a dependence on the thin film preparation technique, and/or the investigational setup for analyzing their photocatalytic performance, i.e. the size and nature of the organic test element used. This reasoning has been confirmed by the IAD experiments using column-grain structure (see Chapter 6).

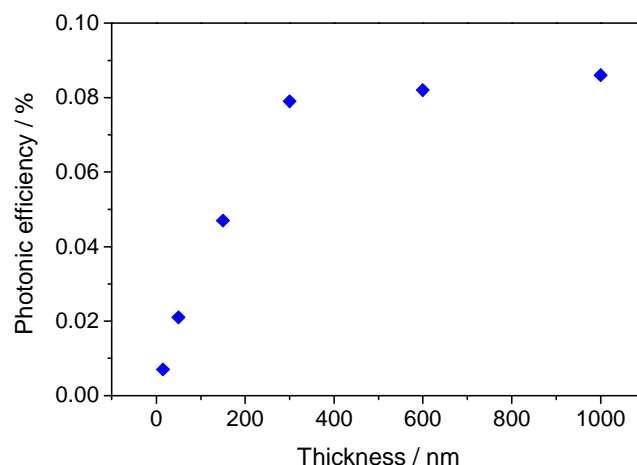
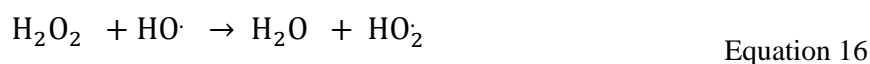


Figure 35. Influence of the deposition thicknesses using Process V on the degradation of methylene blue.

Figure 35 shows that the photocatalytic activity depends on the film thickness and can be presented in three regions: Region I: below 150 nm; Region II: 200 to 550 nm; and Region III: over 600 nm. To understand this dependence, K. Eufinger et al. demonstrated in 2008 that the column-grained film structure explains the reasons the carrier diffusion cannot be the limiting factor for these films. Charge carriers generated inside the grain do not need to diffuse for more than 25 nm to reach its surface<sup>[3]</sup>. Based on these results, it has been discovered that the most of the incoming light is absorbed in the first few 150 nm of the film and that increasing the film thickness leads to greater performance. 150 nm is the critical value for the photocatalytic activity dependent on the methylene blue degradation.

A higher surface area of the catalyst, as a general rule, increases decomposition with the catalyst as there is a greater surface area available for adsorption and degradation, depending on the sample thickness. There is an ideal value available, where the solution opacity increases when above a certain concentration as a result of increased light scattering of the catalyst particles. This then reduces the light penetration in the solution, thus diminishing the rate<sup>[240-242]</sup>. An additional point to consider is that terminal reactions (such as Equation 15 and Equation 16) could be a factor in the photodegradation rate attenuation. The formed hydroperoxyl radical is not as reactive as the HO<sup>·</sup> one:



The ideal catalyst dosage reported for photoreactors has a large range from 0.15 to 8 g/l for different photocatalyzed systems and photoreactors, which only grows with increasing light intensity<sup>[72, 243]</sup>. This ideal dosage is, under certain conditions, significant when designing slurry reactors that make use of the reactor space and catalyst. A photoreactor will be under-utilized if the optical penetration length at any illumination intensity and catalyst concentration is less than the solution layer thickness. In addition to this, TiO<sub>2</sub> immobilized systems also have a prime catalyst film thickness. As a result of the film being porous, the catalyst thickness is proportional to the interfacial region and so catalytic oxidation is favored by thick films. However, increasing the thickness increases the internal mass transfer resistance for both organic species and photogenerated electrons/ holes, which then in-turn will increase the recombination possibility of the electron/hole pair and so decrease performance degradation.

## 5.2 Comparative Analysis of Different Coating Processes Using Other Dyes: Interlaboratory Tests

For systems of activity evaluation, the suitability of methylene blue (MB) has been studied as a representative dye by, for example, comparing the decomposition of acetic acid (AcOH) in its aerated suspension system. Other reference tests have been done. The uncoated side of the same substrate was used as a standard reference for the discoloration of MB, with the commercial samples of Pilkington Activ™ supporting this continual comparison. Other assistance in

comparison came from continuous and parallel complementary work with project partners, such as the stearic acid degradation procedure in Fraunhofer Institute (IST).

Additionally, the IAD samples were sent to German DIN Standardization for the following Interlaboratory tests:

### 5.2.1. Stearic acid and luminescent dye tests, (Fraunhofer Institute IST, Braunschweig)

A series of measurements carried out by IST, using stearic acid and luminescent dyes were gathered (Figure 36) in order to determine the photocatalytic performance of the IAD samples.

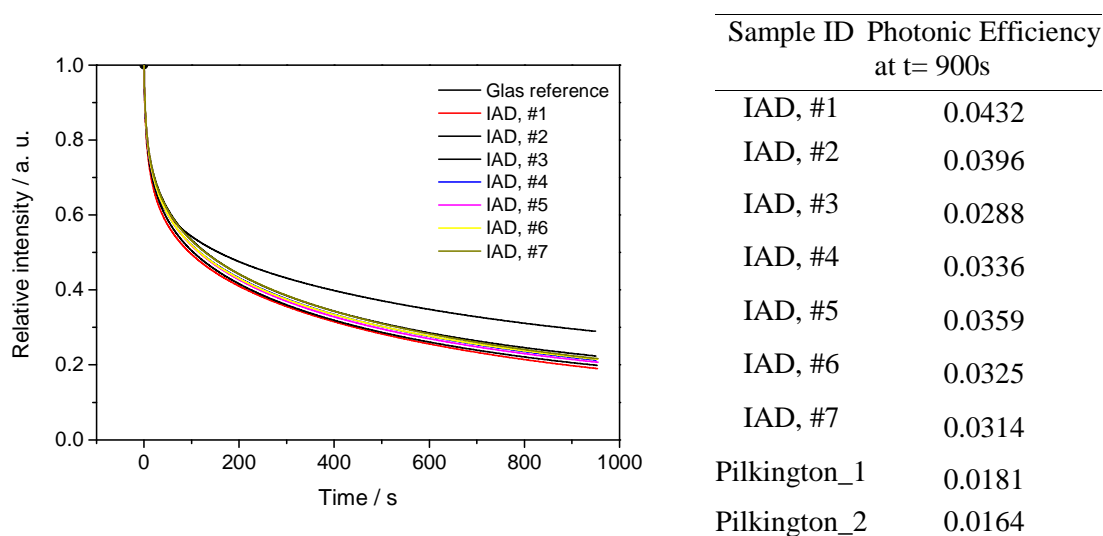


Figure 36. Results of degradation rate using luminescence method (IST).

For thin layers of stearic acid a strong correlation between the light scattering, or the Haze value ( $H$ ) of the layer and the mass density  $\mu$  [ $\text{g}/\text{cm}^2$ ] was observed. This correlation can be described as linear over a wide range of Haze (10% to 70% Haze):

$$H(t) = H_{\max} - [H_{\max} - H(t = 0)] \cdot \exp[r_d \cdot B \cdot t] \quad \text{Equation 17}$$

where  $H(t)$  is the temporal development of the haze,  $r_d$  corresponds to the decomposition rate and  $B$  to the calibration parameter, which is  $7.2 \times 10^6 \text{ mm}^2/\text{g} \pm 9\%$  for the prepared stearic acid layers<sup>[207]</sup>.



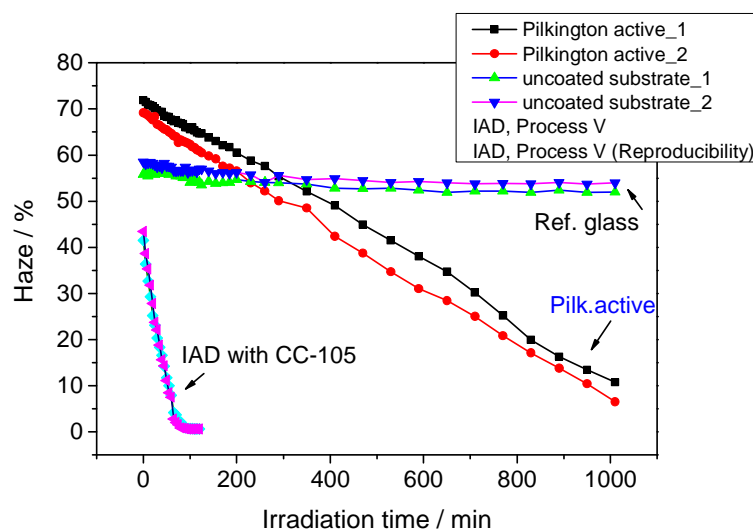


Figure 37. Two Process V IAD sample results of Haze [%] to compare against commercial photocatalytic glass and an uncoated glass (IST).

The results of stearic acid and the decay of luminescence are resumed in the following table:

Table 5. New Developed Stearic acid and luminescent investigation results acquired by Fraunhofer IST.

Sample	Stearic acid Efficiency	Luminescence Efficiency
Pilkington Activ™	0.008	0.017
IAD Process V, with CC-105	0.060	0.035

### 5.2.2. Photocatalytic surfaces based on a solid state luminescent dye

An europium (III) complex showing the typical intense  $5D_0 \rightarrow 7F_2$  transition with an emission wavelength maximum of 615 nm upon excitation at 350 nm (Figure Appendix III). The dyes are deposited onto the samples using an ultra-high-vacuum deposition technique as thin-films spanning from 10 to 100 nm. The procedure is then agitated with  $20 \text{ W/m}^2$  at 365 nm with a LED, and the luminescence is time-dependently monitored with a spectrofluorimeter. The dye luminescence displays only a minor reduction in inactive substrates such as glass, yet exhibits a significant decay on photocatalytically active substrates. <sup>[244]</sup>

Pilkington Activ™ samples were the self-cleaning reference in tests carried out. The IAD samples (A, B and D) were coated via Process V using an ion assisted electron-beam evaporation process operated by Balzers BAK760 plant.

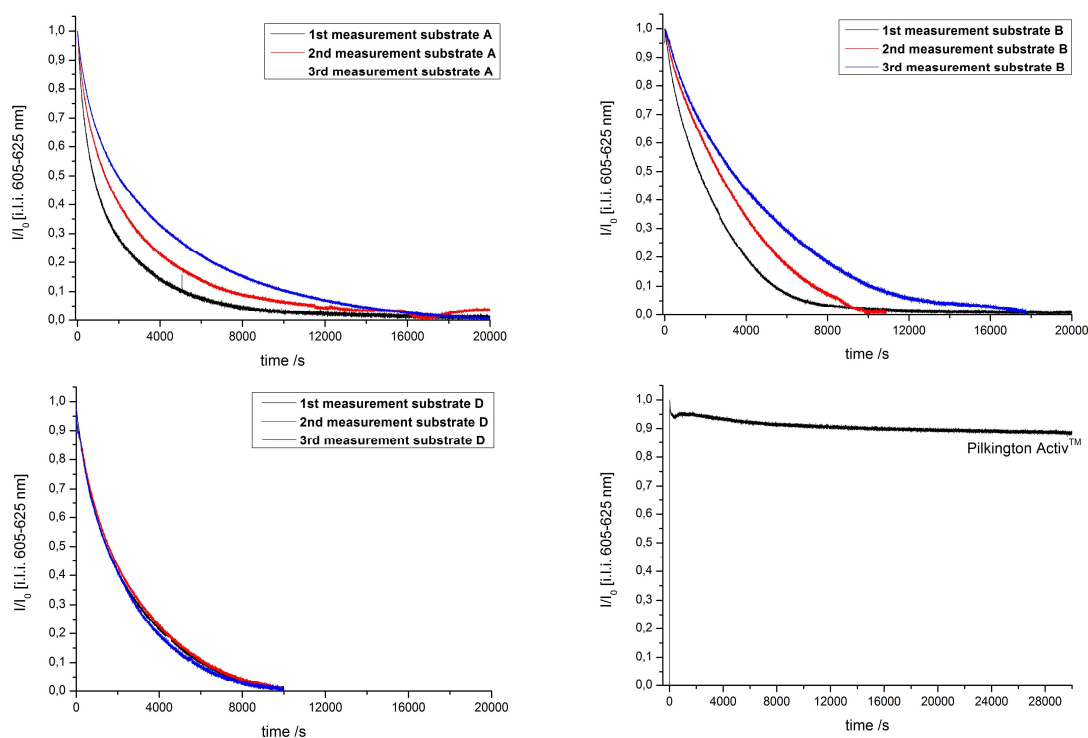


Figure 38. Luminescence results using the new developed solid state luminescent dye method <sup>[244]</sup>. A, B and D: on IAD substrate coated with 20 nm of dye. These substrates were used for a round robin test, in which every substrate was measured three times. Right bottom: no activity of commercial Pilkington Activ™.

The very active IAD samples were able to reduce the luminescence intensity to zero within the measurement time (Figure 38). The characteristic emission lines of the europium complex vanish completely, which expresses a total decomposition of the dye layer.

While the mechanism of the solid state luminescent dye method is not totally cleared, there is proposal that the decay of the dye luminescence is based on the photocatalytic effect.

### 5.2.3. Photocatalytic performances using ‘Reduction of NO<sub>x</sub>’ and Acetaldehyde

The photocatalytic activity of samples from earlier optimization procedure was tested to determine the degradation of NO and acetaldehyde, and was carried out at the University of Hanover by a developed research group consisting of Prof. D. Bahnemann.

Samples created via four different processes, all sized 50 x 100 mm<sup>2</sup>, were used to determine their photocatalytic activity by the degradation of NO and acetaldehyde under UV (A) tested irradiation. These four processes are A: conventional without IAD (Process I), B: IBS (Process II), C: (Process II) and D: Process IV (IAD, CC-105). Before measurements were taken, all samples were preconditioned for 7 days under 1 mW/cm<sup>2</sup> UV-A light.

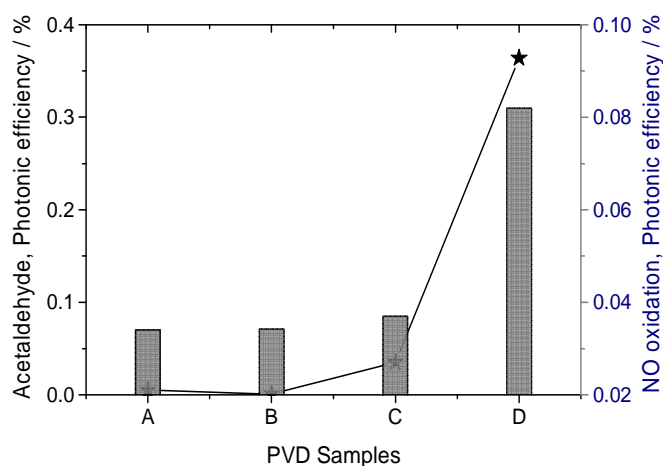
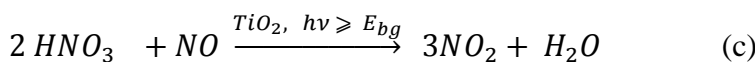
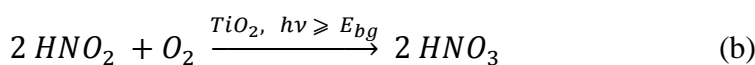
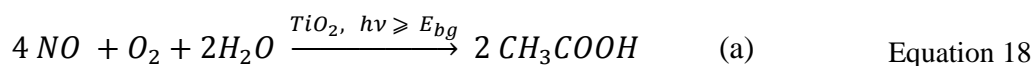


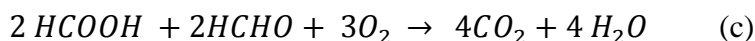
Figure 39. The photocatalytic performance results from *D-TOX*, *c/o Inst. f. technische Chemie, Hannover*. Photocatalytic NO oxidation is measured with an NO content of 1 ppm and a flow rate of 3 L / min. An analysis is performed with a NO/NO<sub>2</sub>-Analysator containing a fluorescence detector with an NO detection limit of 1 ppb. Photocatalytic oxidation of acetaldehyde is measured with an acetaldehyde content of 1 ppm and a flow rate of 1 L / min. An analysis is performed with a capillary gas chromatograph containing a photoionization detector with an acetaldehyde detection limit of 1 ppb.

The titania-sensitised, photocatalytic oxidation of NO proceeds to nitric acid, via nitrous acid and a radical based mechanism<sup>[245-247]</sup>. The key photocatalytic reactions are illustrated in Equation 18(a) and Equation 18(b).

Recent work<sup>[248]</sup> reveals that the accumulation of nitric acid on the surface promotes its photocatalysed reaction with NO that generates the toxic product NO<sub>2</sub>, Equation 18 (c).



Other recent work<sup>[249]</sup> indicates that the acetaldehyde is first oxidised to acetic acid (Equation 19a) and then to formic acid, formaldehyde (the acids being adsorbed onto the surface of the titania) (Equation 19b) and then, finally to CO<sub>2</sub> (Equation 19c):



Kinetics of a heterogeneous photocatalytic reaction is greatly influenced by two major factors: the concentration of the substrate of the interest and the efficiency of charge separation in photocatalyst. Several groups have reported on kinetic studies of the gas-phase heterogeneous photocatalytic reactions<sup>[249]</sup>. In this work, the effects of the adsorption affinity of substrates and the efficiency of charge separation in the photocatalyst on the kinetics of the photocatalytic reactions were investigated. In this regard, three gaseous compounds: acetaldehyde, and nitric acid were picked up as model compounds. They were chosen because of its properties, and they can be considered as representatives compounds, respectively.

After the coating processes were applied to the substrates, they were exchanged with other research partners. Resulting from this exchange, multiple tests were utilized and therefore there was an expectation of either reproducibility of the luminescence loss or a reduced luminescence loss from the deactivation of the substrate. These IAD samples also display the photocatalytic performance as previously observed (see Chapter 5.1). One of the difficulties facing researchers working with qualification methods, that there is still-as-yet no reliably defined and readily available photocatalytic substrate standard, can be solved by these IAD samples. The developed luminescence method can deliver a new method for assessing self-cleaning properties.

The methods of photocatalytic measurements depend on the same principle; they all monitor decomposition of various kinds of model pollutants. They may be gaseous like nitric oxide, liquide or dissolved in water like methylene blue or applied on the sample surface solid film like stearic acid.

### 5.3 Photocatalytic Disinfection and Microbiological Analysis

The experimental set-up for microbial tests using *Sarcina Lutea* as spherical Gram-positive bacteria has been described in-depth in Chapter 3, Experimental. *Sarcina Lutea* is yellow when grown nutrient agar. The microbial evaluation carried using *Sarcinia Lutea* (*Micrococcus Luteus*) in 7 hours with a distinct 5-6-log reduction of the cell count showed high inactivation of microorganism on TiO<sub>2</sub> thin films deposited with PVD-IAD, which proves that the films have a good antimicrobial efficiency.

These results were compared with reference kept in the dark. The results show that *Sarcina Lutea* survived in the dark on all of the surfaces. Most of the studies have concluded that the main mechanism for the killing was HO $\cdot$  attack and lipid peroxidation reaction [73, 248]. The presence of UV/TiO $_2$  in the membrane photocatalytic destroys the microorganism. In the presence of oxygen and water, highly reactive OH-radicals are generated by IAD thin films and ultraviolet exposure. This present study investigated the disinfection of bacteria, with the experimental set-parameters summarized in Table 6 and Figure 40 illustrating this inactivation. The temperature was kept at 350 °C, and the thickness at 300 nm. (More details see Info Appendix 5).

Table 6. Antibacterial study of IAD optimized process (VI)

Sample	Time [h]	Process & Position	
		left	right
<i>a1</i>	7	IAD, 30 sccm , 2 A	in dark
<i>a2</i>	12	IAD, 30 sccm, 2 A	in dark
<i>a3</i>	24	IAD, 30 sccm, 2 A	in dark
<i>a4</i>	12	IAD, 30 sccm, 4 A	-
<i>a5</i>	24	IAD, 30 sccm, 4 A	uncoated
<i>b1</i>	7	IAD, 40 sccm , 2 A	-
<i>b2</i>	12	IAD, 40 sccm, 2 A	in dark
<i>b3</i>	24	IAD, 40 sccm, 2 A	uncoated
<i>b4</i>	12	IAD, 40 sccm, 4 A	-
<i>b5</i>	24	IAD, 40 sccm, 4 A	uncoated
<i>b6</i>	24	IAD, 40 sccm, 4 A	uncoated

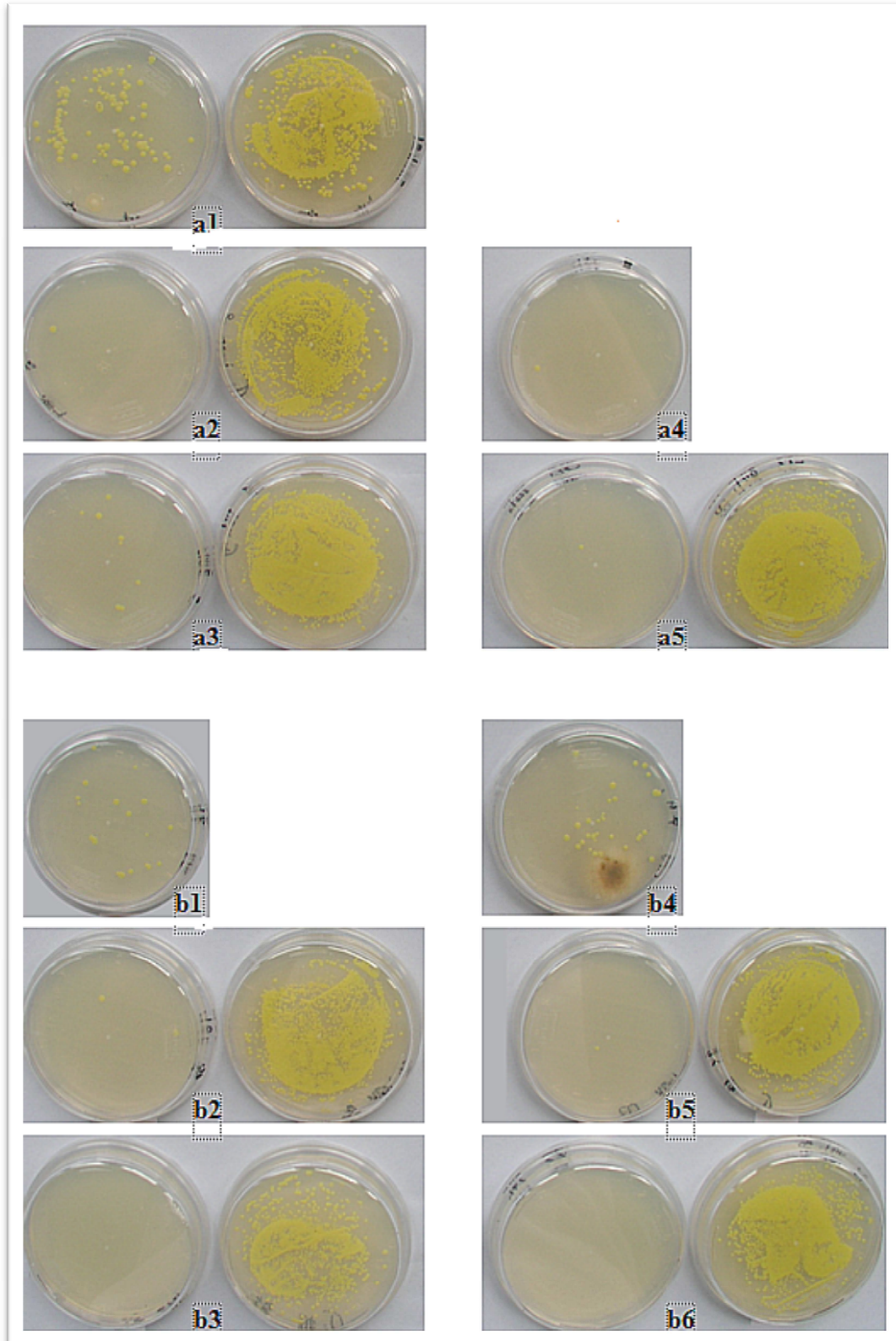


Figure 40. Photographic representations of Titania samples. 'high temperature' refers to 350 °C. (a) Inactivating the test organisms in three stages, after 7, 12 and 24 hours. The samples were coated at high temperature and 30 sccm oxygen flow. (b): Inactivating the test organisms after 7, 12 and 24 hours. The samples were coated at high temperature and 40 sccm oxygen flow.



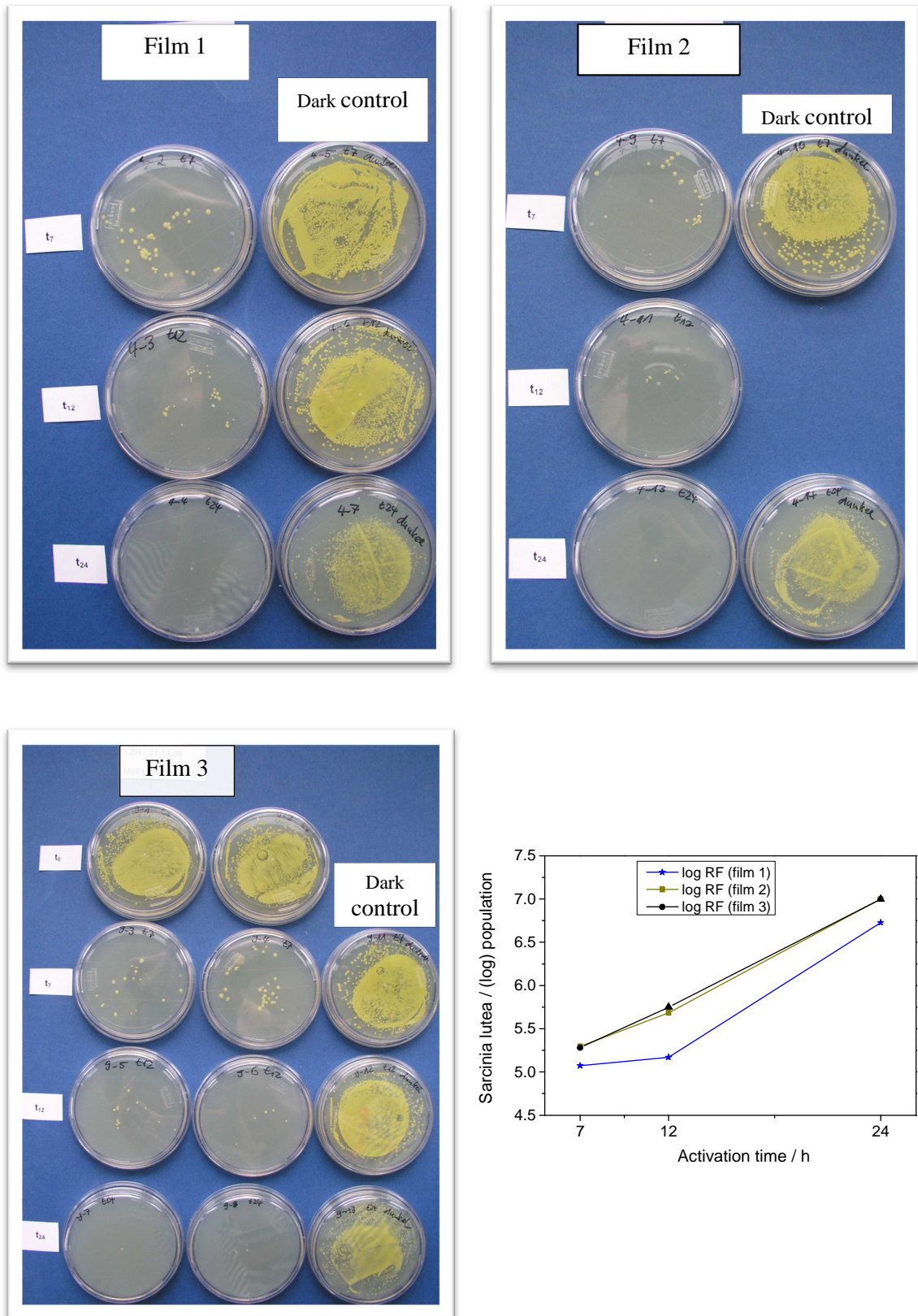


Figure 41. log population results for *Sarcinia Lutea* on IAD samples Film 1 (250 °C, 2 A, 40 sccm, 500 nm); Film 2 (250 °C, 4 A, 40 sccm, 500 nm); Film 3 (350 °C, 4 A, 40 sccm, 500 nm).

The photokilling effect of titanium dioxide thin film on bacteria was selected to be used on the model *Sarcinia Lutea*. Ultraviolet illumination applied alone did not affect the viability of bacteria, and all bacteria survived well in the absence of TiO<sub>2</sub> thin film. The formation of bacterial colonies on the TiO<sub>2</sub> surface decreased significantly. The resulting image of the microorganism in the presence of photocatalytic active films showed that nearly complete killing was achieved after 7 and 14 hours of UV illumination. The samples used without coating and coated in dark help for comparison. The Figure 40 shows that the 40 sccm is more suitable than 30 sccm, and the Figure 41 exhibits that 4 A more effective than 2 A at 250 °C, and more increase in temperature to 350 °C doesn't ameliorate considerably the photokilling.

As explained in Chapter 4, a redox system, along with oxygen and water, is formed on the surface of films upon its exposure to UV illumination. This entails separation of electrons ( $e^-$ ) and electron holes ( $h^+$ ). In the oxidative process, the electron holes play an important role as they generate highly reactive OH-radical from water<sup>[250]</sup>. These radicals are capable of removing germs and bacteria. This eradication of microorganisms is due to the oxidation effect of the surface and the reactive species that can be produced because of TiO<sub>2</sub>.

For possible antimicrobial use with real-time substrate heating or post annealing, currently required for available thin film deposition processes, photocatalytic titanium dioxide films have been extensively studied. Photocatalytic performance of the deposited specimens is tested with methylene blue solution, and antimicrobial efficacy is evaluated through the use of as industrial standard for better understanding the relation between photocatalytic effect and antimicrobial efficacy. The result shows that columnar TiO<sub>2</sub> film with an anatase phase structure can be prepared within a proper coating parameter range (see Chapter 6). The oxygen partial pressure and the ion doses (discharge current) favor the antimicrobial activity. As a result, the photocatalytic efficiency and the antimicrobial activity of the deposited film reaches their maximum potential when ion-source oxygen flow is high (30 to 40 sccm) and the ion-source current is increased (2 to 4 A). The presence of anatase phase is what determines the majority of the photocatalytic efficiency and antimicrobial activity of titania films.

Finally, this chapter shows that the different laboratory tests and different methods used give effective and promising comparative results for photocatalytic performance, even overcoming the problems of the challenging IAD process (Process V), as compared to other processes. This work demonstrates that optics prepared with both the conventional method, that being without ion-source assistance, and the IBS method are not photocatalytically active. These methods are used in the following chapters only as a reference for all previously defined coating methods.



## 6. Structure and Surface Properties of PVD Titania Thin Films

The understanding of surface and microstructure properties was one of the main aims of research, and the goal of surface analysis phase was to examine the morphology of the TiO<sub>2</sub> surfaces. This morphology study is useful to determine the correlation between the optical properties and photoactivity. A spectrophotometer (SPM) is a suitable device to correlate between transmission, reflection, and photoactivity. This characterization also requires measurements of the contact angles for hydrophilicity and hydrophobicity in conformity with the International Organization for Standardization (ISO), the United States Military Standard (MIL-STD), along with abrasion resistance and adhesive strength as per the environmental/Durability Tests.

After the coating process, the layers were examined to evaluate the basic photocatalytic characteristics. The optical characteristics of the thin films are determined by the process geometry, the source and reactive gas parameters, and the activation procedure. The most important aspect in the characterization process is to evaluate the morphology aspect of transparent monolayers. Another important factor to consider is the microstructure, with the former determining optical absorption and the latter affecting the photocatalytic properties and scattering loss of the layers.

### 6.1 Investigation of XRD Crystal Analysis

For XRD crystal analysis and TEM investigation, the following results offer the investigation into the basis of the optimization of coating processes. Already shown in Chapter 2, a review of relevant literature, the evaporation rates for IAD all experiments can be quite high, namely on the order of 10 nm/s. It is possible to obtain crystalline (anatase or rutile) thin films by either heating the substrate during deposition or annealing after deposition. The thin films' microstructure can be managed by the starting materials, the substrate temperature<sup>[104,251]</sup>, the angle of incidence<sup>[6]</sup>, the deposition (O<sub>2</sub>) pressure and the evaporation rate<sup>[252]</sup>. Studies looking at a variety of parameters are given in L. Wanga's work<sup>[208]</sup>. To control the thin film microstructure, a typical IAD layer on a hot substrate was employed. For high crystallinity, the following results are discussed:

- Annealing at temperatures between 300 and 500 °C is needed to obtain crystalline anatase films<sup>[253, 254]</sup>.
- An advantage of PVD is that the process conditions can be controlled to yield crystalline thin films without annealed substrate<sup>[90]</sup>.

- Once diminishing the grain size below ca 10 to 20 nm the degree of crystallinity is strictly reduced due to the high surface to bulk ratio, ever since the grain boundaries represent a high defect state. The photocatalytic activity of such films increases by a factor of almost 3 when crystallizing anatase <sup>[255]</sup>, confirming that a higher degree of crystallinity is indeed beneficial.
- Na<sup>+</sup> can inhibit crystallization by increasing the temperature needed for crystallization <sup>[205]</sup>.
- Often the grain size and/or crystallinity of the thin films are not clearly defined or have a large spread, so that dependencies cannot be defined well. Crystallinity of the thin film increases by increasing the number of crystallites as well as their size. Since the grain surface can be taken as a highly defective, non-crystalline phase the crystallinity increases with grain size (lower surface to volume zero).
- Amorphous or nanocrystalline films are expected to form at low particle energies and low substrate temperatures, which is confirmed by experimental results <sup>[256-260]</sup>.

Figure 42 represents the typical X-ray spectrum of TiO<sub>2</sub> coated using the IAD process.

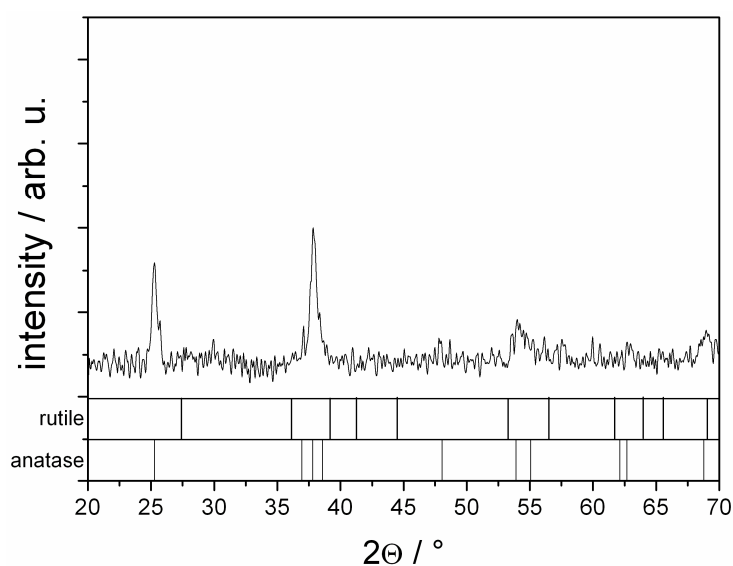


Figure 42. Typical X-ray diffraction spectrum with corrected background for TiO<sub>2</sub> layers coated using IAD.

The result of the IAD layer shows a high diffraction reflex (004) and depicts a preferential crystal orientation. The X-ray diffractions show that the microstructure is anatase, with the anatase crystal structure having diffraction reflexes (101) for  $2\theta = 25^\circ$  and (004) for  $2\theta = 37.7^\circ$ . The lattice distances are 3.50 Å and 1.87 Å, and are in accordance with ones obtained from anatase (101) and (200). These diffraction reflexes are in agreement with those documented in the literature (XRD data base: ICDD PDF 21-1272) for lattice distances of 3.52 Å and 1.89 Å.

The above results are caused by the influence of ions or high energy neutral particles, meaning that the suitable evaporation procedures are those that work with oxidic raw materials or Ti-metal combined with ion-sources. Several process concepts, with particular attention given to the deposition of TiO<sub>2</sub> layers during the production of high optical function layer systems (Chapter 7). This investigation showed that there was a good possibility to adapt process concepts in the optical functional layers range. Additionally, An allocation of the 2 theta shift at 39°, high (004) reflex, was also observed in an external XRD investigation (Figure Appendix IV).

## 6.2 TEM and DS Examination

Crystal analysis is illustrated in the following set of pictures, Figure 43.

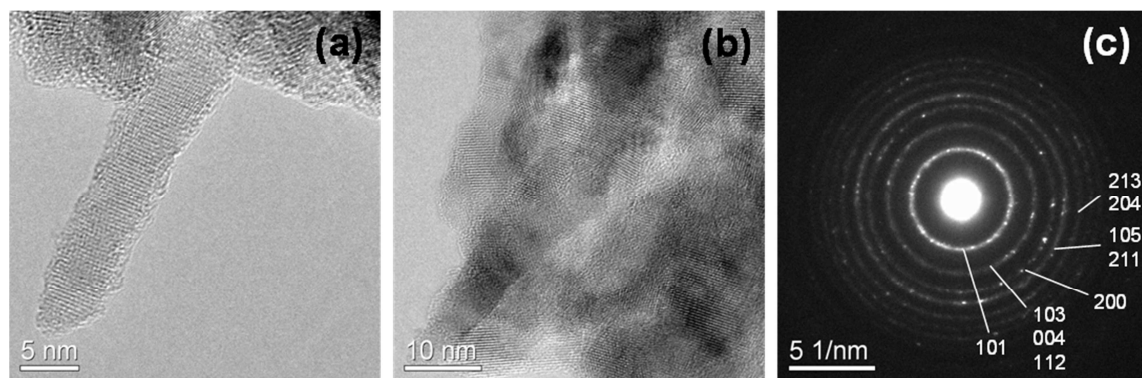


Figure 43. TEM investigations (A, B) and SAED admission (C) of IAD with CC-105 optics coated at 250 °C, 30 sccm and 300 nm.

Shown above (A) are nanocrystals with diameters of 5 to 10 nm, and the nanostructure of glass coated with titanium dioxide is clearly recognizable due to its crystal orientation in above (B).

The sequence of the Debye Scherrer rings in Figure 43 (C) is typical for TiO<sub>2</sub> anatase, as the rings (101) and (200) are recognized clearly in the process. All rings are well-developed and show a high portion of oriented crystals, which is made obvious on the basis of the ring (101).

Using a transmission electron microscope and SAED, the captured images of the surface microscope shows that IAD coating under defined process parameters (250 °C, 30 sccm and 300 nm) enabled high crystallinity, i.e. more than 95 % of crystallite phase and a high photo activity due to the presence of high anatase portion.

## 6.3 Modification of Surface Morphology

The two most important factors that add value to a coated surface are the adhesive strength and the durability, both of which make the coated surface more practical. It is essential for substrates to undergo appropriate preconditioning processes in order to gain these characteristics. These preconditioning processes can have an impact on the crystallinity and surface morphology of the thin films and can also be carried out by conventional means such as lacquer finish, the manual usage of chemicals, and plasma etching. The latter two conventional processes, application of chemicals and plasma etching, were investigated. In order to analyze the microstructure and morphology of the surface, the following techniques were employed: Scanning electron microscope (SEM), Atomic force microscopy (AFM), Qualitative chemical Analysis (EDX), X-Ray Diffraction (XRD) and Debye Scherrer (DS), Transmission electron microscopy (TEM) and Contact Angle Measurement (CAM).

### 6.3.1 Energy-Dispersive X-ray Spectroscopy Chemical Analysis

Both Menzel glass and Suprasil glass were used as substrates for the EDX chemical analysis. Suprasil substrates were utilized to avoid the negative impact of impurities, such as sodium and potassium, on the photocatalysis.

The EDX diagrams in Figure 44 (a, b) show the chemical composition, layer and substrate, of TiO<sub>2</sub> layers on Menzel and Suprasil quartz samples.

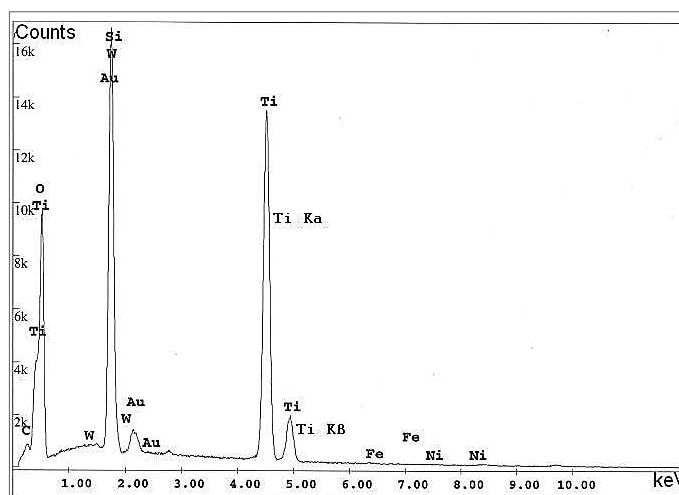


Figure 44.(a) Measuring curves of the EDX analysis of titania thin films with IAD Process V using CC-105. Substrate: Suprasil glass.

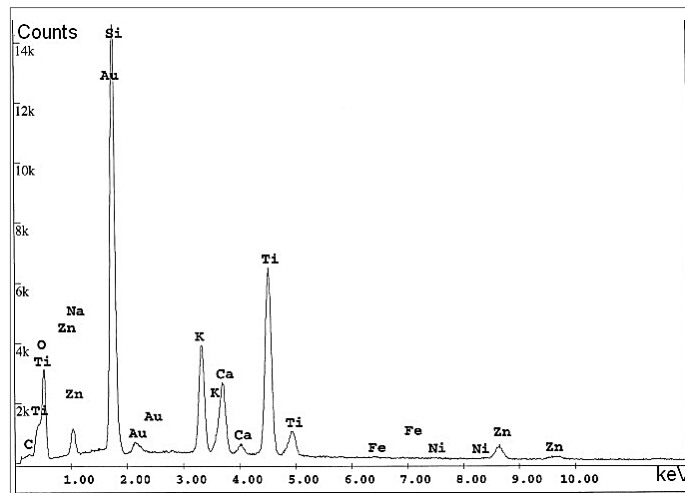


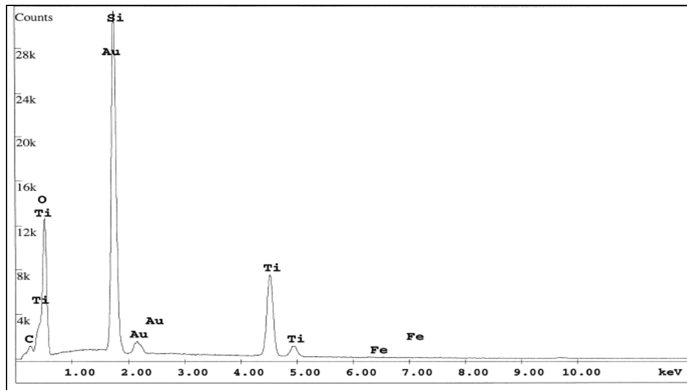
Figure 44 (b). Measuring curves of the EDX analysis of two titania thin films with IAD Process V using CC-105. Substrate: Menzel glass.

The chemical impurity comparison of Suprasil and Menzel quartz glass in the graphs demonstrates that the two types provide different results.

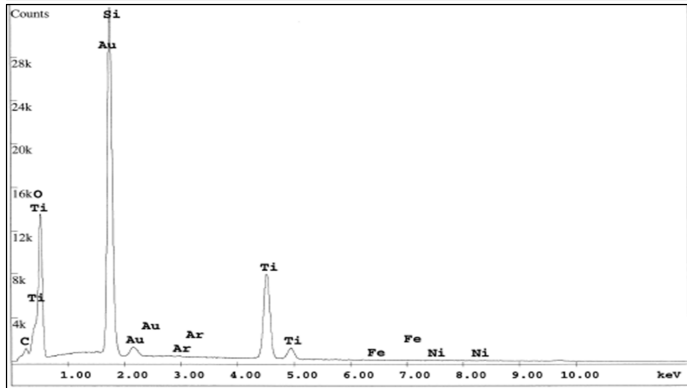
EDX analysis of the two uncoated substrates confirms the presence of various elements on Menzel glass, such as Na, K, and Ca. These chemical impurities limit the use of Menzel where high purity and OH content affects the morphological and optics properties.

The presence of such elements affects the coating process, and also the photocatalytic ability of a surface (Figure 45). Pure quartz Suprasil was found to be free of these elements, which resulted in a higher visual quality as compared to Menzel, making it more suitable for use when high optical quality is desired. Though Menzel has a lower visual quality, it does have its own benefits as a borosilicate glass, namely a resistance to chemicals. It is also more commercially available and there is little difference in the anti-bacterial characteristics and morphological properties of the two. This makes Menzel useful for certain purposes and is a good choice when comparing different substrates.

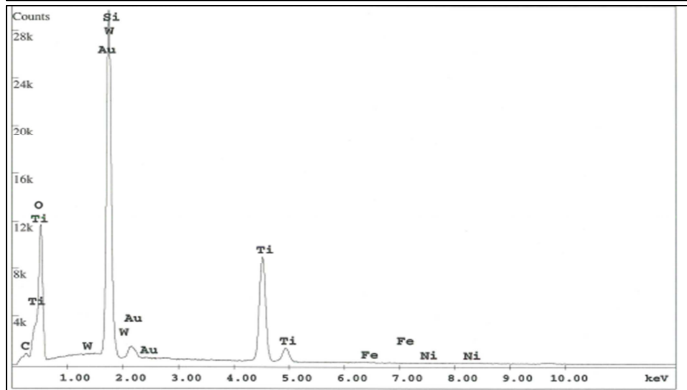
It has been discovered that the photocatalytic activities of  $\text{TiO}_2$  PVD thin films are reliant on the type of substrate that is used. The presence of argon in the EDX spectra of films coated using the APSpro ion-source, Process II, is due to argon being used as a reactive gas.



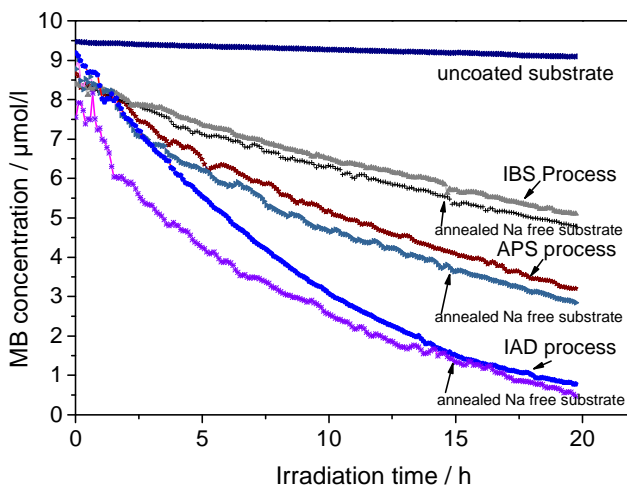
(a) Process II:  
APSpro investigation  
(250 °C, 300 nm, Bias 60).



(b) Process III:  
IBS deposition  
(250 °C, 300 nm).



(c) Process V:  
IAD with Denton CC-105 (250  
°C, 300 nm, 25 sccm, 2.5 A).



Investigated coating concepts  
in comparison. Influence of Na  
free substrate on the  
demineralization process

Figure 45. Energy–Dispersive X-ray Spectroscopy Chemical Analysis.

A suspected influence on the activity of the film was the ions diffusing from the substrate into the film. The decline in photocatalytic activity was associated to the effect of Na on the grain growth in the thin film upon different processes<sup>[204]</sup>.

Na may inhibit the crystallization of anatase while also increasing the particle size in the film. It is thought that, by annealing films, Na creates a shallow donor state in TiO<sub>2</sub>, making it an unlikely recombination center.

All of this makes it possible to conclude that Na in the films, by changing the particle size and not by acting as recombination center, affects the photocatalytic activity. This clarification leads to using Suprasil quartz for the analysis in Chapter 7.

Due to this influence, most investigators wish to avoid incorporation of Na when a heat treatment step is needed after deposition, and so use glass free substrates<sup>[194]</sup>.

From the above it can be concluded that the best strategy regarding the influence of Na on the of TiO<sub>2</sub> properties is by the correct selection of glass substrate to escape Na-contamination.

### 6.3.2 SEM Analysis

The SEM pictures shown in Figure 46 reveal that samples deposited using conventional method, APSpro ion-source and Denton CC-104 and ion-beam sputtering process exhibit small grain sizes.

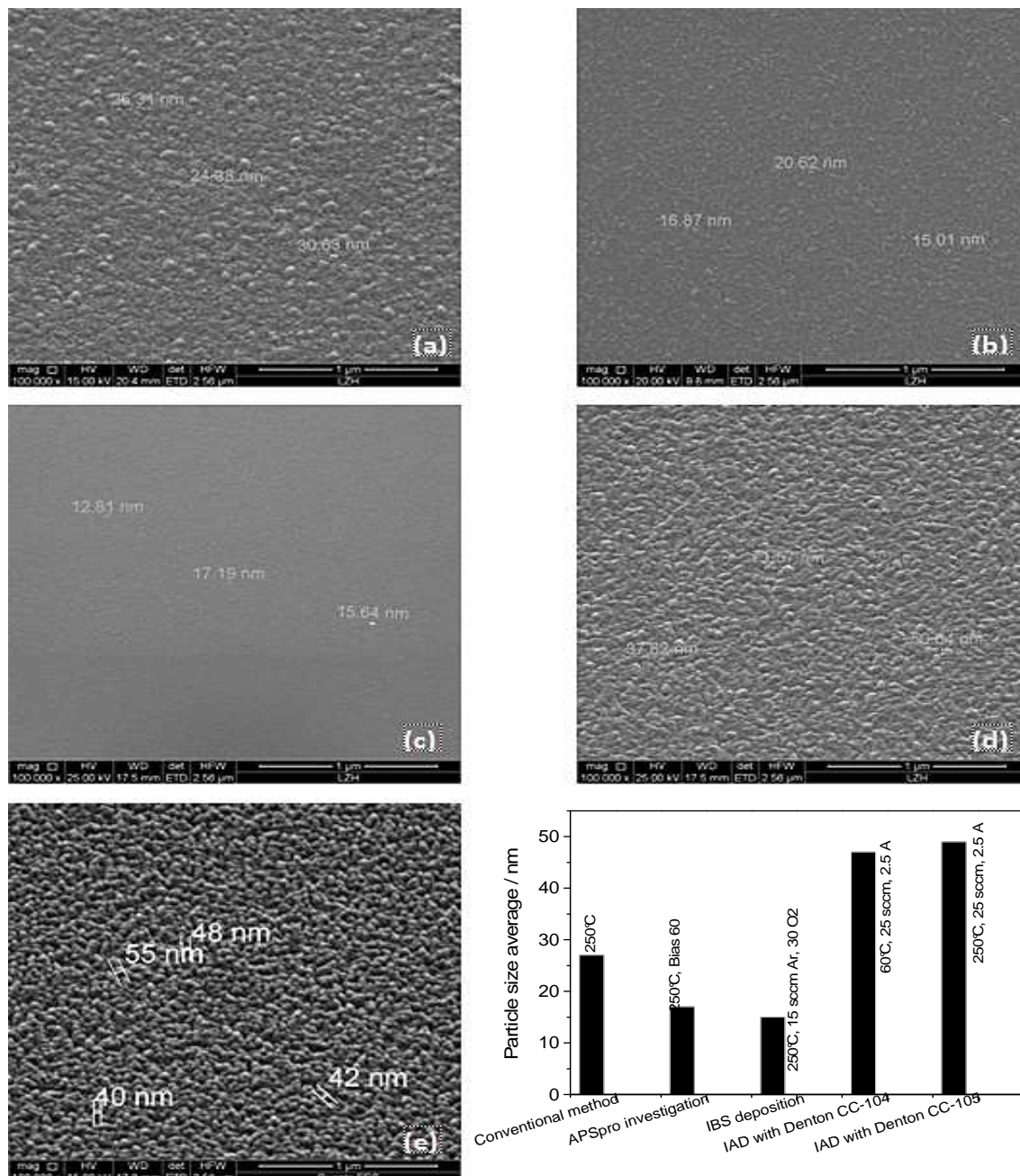


Figure 46. SEM Results of different deposition processes. (a) Process I: Conventional method (250 °C, 300 nm). (b) Process II: APSpro investigation (250 °C, 300 nm, Bias 60). (c) Process III: IBS deposition (250 °C, 300 nm, with 15 sccm Ar, 30 sccm O<sub>2</sub>). (d) Process IV: IAD with Denton CC-104 (60 °C, 300 nm, 25 sccm, 2.5 A). (e) Process V: IAD with Denton CC-105 (250 °C, 300 nm, 25 sccm, 2.5 A).



However, if the films were deposited using an IAD e-beam evaporator with CC-105, they showed a bigger grain size. It is possible to retain the particle size of Merck's commercially available Titania P25. Commercially available anatase is typically less than 50 nm in size. These particles have a band gap of 3.2 eV, corresponding to a UV wavelength of 385 nm.

The cross section SEM results obtained for the deposition processes are shown in the following figures. Their images are representative of various deposition set for a comparison between the optimized process (Process VI) and other processes.

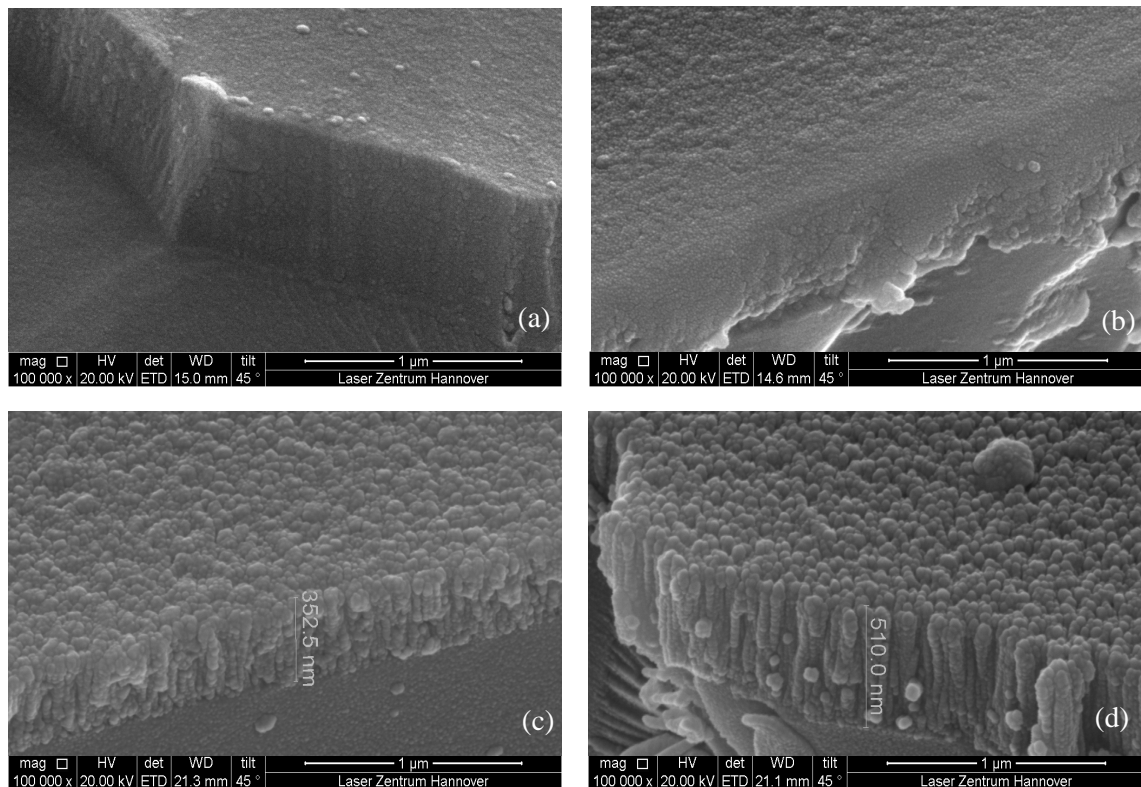


Figure 47. Representative cross section comparison between different processes. (a): using APSpro (250 °C, 300 nm, Bias 60); (Pr. II), (b): Ion sputtering technology (250 °C, 300 nm, with 15 sccm Ar, 30 sccm O<sub>2</sub>); (Pr. III), (c): IAD (Pr.V) (150 °C, 300 nm, 25 sccm, 2.5 A) and (d): optimized IAD (Pr. VI). (350 °C, 300 nm, 23 sccm, 2.5 A)

Figure 47 shows a SEM cross-section of the columnar structure of the deposited titania by different process parameters. The IAD films feature uniform cross-sectional structures for IAD processes. Additionally, the average particle size of the columnar structure was calculated using the values obtained from several SEM micrographs. The morphology of a titania thin film is facilitated by its roughness. Films deposited by APSpro and by IBS show a smoother surface, and therefore might be more hydrophobic than the films deposited by IAD process as shown in 6.1.3 and in Chapter 7.

The ion flux value of the samples consistency does not play as big a role in this regard as it does for other coating types. Comparatively low energy (~300 eV) ions are more desirable than higher energy ions when attempting to minimize substrate sputtering while still maintaining enough energetic activity to result in the above effects.

The ion-source used grants a monoenergetic, neutralized ion beam that is focused coated substrates. This configuration grants several additional features over conventional plasma preparations providing ion bombardment of the substrate, including intrinsic control through the ion beam, the independence of the bombardment process from the deposition process, and the ability to precisely measure all critical deposition parameters. Another characteristic regarding IAD is that substrate cleaning can be quickly accomplished prior to deposition by controlling the appropriate gas through the ion-source.

SEM analysis reveals that the samples deposited using Ion Beam Sputtering have a smoother surface than samples deposited using a thermal evaporation method, as shown in Figure 46. From the results it can also be seen that samples deposited using IAD can produce a surface with a rough morphology, and at approximately 250 °C, the IAD process improves the photocatalytic property of the surface when compared to the IAD process at approximately 60 °C.

If a thin film has a flat surface and a fully dense structure, the geometrical area of the substrate equals the active surface area. If it has a rough surface, however, it will have a larger area gaining more photocatalytic activity. It is possible to approximate this area increase on the supposition that the surface consist of a collection of semi-spheres <sup>[3]</sup>.

The layers appeared with a granular morphology, which is of interest as this increases their photocatalytic activity. The analytical methods of SEM and AFM characterized the morphological properties. It was found by scanning electron microscopy that all TiO<sub>2</sub> thin films were homogeneous and continuous. It is possible for smooth TiO<sub>2</sub> films (Process II and III) to offer numerous useful optical and corrosion-protective properties, and in addition the roughness on TiO<sub>2</sub> films (Process IV and V) can improve the inherent photocatalytic activity. TiO<sub>2</sub> films prepared with IBS (Process II) showed poor photocatalytic activities because of the defect level generation caused by the bombardment of the high-energy particles on the growing film surface.

### **6.3.3 Scanning Probe Microscopy by Means of AFM**

To analysis the optical surface quality, all the titania films were 300 nm thick. To examine the sample surfaces, AFM was used due to its high resolution, of 1 μm. Figure 48 shows two-dimensional TiO<sub>2</sub> film pictures deposited with ion beam assistance for samples from cold and heated processes with a varying reactive oxygen level and ion current assistance. It obvious that

the surfaces of the films exhibited a high degree of roughness and the films became rougher when the deposition temperature increased. To compare between coating with and without ion-source assistance, the three-dimensional AFM photos below show the surface structure and the densification of operated films.

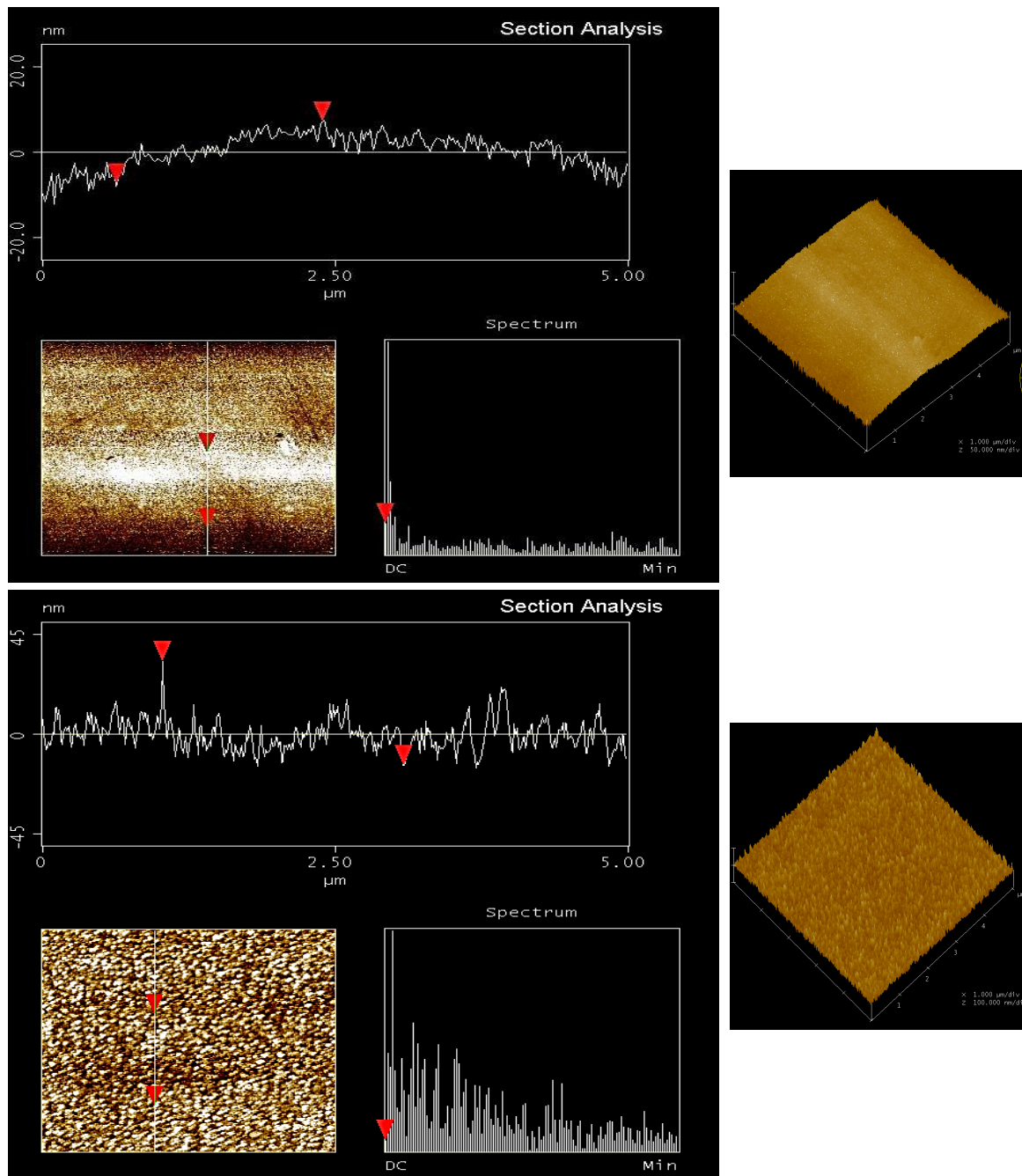


Figure 48. AFM investigation for films with and without Denton CC-105 for the scan area of  $5\ \mu\text{m} \times 5\ \mu\text{m}$ . Left: Conventional method without IAD ( $250\ ^\circ\text{C}$ ,  $300\ \text{nm}$ ). Right: with IAD method ( $250\ ^\circ\text{C}$ ,  $300\ \text{nm}$ ).

An area of  $2\ \mu\text{m} \times 2\ \mu\text{m}$  was scanned for titania layers extracted from the AFM images to contrast the grain sizes and roughness of titania coatings created both with and without IAD. Two essential

pieces of information were identified from this comparison, the first of which being that the width of the column is approximately 6 nm for the conventional process and 26 nm for the heated IAD sample. The second point gained was the rough mean square (*RMS*), given in formula as such:

$$RMS = \sqrt{\frac{\sum_{n=1}^N \sum_{m=1}^M Z_{nm}^2}{NM}} \quad \text{Equation 20}$$

where  $Z_{nm}$  is the height of column extracted from AFM data's. That *RMS* depends strongly on the scan size gives an indication that the surface has fractal behavior<sup>[261]</sup>.

IAD-TiO<sub>2</sub> are rougher, having a *RMS* higher than 6 nm while also displaying a more open surface than conventional TiO<sub>2</sub> layers, whose roughness is typically less than 3.2 nm.

Figure 48 shows the difference aspects of 'Section Analysis' of samples heat-treated, for the titania using ion assisted source. The coating with APS source is amorphous. It can be concluded that deposition with Denton CC-104, the particles of titanium dioxide remain more agglomerated, and the crystallization rate of titania is reduced. These AFM pictures show that the morphology of the layers is influenced drastically on the deposition process used.

The results illustrated in both Figure 46 and Figure 48, clearly show the difference between the conventional method and the IAD process. It can be seen from an SEM investigation of TiO<sub>2</sub> film without Ion Beam Assistance that the grain size exhibits 30 to 110 nm. This demonstrates that the lateral grain size on the layer surface amounts to 20 to 80 nm for the films deposited with Ion Beam Assistance, which is smaller when compared to the conventional technique.

Additionally, the average roughness value is between 4 to 8 nm, shown in Figure 48, left, and between 15 to 30 nm, Figure 48, right, which also varied depending on the type of ion-source used and the ion-source parameters.

Generally, the 300 nm thick layers investigated are significantly smoother with the conventional method and rougher with the ion assisted deposition method, which is indispensable for the hydrophilicity effect and an increase of photocatalytic activity.

In general, this same observation of a smooth surface can be made using IBS technology, Process III (Figure 47b). It was observed that the amorphous TiO<sub>2</sub> films have a very smooth surface. AFM images shown in Figure 48 are for Process V, which is the deposition method with a varying ion-source current, reactive gas flow, and substrate temperature. It was seen from the TiO<sub>2</sub> films that they had a rough surface with uniform grains and mainly spherical particles. The surface

morphology reveals the nanocrystalline TiO<sub>2</sub> grains; creating a denser film with increasing temperature. An ion-assistance method with a high oxygen flow value conveys a significant change in the structure and at 2 A and 40 sccm the grains get larger but the basic structure remains unchanged.

Rough surfaces comprised of distinguishable grains of the anatase phase are demonstrated by AFM patterns.

An alteration in the grain size is needed to gain a larger surface area for a TiO<sub>2</sub> thin film. The majority of photocatalytic materials have a grain or crystallite size under 100 nm, making them nanocrystalline. Defective lattice producing grain boundaries start to dominate the material when the crystallite size is below approximately 10 nm<sup>[262]</sup>. As this result in trap sites for the photogenerated charge carriers, which will then increase their probability of recombination, imperfections in the lattice structure are detrimental to the photocatalytic activity. This is the reason that an highly defective amorphous state is expected to show either no or very little photocatalytic activity<sup>[262, 263]</sup>.

In addition, surface area is always a key factor in heterogeneous catalysis process. It is known from AFM pictures that the crystallite size is smaller for the TiO<sub>2</sub> films deposited with the Ion Beam Assisted Process, and so can be concluded that the surface area of the TiO<sub>2</sub> films with Ion Beam Assisted Deposition is larger than those deposited without Ion Beam Assistance.



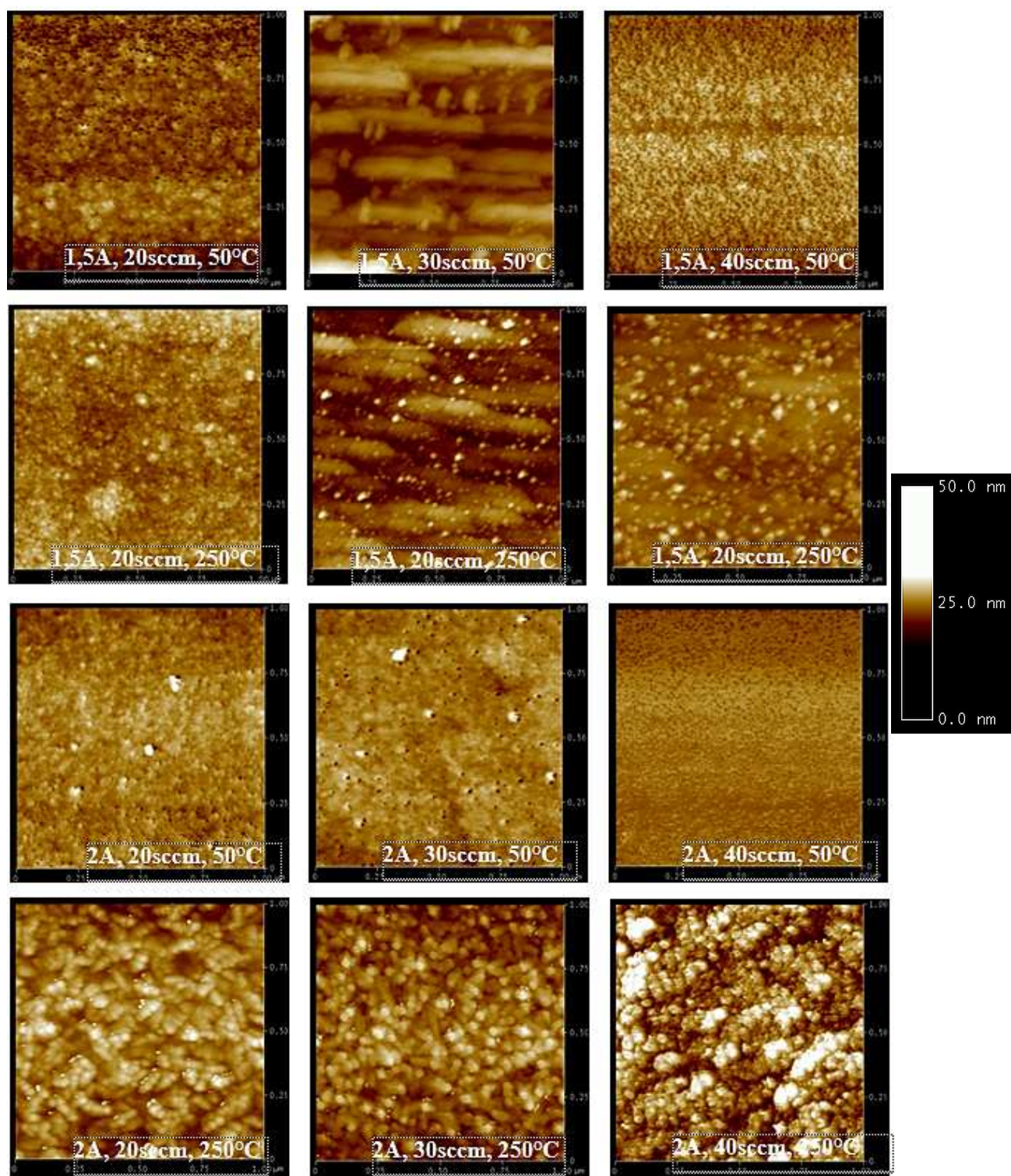


Figure 49. Two-dimensional Atomic Force Microscopy results of IAD samples at a scan size of  $1 \times 1 \mu\text{m}$ . in height mode. Tapping- mode AFM images were taken for 300 nm thick single titania layer. Oxygen flow was varied between 20 to 40 sccm, the discharge current between 1.5 to 2 A, and the substrate temperature: cold and heated at 250 °C. The scanned area was  $1 \mu\text{m}^2$ .

The AFM image above (Figure 49) depicts the surface with different grain sizes. Although the  $\text{TiO}_2$  grains sizes reach 2 Å at 20 to 40 sccm at 250 °C, they have smaller proportions in either cold coated film or with 1.5 Å. AFM study of the imaged region reveals that grain sizes differ from low oxygen assistance to high values, and it was also discerned that there was a lack of cracks and a non-compact morphology of the deposited  $\text{TiO}_2$  film. Below, the influences of thickness, temperature and discharge voltage the roughness of the films are discussed.

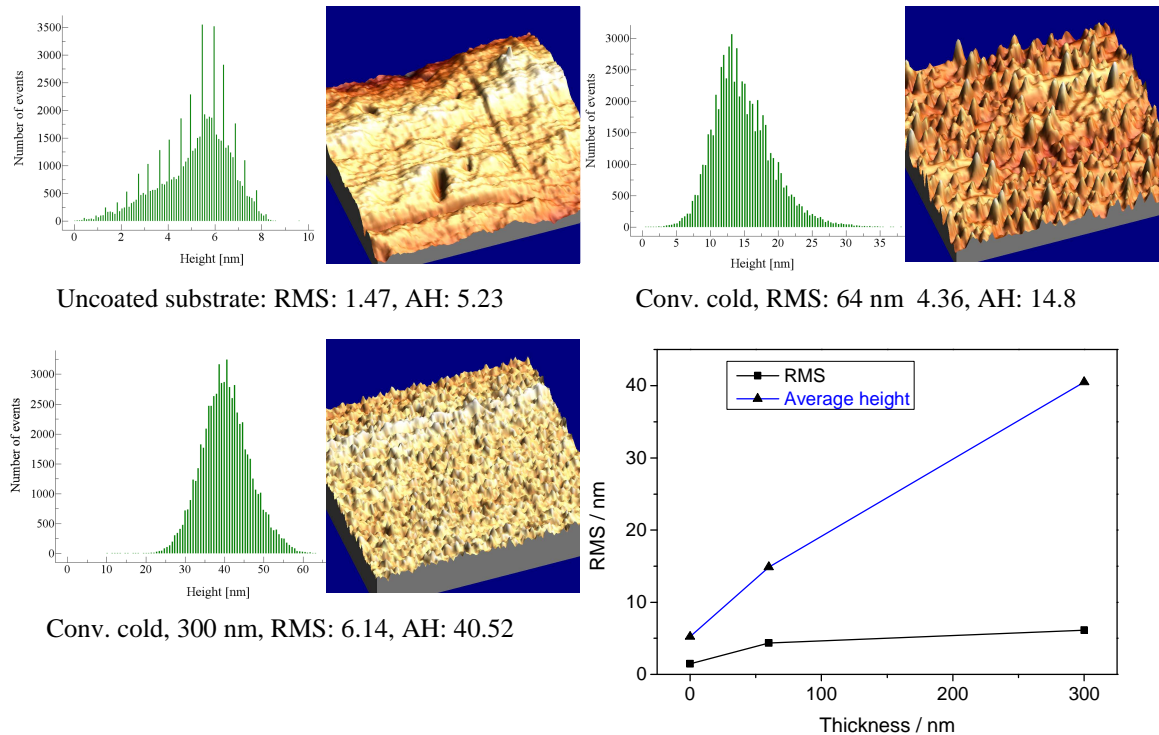


Figure 50. AFM study of reference samples: uncoated glass and titania film coated without IAD. Ironed surface:  $1 \mu\text{m}^2$ . RMS: roughness, AH: Average Height.

AFM studies have shown that an increase in process thickness causes considerably greater roughness. AFM pictures exhibits that deposited thin films with 30 sccm have nanocrystalline structure. Density of grains packing was four times bigger in cases of thin films deposited by 2 Å and high temperature of 250 °C ( $RMS$ : 10.54) as compared to thin films deposited at lower voltage (1.5 Å), and seven times higher than compared to a cold process.



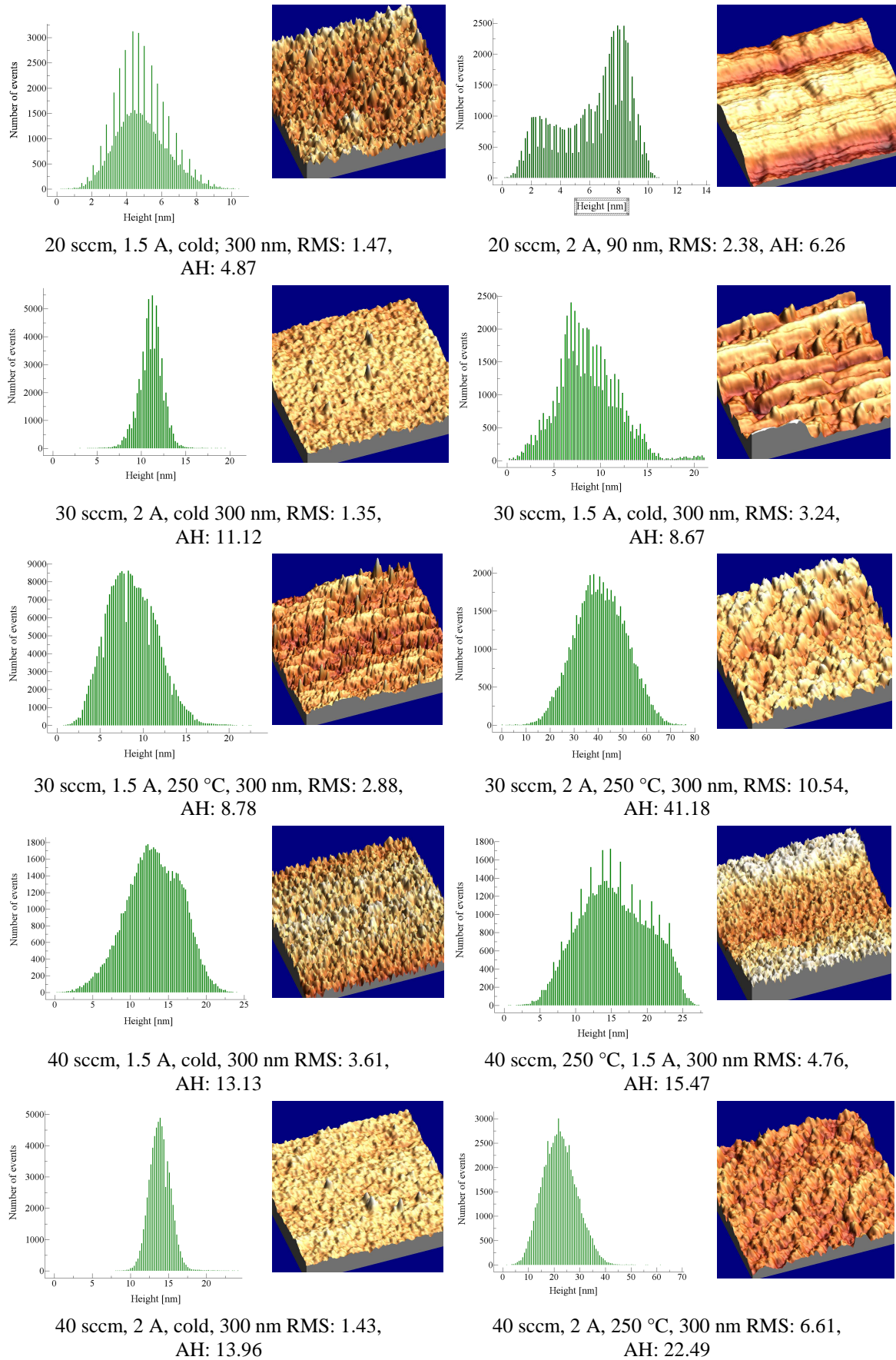


Figure 51. AFM study of IAD films for an ironed surface:  $1 \mu\text{m}^2$ . RMS: roughness, AH: Average Height.



When compared to thin films from IAD using 60 °C, 1.5 A and a thickness lower than 100 nm, a higher variation of the surface topography can be found for those TiO<sub>2</sub> films obtained from an IAD process with 250 °C, a thickness of 300 nm, and 2 A. These results were determined based on *RMS* (Root Mean Square) parameter as shown in Figure 52. Process V generated higher *RMS* values for TiO<sub>2</sub> thin films. The structure of Process V TiO<sub>2</sub> films are considerably more homogenous than those prepared via other processes (such as with a low temperature). Local minimum and maximum height values on AFM images, which have also been sharply outlined on histograms (Figure 51), may theoretically cause errors in the *RMS* value.

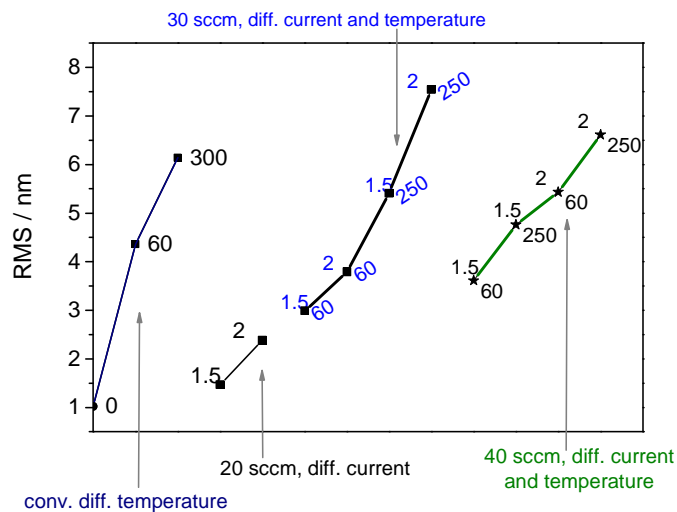


Figure 52 Influence of different coating parameters on TiO<sub>2</sub> film roughness when deposited via Process V (with IAD) and the conventional method.

As display in Figure 52, the *RMS* values' development similarly follows the previous discussed of AFM results in Figures Figure 48 and in Figure 49. The *RMS* values increase considerably from 1.43 to 7.5 nm when the temperature rises from 60 to 300 °C and the discharge voltage reaches 2 A. The reason for the increase in roughness is the growth of grain size and, theoretically, a process leading to rougher surfaces is more favorable for the adsorption of organic pollutants. A study of *section analysis* was performed on the AFM images, as shown in Figure Appendix V. The employment of all AFM investigations was carried out to perceive the surface and texture properties of the synthesized titania films.

This was so as to completely understand the surface morphologies reliance on the optimized parameters. Titania sample films are comprised of interconnected spherical nanoparticles. Whereas uniform and dense spherical grain-like structures at the same altitude compose the surface of the conventional and IBS processes, the IAD Processes films show rough structures of nanoparticle agglomerates. Through calculation of the related AFM images, the average grain sizes of TiO<sub>2</sub> particles (see Figure 46) are divided in two categories. The first category is 'low':

approximately 27 nm for conventional, 16 nm for APSpro, 16 nm for IBS. Category two is 'high': approximately 42 nm for IAD with CC-104 and 51 nm for IAD with CC-105, making them in agreement with the photocatalytic results previously gained in Chapter 5. To ascertain the photocatalytic activity other vital parameters in addition to grain size include the maximum height ( $R_{max}$ ), the average roughness value ( $R_a$ ) and the root mean ( $RMS$ ) of surface features (Figure 52 and Figure Appendix V). IAD Processes IV and V provided a comparatively higher  $RMS$ , especially for high temperatures, and lower values were observed for conventional and IBS processes.

The IAD Processes have a rougher surface and a higher particle size, making it favorable for the adsorption of organic pollutants. It can be suggested from these results that the films exhibiting various photocatalytic and morphological aspects can be synthesized at different designed experiment conditions.

#### 6.3.4 Influence of the Process Parameters on Hydrophilicity

Determining the hydrophilic effect is essential for photoactivity. Thus, contact angle measurements were carried out to determine the hydrophilicity of the samples and correlated to the results of the MB demineralization.

Table 7. Comparisons of the contact angular measurement

Sample #	O <sub>2</sub> / sccm	current / A	Temperature / °C (±10 °C)
S5	20	1.5	60
S11		2	250
S4	30	1.5	60
S10			250
S3		2	60
S9			250
S2	40	1.5	60
S8			250
S1		2	60
S7			250
S6			without reactive gas

The samples from Table 7 were coated with 300 nm TiO<sub>2</sub> using IAD process V, and rod-shaped particles were found on samples S8 and S9. The particles in samples S6 and S7 have only a spherical geometry, similar to those found on S8 and S9. The influence of ion assistance in the coating process is shown upon microscopic investigation, in which S6 and S7, prepared with an ion assistance of 2 A, shows a greater quantity of spherical geometry than S8 and S9, which were

both prepared with 1 A. The demineralization results of methylene blue establish that spherical structures are highly effective in regards to the photobleaching of methylene blue, which allows for the creation of a more concentrated cluster of methylene blue molecules.

In regards to adhesive strength, although the particle size was seen to have grown upon annealing at 400 °C, the deposited films were highly stable. Increasing the annealing temperature above 400 °C adversely affected the morphology of the films, to the point of forming cracks when annealed over 500 °C for 12 hours. Table 7 provides an overview of the influence of process parameters, such as unloading current, O<sub>2</sub> flow, and temperature (cold: 60 °C; hot: 250 °C). A better result can be obtained with higher process temperatures, and the addition of oxygen plays such a major role in photocatalytic coating that attempts with oxygen addition were not continued as this could possibly result in a non-stoichiometry effect of less than 15 sccm.

A comparison of layers shows that better hydrophilicity can be achieved with an O<sub>2</sub> level at 30 sccm, rather than at 40 sccm. The contact angles also change with the level of current as they increase as the current is reduced, and vice versa. Some of the samples also showed an increase in contact angle under UV exposure. The samples S6, S7, S8, and S9 showed an improved hydrophilic effect when compared to samples S7 and S9, which were produced with UV exposure and showed a large contact angle. The manufactured samples were coated with TiO<sub>2</sub> and divided in 3 test rows: addition of O<sub>2</sub> in 20, 30 or 40 sccm; temperature in cold and 250 °C; discharge current in 1.5 or 2 A (Table 7). Figure 53 shows that the samples have amphiphilic surfaces. The sample surfaces on which the contact angle is smaller after UV-irradiation than it was before are to be called hydrophilic or super-hydrophilic. In Table 7, the samples are sorted according to O<sub>2</sub>, ion-source current and temperature.

With the comparison of the temperature dependence, it becomes clear that the layers produced under higher temperatures are more suitable than the ones produced with cold process. O<sub>2</sub> plays a significant role in coating. With a decrease in the flow of oxygen, the contact angle also changes. The contact angle drops with rising intensity. Some samples show a very large contact angle after the effect of UV irradiation.

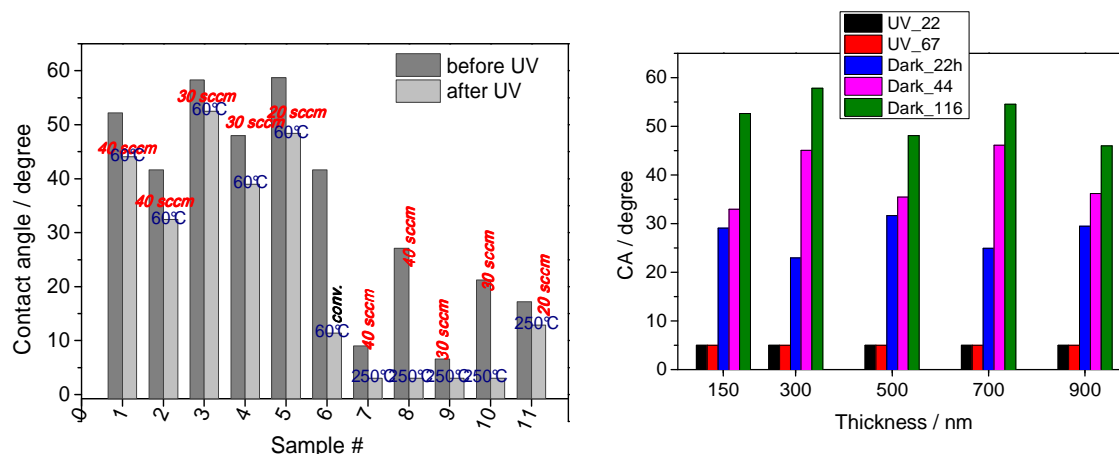


Figure 53. Hydrophilicity analysis results for cold processes and process at 250 °C with and without UV exposure, and after dark experiment.

The surface free energy of solid determines the wettability of a flat surface. For a non-flat surface, it is the surface roughness that affects the wettability<sup>[12, 79]</sup>. Wenzel expanded Young's equation by including the surface roughness to obtain the following equation<sup>[264]</sup>.

$$\cos \theta' = r \cdot \cos \theta \quad \text{Equation 21}$$

where  $\theta'$  is the apparent contact angle and  $r$  is the surface roughness ratio between the actual surface area and the apparent surface area. This equation indicates that, as the  $r$  value is always greater than 1, the surface roughness improves hydrophilicity for surfaces under 90° and also the hydrophobicity of surfaces greater than 90°. Resulting from the contact angle of a flat TiO<sub>2</sub> surface always being less than 90°, the hydrophobic TiO<sub>2</sub> surface cannot be attained through consideration of only the Wenzel equation.

Superhydrophilic properties were also displayed by the films when under UV light for 67 hours, and they turned hydrophobic after being stored in the dark for 116 hours (Figure 53, right). The CA of the samples reached approximately 50° when kept in the dark for 5 days, suggesting that alternating between UV irradiation and dark storage can control the surface wettability.

### 6.3.5 Industrial application

Glass, plastics, ceramics and metal samples of different sizes were obtained from the commercial entities Sartorius AG, Duscholux and Villeroy & Boch and deposited with titania thin films and then analyzed for their self-cleaning characteristics. A comparative analysis of these samples is given in Table 8, which also shows the results obtained from the deposited standard Suprasil and Menzel glass samples.

Table 8. Results of the accomplished contact angle

Substrate	Processes and Coating Materials	Parameters	Angle [°] without UV	Angle [°] with UV
Comparison between PVD- Coating Processes, 250 °C, ~300 nm				
Quartz glass	Suprasil	heated with IAD, Pr V	< 23	< 5
	AF 37 alkali free	heated without IAD, Pr V	< 20	< 5
Borosilicate glass	D263 Menzel	heated without IAD, Pr V	74	< 5
	D263 Menzel	heated with APS, Pr III	39	16
IAD application on different substrates using Process V , ~300 nm				
Sartorius AG				
BK 7 glass	bubble and inclusion free	With ITO	82	50.4
Multi-layer glass	front windows	Without ITO	79.6	57
Duscholux				
PMMA	as dip coating Method	1.5 A, 30 sccm	-	-
	as Primary Material	1.5 A, 20 sccm	27.7	< 5
	reference	1.5 A, 30 sccm	69.4	41.8
Villeroy and Boch				
Ceramic	white Painted	1.5 A, 30 sccm	66.9	38.7
Iron steel	metal Sample	Without IAD	13.3	< 5
	metal Sample	1.5 A, 30 sccm	89.4	< 5
Aluminium	reference	1.5 A, 30 sccm	15	< 5

This table displays the results of the TiO<sub>2</sub> surface both before and after UV irradiation for the industrial application of this research. For both a multilayer glass with an ITO layer and BK 7 glass (Sartorius AG), TiO<sub>2</sub> films coated with IAD display an initial CA of several tens of degrees, which varies depending on the surface conditions, with surface roughness being the chief property. Ion e-beam evaporation sources after UV irradiation produce higher deposition rates than conventional sources, which lends itself to large-area hydrophilicity industrial application. Water also begins to show a decreasing CA after this irradiation, with the CA finally reaching near 0 (<5) as shown in Table 8 and Figure 54. At this stage, the surface becomes fully non-water-repellant and retains a CA of a few degrees for a day or two when under the ambient condition and no exposure to UV light.

When coated, the surface energy of these layers is greater than that of the industrial surface covered with the initial OH groups. As a water droplet is significantly larger than the hydrophilic areas, it instantly and completely spreads on such a surface and thus resembles a two-dimensional capillary phenomenon.

In some cases, another polymer film (from Duscholux) can be used as a seed layer, which then provides the hydrophobic surface that is generally preferred by these films. In this case, the CA again reaches near 0, which is the same as for aluminum and ceramic. In contrast to this, uncoated PMMA exhibits no hydrophilicity. With this basic appreciation of these substrates coated via ion assisted deposition with a varied discharge current, surface temperature and oxygen flow, the produced samples are suitability for production of easy to clean applications with the intention to coat a large selection of surface material.

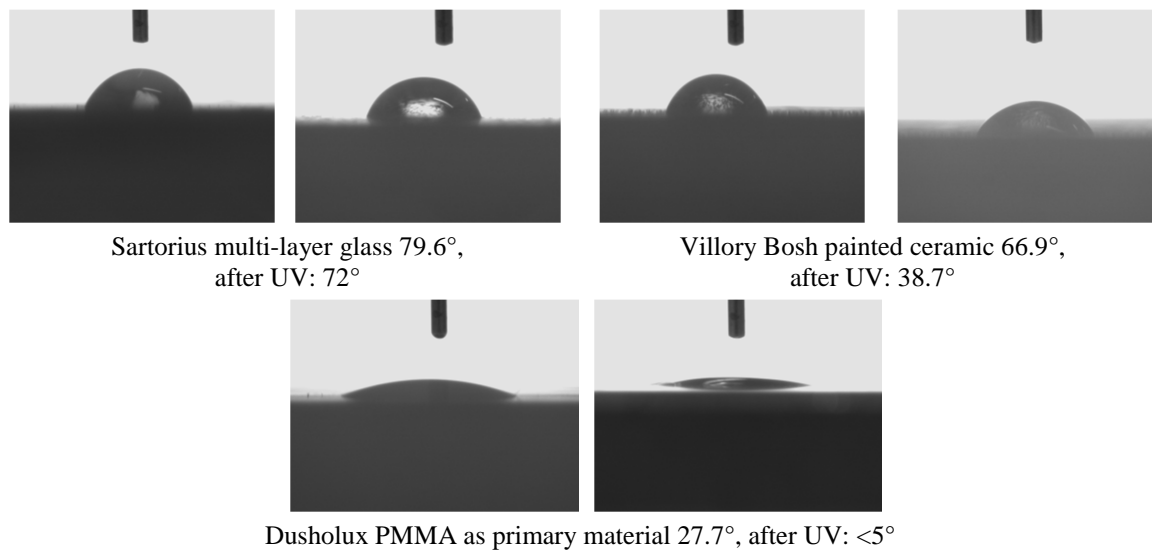


Figure 54. Process V CAM results of post-IAD application on different industrial substrates.

## 6.4 Durability Tests: Mechanical and Environmental Stability of TiO<sub>2</sub> Layers

The mechanical stability experiments were conducted with the coatings, with their resistance under environmental influences being analyzed. It is important to note that there were more than 200 coatings, classified into the 5 previously-defined coating processes, I to V. A minimum of 10 samples, were produced in each coating batch. One sample was used for optical monitoring, and the rest for different optical, morphological, multi-functional and structural characterization, all within the MIL (MIL-C-48497) and DIN Standards (DIN 52348, DIN ISO 9211-4) (more can be found in Figure Appendix VI). The durability condition is vitally important for the thin films as it has an impact on characteristics of the films' growth.

### 6.4.1 Layer Adhesion Test

In the tests done following the MIL-C-48497A model, the coated samples were subjected to an adhesion test using wide cellophane tape. This tape was pressed, with 1 kg pressure, firmly

against the coated surface and then quickly removed at an angle normal to the coated surface. The results in Figure 55 show that the layers maintained their original form and exhibited no damage to the surface, with below (left) displaying the surface before testing, and below (right after testing). The Process V IAD sample is used here as a representative example.

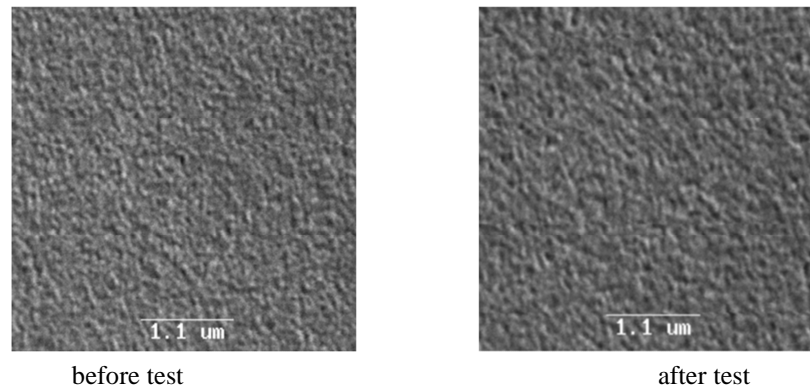


Figure 55. Durability test SEM results of a TiO<sub>2</sub> 300 nm thin Suprasil substrate coated via Process V (250 °C, 2.5 A, 25 sccm, 0.15 nm/s).

#### 6.4.2 Moderate Abrasion

To test moderate abrasion, a 3.8 inches (0.91 cm) wide and ¼ inches (0.61 cm) wide cheesecloth was placed over the coated side of the sample and then rubbed back and forth using the machine shown Figure Appendix VI. Though this process was repeated 50 times with a contact pressure of 1 pound (0.45 kg), the results (Figure 56) showed no indication of abrasion on the layers.



Figure 56. Nomarski-microscope magnification inspection of a 300 nm thin Suprasil substrate coated via Process V (250 °C, 2 A, 30 sccm, 0.15 nm/s). Eraser test is according to MIL-E-12397B.

This test establishes the high durability requirements for thin films. The surface of test sample showed no evidence of coating removal or scratches. Generally, all coated IAD titania films show no signs of deterioration or abrasion.

### 6.4.3 Severe Abrasion Resistance Test

For abrasion resistance testing, the samples were rubbed with a standard eraser 20 times with a pressure of 2 pound (0.9 kg). The results of this, shown in Figure 57, demonstrate that the samples were unchanged and no scratches were formed. Figure 57, (left) shows the surface before abrasion resistance testing, and Figure 57 (right) shows the surface after this test.

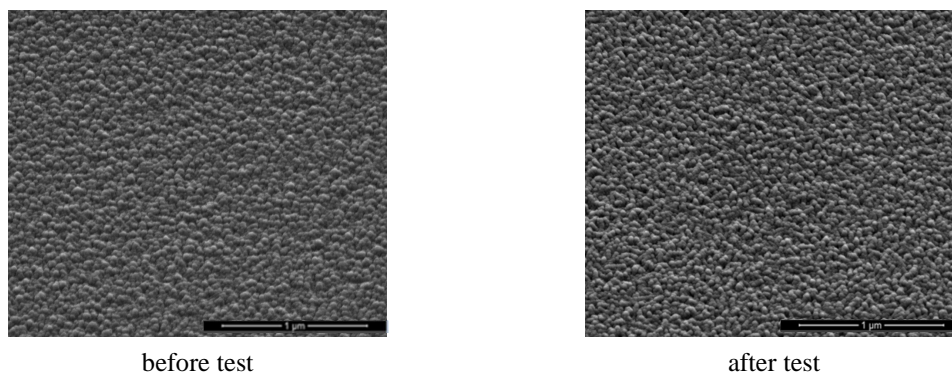


Figure 57. Example images of severe abrasion test controlled with SEM, as good representative for more than 200 coating batches. This test was carried out on a 300 nm thin Suprasil substrate coated via Process V (250 °C, 2 A, 30 sccm, 0.15 nm/s).

### 6.4.4 Sand Erosion Test

This test is according to the DIN 52348, and ISO 9211-4. The coated sample was first cleaned and the transmission was measured as-deposited. The sample was rotated and a controlled 10 g of sand (grain size: 0.2 mm) was funneled from a distance of 60 cm through a cylinder (diameter: 8 mm).

To ensure the environmental stability of the layers, the method was precisely reproduced five times. After every step, the transmission curve was measured to determine the damage caused by these small particles and any resulting surface defects. The transmission curve was found to have decreased after every measurement (Figure 58).



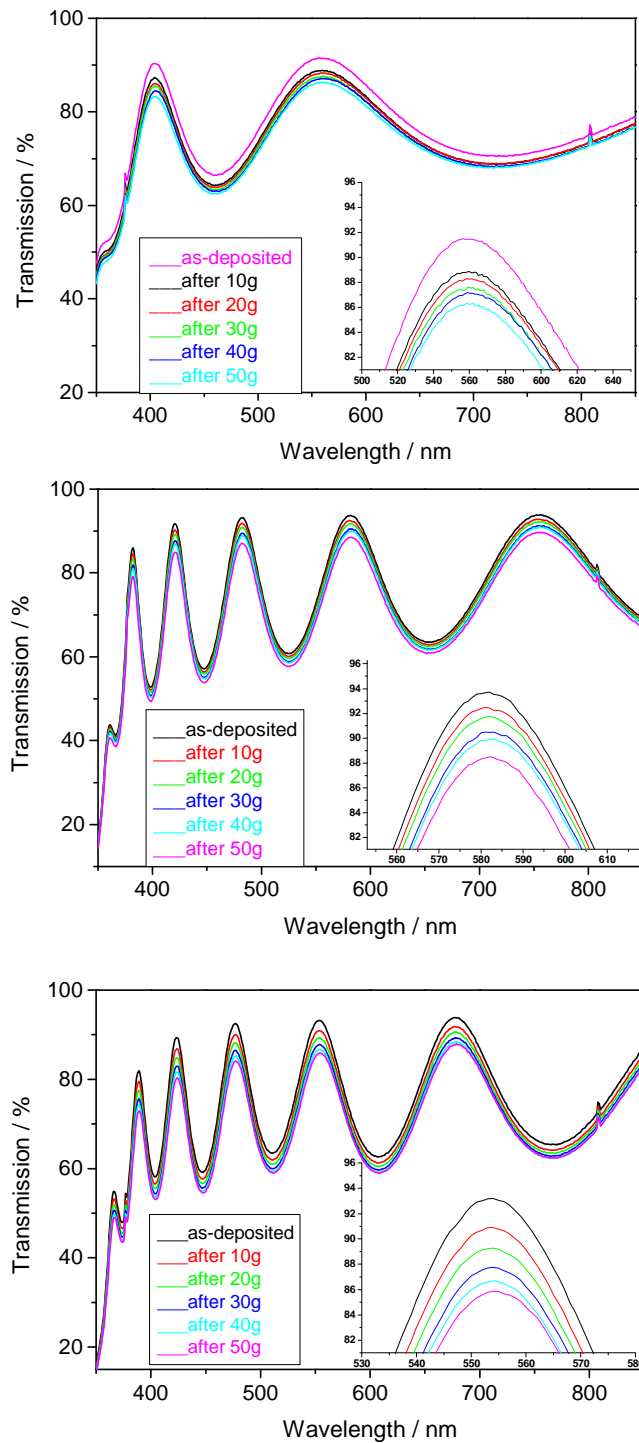


Figure 58. Sand erosion test. First row coated via Process I: without IAD, 250 °C. Second row via Process IV: IAD with CC-104. Third row via Process V: IAD with 2.5 A, 300 °C.

This exact test was repeated using different coating processes to generate points of comparison. The difference in transmission is approximately 7%, showing a decrease in the stability that normally characterizes this sand erosion test. This difference can be reduced through the future use of cleaning techniques, which can allow for complete removal of sand traces. A higher change is observed for the process without IAD, of which the first 10 g show a significant loss of

transmission. The transmission loss via this test over the three coating processes is beneficial in determining the most efficient way to clean coated samples before characterization methods and other industrial applications.

#### **6.4.4 Solubility Test**

For the solubility tests, in each case the optics were first placed into a container housing acetone for 15 minutes, and then another 15 minutes in a container carrying isopropanol. In both cases the optics were completely submerged into these solutions and dried after removal. The results of this showed that no e-beam layers detached from the glass surface. Also dependent on layer and the substrate surface are environmental properties such as solubility, abrasion or adhesion, in such a way that their resistance and performance may be used to determine the limits and possibilities of TiO<sub>2</sub> thin film operation under real conditions (Figure Appendix VII).

The thin film properties when coated via Ion Beam Sputtering include greater adhesion and denser film structure, both credited to the higher energy of the sputtered particles. The intent in both instances is to impart the thin film adatoms on the substrate with increased energy, and thus increased mobility prior to nucleation. An improved durability was observed for films produced with IBS and IAD when compared to other deposition method, such as sol-gel. The ion bombardment is generally beneficial for film adhesion and nucleation. The processes fulfill the high demands of present optical technologies, with some of the major aspects covered being a compact microstructure, an enhanced optical quality, a higher mechanical resistance and an adjustable film stress.

#### **6.4.5 Experiments with Polymers**

The polymer may not, in several cases, have good adhesion to the surface of the substrate unless either an adhesion promoter or SiO<sub>2</sub> layer is used prior to the polymer coating.

Because of its importance in countless daily-use and sophisticated products, the use of thin films on polymers is very much worth considering. To investigate the possible use of thin films on polymer, experiments were carried out using Poly (methyl methacrylate) (PMMA). The three main demands for this industrial product were:

- Preparation of a homogenous highly active photocatalytic coating.
- The color impression should not be or only slightly changed by the coating.
- Highly mechanical and chemical resistance of the coating as the product has normally a long lifetime and is exposed to chemical and mechanical destructive pollutants.

To guarantee good mechanical stability of the photocatalytic surface there is first a need for a more suitable adhesive layer. Both the moderate test and the solubility test show high mechanical resistance. The severe abrasion test, however, exhibits surface scratches (Figure 59). The influence of  $\text{SiO}_2$  as a basic layer directly on PMMA should inhibit the presence of these deformities. The plasma pretreatment can achieve a better adhesive strength via the possibility of obtaining increased wettability due to the sufficient surface energy, and via the presence of more free-radicals for strong bonds with the polymer surface.

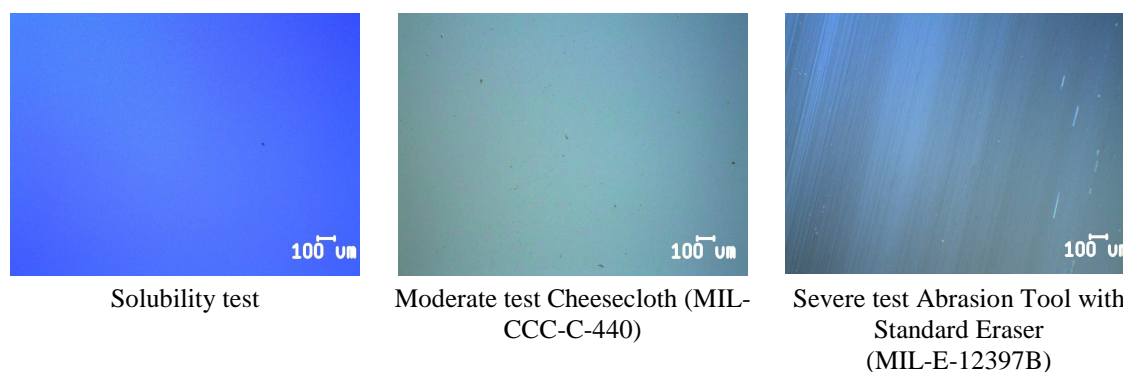


Figure 59 Nomarski-microscope inspection of Microscope magnification of a 300 nm thin PMMA substrate, coated with Process V (cold, 2 A, 30 sccm, 0.15 nm/s), before using  $\text{SiO}_2$ .

A deposition process has been made with thin layers of  $\text{SiO}_2$  between 15 and 50 nm. Yet other correlational experiments have shown that it is possible to synthesize  $\text{TiO}_2$  on a polymer substrate, using sol-gel method, with surface composition and chemistry, crystal phase and size, UV transmission and morphology similar to those of commercially available CVD glass substrates<sup>[251]</sup>.

Previously defined IAD methods produce laboratory glass films in certain cases even better, photocatalytic performance than commercially available films. For as-received/unreacted films, photocatalytic efficiency depends on surface roughness, i.e. high level of crystal size and roughness causes higher photocatalytic efficiency. Stearic acid reaction in model solutions such as neutral, acidic and basic, alter the surface compositions i.e. Si/Ti, Ca/Ti, and roughness and also enhance photocatalytic efficiency of films after reaction. Photocatalytic efficiency does not decrease with Si-rich surface layer on films<sup>[3]</sup>.

Other research proves that the photocatalytic and super-hydrophilic efficiency of  $\text{TiO}_2/\text{SiO}_2$  films depend on the content of  $\text{SiO}_2$ . Research shows that optimum level of photocatalytic activity can be achieved by adding 10 to 20 mol % of  $\text{SiO}_2$  on a thin film, and for hydrophilicity adding approximately 30 to 40 mol % of  $\text{SiO}_2$  can give optimum results greatly depending on the particle geometry. An increase in the  $\text{SiO}_2$  level, up to 30 to 40 mol %, can decrease the quantity of

absorbed organic substances. There exists a correlation between photocatalytic efficiency and hydrophilicity, as both augment each other and together they produce the self-cleaning effect.  $\text{SiO}_2$  increases the acidity level on substrates <sup>[104]</sup>.

Suitable IAD methods were applied to different plastics, with a focus on PMMA substrate. Example morphological and optical results are found in the following Figure 60.

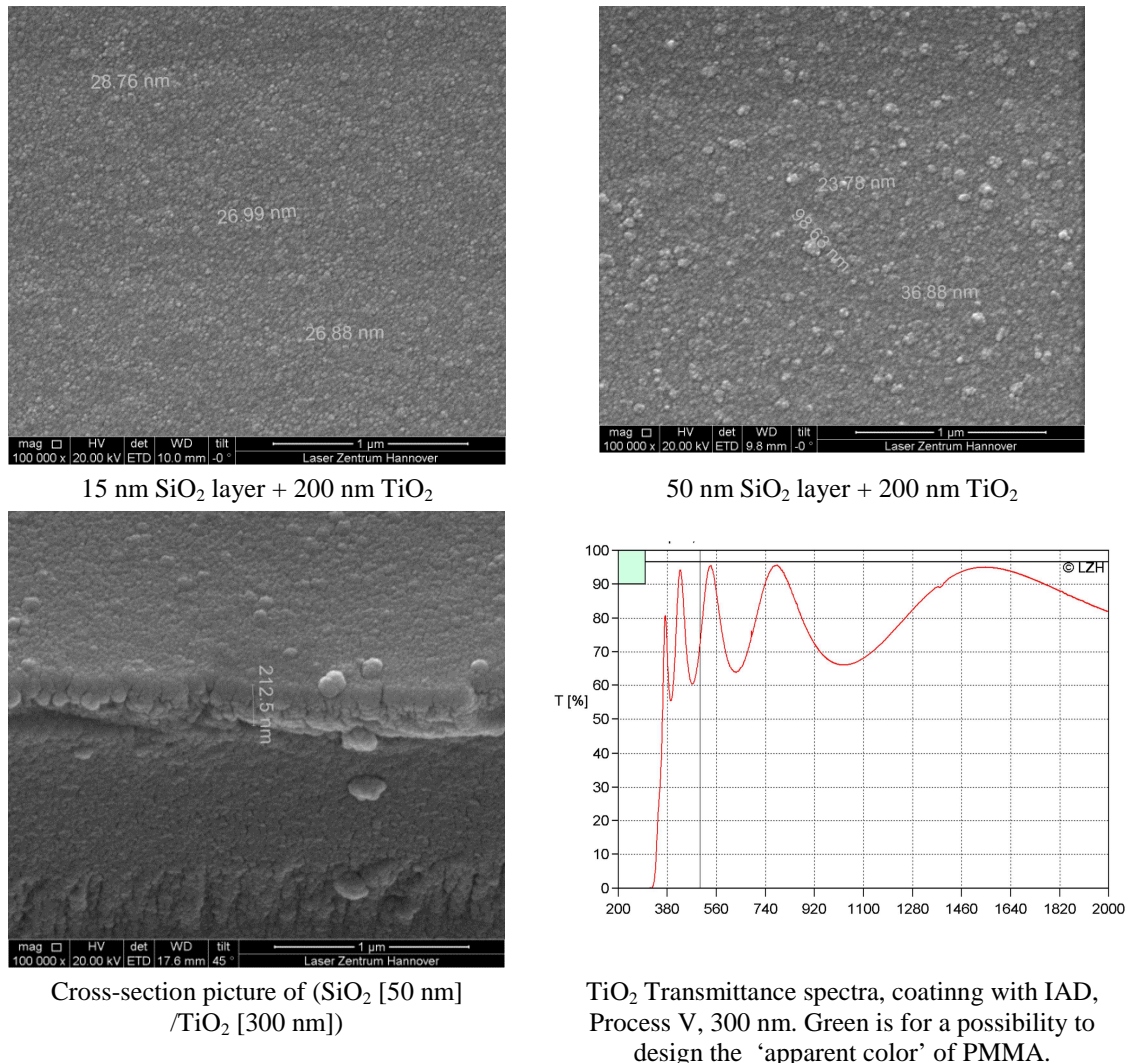


Figure 60. Morphological quality of multi-layer systems on PMMA coated via Process V (2 A, 30 sccm, 0.15 nm/s).

As is clear from Figure 60, the grain size for the titania added with 50 nm is larger than with a 15 nm  $\text{SiO}_2$  layer. This could be due to a more compact arrangement of particle adsorption. Covalent bonds are formed during the e-beam deposition of oxide film onto a polymer substrate, and this formation can be influenced by a complex interplay between coating growth, interface structure, defects and an internal stress state. There is a correlation between the grain size and the coating thickness chosen for the titanium and silica in situ-deposition process. In both of these

cases, the deposition process was carried out at a cold temperature, 50 °C to 60 °C, with an ion-source current of 2 A and 250 V, and a deposition rate of 1.15 nm/s.

In terms of adhesive strength, the stability of the films was outstanding on the surface of PMMA, which is not an easy surface to work with when compared to mineral silica. The mechanical stability tests were performed on the films by immersing them in a solution of water and diluted acetone. This also showed positive results, as no scratches and abrasions were noticed on the surfaces. The important role that hydrophilicity plays in maintaining the self-cleaning effect of the surface was investigated. The contact angle after UV-irradiation decreased from 79° to 12° (Figure 61). Not displayed in this figure is that the contact angle of multilayer PMMA and SiO<sub>2</sub> does not change before and after UV exposure. The predisposition of an exterior surface to soiling is closely related to its contact angle with water, so a material used on the outside is actually more likely to be soiled if it is more water-repellent. Because of this, plastic is more likely to be soiled than sheet glass or tiles.

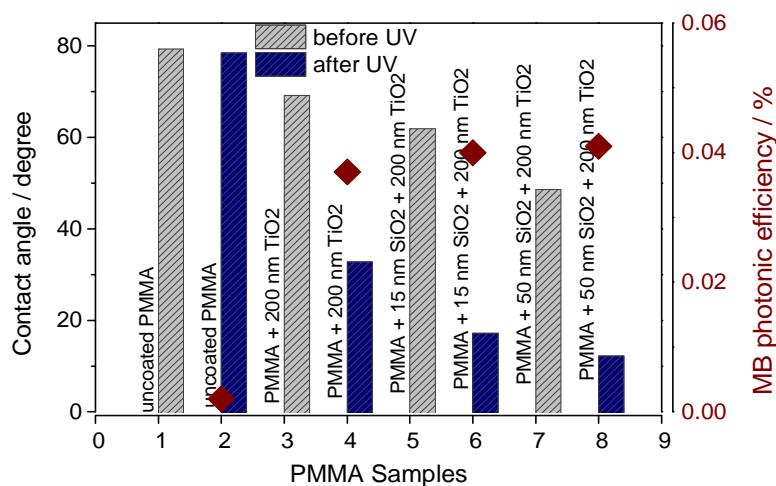


Figure 61. Contact angle result for PMMA samples coated via Process V (2 A, 30 sccm, 0.15 nm/s) showing the hydrophilic efficiency of TiO<sub>2</sub>/SiO<sub>2</sub> films irradiated under 1 mW/cm<sup>2</sup>.

One major reason that the aspect of the IAD method's potential has not yet been utilized is that it is challenging to realize suspension and dispersion of the multilayer supported catalysts. The acidity of the composite oxide is enhanced with an SiO<sub>2</sub> additive to the TiO<sub>2</sub> film, and thus water molecules that would normally result in hydroxyl groups are adsorbed. It is possible that this enhancement could be why a purely TiO<sub>2</sub> film adsorbs more organic substances when subjected to air. Acidity growth is hypothesized to be the main cause for the enhancement in photocatalytic performance and hydrophilicity of these layers. This improvement is significant due to the vital nature of good hydrophilicity self-cleaning technologies. It has been suggested in 1974 by Tanabe et al. [265] that a greater absorption of hydroxyl radicals can be gained through increased surface acidity. The silicon cations (such as Ti–O–Si ligand) capture and bind the hydroxyl radicals from

surface-adsorbed H<sub>2</sub>O molecules. In contrast to this, H<sup>+</sup> ions from the adsorbed H<sub>2</sub>O molecules easily bind to O<sub>2</sub><sup>+</sup> ions, leading to a greater concentration of hydroxyl radicals on the composite surface, as opposed to a pure TiO<sub>2</sub> coating.

The increased hydrophilicity and photocatalytic performance of the TiO<sub>2</sub>/SiO<sub>2</sub> film, as a result of the above, are hypothesized to be a consequence of the increased surface hydroxyl groups. The water contact angle measurement can be easily applied to SiO<sub>2</sub> supports. It was revealed from previous results that these supports offer a base with a high mechanical stability. Although no physical degradation of the polymer support was perceived, there is still the option to further lessen degradation chance by UV irradiation through the choosing of high UV-resistant thermoplastic substances, such as acrylic or polyallomers. It is essential, due to the transfer of heterogeneous photocatalytic oxidation processes in their attempt to find industrial applications, that economically viable solutions to the expensive post-treatment separation are found. In today's world, the utility of plastics for industrial and non-industrial use is remarkable, which can pave the way for its use in innumerable products. As evidence of that, Figure 62 shows that TiO<sub>2</sub> layers can be applied to plastic surfaces without drastically affecting the overall optical quality. While the real challenge in using this technology on plastics is maintaining a sufficient adhesive strength of the layers, the experiments conducted strongly suggest that this could be theoretically met with success.

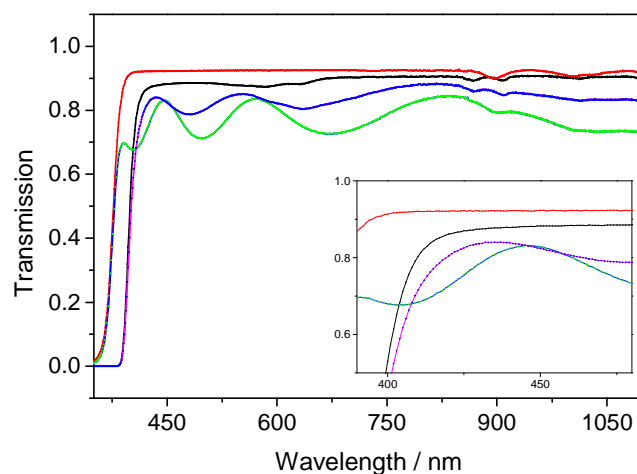


Figure 62. PC & PMMA with TiO<sub>2</sub> optical characteristics for photocatalytic transparent TiO<sub>2</sub> layers  
PMMA: Red: uncoated; Green: with ~300 nm TiO<sub>2</sub>. PC: Black: uncoated; Blue: with ~200 nm TiO<sub>2</sub>.

The transmission values of PMMA and PC plastics, with and without TiO<sub>2</sub> coating, are shown in the graph of Figure 62. Owing to the high transmission, between 70 to 85%, of the successful coating plastics, the methods developed during this research appear to be very suitable for industrial optical application.

## 7. Optical Properties of IAD Photocatalytic Thin Films

The aim of this chapter is to investigate in the correlations between the optical quality, the morphology and the photocatalytic performance of titania thin films produced using ion assisted deposition (IAD). To investigate this, transparent TiO<sub>2</sub> thin films were deposited with different IAD coating parameters to analyze their structural and optical properties. The influence of the deposition parameters on the morphological properties of the titania films was determined through SEM and EDX analysis. The process parameters chosen for this research were (1) coating and annealing temperatures, (2) ion-source parameters, such as oxygen flow, and (3) TiO<sub>2</sub> thin films of different thicknesses.

### 7.1 Deposition and Annealing Temperature Influence

Experiments carried out using different coating parameters have been previously discussed in Chapter 5, explaining the following points.

- a) The films coated using BAK 640 and Denton CC-105 displayed a photodecomposition rate of methylene blue was greater than uncoated substrates and greater than commercially available products having self-cleaning ability.
- b) Comparisons showed that Balzers BAK 760 with Denton CC-105 achieved the fastest demineralization of methylene blue at high temperature and resulted in a near colorless solution. This contrasts to other processes that had a 50% decrease in the concentration, from 10 µmol/l to 5 µmol/l.
- c) The thin films' thickness resulted in a related increase in photocatalytic efficiency, up to a limit. Up to a thickness of 150 nm, the influence was negligible. However, between 200 nm and 550 nm a large increase in photocatalytic efficiency could be gained.

#### 7.1.1 Optical Properties of TiO<sub>2</sub> Thin Films

Optical properties of the deposited thin films, such as the refractive index  $n$  and the optical band gap, can be influenced by the coating temperature, the temperature during annealing, various deposition parameters of the ion-source and the deposition rate. Results were gathered as-deposited and after annealing to allow for comparisons. Following parameters are fixed:



Table 9. Fixed deposition coating parameters

Vacuum chamber			Source					Process	
U	I	O <sub>2</sub>	Neutralizer		U	I	O <sub>2</sub>	Rate	Thickness
HV[kV]	E[A]	[mbar]	U[V]	I[A]	[V]	[A]	[sccm]	[nm/s]	[nm]
8	0.35	3.10 <sup>-4</sup>	10	27	250	3	25	0.15	150

**(a) As-deposited**

The transparency of the films exhibits a sharp decrease in the UV region as shown in the transmittance spectra (Figure 63). The character of the transmittance spectra shows a series of transmittance maxima and minima of different orders. As the film characteristic changes, location of a particular transmittance extrema ( $T_{\min}$  or  $T_{\max}$ ) shifts towards longer wavelength side. The films also show a sharp decrease of transmittance in the ultra-violet region which is a result of the fundamental absorption of the light <sup>[266, 267]</sup>. This interference is due to the thin film characteristics, such as the thickness or the effective refractive index of the film medium.

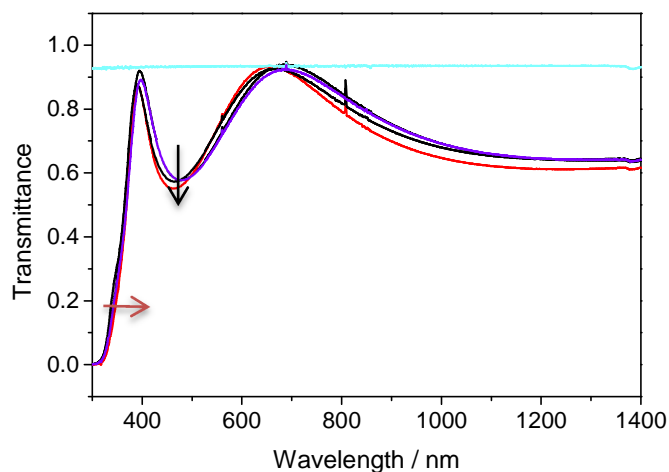


Figure 63. Transmission spectra for 50 °C, 150 °C and 350 °C in IAD (3 A, 25 sccm O<sub>2</sub> and different thicknesses in the area of 150 nm). Dark violet: 50 °C. Black : 150 °C. Red: 350 °C. The cyan line (~94%) corresponds to the uncoated side of the substrate.

The refractive index of the shifted curves can be compared in cases where the curves have no absorption in relation to the uncoated curve. If there is inhomogeneity, there is more than one layer and a refractive index of more than one. A comparison of the refractive index of the shifted curves can only be correct if both curves have no light absorption. If there is an exact overlap with the uncoated substrate curve, this is due to the influence of  $n$ .

Due to multi-reflections at the film-air and film-substrate interfaces, the UV-Vis spectra displayed noticeable interference effects. Once a high refractive index transparent thin film achieved on a transparent substrate of a lower refractive index, the transmission maxima are obtained when the



film optical thickness corresponds to even multiples of the quarter-wavelength. Once these transmission minima are gathered, the reflection deficits caused by the refractive index divergences between substrate and titania layer are maximal <sup>[179]</sup>.

From this graph it can be seen that the titania coated thin films are transparent within the visible and the IR range. The minima and maxima transmission spectra for the samples coated at different temperatures indicate that the temperature and thickness of the deposition has an influence on the optical quality of thin films. Generally, the transmission was increased faintly with a rise of temperature.

For wavelength above 400 nm, the transmittance of the films was almost constant. The decrease below 400 nm is caused by the quartz substrate and by titania absorption <sup>[268]</sup>. The above figure shows that homogeneity becomes adversely affected at approximately 750 nm if the coating temperature is raised to 350 °C. Figure 63 also indicates the complex interdependence between various deposition parameters and the coating quality, as at 650 nm the optimized optical quality is achievable if the coating temperature is maintained at 150 °C. Using this same temperature for 550 nm, optimized results for the refractive index can be gained at 2.63. At cold, 50 °C, and hot, 350 °C, temperatures, the refractive index goes down to 2.51 and 2.55, respectively.

The envelope method and experimental expression <sup>[269]</sup> were used to analyze the TiO<sub>2</sub> films' refractive indices. As can be discussed, it is possible to draw the envelopes through the maxima,  $T_M$ , and minima,  $T_m$ , of the transmittance curve. The film refractive index  $n_f$  in the transparent and weak absorption (high temperature) area was calculated from Equation 22:

$$n_f = \sqrt{N + \sqrt{N^2 - n_s^2}} \quad \text{Equation 22}$$

where

$$N = 2n_s \frac{T_M - T_m}{T_M T_m} + \frac{n_s^2 + 1}{2} \quad \text{Equation 23}$$

$n_s$  stands for the refractive index of substrate.

In these equations, maxima and minima of the envelope in transmittance spectra are respectively represented by  $T_M$  and  $T_m$ , refractive index of the glass as  $n_s$ , computed with the help of the transmittance  $T_s$  of glass by Equation <sup>[35]</sup>. The experiments showed a 90% transmittance of the glass in the visible range.

$$n_s = \frac{1}{T_s} \left( \frac{1}{T_s^2} - 1 \right)^{1/2} \quad \text{Equation 24}$$

Figure 64 illustrates the evolution of refractive indices as a function of wavelength for TiO<sub>2</sub> film annealed, obtained with the methods mentioned above.

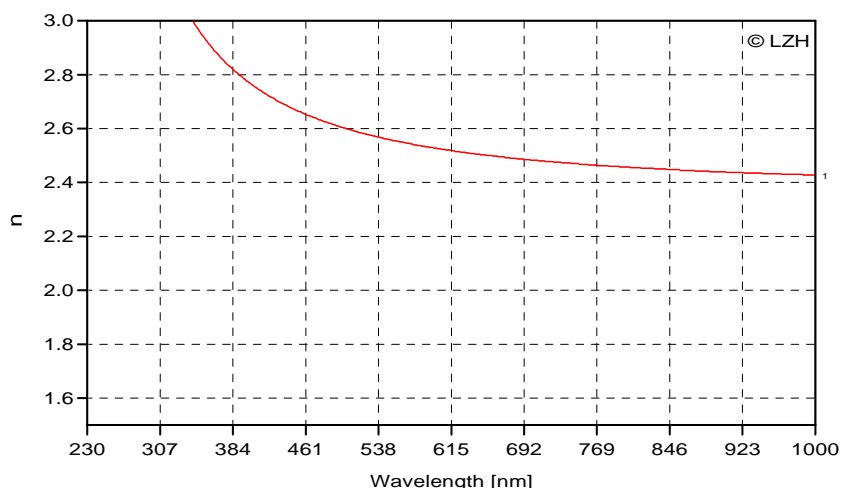


Figure 64. Refractive index of TiO<sub>2</sub> film at 350 °C. At 550 nm, the value is 2.548.

The transmittance ‘extrema’ of the curve for the ion assisted coating contain greater differences than the conventional e-beam evaporated coating curve. A greater ion assisted coating refractive index value  $n$  is signified as a result of these larger differences. Good coating condition for coated film was obtained for the ion-operated bombardment, as signposted by the lack of quantifiable absorption at wavelengths for which the film is multiple half-wave in optical thickness, down to approximately 350 nm. An absence of refractive index inhomogeneity was inferred.

### (b) After Annealing

The annealing process and its parameters can affect the optical properties of the films. Figure 65 shows the transmission spectra for the process of deposition at 150 °C, and annealing at 450 °C, both after 4 hours. The use of 450 °C as the annealing point is not only for the layer growth of titania according to the microstructure variation, but also appropriate in the characterization of titania films as useful in photocatalytical electrodes and other applications <sup>[179]</sup>.

The annealing process increases the transmission curve to near that of the uncoated curve, meaning that it can be used for optical correction. The resultant dense or compact layers also show that there was low light shift on the maxima points. Using 25 sccm, a reactive O atom is added on the crystal lattice with an atomic arrangement correction <sup>[163]</sup>.

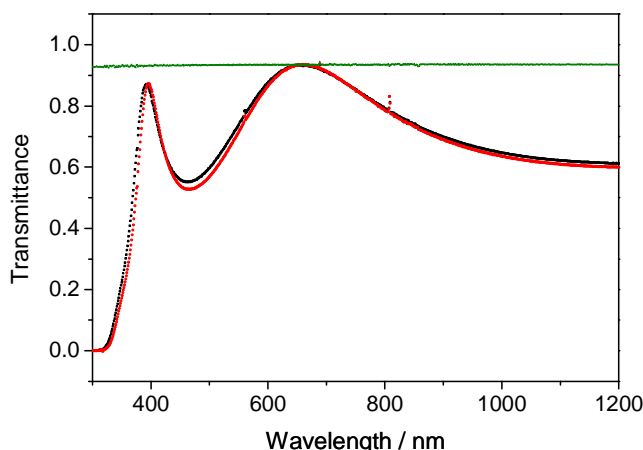


Figure 65. Transmission curve showing the influence of annealing, IAD (250 nm, 3 A, 25 sccm, 150 °C). Red: As-deposited at 150 °C. Black: After annealing at 450 °C. Green: uncoated substrate.

The Figure 65 shows that transmission losses increase up to 3% between 400 and 470 nm. The transmission maxima observed between a spectral range of 470 appears to be only 2% below the transmission level measured for the uncoated side of the glass. This feature shows that optical losses in the visible range are small. It was observed during the experiments that the annealing parameters above have little-to-no effect on the optical properties of the coatings. Thus, it can be concluded that the films deposited using the IAD process have the stability to resist a high annealing temperature. Moreover, the annealed films did not show any considerable damage to the layer.

From Figure 65 it can be calculated that the average transmittance of as-deposited and annealed TiO<sub>2</sub> film, in regard to the reference of blank glass substrate, is greater than 80 % in the visible region<sup>[270]</sup>. It was also shown that the slight decrease in transmittance was a result of the annealing temperature of 450 °C, which can be accredited to the light scattering effect for its higher surface roughness. The as-deposited TiO<sub>2</sub> films in the visible spectral region were discovered to have an average transmittance of above 70 % for films on glass and quartz substrate<sup>[189, 271]</sup>. The annealing of TiO<sub>2</sub> films at a higher temperature, of above 600 °C, typically results in a lower transmittance, hence the reason that the maximum annealing temperature used throughout this study was generally 500 °C.

Generally, and according to the microstructure, an increase in the substrate temperature during the annealing phase leads to an increase in the refractive index. This can itself lead to the presence of the rutile phase<sup>[189, 208, 263]</sup>.

(c) **Band Gap Calculation with Tauc Preliminary Method**

The optical transmittance spectra of both the as-deposited films and the annealed films exhibited good transmission in the visible light range and a sharp decrease in the UV region, which corresponds to the band gap. The optical absorption coefficient  $\alpha$  was calculated using the formula:

$$\alpha = \frac{\ln\left(\frac{T}{(1-R)^2}\right)}{d} \quad \text{Equation 25}$$

where  $T$  is the transmittance of film at each wavelength, and  $d$  is the thickness of the film. The absorption rate reaches its minimum point at low energy and increases with optical energy in a similar manner to the titanium dioxide absorption edge. The transmission films shown that the absorption coefficient  $\alpha$  decreases rapidly when wavelength is lower than 350 nm, which corresponds to the  $E_g$  values below 3.5 eV. The band gap  $E_g$  was calculated using the Tauc equation <sup>[272]</sup>.

$$\alpha = \frac{k(h\nu - E_g)^n}{h\nu} \quad \text{Equation 26}$$

where  $k$  is a constant,  $h\nu$  is the photon energy (eV), and the value of  $n$  can be  $\frac{1}{2}$  or 2 depending on whether it is a direct or indirect transition <sup>[38, 273]</sup>. The optical band gap was estimated by extrapolating the straight line portion of the  $(\alpha h\nu)^{\frac{1}{2}}$  vs  $h\nu$  plot. Therefore, it is expected that for values of  $h\nu \leq 3.5$  eV,  $h\nu$  is near to 0, but not equal to 0 due to optical interference. The absorption coefficient  $\alpha$  for directly allowed transition,  $n = 2$ , can be ascribed to a function of incident photon energy, and the optical band gap was calculated for different deposition process parameters. The band gaps of the IAD deposited films, coated at 60, 150, and 350 °C, are displayed in Figure 66.

- (A) Band gap for the film deposited at 50 to 60 °C (as-deposited).
- (B) Band gap for the film deposited at 150 °C (as-deposited).
- (C) Band gap for the film deposited at 350 °C (as-deposited).

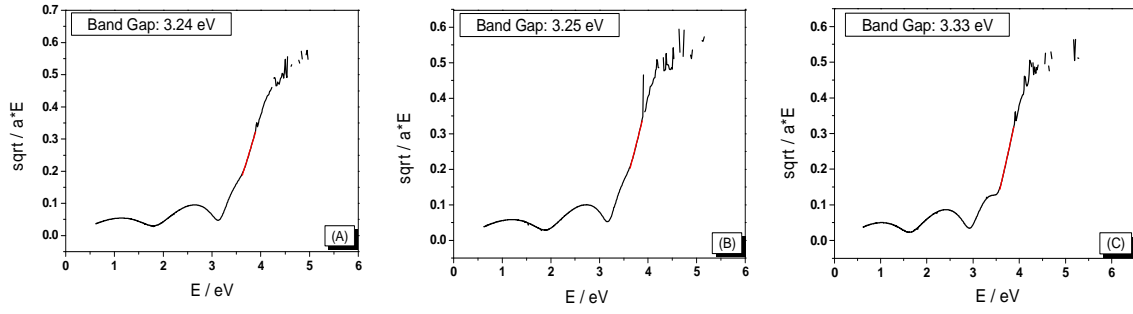


Figure 66. Band gap of different TiO<sub>2</sub> films deposited using IAD at different temperatures.

The dependence of  $(\alpha h\nu)^{1/2}$  against photon energy over the threshold of fundamental absorption is a constant. TiO<sub>2</sub> has different band gap transitions: for rutile and anatase the exact position of the transition are slightly different, but there are two indirect transitions at approximately 3.0 and 3.2 eV, while there is a direct transition at 3.7 eV. It should be noted that all the samples had the same thicknesses (300 nm). As seen above, the band gap was 3.24, 3.25 and 3.33 eV for films deposited at 50, 150, and 350 °C, respectively, showing that the band gap increases with an increase in the temperature and can be associated to the band gap of bulk anatase TiO<sub>2</sub> (3.2 eV). To compare these results to those of the literature, the anatase band gaps vary by as much as 0.05 eV, from 3.48 eV for glass to 3.43 eV for ITO as a substrate. This small difference can be related to the measurement precision. There is also a difference in the band edge energy of anatase from the bulk material with results varying from the literature by up to 0.2 eV [274-276]. Vasanthkumar et al. [277] suggested that the change in the optical band gap of the TiO<sub>2</sub> films with annealing temperature might be the result of the change in film density and increase in grain size. The observed values for IAD sample at 350 °C is higher than the band gap of both bulk material (3.18 eV) and thin film TiO<sub>2</sub> in the anatase phase (3.23 eV). The higher band gap observed can be associated with the crystalline nature of the films. An inverse square relation between  $E_g$  and grain size can be expected [277].

$$\Delta E_g = E_g - E_g^{(bulk)} = E_b \left( \frac{\pi a_B}{R} \right)^2 \quad \text{Equation 27}$$

where  $E_g$ ,  $E_g^{(bulk)}$  are the measured band gap energy and the excitation binding energy, respectively.  $a_B$  is the Bohr radius and  $R$  is grain radius.

When a wavelength of 550 nm was used, the refractive index of the film deposited at 350 °C corresponds to 2.41. From Mathews et al. [273] it can be concluded that the refractive index is directly proportional to the temperature. After implementation of the previously mentioned

sample analysis, the IAD sample results follow that of other analyses in the literature, such as the work of Mathews et al. There is a very good correlation with the proportionality factor (Fig. 67).

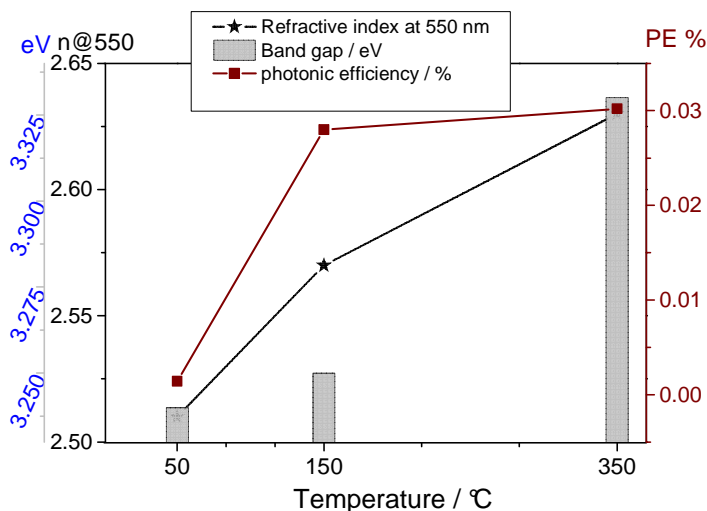


Figure 67. Correlation between refractive index, temperature and photocatalytic activity.

### 7.1.2 Morphology of IAD Optics

#### a. Hydrophilicity

The hydrophilic property of coating samples was evaluated by measuring the contact angle (CA) of a water droplet on the films under an ambient condition in air atmosphere.

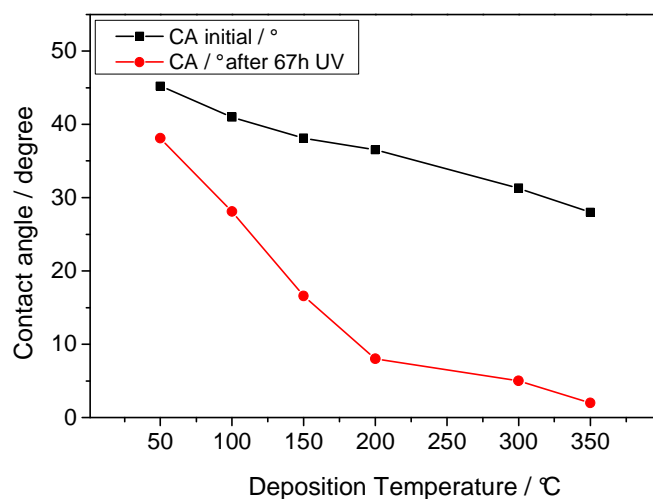


Figure 68. Results of films coated at different temperatures. Black: CAM Initial. Red: After 67 under UV, 1 mW/cm<sup>2</sup>. This result is in accordance with the results discussed in Chapter 6, in which the UV irradiation markedly changed the surface wettability under higher temperatures and high ion-dose energy (oxygen and ion-source current).

The entire process was carried out twice. First under the initial conditions and then after 67 hours. The results obtained from the films are given in Figure 68. Depending on the surface conditions, primarily surface roughness, a  $\text{TiO}_2$  thin film exhibits an initial contact angle of greater than 20 degrees. When this surface is under to UV light, water starts to exhibit a decreasing CA, i.e. it tends to disperse flatly instead of beading up. The superhydrophilic surface becomes wholly non-water-repellant after UV-Illumination for thin films coated at higher than 200 °C. This behavior was expected due to the energy introduced by UV light, which was able to break the surface Ti-O-Ti under atmospheric moisture and create an enhanced formation of surface Ti-OH groups responsible for the better wetting. The above-mentioned experiments and analysis lead to the conclusion that the linear trend in the decline of the contact angle also shows that it is inversely proportionate to the deposition temperature. In addition to these two factors, high process temperature results in a rough morphology of the surface, which in-turn increases the self-cleaning property. A morphological study via SEM investigation was carried out in an attempt to gain further clarification.

#### b. SEM Microstructure and Size Particle Determination

To complement the morphological study in 7.1.2, the microstructure was also investigated using SEM. The SEM images of the films coated at a cold temperature, 50 °C to 60 °C, and at 350 °C are shown as-deposited and after annealing in the Figure 69. Additionally, an average particle size was calculated from the different values obtained in each image.

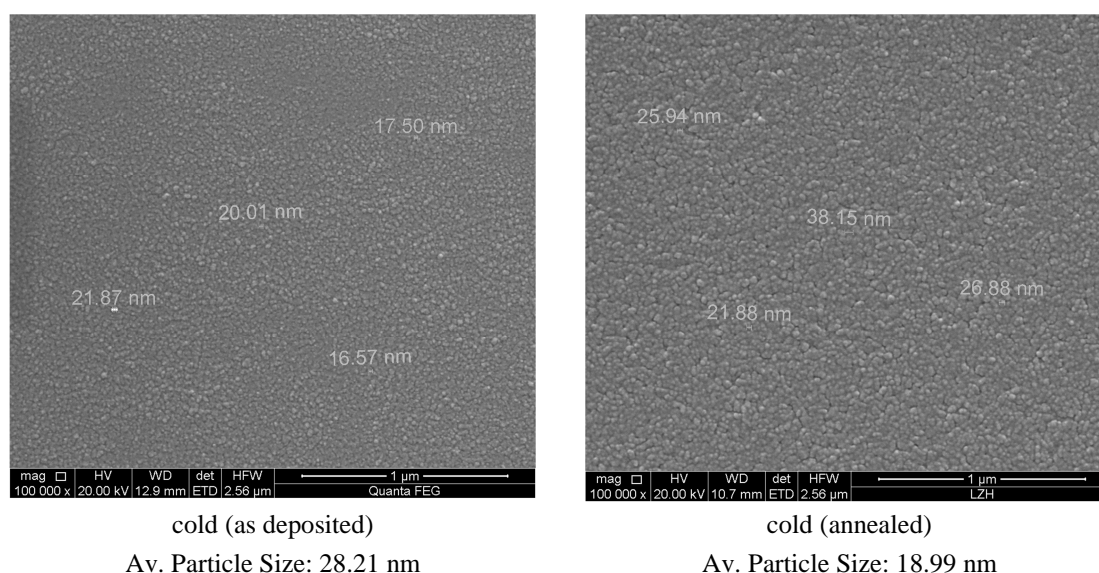


Figure 69 (a). Examples of SEM micrographs of  $\text{TiO}_2$  films, both as-deposited and after annealing.

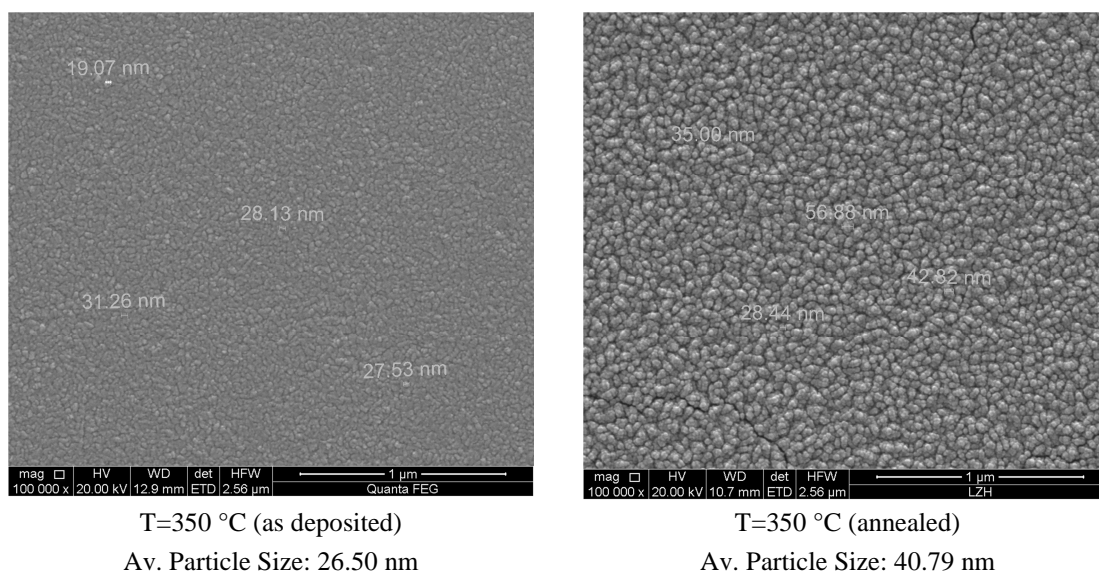


Figure 69 (b). Examples of SEM micrographs of TiO<sub>2</sub> films, both as-deposited and after annealing.

As shown in Figure 69 (a,b), annealing at 350 °C for 20 hours increases the particle size. The surface was found to have homogeneity for all the particles, except in cases of films produced after annealing, in which very small cracks appeared randomly on the surface. This cracking was due to the stress of irregular thermal expansion, interfacial roughening, and voids formed during high-temperature annealing. After a series of experiments regarding TiO<sub>2</sub> layer stability post-annealing, for example those published by Lappschies in LZH<sup>[278]</sup>, higher annealing, layer cracking (identical to those in Figure 69b, right) and morphological deformations were observed for the samples annealed over a long period (for more than 10 hours) and / or if the annealing temperature is greater than 450 °C. To add to the research, annealing time was set to a short duration, for example 4 hours, and the temperature kept at 450 °C.

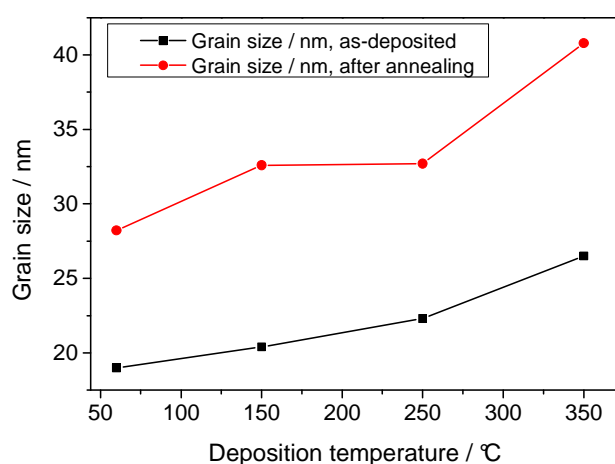


Figure 70. Growth of grain size values, depending of the deposition temperature and annealing temperature.



From the SEM micro-graphical analysis, the average particle size was obtained from each sample with or without annealing and at cold and hot temperatures. It is apparent from both the SEM and the particle size obtained from these pictures that grain size increases with the coating temperature and the annealing temperature. There are undefined particles on the surface of the films deposited at cold temperature. The biggest particle size was observed on the films coated at 350 °C after annealing. The thin films appear to be formed of larger aggregates of granulates, rather than being morphologically smooth.

Optical analysis shows that the transmittance feature of the films increases with the increase in deposition temperature. This increase is due to enhanced structural homogeneity and the decrease of crystal defects <sup>[42]</sup>. In the case of ion assisted deposition, the films prepared were shown to have a very high refractive index (a value of 2.75 at 550 nm was calculated for a sample coated via IAD with Process V, at 350 °C, 4 A and 30 sccm). When compared with common PVD, the atoms deposited on the substrate can get more energy from ion bombardment in the ion assisted deposition, which consequently benefits in the formation of more compact structures, uniform layers, and a higher refractive index. The optical band gap increases with the increase in the deposition temperature. The quality of the optical band gap correlates to the grain size.

The higher particle size caused by the annealing temperature can be explained as follows: if the temperature is increased, the agglomeration of the particles also increases, therefore roughness increases. Higher surface roughness leads to a higher rate constant, thus the free surface area for adsorption of molecules is higher. On a rough surface, the drops of water expand between the particles and thus facilitate formation of a hydrophilic surface. Films deposited on a cold substrate show a smoother surface and can therefore have more hydrophobic properties than the films deposited on a hot substrate.

## 7.2 Oxygen Flow Influence

The experimental set-up used to carry out varying oxygen flow levels has been discussed in detail in Chapter 3, detailing that the oxygen flow in the experiments was varied between 21 and 30 sccm. The results of the experiments done to study the effect of the reactive oxygen flow on the layer properties annealed at 450 °C on as-deposited samples. Following parameters are fixed.

Table 10. Fixed deposition coating parameters

Vacuum chamber				Source				Process	
U	I	O <sub>2</sub>	Heater	Neutralizer	U	I	Rate	Thickness	
HV[kV]	E[A]	[mbar]	[°C]	U[V]	I[A]	[V]	[A]	[nm/s]	[nm]
8	0.35	3.10 <sup>-4</sup>	350/NO	10	27	250	3	0.15	150

### 7.2.1 Optical Properties of the TiO<sub>2</sub> Thin Films

#### (a) As-Deposited

The influence on transmission properties of the films deposited at 350 °C with different flows of oxygen is shown in the Figure 71.

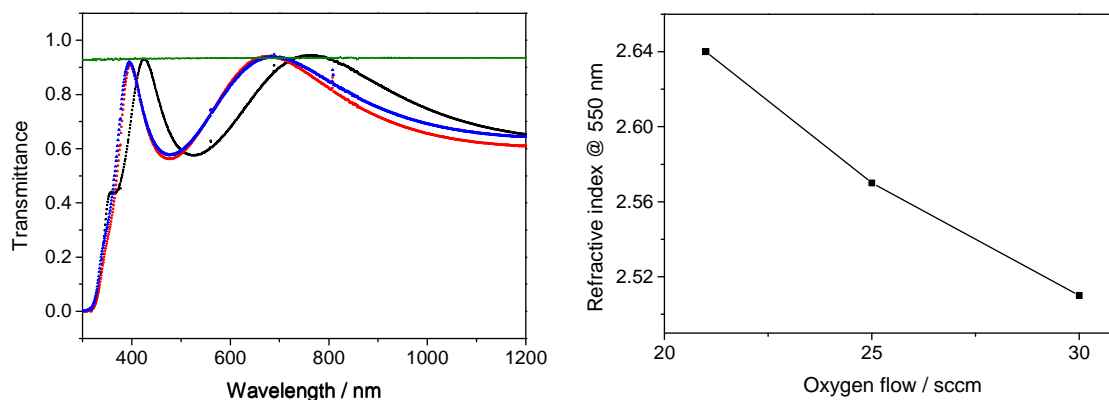


Figure 71. Example of oxygen flow influence on the optical properties. Left: Transmission spectra for deposition with different oxygen flows ( $T=350$  °C). Red: 21 sccm. Blue: 25 sccm. Black: 30 sccm. Green: uncoated substrate. Right: Refractive indices at 550 nm for the films coated with varying oxygen flows ( $T=350$  °C). To gain ion-source stability, O<sub>2</sub> flow was increased. Coating parameters used were 2.5 A, U = 200 V.

From these figures it can be seen that the coatings done with 21, 25 and 30 sccm showed a high transparency within the visible and IR range.

The transmission spectra obtained for the three samples was almost identical, which indicates that the oxygen flow has either little-to-no impact on the optical quality of the films. Due to the changeable rate of the deposition process and other factors, films deposited at 350 °C with an oxygen flow of 25 sccm adversely affect homogeneity; the refractive indices obtained for the films deposited at 350 °C with 21, 25 and 30 sccm oxygen flow were 2.64, 2.57 and 2.51 respectively.

Figure 71 (left) shows a gradual and linear decrease in the refractive index with an increase in the oxygen flow, and in cases of films coated using the cold process, it was observed that there was no change in optical quality when different oxygen flows were used. The transmission spectra of the deposition done at cold temperature with varying oxygen flows are displayed in Figure 72.

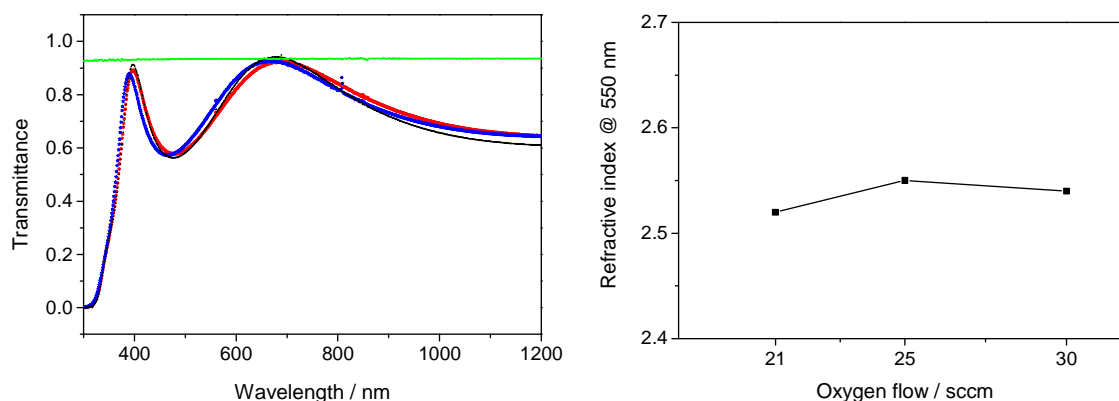


Figure 72. Example of oxygen flow influence on the optical properties at cold temperature. Blue: 30 sccm, red 25 sccm and black: 21 sccm. Green: uncoated substrate. Left: Transmission spectra for deposition with different oxygen flows ( $T=50\text{ }^{\circ}\text{C}$ ). Right: Refractive indices at 550 nm for the films coated with varying oxygen flows  $T=50\text{ }^{\circ}\text{C}$ .

The refractive indices of films deposited with an oxygen flow between 25 and 30 sccm at  $50\text{ }^{\circ}\text{C}$  remained constant, as opposed to the refractive indices obtained at  $350\text{ }^{\circ}\text{C}$ . Generally, high refractive indices of oxide layers can be obtained by applying high kinetic energy using an increased oxygen flow through the IAD process with CC-105<sup>[213]</sup>. When estimating the surface area of the films coated on a hot substrate, this resulted in a decrease of the surface area due to the smoother surface of the nodules, which should be more than compensated for by increasing the initial surface area. This issue is referred to again in Chapter 6 when discussing the density of the thin films as estimated from the refractive index.

#### (b) After Annealing

The films deposited using different oxygen flows were then subjected to annealing at  $450\text{ }^{\circ}\text{C}$  for 4 hours. As per the results shown in Figure 73, the films prepared using different oxygen flows did not show very different results in terms of transmission spectra. Differences in the spectra of the annealed films were only noticeable at the minima, between 420 and 520 nm, and also at the maxima, above 710 nm.

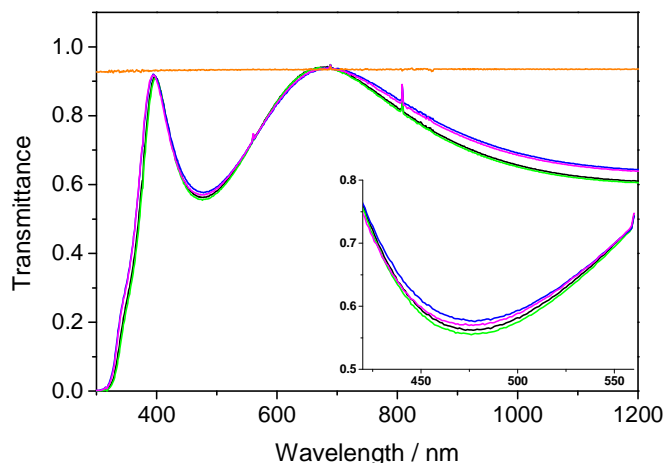


Figure 73. Transmission of IAD deposition using different oxygen flows after annealing. Pink: 21 sccm. Blue: 21 sccm annealing. Green: 30 sccm. Black: 30 sccm annealing. Orange: uncoated substrate.

In the visible region, the optical property of as-deposited  $\text{TiO}_2$  films is high and an obvious absorption edge is observed at around 370 nm. Also in the visible region, the average transmittance of a  $\text{TiO}_2$  film under different process parameters generally higher than 70% [270]. The absorption edge for the resulting films slightly shifts toward longer wavelengths. The influence of the reactive oxygen on the transmission is the cause of this shift to lower than 4 %.

### (C) Band Gap Calculation

The optical band gap of films was calculated on the basis of Equation 25 (mentioned in 7.1.1.c). The following graphs show the results of these calculations, with Tauc extrapolation, on thin films as-deposited at 350 °C under different levels of oxygen flow. (See Figure 74)

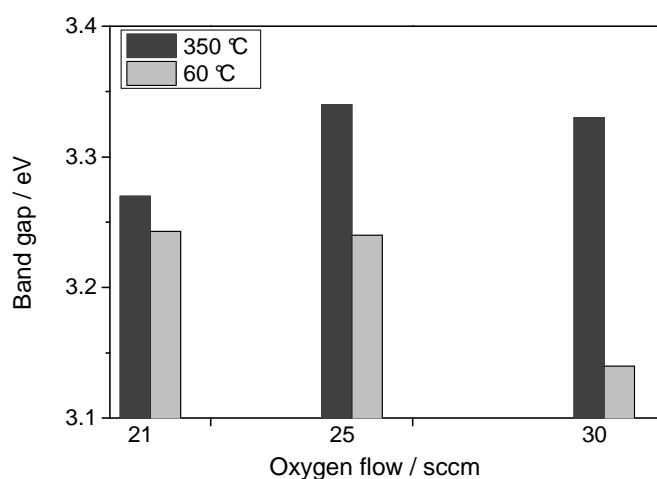


Figure 74. Band gap for IAD coated  $\text{TiO}_2$  films using different oxygen flow values. The measurement precision was ~2 %.

With oxygen flows for 21, 25 and 30 sccm of oxygen flow, the band gap was 3.27, 3.33 and 3.34, respectively. Thus, band gap increases with a higher flow of oxygen during deposition process. In comparison with the processes carried out at high temperature, Figure 74 shows also band gap calculation of films deposited at a cold temperature, 50 to 60 °C, with varying oxygen flow. The band gap of TiO<sub>2</sub> films on glass substrates varies depending on the process of deposition and the parameters used. The films prepared at levels between 21 to 30 sccm show a transparency in the long wavelength range. If the flow of oxygen is kept between 25 to 30 sccm, the band gaps would fall to the range of 3.24 to 3.14. Existing research shows that this is due to the film's thermal stress<sup>[3]</sup>. Films processed at cold temperatures of around 50 °C show that the band gap values are less than those for anatase, at 3.2 e.V.

### 7.2.2 Morphology of IAD Optics

The hydrophilic property of the coating samples was calculated by measuring the contact angle in exactly the same manner as mentioned in 7.1.2. The measurements were obtained using the initial conditions and after 67 hours of UV light. The results obtained from the films are as Figure 75:

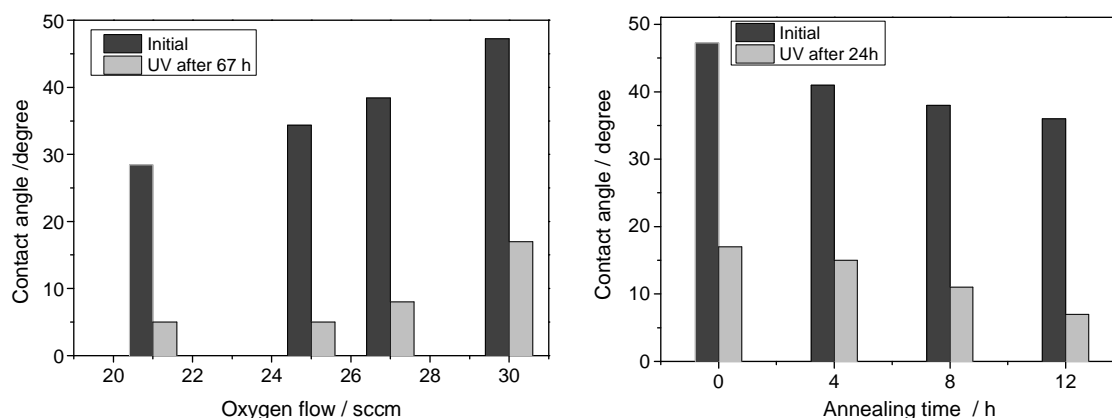


Figure 75. Contact angle results measured before and after 67 hours of UV irradiation. Left: Coated at 350 °C with different oxygen flows. Right: Coated with 30 sccm oxygen flow and annealed at 400 °C at different times.

Depending on the IAD oxygen assistance, thin film exhibits an initial contact angle of greater than 30 degrees (Figure 75 right). When this surface is under to UV light, water starts to exhibit a decreasing CA, i.e. it tends to disperse flatly instead of beading up, except for 30 sccm. For that, the Figure 75 (left) exhibits the CA for thin film kept at 30 sccm, but with different annealing time kept at 400 °C. Once exposed to UV irradiation, the films become super-hydrophilic as a result of the effect of the temperature and the oxygen.

The superhydrophilic surface becomes wholly non-water-repellant after UV-Illumination for thin films coated at lower than 30 sccm and annealed for more than 8 hours at 400 °C.

It can be concluded that the films coated under the above-mentioned parameters exhibit a very high transparency and refractive index. The refractive index for the films deposited at 350 °C increased when the flow of oxygen was decreased. The band gap has a correlation with the oxygen flow and all the films become super-hydrophilic after UV light.

### 7.3 Thickness Influence

To study the effect of different thicknesses on the films' properties, the following parameters were fixed:

Table 11. Fixed deposition coating parameters

Vacuum chamber				Source					Process
U	I	O <sub>2</sub>	Heater	Neutralizer		U	I	O <sub>2</sub>	Rate
HV[kV]	E[A]	[mbar]	[°C]	U[V]	I[A]	[V]	[A]	[sccm]	[nm/s]
8	0.35	3.10 <sup>-4</sup>	350	10	27	250	3	25	0.15

As mentioned in the chapter *Experimental Set-Up*, 3.1.6.3, and Table 11, the samples used in the experiments varied in thickness ranging between 150 nm and 900 nm using the fixed deposition rate, i.e. 0.15 nm/s.

The samples were annealed under different conditions; for example, the first group was first annealed at 450 °C for 4 hours and later re-annealed at 400 °C for 7.5 hours.

The second group of samples was annealed at a lower temperature of 250 °C for 8 hours. The transmission spectra of films varies depending on their thickness, which is described in detail in the below subheadings.

#### (a) As-Deposited

The difference in the transmission spectra for the films deposited with different thickness, 150, 300, 500, 700, and 900 nm, is shown in Figure 76:

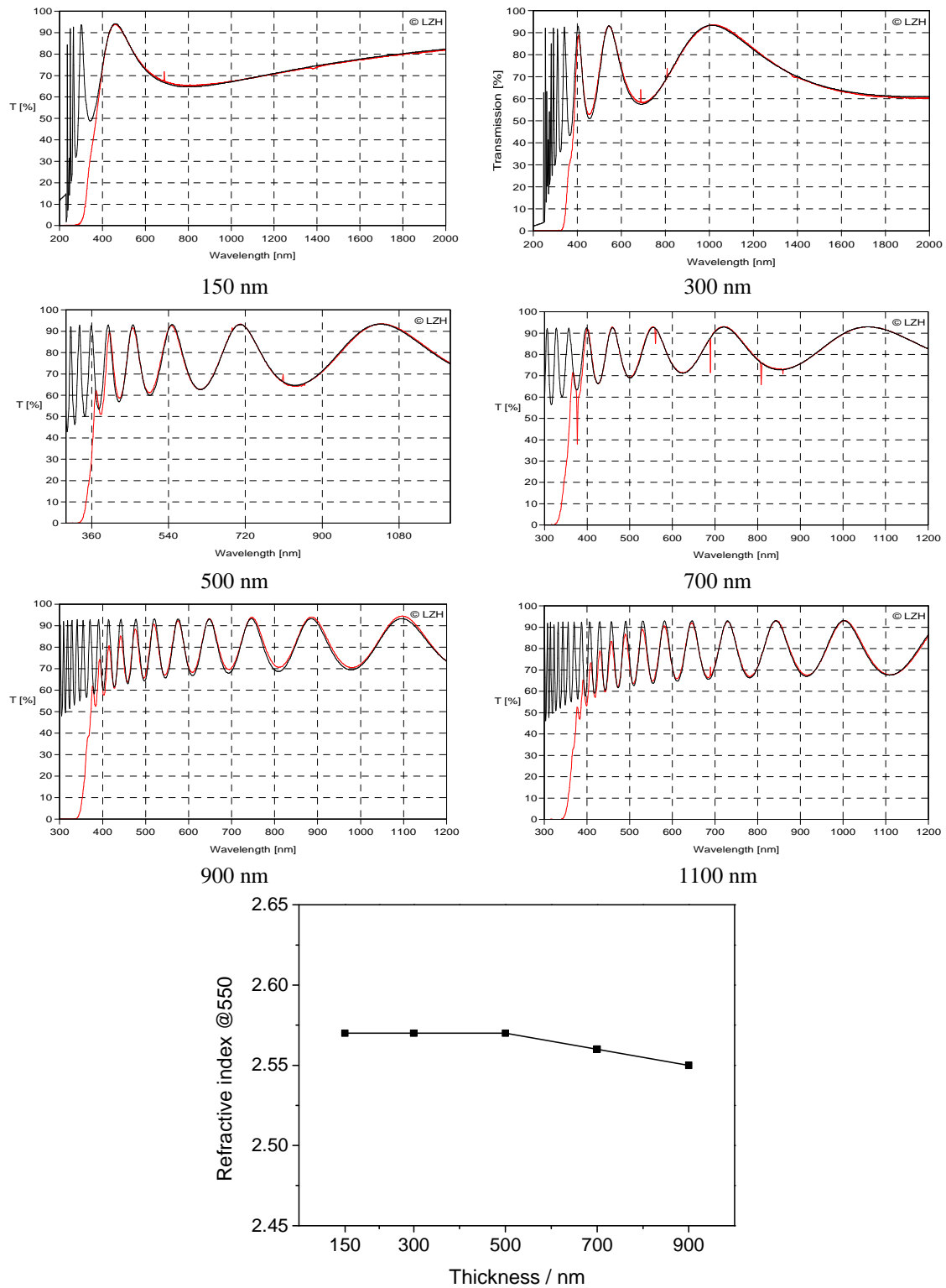


Figure 76. Range of the transmission spectra as-deposited films with varying thicknesses. Black: Programmed titania design layer. Red: the obtained IAD film.

In Figure 76, the coatings are transparent within the visible and IR range, independent of the thickness of the coating. It is important to notice that the experimental and simulated data are in a very good agreement. Concerning the process development, the design curve allows a detailed

analysis of inhomogeneities and optical properties during the growing layer via different thicknesses. The transmission spectra obtained are different and characteristic for each thickness. Figure 76 shows the range of the transmission spectra from 350 to 900 nm. The light transmission at different wavelengths varies with thickness of films. The refractive indices calculated for 150, 300, 500, 700, and 900 nm thickness were 2.57, 2.57, 2.57, 2.56, and 2.55 respectively, thus it can be concluded that the refractive index remains more-or-less constant with the varying thickness of films.

To close, good optical characteristics were seen from those layers coated with oxygen ion current densities up to near their critical values. A stable CC-105 optic operation is demanded. This relates not only to the possibility to apply correctly various coating parameters but also on the progressive stability. As total layer thickness increases, the optical absorption of the coatings increased. Moreover, no long-term drift of the variables ion energy distribution and ion current density distribution characteristics must be detectable. This could be caused for example by progressive electrode consumption or contamination effects during the process.

#### (b) After Annealing

The following graphs in Figure 77 show that annealing done at 450 °C for 4 hours effects light transmission considerably.

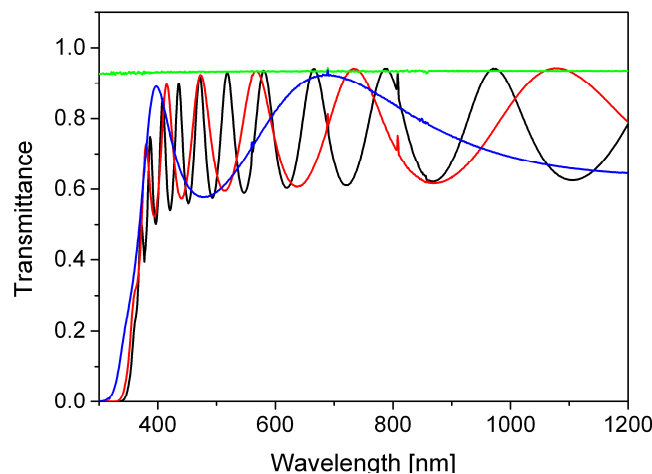


Figure 77. Range of the transmission spectra for coatings with different thicknesses. Blue: 300 nm; red: 500 nm; black: 900 nm. Green: uncoated substrate.

It can be observed that when annealed under the conditions described above, there is negligible impact on the transmission spectra of the films, which can be observed from no optical losses to the uncoated curve (dark line). The optical quality of the films remains the same after annealing at 450 °C for 4 hours. The above graphs show transparency of the film thickness, between 350 nm and 900 nm at the as-deposited stage, both after annealing at 450 °C for 4 hours and re-annealing



at 400 °C for 8 hours. The three films showed an almost identical transmission spectrum which leads to the conclusion that the annealing process, if carried out in the manner described above, does not considerably affect the optical quality of thin films. Other conditions of annealing were tried on the substrates coated with different thicknesses. To observe the possible effects that different annealing temperatures may have on optical properties and photoactivity, different samples were annealed at high temperatures, such as 400 °C, and at a relatively lower temperature of 250 °C for 8 hours. The optical transmittance data revealed good transmission in the visible region of the as-deposited and annealed films and a sharp fall in the UV region, which relates to the band gap. It can be clearly observed in Figure 78 that the optical quality of the annealed films is lower than the as-deposited films of the same thickness.

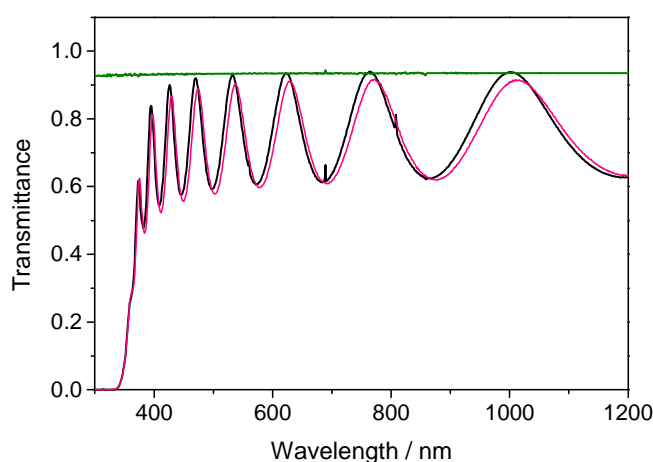


Figure 78. Transmission spectra of a film with 700 nm thickness. Pink: 700 nm as-deposited ( $n@550$ : 2.56). Black: 700 nm anneal ( $n@550$ : 2.57).

Figure 78 indicates that there is a change in the optical properties of the films after annealing when under the same conditions. A comparison was made between the different experiments using different substrates, such as Suprasil for the as-deposited films and Menzel for annealed films.

### (c) Band Gap Calculation

The optical band gap of the films was measured using Tauc equations, previously mentioned in 7.1.1 (c), and the graphs with extrapolation obtained for the as-deposited films of different thicknesses are shown in Figure 79. The band gaps calculated for 150, 300, 500, 700, and 900 nm were 3.33, 3.32, 3.30, 3.29, and 3.26 eV respectively, as can be seen in Figure 79. (Band gap graphs are illustrated Figure Appendix VIII).

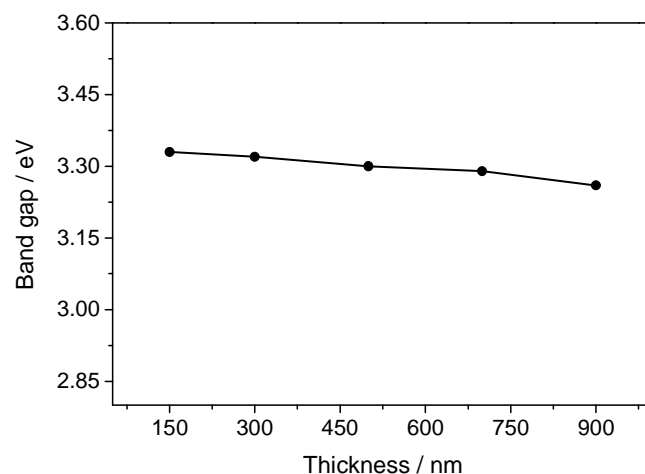


Figure 79. Band gap for TiO<sub>2</sub> films coated with different thickness. With an increase in thickness, absorption increases and band gap decreases, showing a trend similar to that of Figure 76.

The magnitude of the absorption band gap of TiO<sub>2</sub> film deposited can be determined by representing  $A(h\nu)^2$  ( $A$ , absorption coefficient from the UV-Vis spectra) against  $h\nu$  and extrapolating to zero the straight zone of the plot. From Figure 79 it can be observed that the band gap energy of each sample decreases (only slightly) when deposition thickness increases.

Additionally, the comparison of photo-induced hydrophilic activity of TiO<sub>2</sub> thin films with the different thicknesses was shown in Figure Appendix IX. The initial water contact angle was approximately 40°. After the film surface was irradiated by UV light, the water contact angle decreases. All samples had low water contact angle of about 5° after illumination, which indicated good photo-induced hydrophilicity of these films. Among the thin films, the superhydrophilic activity was achieved from the films thickness of 150 and 900 nm corresponding to layer structure dependence.

#### **7.4 Correlation between Refractive Indices at 500 and 1064 nm and the Different Coating Parameters**

In order to measure the refractive index, different samples were investigated by coating under varied parameters, namely ion-source current, coating temperature and coating thickness.

When using an IAD process, the dense microstructural layer minimizing the water content of the titania films leads to an improved thermal stability.

The physical dependence of the refractive index on the temperature or the thermal expansion of the layers causes the small positive shift of the refractive index. These are not detectable in conventional coatings prepared by the induction of an undesirable shift by water desorption.

Figure 80 illustrates the evolution of the refractive indices at 500 and 1064 nm as a function of ion-current dependence; reactive oxygen gas used at high and low deposition temperatures, substrate heating during the coating process, and thickness.

These experiments show that when the ion-source current is increased from 1 to 5 A, the refractive index increases slightly until 3 A, at 500 nm wavelength, yet when further increased to 5 A, the refractive index starts increasing considerably. The results remained the same even with the refractive index at a wavelength of 1064 nm.

A compaction of the layer is induced by ion bombardment, which improves the densification and the intra-columnar structures remain. This leads to water absorption and produces an increase in the refractive index.

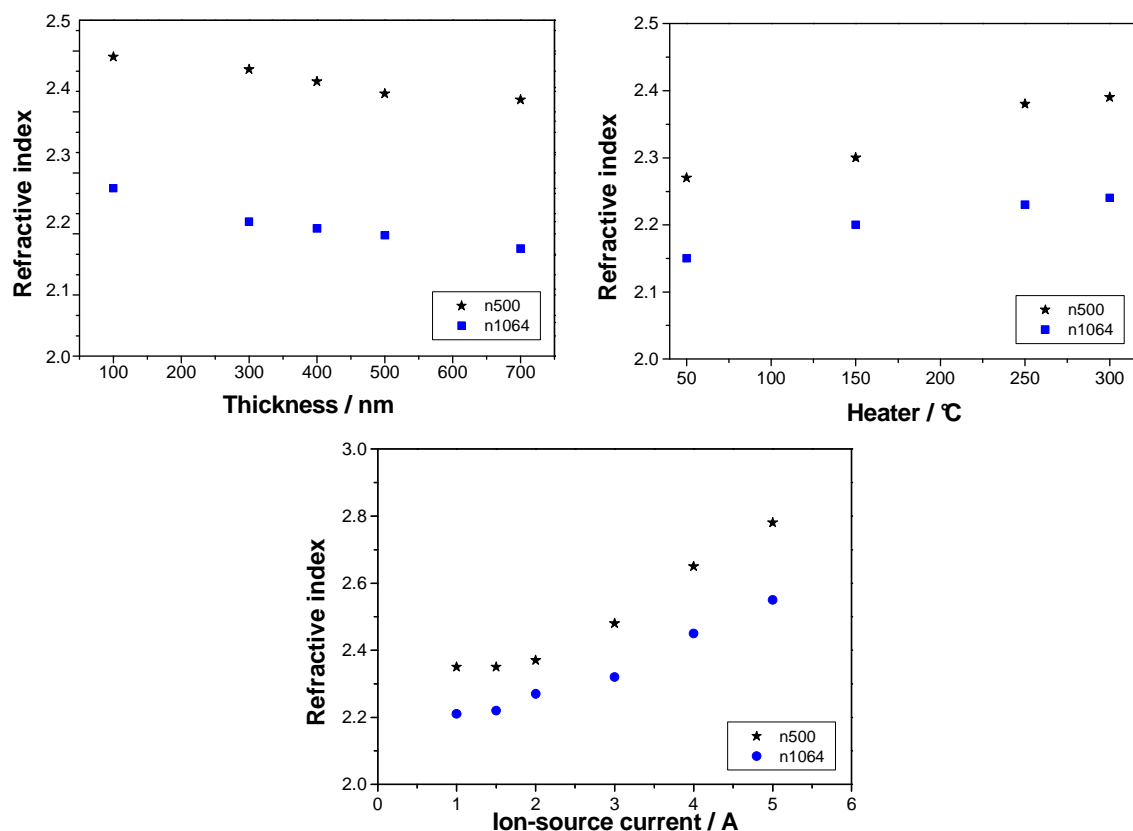


Figure 80. Dependence of the refractive index of the coating parameters at different wavelengths (Black: 500 nm. Blue: 1064 nm).

Above this point, the film is stable and indifferent to its environment. These changes were anticipated not only in the layer density and the refractive index, but also in the crystalline structure, displaying a high transparency. TiO<sub>2</sub> films deposited at a high ion dose have a higher transparency resulting in the photocatalytic film having the best optical property. The use of overhanging atoms casts a favorable light on the structural model. The process temperature also

has an effect on the refractive index of photocatalytic active films, as the index increases with an increase in the temperature, and reaches its maximum at 250 °C. This result can be attributed to the formation of thin films with high refractive index, which conforms to the research of Yoshida et al. [279]. Although the transmittance of as-deposited TiO<sub>2</sub> films is fairly good, its refractive index at 500 nm is low and some absorption has been observed. After being heated, the refractive index of the TiO<sub>2</sub> film at 500 nm increases. When the annealing temperature is high (up to 450 °C), the transmittance (shown in Chapter 7) deteriorates slowly. For the thin film's thickness, no considerable proportionality to the refractive index is found, since an increase in thickness from 100 to 700 nm decreases only very slightly the index.

## 7.5 Scattering Tests Correlating to IAD Parameters

The quality of optical components after coating can be investigated by means of the light scattering analysis. In particular, the state of cleanliness and the roughness of an optical surface [215, 280] can be evaluated with the help of the Total Scattering (TS) measurement. According to the international standard ISO 13696, TS is the integration of the scattered light in the angle range from 2° to 85° in the frontal hemisphere of the investigated specimen. TS is calibrated as the ratio of the scattered power  $P_s$  divided by the incident power  $P_0$ . Thus, TS is dimensionless.  $P_0$  is measured by using a calibration sample which is a diffuser with an exactly known reflectance at the investigated wavelength. The scatter characteristic of the calibration sample has to be Lambertian (cosine-scatter distribution). Because of the low level of the scatter losses, TS is expressed in terms of ppm (0.000001, parts per million).

The scatter loss depends on the roughness and spectral reflectivity of the sample. The relationship between the scattering in backward direction and the roughness of the opaque surfaces can be expressed as:

$$TS = R(\lambda) \cdot \left( \frac{4\pi \cdot \sigma}{\lambda} \right)^2 \quad \text{Equation 28}$$

where  $\lambda$  corresponds to the test wavelength. For the calculation of RMS-roughness  $\sigma$  of a sample, its spectral reflectivity  $R$  has to be exactly known. The TS results presented in this work are used only to indicate the evaluation of the surface quality and not for the exact determination of  $\sigma$ . For the evaluation of the TS results presented in this thesis, mappings ( $\varnothing = 22$  mm) are performed in the center of the samples. The “optimized mean value” of the TS direction is calculated according to the corresponding data evaluation procedure in ISO 13696. The distance between two points on the mappings amounts to 25  $\mu\text{m}$  and the measurements are done at wavelengths of 633 nm or

532 nm. Figure 81 shows an example of a scattering map for a coated sample. The detection limit (background) of the involved TS-set-up amounts to 0.1 ppm and thus, smooth samples with a RMS-roughness in the range down to 1 Angstrom can be investigated<sup>[215]</sup>. The realized set-up at LZH allows for a fast mapping of the samples in a few minutes.

Mean: 0.356  
 Standard deviation (std): 1.85  
 Optimized mean: 181 ppm  
 Number of data points: 605.000  
 Optimized standard deviation: 37.2 ppm  
 Used number of data points: 556.000. Iterations: 9

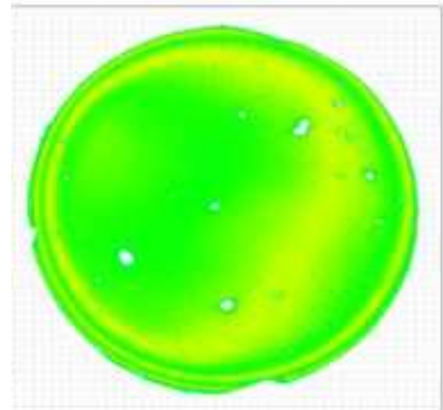


Figure 81. TS map at 633 nm coated single layer and the calculated statistical parameters (Table Appendix 2). Mean is the average of all measurement points (raw data). The mean value  $S_m$  is sensitive against fluctuations. Therefore, the optimized mean value is calculated by removing the points with a very high ( $S > S_m + 2std$ ) level of scattering. The procedure of data reduction is iterated 9 times.

### (a) Fast Scattering Test for the Ion-Source Parameters Dependence

In order to evaluate the influence on the Denton CC- 105 parameters by the coating, scattering maps of the samples were investigated to monitor the effect of the ion-source current and oxygen flow. The results of these tests are depicted in Figure 82.

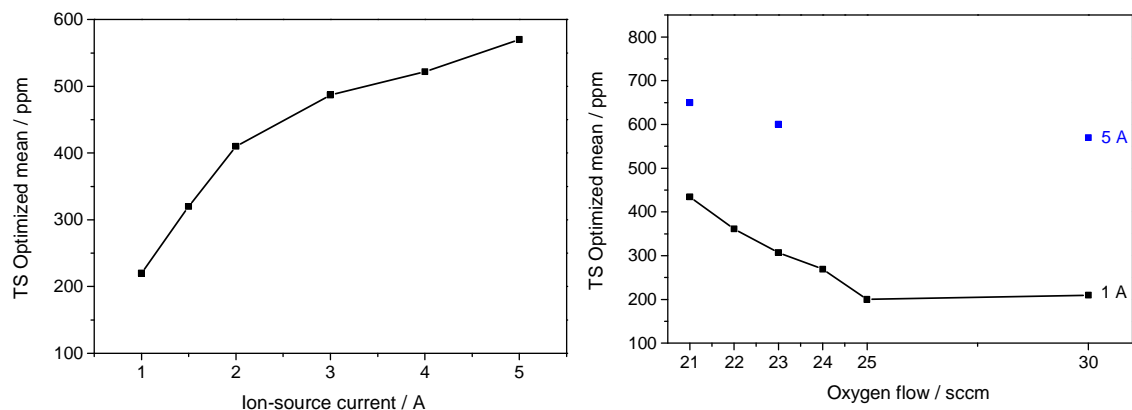


Figure 82. Results of scattering test on different ion-source parameters. (Left) Ion-source current comparison with 30 sccm  $O_2$ . (Right) Oxygen comparison at low temperature at 100 °C, using 1 A (dark) and 5 A (blue), at ~ 300 nm.

In the left graph, the increase of the ion-source current causes the increase of the scattering. It indicates that the ion kinetic energy has an effect on the surface morphology and on the production of agglomerates of crystallites. Scattering increases considerably if the ion-source is operated with a high discharge current such as 4 A or 5 A. A small variation can be observed when the ion-source is operated with oxygen as the reactive gas. An improvement (from 450 ppm to 200 ppm) of the scatter level is observable due to a high level of oxygen assistance. The ion energy distribution and the ion current density have an affect on the surface morphology and the production of agglomerates of crystallites.

### (b) Fast Scattering Test for Thickness and Temperature Dependence

In Figure 83 the measured scatter losses of a  $\text{TiO}_2$  layer series are illustrated. The thickness of a single layer varies from 100 to 700 nm. An increase of the scatter level can be observed when layer thickness increases. The change of the samples' reflectance is about 4%. However, the scattering of the layers increases from 250 ppm to 4500 ppm. This is an indication that the roughness of the layers increases strongly with their thickness.

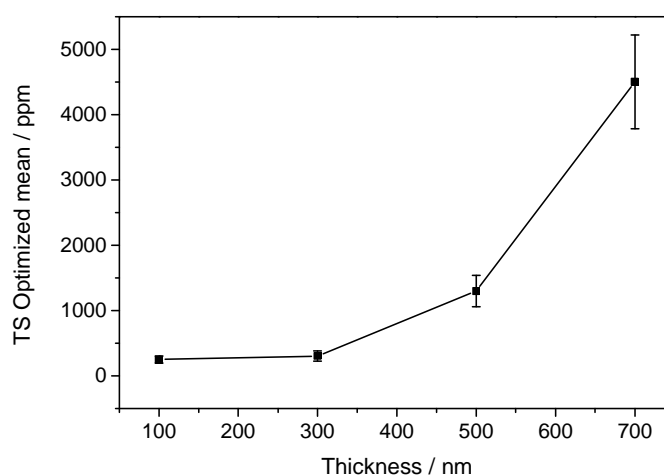


Figure 83. Influence of the deposition thickness on the optimized mean values.

The roughness of the single layer correlates strongly to the surface roughness of the substrate (before coating)<sup>[280]</sup>. Therefore, fused silica samples (Suprasil) with a RMS-roughness of about 1.47 nm (Figure 50) are used. In order to investigate the effect of the sample, AFM-profilometry tests of coated and uncoated substrates are performed. The corresponding AFM images reveal that pronounced agglomerates of crystallites in the layer are the cause of the roughness effect.

A test series is performed in order to verify the effect of the temperature on the coating roughness on Suprasil samples. The thickness of the layers was equal in all samples (300 nm  $\pm$  15 nm). The

results are shown in Figure 84. They are in considerable agreement with the measured sample scattering, that the change of the reflectivity is not considerable.

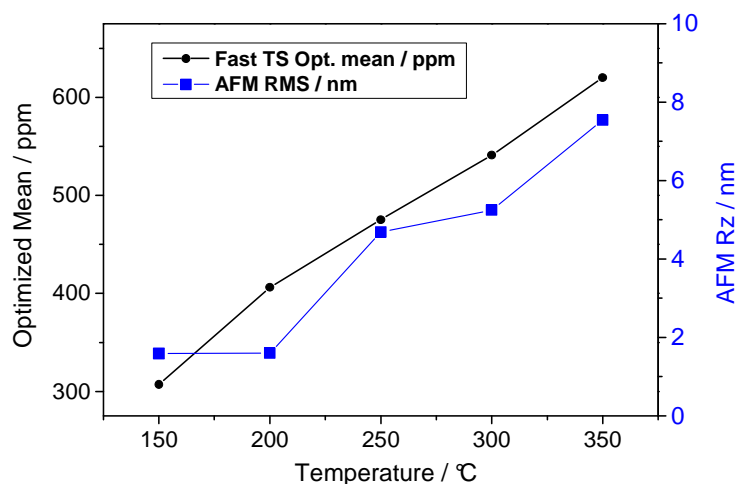


Figure 84. Accordance between the scattering result and the roughness of the single TiO<sub>2</sub> layer by different coating temperature, at ~ 300 nm.

It can be concluded that there is a linear correlation between the scattering values and the coating temperatures. Adjusting the ion-source parameters does not have greatly influence the scattering level. The results obtained from the experiments can be used to understand the correlation between the morphology, optical characteristics, and the photocatalytic activity based on an optimized coating matrix. Total Scattering measurements, according to the ISO 13696 standard, can be involved for a precise and fast testing procedure for the determination of the surface roughness quality [27, 215].

## 7.6 Chapter Conclusions

To summarize the above headings, the coating temperature, oxygen flow, and film thickness were varied in the experiments conducted to assess functional properties of TiO<sub>2</sub> films using the optimized IAD process (VI). These parameters were used on as-deposited and annealed films. To evaluate the processes and correlation among different parameters, three different methods were used, namely spectrophotometry, SEM, and EDX. To compare the hydrophilicity of different samples water, CAM was used. During the experiments, all films prepared using these different process parameters showed a high transparency and high refractive index. The films also showed superhydrophilic properties under UV light and became hydrophobic after being stored in the dark. An increase in process temperature and annealing temperature improves hydrophilicity and structural and optical properties of transparent films. The most suitable results in terms of hydrophilicity were observed in cases of films coated at a process temperature of 350 °C. The

films processed under these conditions have the largest particle size, most roughness, and the highest hydrophilic properties.

The annealing of TiO<sub>2</sub> films at a higher temperature of above 600 °C typically results in a lower transmittance. Therefore, the motive that the maximum annealing temperature operated during this study was generally 500 °C. The refractive index is proportional to the substrate temperature.

Additionally, the refractive index for the films deposited at 350 °C increased when the flow of oxygen was decreased.

The transmission spectrum of films differs depending on their thickness, If the thickness of the films is increased the particle size increases. The refractive index rests more-or-less constant with the changing thickness of films.

Finally, the surface turns into a highly hydrophilic state and remains unchanged for up to one week. It can therefore be expected that various glass products, i.e. mirrors and eyeglasses, can use this technology to gain anti-fogging functions. All with simple processing and a low cost. The TiO<sub>2</sub> films prepared via PVD display low packing density resulting in low refractive index values and a high sensitivity to the environment <sup>[281]</sup>. It is for this reason that ion-activated technologies have been developed. One of which being ion assisted deposition (IAD) which is largely used due to its good acclimatization to the coating chambers <sup>[163, 179]</sup>.



## 8. Correlation between Photocatalytic Activity, Crystal Microstructure and Morphology of IAD Transparent Titania Thin Films

Whereas previous chapters have analyzed the various titania layer functionalities over different processes, discussed here is the correlation between these functionalities on the basis of the drawn conclusions. Previously considered were general studies regarding PVD inclusive comparison with conventional and ion beam sputtering and other processes, summarized as follows:

- As previously mentioned in Chapter 6, the photocatalytic activity may also simply be connected to roughness. When a thin film has both a completely dense structure and a flat surface, the active surface area is equal to the geometrical area of the substrate. A rough surface, on the other hand, will have a larger area <sup>[3]</sup>.
- Varying levels of thickness result in different transmission spectra. However, annealing does not make a considerable difference on transmission spectra and the refractive index of films is affected by the temperature used. The band gap also increases with a higher flow of oxygen during the IAD deposition at 350 °C.
- All the films used in the experiments exhibited super-hydrophilic properties after being exposed to UV light.
- The SEM results show a direct correlation between the size of the agglomerate, the coating thickness, and the annealing effect. An increase in the coating thickness increases the size of particle. The same can be achieved by the annealing procedure, which results in an anatase structure. An increase in the size of the particle also increases the active surface area, which then improves the affixing of OH-radicals and consequently, the level of photoactivity ameliorates.

Striking a compromise between a sufficiently high optical quality and a ‘multi-functional structure’ gives the appropriate optimization range of the coating processes. With a sufficiently high optical quality, it is possible to produce a dense transparent structure, which is needed to provide good photocatalytic characteristics. Generally, if a thin film has a completely dense structure and a flat surface, the active surface area is equal to the geometrical area of the substrate. A rough surface, on the other hand, will have a larger area.

Chapter 8 here discusses a final correlation and the optimal phase for important IAD parameters. Crystallinity, photoactivity, self-cleaning, and hydrophilicity are some of the functionalities analyzed, and thus the correlation between these form the subject matter of this chapter.

Owing to this, reaching a balance between an optical characteristic, such as, the change of the refractive index with wavelength (dispersion) and the stability of the monolayers is a fundamental issue to the microstructure and functional properties correlation section of this research, along with the understanding of hydrophilicity, photocatalytic performance and microstructure, use has.

## **8.1 Correlation between Grain Size, Photonic Efficiency and Hydrophilicity with Ion-Source Current as a Variable**

The ion-source Denton CC-105 was operated with 30 sccm oxygen using a standard 0.64 nm diameter tungsten wire as the filament lit under an ion-source discharge current between 1 and 5 A. The typical operation parameters are that of oxygen flow, temperature, coating rate, thickness and ion-source gas flow. With the aim of influencing of the discharge current, all of these parameters were kept at a constant, with the exception of the ion-source current. With the aim of managing the stability of the ion energy distribution and understanding the correlation of the ion-source current with the morphology and the photocatalytic performance, the ion-source voltage was kept constant at 200 V. To technically attain this constant rate, the CC-105 neutralizer was adjusted to stabilize the ion-source voltage, and the neutralizer potential was altered according to the goal process parameter.

Ehlers et al.<sup>[211]</sup> demonstrated by RFA measurements, that the long term stability of the ion energy distribution and ion current density is vitally important for the production of both complex and stable optical results, involving homogenous titania films. The measurement conditions for BAK 760 assisted with Denton CC-105 have already been investigated<sup>[213, 235]</sup>. The RFA measurement shows how optical conditions in thin film reach stability. At that point, the stability of this ion- source is related to the discharge current and voltage, the filament current and voltage and the flow of oxygen as a reactive gas.

One purpose of the ion-source is the formation of ions from the sampled gas molecules and atoms, which is done through electron impact, with another purpose being to focus and accelerate these ions. The detector is responsible for the ion current collection and measuring, and is usually based on a RFA ion collector. The majority of detectors are provided to amplify the ion current. A methodical analysis is shown from the resulting ion energy distributions: Increasing the discharge current from 1 to 5 A alters the peak positions for the ion energy distributions to gain better kinetic energies, which corresponds to a higher ion current density. Also in the RFA study, it was

shown that a quadratic fit is a good approximation and proved the reliance of the ion-source total energy as a function of discharge current.

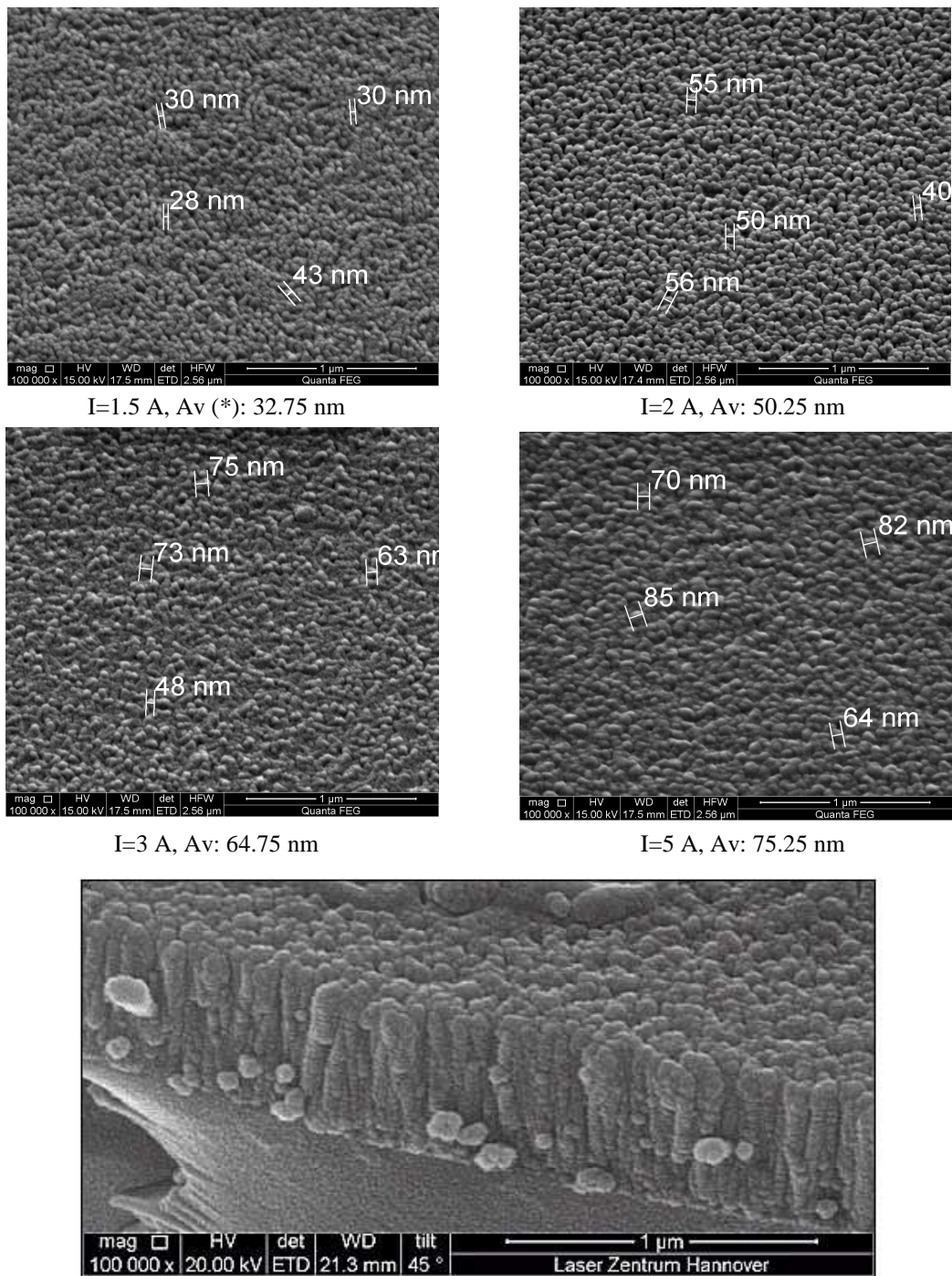


Figure 85. Results of the scanning electron microscope photographs. The ion-source current is varied, yet the oxygenation, layer thickness, coating rate and coating temperature are kept constant. Bottom-most picture: a representative cross-section of an IAD Process (I= 5 A, 300 nm, 30 sccm). Legend: (\*) Av: average value. mag: magnification; HV: high voltage; det: detector; ETD: secondary electron 'Everhart-Thornley Detector'; WD: working distance, tilt: angle sample to axe.

The grain size of the TiO<sub>2</sub> thin films was determined with the support of SEM in which different and randomly chosen regions of the coated samples were examined. The grain size was determined by taking the average sizes of these examined samples. These sizes are chosen with a representative methodology for the examined morphological area. The four images shown as Figure 85 show the grain size of the samples coated using varying ion-source currents, 1.5, 2, 3 and 5 A.

SEM showed that a TiO<sub>2</sub> film is composed of 30 - 80 nm grains and increases in proportion to the ion-current, which is evident in Figure 86.

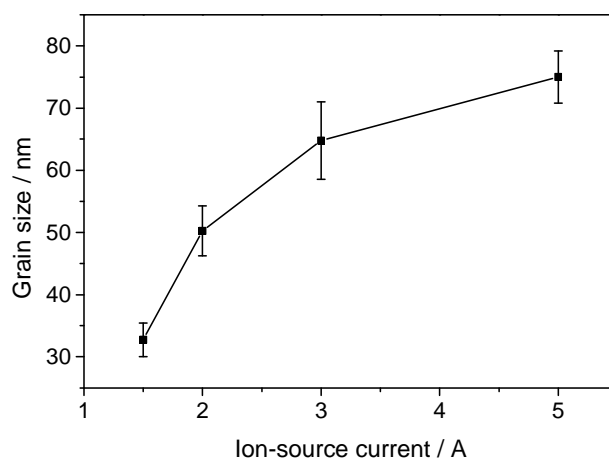


Figure 86. Correlation between grain size of the monolayer TiO<sub>2</sub> and the ion-source current.

The films exhibited, from a top-side view, a uniform structure of the column and granular surface with a fine grain for low ion current values of 1.5 and 2 A, as compared to higher levels of 3 and 5 A which show a large grain size. This change in the grain size appears to be due to the enhancement of the crystallization. Films prepared with a high ion-current level possess a strong adhesion to the substrate, and the crystallinity of the samples coated using 30 sccm is shown in the following Figure 87:

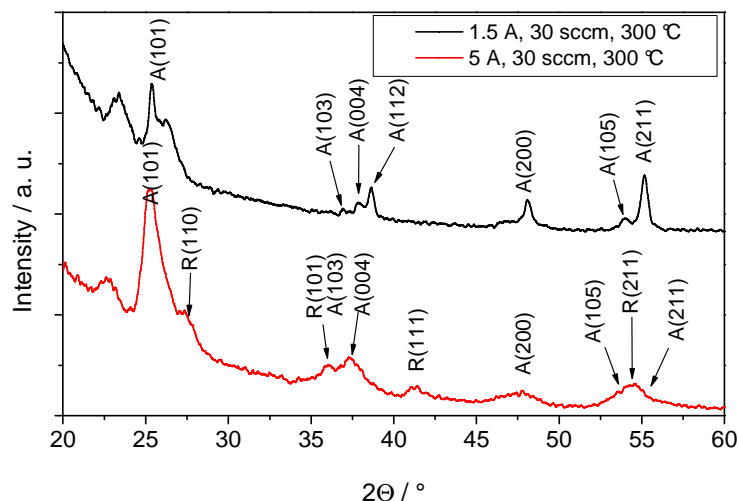


Figure 87. XRD pattern of the prepared  $\text{TiO}_2$  thin films with a variation of ion-source current at 1.5 A and at 5 A.

For the sample prepared at 1.5 A, an almost exclusively anatase modification is found. A slight shoulder at a  $2\theta$  angle (101) of about  $26^\circ$  is visible, but cannot be attributed to the rutile (110) reflection usually situated at  $27.45^\circ$   $2\theta$ . Interestingly, the photonic efficiency is significantly decreased to 0.045%. Additionally, XRD study shows an increase in the ion-current to a value of 5 A, which is the maximum level possible with the Denton CC-105 ion-source providing a stable energy distribution. The higher ion current of 5 A provides well crystallized films. The preferred orientation of the anatase crystallites is (101). The columnar structure of the (101) preferred orientation  $\text{TiO}_2$  prepared by IAD was similar with that produced using the sputtering in a previous study <sup>[103, 273]</sup>. Obviously, all the other anatase reflections are weakened, which can be in accordance with the preferred columnar growth shown in the SEM cross section image. A good degree of crystallinity leads to a quite high photonic efficiency of 0.077%. Possibly, the mixed phase composition of rutile and anatase found also in the prominent titania photocatalyst Degussa P25 has a positive effect on the photocatalytic activity as well <sup>[70, 71]</sup>.

Raman bands at 141, 393, 514, and  $636\text{ cm}^{-1}$  (Figure 88) are designated to the anatase phase. Those displayed at  $320\text{ cm}^{-1}$  and  $450\text{ cm}^{-1}$  correspond to the rutile phase. In all of the coated samples, the dominant titania phase is anatase.

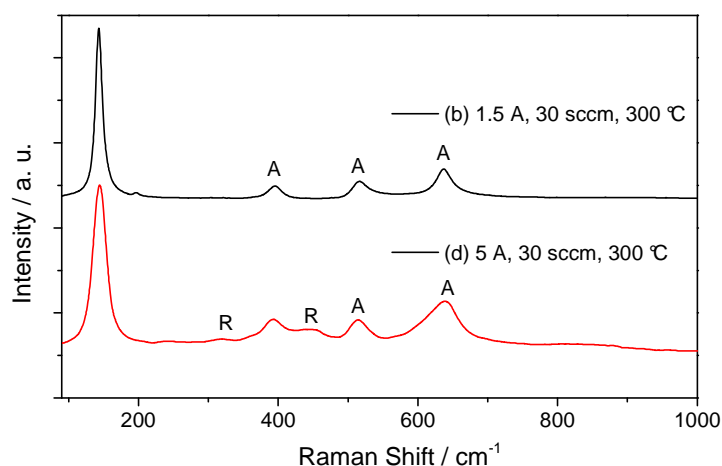


Figure 88. Raman spectra of TiO<sub>2</sub> at various ion-current (minima 1.5 A, and maxima 5 A).

As has already been noted before, the ion energy increases with an increase in the ion-source current, from 1 to 5 A. This results in an increase in the ion dose and therefore a denser layer. Additionally, when the energy is high, i.e. 5 A ion current discharge, the distribution of crystal atoms can change with the formation of the rutile phase parallel to the anatase. The SEM pictures also show that there was columnar growth, which leads to an enhanced photocatalytic performance.

In order to clarify the effects of ion bombardment on film growth, a microstructure study was conducted. This study demonstrated that the films obtained at a high ion-current are polycrystalline, consisting of anatase and rutile phase. These same conditions also improve the rough surface and a columnar cross-sectional structure. Rough surfaces are determined using the SEM images and have a high discharge current (higher than 3 A).

In order to clean the substrates, ion bombardment prior to film deposition was conducted (Figure 89). Ion bombardment during film deposition produces one or more advantageous effects, including sputtering of loosely-bonded film material, desorption of gases, low-energy ion implantation, modification of a large number of film properties and conformal coverage of contoured surface.

The source material is not required to be derived from a target as it can also originate from an evaporation source that reacts to the condensed constituents to form compounds.

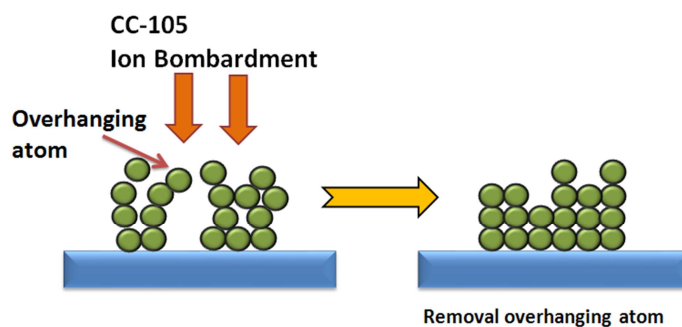


Figure 89. Explanation of the influence on the atomic adsorption of ion-source bombardment.

The basis of the surface treatment procedures is that some chemical reactions are hastened at a given temperature in the presence of energetic reactive-ion bombardment plasma oxidation, which is basic for the 'overhanging atom'. The return will be essentially identical for the bombardment of a surface with an ion or an atom of the same energy; e-beam PVD relies on the transfer of physical momentum and kinetic energy from the incident particle to the surface atoms, which is independent of the particle's charge. Not only are the same parameters known, but they are for the most part controllable. Together with previously mentioned proper e-beam techniques, this makes the process useful during the early stages of film growth for bombardment.

The ion bombardment persuaded not only the condensation of the adsorbed atoms, but also a growth of the crystal from an anatase crystalline phase to an anatase-rutile mixture using the same oxygen-atom flux of 30 sccm. This variation on the microstructure affects also the photocatalytic performance.

In addition, the roughness can have a significant influence on the heterogeneous catalysis process. Adsorption of molecules is typically related on steps and edges to rough titania surfaces. Roughness enhances hydrophilicity and affects the wettability, meaning that the layer is consequently more photoactive. As a result of the large aggregates formed by the interconnected  $\text{TiO}_2$  particles, the  $\text{TiO}_2$  surfaces show important roughness, depending on the scan sort, preparation method and fractal dimension range (see chapters 6 and 7).

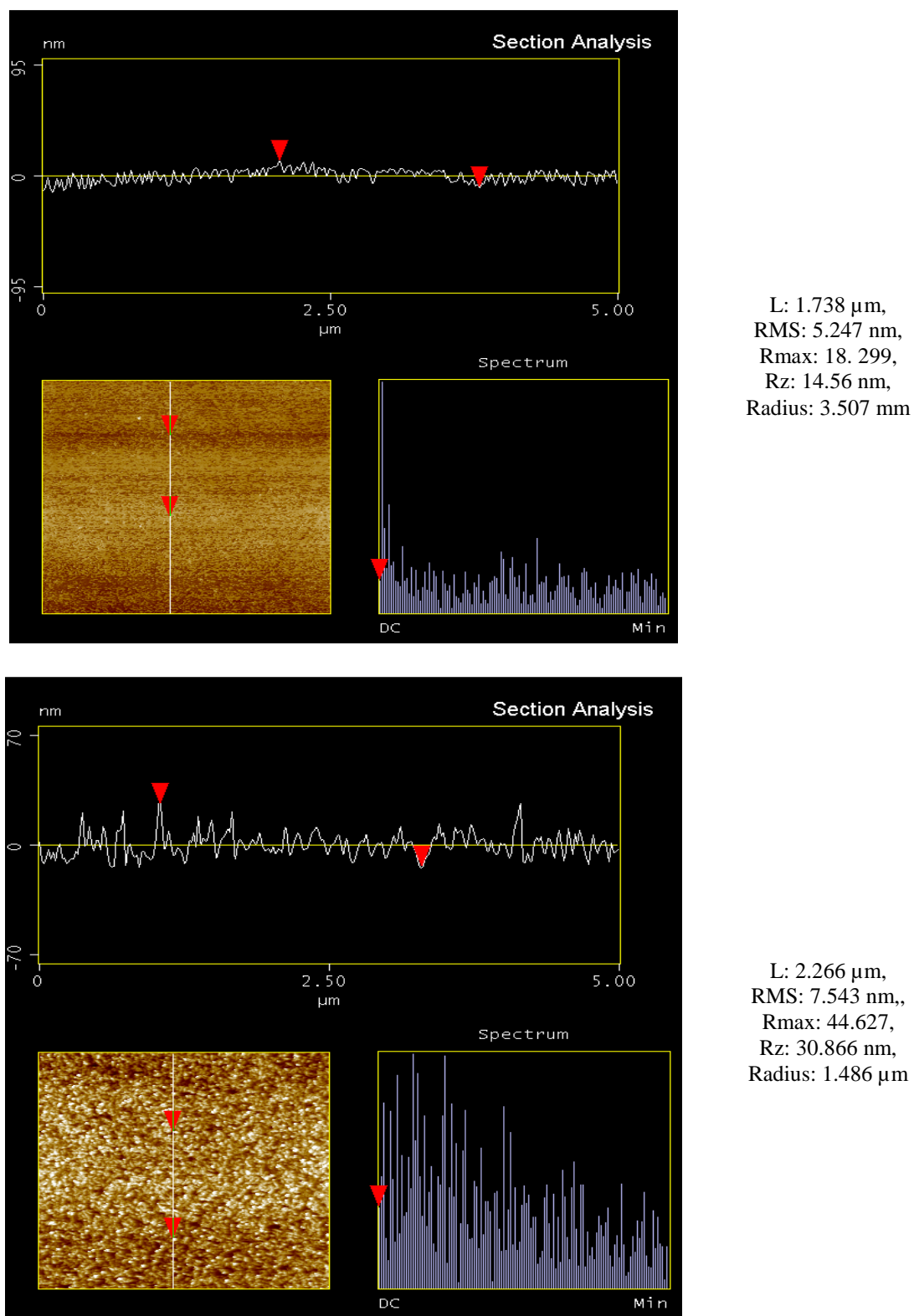


Figure 90. AFM investigation of coated titania thin layers with different process parameters. Top: without IAD, Bottom: the crystallite size is larger for  $\text{TiO}_2$  films deposited with Process V, CC-105, at high discharge current.

This may be one more reason for the improvement in the photocatalytic activity of  $\text{TiO}_2$  films, as a larger size results in more active sites being available for photodegradation. There is usually no



direct correlation between the surface and the activity of the individual sites. It is also known from AFM pictures, Figure 90, that the crystallite size is larger for TiO<sub>2</sub> films deposited with CC-105, at high current values. As the ion-beam current is increased from 1 A to 5 A, the crystal's grain size increases and becomes rougher, leading to an increase in the photocatalytic performance of the TiO<sub>2</sub> films. A current of 1 A corresponds to a root mean square *RMS* equal to 5.247 nm, with an average maximum height (*Rz*) equal to 15 nm. At 5 A, the values are 7.543 nm for *RMS* and 31 nm for *Rz*. The *RMS* values (*RMS* being the standard deviation of the *Z* values, *Z* being the total height range analyzed) for both films show that the TiO<sub>2</sub> films present surface characteristics of greater size when compared with heated IAD films.

To accomplish suitable conditions for high crystallinity, a columnar growth observed via SEM, a good crystal orientation, a rough surface and high ion-energy dose (via high temperature upper than 250 °C and via discharge current higher than 3A) are required.

After determining the grain size and the roughness, the next step was to measure the contact angle, both with and without UV illumination. The correlation of the photonic efficiency, microstructure, and contact angle, before and after UV illumination is depicted in the Figure 91 and Figure 92.

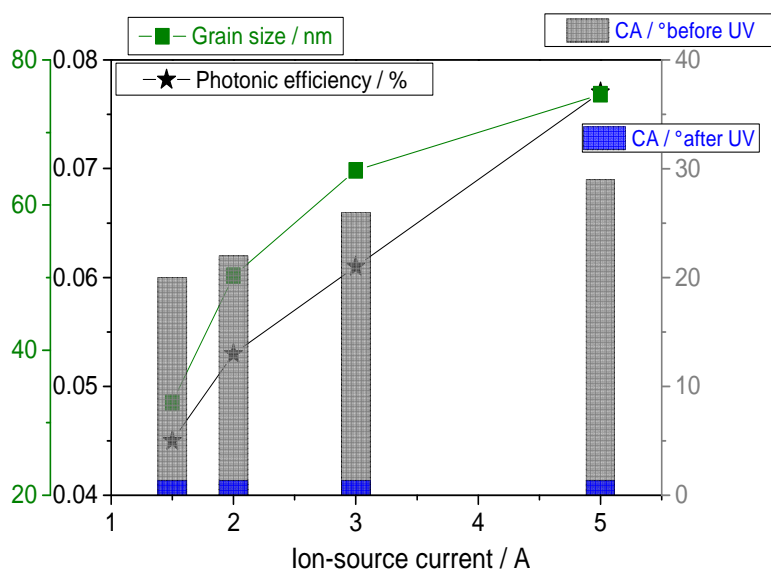


Figure 91. Correlation between grain size and CAM for different ion-current values. The contact angle is both before and after UV irradiation.

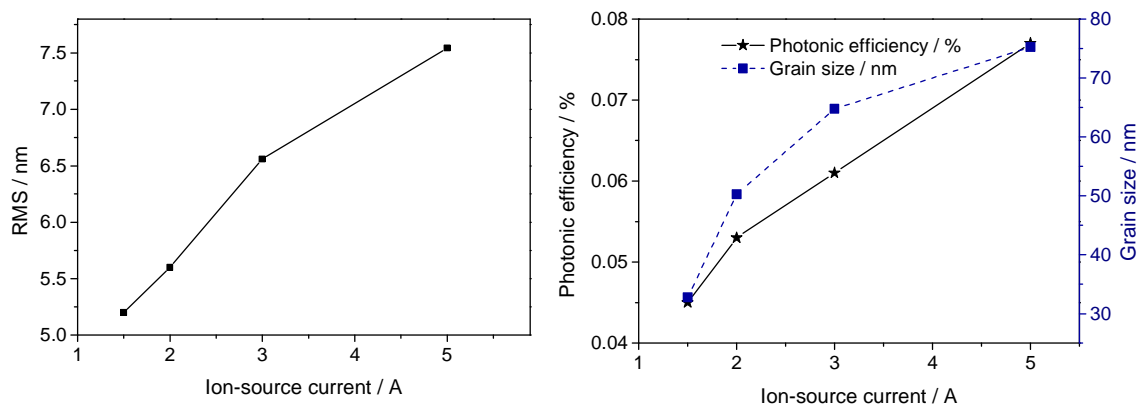


Figure 92. Correlation between photonic efficiencies and grain size for different ion-current values. ( 1 to 5 A, 300 nm, substrate heated via high temperature)

Figure 91 to Figure 93 show that the high photonic efficiency of the coated substrates is slightly above 0.070%, and also displays the structural sizes obtained from the experiments. The results represent good demineralization of methylene blue. The CAM results showed a hydrophilic structure after UV exposure, but a relatively higher contact angle was observed on the sample treated under high ion-source current, of 5 A. It can be concluded from these different phases that the microstructure of coated films changes with different levels of the ion-source current.

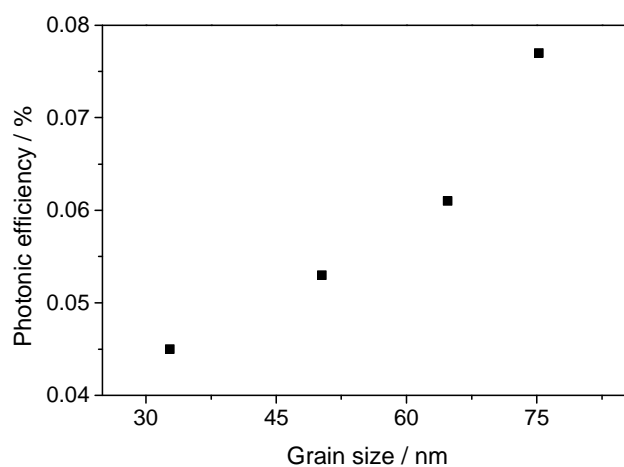


Figure 93. Correlation between photonic efficiencies and for different grain size values.

The synergetic effect of photocatalysis and hydrophilicity can be explained as follows. As it is possible with hydrophilicity to adsorb more OH groups on the surface, the photocatalytic activity is enhanced, therefore hydrophilicity can improve photocatalysis.

It is also possible for the film surface to adsorb particles, which can then turn the hydrophilic surface to a hydrophobic surface. The organic compounds on the film surface can be decomposed through photocatalysis, which brings about the restoration of hydrophilicity. Photocatalysis can then improve hydrophilicity and preserve this trait for a long duration. The self-cleaning effect of

hydrophilic  $\text{TiO}_2$  film can be expressed as in Figure 94. There is a layer of chemisorbed  $\text{H}_2\text{O}$  on the film due to its hydrophilicity. The chemisorbed  $\text{H}_2\text{O}$  can further adsorb layers of water by Van der Waals forces and hydrogen bonds that hinder the close contact between surface and adsorbed contaminants. So the soiled substance adsorbed on the surface can be easily removed by spread water and the glass shows self-cleaning effect. The self-cleaning effect can stay a long time due to the synergetic effect of photocatalysis and hydrophilicity as is related above.

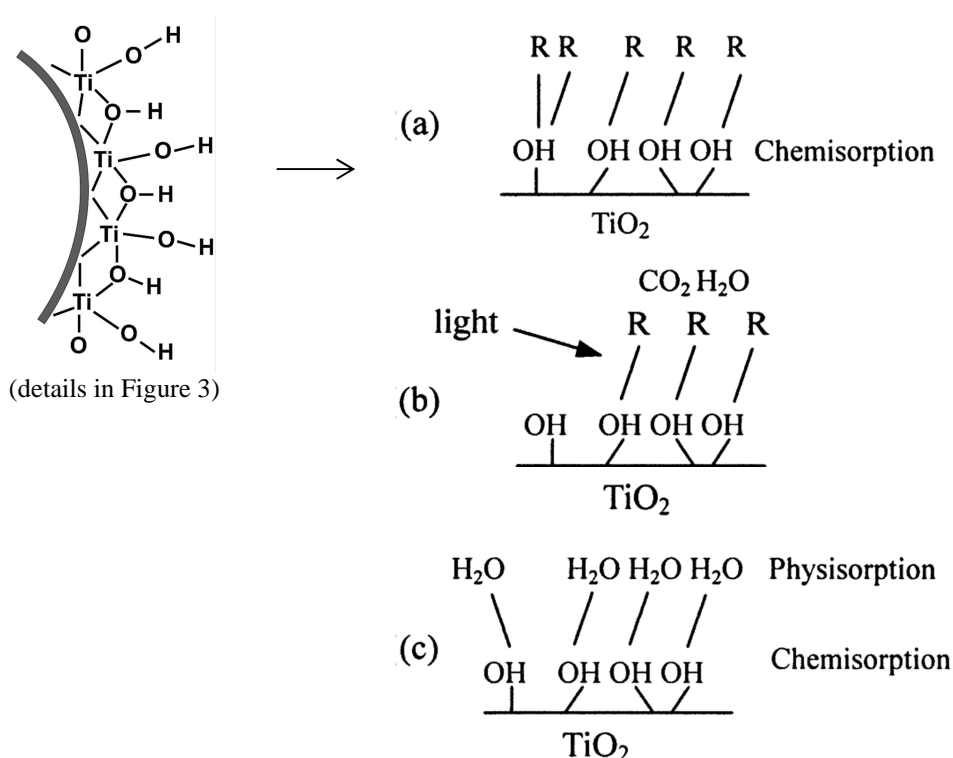


Figure 94. Self-cleaning mechanism of hydrophilic  $\text{TiO}_2$  thin films<sup>[104]</sup>.

As shown in Chapter 7, in addition to the ion current, oxygen ions and electrons, from the Hall ion-source, play a role in increasing transfer energy. The momentum transfer of the IAD ion-beam bombardment on the growing titania films may result in an improvement of the microstructure, the absorption of UV-light and the generation of more electron-hole pairs, thereby increasing the photocatalytic performance<sup>[2, 3, 65, 87, 213]</sup>.

## 8.2 Effect of the coating parameters on microstructure and photocatalytic activity

Different deposition parameters were set to find the most suitable method to produce titania films with optimized optical and morphological properties. The fixed parameters were  $3 \times 10^{-4}$  mbar  $\text{O}_2$  gas, 0.15 nm/s coating rate, and 300 nm film thickness. To analyze its impact, the other

parameters were held in a substrate temperature range between 60 to 300 °C, an ion-source discharge current (I) of 1 to 5 A, and oxygen as a reactive gas of 20 to 30 sccm. Figure 95 presents the time-dependent photocatalytic degradation obtained from the UV-illumination of the titania coated samples. The initial concentration of methylene blue was kept at 10  $\mu\text{mol/l}$ . A comparison of the methylene blue degradation on the coated surfaces prepared with different deposition parameters is presented in following Figure 95, with uncoated glass as the reference sample.

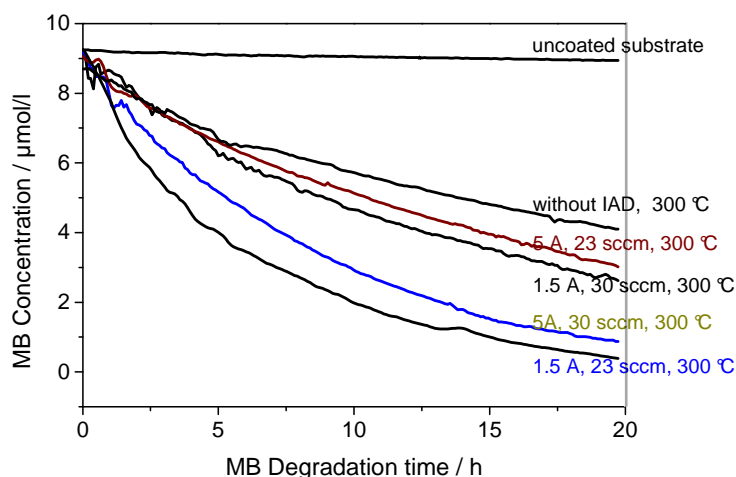


Figure 95. Photocatalytic degradation of titania films with different processes methods at 300 °C.

An analysis of the photocatalytic activity was conducted from the calculation of the photonic efficiency values. Prior to this, both the rate of demineralization of methylene blue over 20 hours and the variation of the ratio of  $\ln(C/C_0)$  versus time were determined (Figure 96).

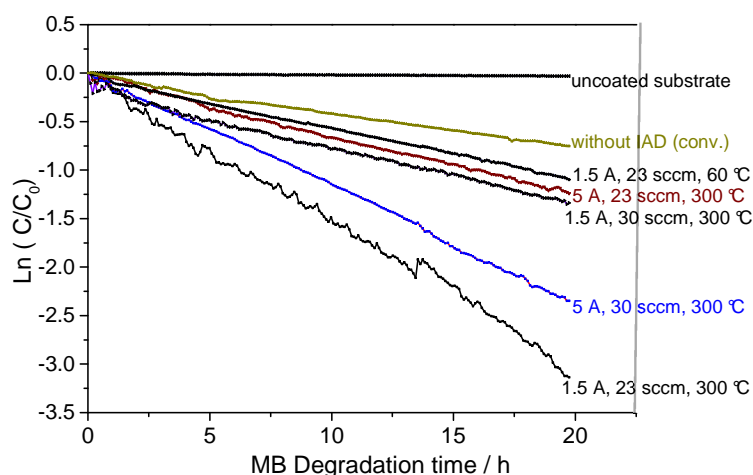


Figure 96. Photocatalytic activities of different coating processes. Uncoated represents the pure  $\text{SiO}_2$  substrate (Suprasil).

The samples with the two parameter sets of 1.5 A, 23 sccm, and 250 °C, and 5 A, 30 sccm, and 300 °C show the expected linear behavior and a high photocatalytic activity. Another tendency is that MB adsorbs onto TiO<sub>2</sub>, and the oxygen-saturated conditions influence the photobleaching mechanism<sup>[61]</sup>.

The resulting values in Figure 96 show an influence of process parameters on the dye demineralization mechanism rate differences via the production of electron hole pairs on titania surfaces (as explained in 5.1. pp.70-78). Table 12 demonstrates the increase of photonic efficiencies using the IAD method at 60, 165, 250, and 300 °C.

Table 12. Result of the photocatalytic activities of the coated samples using different deposition parameters.

Deposition parameters	Photonic efficiencies [%]
conventional, 300 °C	0.035
1.5 A, 23 sccm, 60 °C (cold)	0.038
1.5 A, 23 sccm, 165 °C	0.054
1.5 A, 23 sccm, 250 °C	0.097
1.5 A, 23 sccm, 300 °C	0.098
1.5 A, 30 sccm, 300 °C	0.045
5 A, 23 sccm, 300 °C	0.039
5 A, 30 sccm, 300 °C	0.077

In the first deposition experiment, the sample was coated by the conventional method, without the use of the ion-source. The process temperature was kept at 300 °C and a thickness of 300 nm was maintained for the prepared titania films by utilization of an ion-source. In a past paper<sup>[123]</sup>, titania films prepared using the conventional method, without the IAD method, and at a thickness of 300 nm, exhibit only low photocatalytic activity. The X-ray diffraction spectra of the conventionally prepared film are shown in Figure 97a. Although a pure anatase phase is identifiable, the film exhibits a very low degree of crystallinity indicated by the exclusive presence of a low-intense anatase (101) reflection. The low crystallinity results in the lowest photonic efficiency of all tested samples, of only 0.035%.

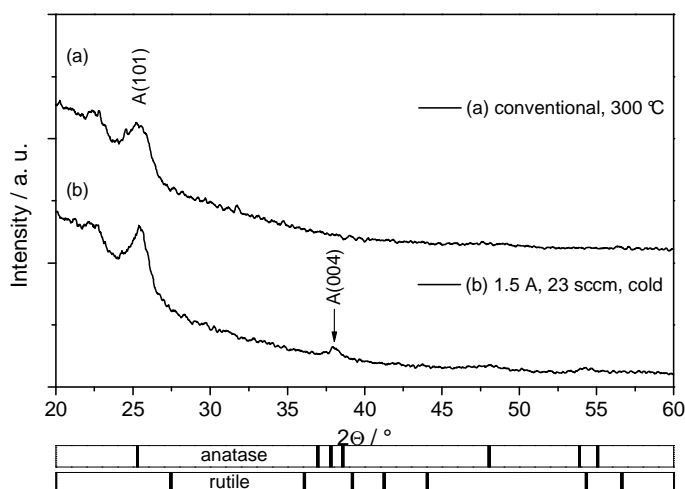


Figure 97. XRD pattern of the prepared  $\text{TiO}_2$  thin films with the conventional method and with cold IAD process.

Figure 97b represents the XRD data of a thin film prepared with the ion assisted deposition method, but at a process temperature of approximately 60 °C as a cold substrate temperature. The ion-source current and the oxygen flow rate were maintained at 1.5 A and 23 sccm, respectively. The thickness of the deposited film was fixed at 300 nm. Although the degree of crystallinity is improved compared to the conventional film, it is still quite low. Besides the (101) reflection, the (004) reflection can be assigned to the anatase phase. Consequently, the photonic efficiency is marginally increased, to 0.038%.

As the conventional method and the cold IAD preparation lead to almost amorphous films, and consequently to low activities, the process temperature was optimized.

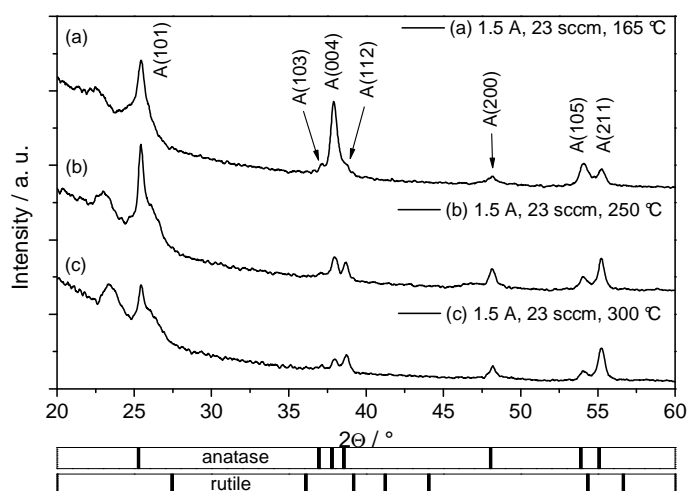


Figure 98. XRD pattern of the prepared  $\text{TiO}_2$  thin films with a variation of IAD process temperature.

The ion-source current, the oxygen flow rate, and the film thickness were fixed at 1.5 A, 23 sccm, and 300 nm, respectively. The X-ray diffraction data of the samples prepared at 165 °C (a), 250 °C (b), and 300 °C (c) are presented in Figure 98.

The degree of crystallinity is significantly improved for all samples indicated by the presence of all common anatase reflections in the investigated angular range. The samples are free of the rutile phase, yet more importantly, the process temperature affects the growth of crystal faces leading to a preferred orientation of the anatase particles. Beside the (101) reflection being of a high intensity in the whole temperature range, the anatase (004) diffraction reflex becomes very intense by applying a process temperature of only 165 °C (Figure 98a). This reflection decreases when the process temperature is increased. A similar behavior is also found in the anatase (105) diffraction reflex, yet both the anatase (211) and (112) reflections develop the opposite way. As with the cold-prepared ion assisted sample (Figure 98b), the most intensive reflections of the thin film deposited at a relatively low temperature of 165 °C, are still found with (101) and (004) indices. However, the latter index features represent a higher degree of crystallinity, leading to an improved photonic efficiency of 0.054%. By raising the process temperature to 250 °C, the photonic efficiency is significantly enhanced to 0.097%, and a further increase to 300 °C leads to a slightly higher efficiency of 0.098%. Therefore, a (004) preferred orientation of anatase crystallites seems to be unfavorable for photocatalytic activity. Tung et al.<sup>[282]</sup> reported about a low carrier concentration and a poor mobility of photo-excited electrons in TiO<sub>2</sub> anatase thin films with (004) preferred orientation. This corroborates very well with our finding that preferred orientations in the (211) and (112) lattice planes greatly increase the photonic efficiency.

The process parameter of the oxygen flow rate was increased from 23 sccm to 30 sccm to determine its effect on the structural characteristics and the photocatalytic activity, whereas the ion-source current, the process temperature, and the film thickness were kept at 1.5 A, 300 °C and 300 nm, respectively. Figure 99 shows clearly that the oxygen flow rate has no influence on the preferred orientations of the crystallites. Interestingly, the photonic efficiency is significantly decreased to 0.045%.

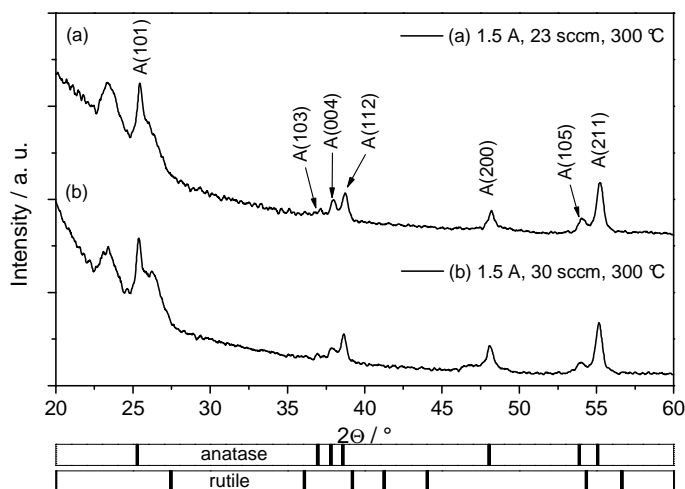


Figure 99. XRD pattern of the prepared TiO<sub>2</sub> thin films with a variation of oxygen flow rate using the IAD method.

Additionally, thin film samples were prepared by increasing the ion-current to a value of 5 A, which is the maximum level possible with the Denton CC-105 ion-source providing a stable energy distribution. Whereas film thickness and process temperature were maintained at 300 nm and 300 °C respectively, the oxygen flow rate was adjusted to 23 or 30 sccm. Figure 100 (b) shows the X-ray diffraction data obtained with 23 sccm oxygen flow, indicating a low degree of crystallinity, but the presence of a small amount of rutile as a second titania phase. Once more, the low degree of overall crystallinity leads to a low photonic efficiency of 0.039%. The higher ion current of 5 A requires an increased oxygen flow rate of 30 sccm to provide well crystallized films (Figure 100a).

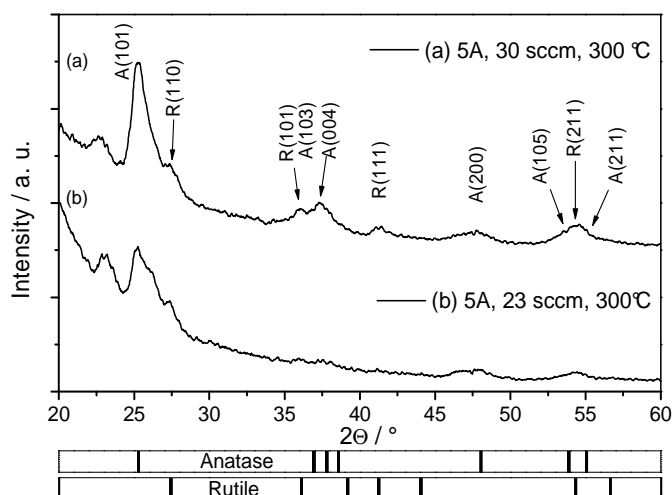


Figure 100. XRD pattern of the prepared TiO<sub>2</sub> thin films with a variation of oxygen value at high ion-source parameter and at 300 °C.



The results are presented in Figure 101. The Raman bands centered at 141, 393, 514, and 636  $\text{cm}^{-1}$  are assigned to the anatase phase and those performing at 320  $\text{cm}^{-1}$  and 450  $\text{cm}^{-1}$  correspond to the rutile phase. Anatase is the dominant titania phase in all measured coating samples. Raman displays a rutile by-phase clearly in the 5 A-film deposited at a high oxygen flow of 30 sccm.

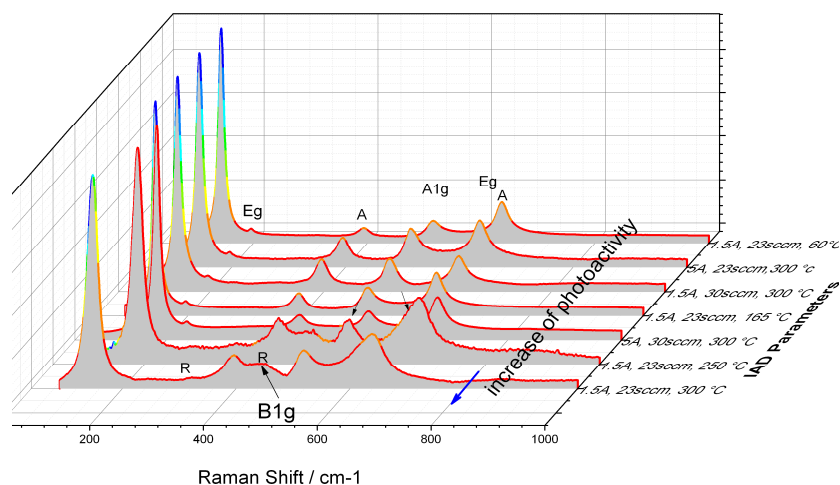


Figure 101. Raman spectra of  $\text{TiO}_2$  at various deposition parameters.

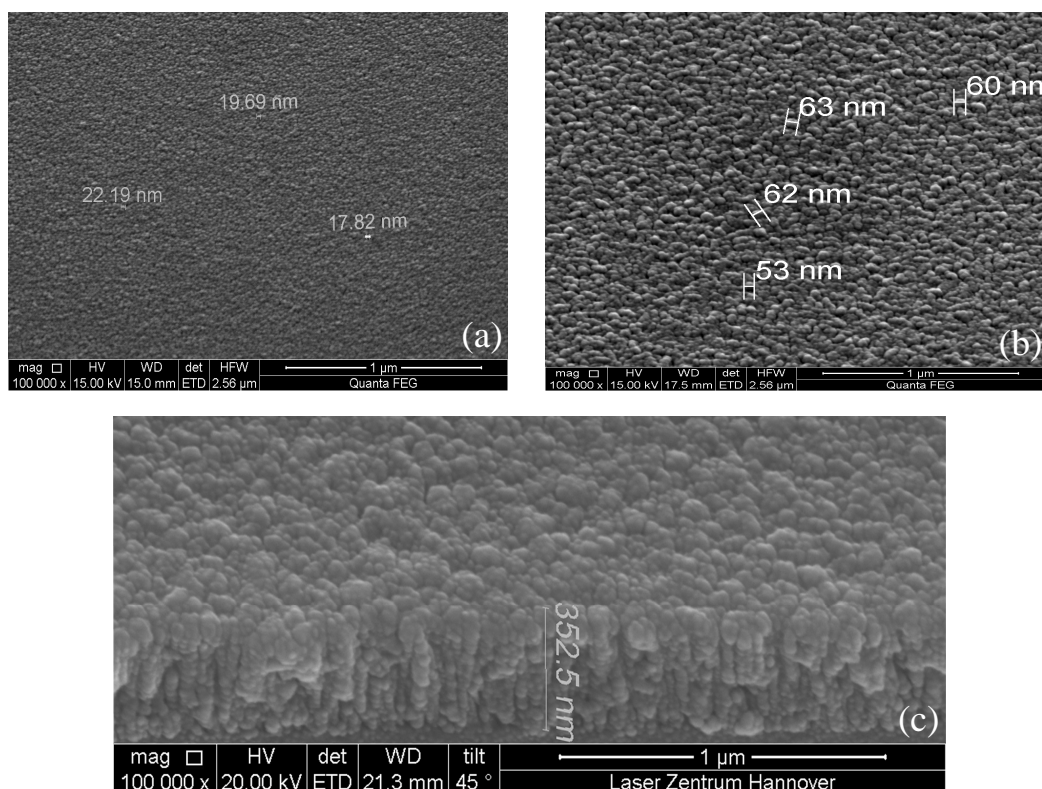


Figure 102. SEM micrographs of  $\text{TiO}_2$  films. (a) Conventional process at 60 °C. (b). IAD process at 300 °C with 1.5 A, 23 sccm. (c) Representative cross-section picture of a sample made by the IAD process: 1.5 A, 23 sccm, 300 °C. The difference in this SEM analysis (c) is the use of the coating matrix, which correspond to a highest photocatalytic activity (optimized Pr. VI).

The SEM micrographs shown in Figure 102 reveal that the sample deposited using conventional PVD without IAD (a) has a smoother surface than the samples deposited by a thermal evaporation method (b, c). Figure 102c displays a cross-section of the columnar structure of the deposited titania with an approximate thickness of 350 nm. The films have uniform cross-sectional structures. A smoother surface is shown for the conventional coated, and therefore has less pronounced hydrophobic properties than the films deposited at 300 °C.

The film porosity can influence the active surface area, which in turn has a strong effect on the photocatalytic activity. From optical transmission measurements, a simple way to estimate the porosity can be determined<sup>[269]</sup>. The microstructure (porosity) of the thin films generally enlarges the surface area<sup>[3]</sup>.

It is known that the packing density of the films can be checked by measuring the optical property of the films as follows<sup>[283, 284]</sup>:

$$Porosity = \left( 1 - \left( \frac{n^2 - 1}{n_d^2 - 1} \right) \right) \cdot 100\% \quad \text{Equation 29}$$

where  $n_d$  is the refractive index of pore-free anatase  $\text{TiO}_2$  (2.3), and  $n$  is the refractive index of the deposited  $\text{TiO}_2$  films. A pure  $\text{SiO}_2$  (Suprasil) was used with a  $T_s$  equal to 0.936, and a refractive index: 1.44.

Table 13. Estimation of porosity using an IAD and conventional examples

	n @550	T maxima	T minima	Porosity (%)
conventional (picture a)	2.41	0.87	0.65	39
IAD (picture b)	2.52	0.92	0.58	27

The refractive index, with a wavelength of 550 nm, was 2.52, a higher result than values that have been previously garnered. Table 13 shows that there is a reduction in porosity as the deposition temperature increases. This remark also corroborates with the above explanation that one reason for the decrease in band gap with temperature could be IAD film densification.

The column-grains have rounded tops and an elongated, approximately cylindrical shape. The rounded tops will in all cases increase the surface available for catalysis. The side surfaces of the column-grains can only participate when the inter-grain spacing is large enough to allow diffusion of the reactant and reaction products. This inter-grain spacing actually defines the pore size in the thin film. If a thin film has a completely dense structure and a flat surface, the active surface area

is equal to the geometrical area of the substrate. The surface can consist of a collection of semi-spheres (the tops of the individual grains).

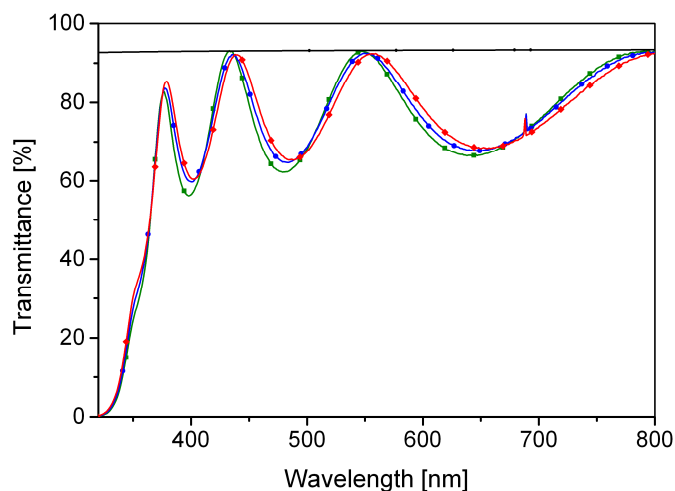


Figure 103. Transmittance measurements of  $\text{TiO}_2$  thin films prepared by IAD at 1.5 A, 23 sccm  $\text{O}_2$ , as a function of the process temperature: Green: 165 °C, Blue: 250 °C and Red: 300 °C.

From the transmission spectra, it can be deduced that the transmission rate of the coated samples is qualitatively high. Figure 103 shows the transmittance of thin films prepared with 1.5 A, 23 sccm  $\text{O}_2$  at different temperatures. A transmittance of 93% value, nearly the value of the uncoated side, at 550 nm shows an obvious result regarding the thickness of the titania coating of 300 nm. The difference between the curves of Figure 103 at high wavelengths indicates a slight variation in terms of thickness. The refractive indices are estimated to be 2.52, 2.53, and 2.54 for process temperature 165, 250, and 300 °C respectively.

During the IAD process, the crystallite grain size influences the absorption edge of the titania thin films, as demonstrated by Wang et al. <sup>[5, 54]</sup> A relationship can be determined between the morphology and the optical properties that can be more heavily specified using a correlation with the photonic efficiency values (Figure 104). Furthermore, it appears that some of the oxygen ions and electrons from the ion-source might play a role in increasing the MB deposition rate (Chapter 5). The momentum transfer of ion-beam bombardment on the growing IAD layers can result in augmenting the packing density of the microstructure and absorb more UV-light quanta, which provide high photocatalytic activity.

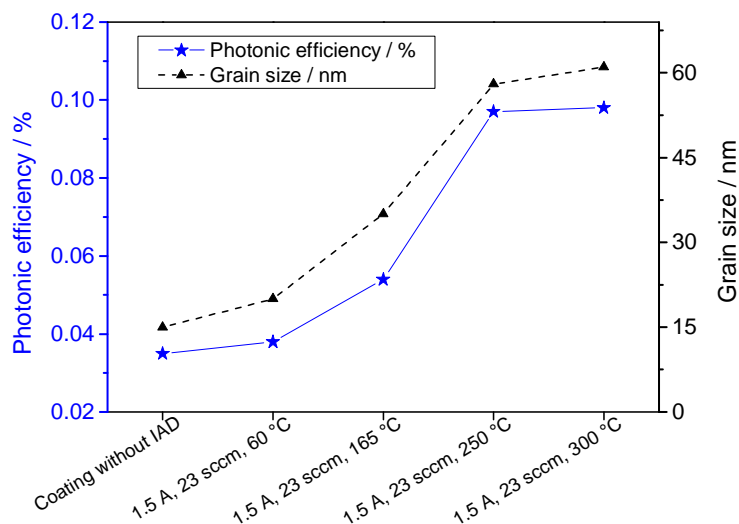


Figure 104. Correlation between average grain size values and photonic efficiencies for different process parameters (substrate temperature) operating with 23 sccm oxygen and 1.5 A current.

The results illustrate that the photocatalytic activity strongly depends on the roughness of the thin films prepared by IAD (Figure 104). A high ion-source current and a low reactive gas, or vice-versa, is unfavorable in obtaining high grain sizes. The sample coated with the conventional method without ion-assistance is used as a reference.

The process conducted without using an ion-source showed a low presence of anatase on the XRD and Raman data. An increase of temperature positively influences the photo-mineralization. A mixture of anatase and rutile can provide high photoactivity. Anatase and rutile phases bear an influence on certain coating parameters, such as, the substrate temperature or the ion-source parameters.

Hence, another conclusion of this study is that the factors adversely affecting crystallinity are mainly fourfold; that of the ion assistance used, the temperature applied, the ion-source current value, and the oxygen level when used as the reactive gas. The factor that positively and substantially influences the crystallinity is the maintenance of the pre-defined values between the ion-source current and the reactive gas. The temperature was kept between 60 °C and 300 °C and the thickness was kept at a constant of 300 nm, which influenced the photonic efficiency and crystallinity. This leads to the conclusion that for a suitable level of crystallinity and photoactivity, a precise level of an ion-source current and a reactive gas plays an important role.

## 9. Future Research and Utility

The innovative measurement systems, that were optimized, can be put to approve for further use and innovation. Some research ideas have already been initiated, some of which involve research on extraction of TiO<sub>2</sub> from sun-protective agents, photocatalytic activity of commercially available sun-protective glasses, and the determination of TiO<sub>2</sub> content of these examined sun-protective agents. There are many areas where this research is of use. Two of the most applicable of these, photocatalytic transparent films under visible light, coating potential on laboratory equipment, have been discussed below.

### 9.1 Photocatalytic Transparent Thin Films under Visible Light

One section of the research for this thesis was conducted specifically to understand the functionality of TiO<sub>2</sub> thin films under visible light as opposed to UV, which has been thoroughly discussed in previous chapters. It was necessitated primarily by the need to increase the scope of utility in coating to visible range. Recent efforts have been made to increase the efficiency of TiO<sub>2</sub> as a photocatalyst under visible light and for this purpose research has been conducted to produce thin films doped with certain elements including Silver (Ag) and Gold (Au) <sup>[78, 89, 130, 149, 285-287]</sup>. Due to surface plasmon resonance, which is a light-induced collective oscillation of conducting electrons on the surface, silver and gold absorb light in the visible range. For the purpose of obtaining structures which can facilitate high performance catalysis, many chemical and physical methods, such as, co-precipitation <sup>[288]</sup>, chemical vapor deposition <sup>[289]</sup>, co-sputtering <sup>[290]</sup>, deposition– precipitation <sup>[291, 292]</sup> and gas-phase grafting <sup>[293]</sup> have been developed. To produce gold metal nanostructures, several procedures have been published <sup>[294]</sup>. Mesoporous TiO<sub>2</sub> films with defined mesoporosity, that is, narrow pore size distributions, synthesized via sol-gel technique were used recently <sup>[89]</sup>.

Ag and Au were used in this research with their differences when expending the ion assisted deposition (IAD) method being a focus. The photocatalytic activity of the titania thin films produced was evaluated. The doped Ag- titania films, was deposited as co-e-beam evaporation in BAK 760, with Denton CC-105. The voltage of the plant, Balzers BAK 760, was kept at 8 kV, the voltage of the ion-source, at 2.5 A. The flow of oxygen, as a refractive gas, was kept at 20 sccm. The substrates were heated at 350 °C.

A different process was employed for Au. First, the substrates were coated with TiO<sub>2</sub> thin films and were placed inside a furnace to anneal for 12 hours at 400 °C. After this, the Au was added with a pressure of 10<sup>-1</sup> mbar while operating 10 mA current, with Bio-Rad Polaron Division TEM Dehydrator Model E500M utilized for this process. Once the deposition process was completed, the substrates were again placed inside the furnace for 12 hours at 400 °C to anneal.

### 9.1.1 Optical Properties

The samples of thin films produced with metal doped TiO<sub>2</sub> process were studied for optical quality, total scattering, photocatalytic properties, contact angle, crystal structure, and anti-bacterial properties. Each of these will be discussed below. The optical quality of each sample was estimated using the transmission curves mentioned earlier in Chapter 7 (IAD and its functional properties). The following Figure 105 shows the area, which corresponds to the transverse surface plasmon band of spherical gold nanoparticles [295, 296].

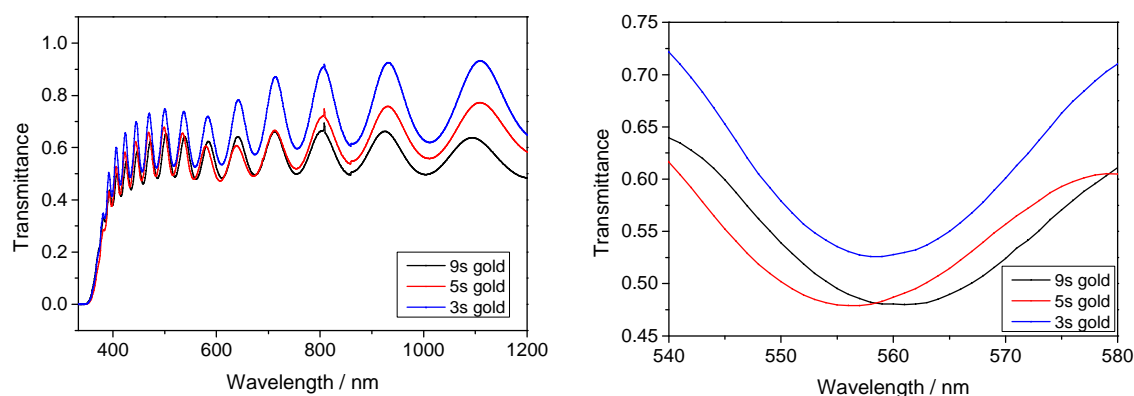


Figure 105. Transmissions spectra of TiO<sub>2</sub>-Au with presence of the plasmon resonance peak at approx. 560 nm. Blue (Top): TiO<sub>2</sub> + Au-3s, Red: TiO<sub>2</sub>+Au-5s, Black: TiO<sub>2</sub>+Au-9s.

For metal nanoparticles of Au, the plasmon absorption arises from the collective oscillations of the free conduction band electrons that are induced by the incident electromagnetic radiation. For Au/TiO<sub>2</sub> samples, the intensity of absorbance band is related to the size of Au particles and the content of Au in Au/TiO<sub>2</sub>. There is only a slight increase of the absorbance intensity when the time of gold increases from 3 to 9s. According to the relevant references [297, 298], the size of Au has no evident increase.

As reported by I. Bannat et. al, the comparable spectrum wavelengths of the surface plasmon resonance band designate that there is no further effect of the refractive index and of the dielectric constant of the transparent thin TiO<sub>2</sub> film on the position, which normally indicates a presence of a characteristic red shift depending on the film thickness. A very slight color spectrum was observed due, may be, to the small thickness and preparation method to compare with mesoporous sol-gel samples.

Other transmission spectra obtained, TiO<sub>2</sub>-Ag are shown in Figure 106. The shift of the band gap to the visible region was clearly observed with the increase of Ag amount.

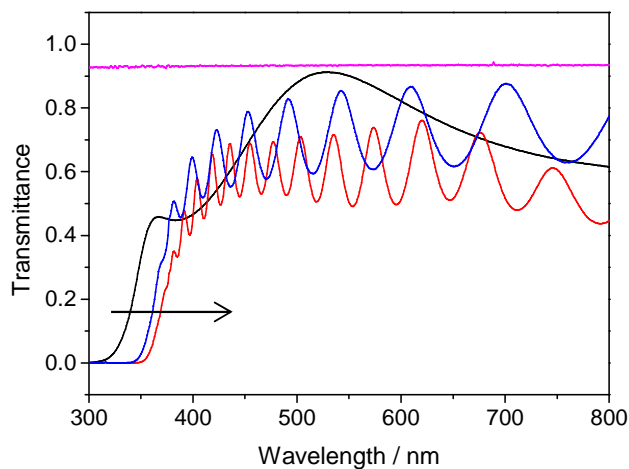


Figure 106. Transmission spectra of TiO<sub>2</sub>-Ag. Black: 100 nm TiO<sub>2</sub> and 15 % Ag, Blue: 200 nm TiO<sub>2</sub> and 10 % Ag, Red: 300 nm and 20 % Ag.

The position of plasmon bands of the Ag-TiO<sub>2</sub> films on Suprasil glass confirms the formation of Ag nanoparticles. As the figure shows, the transmission is recognized to shift toward the visible region depending on the percent of silver implanted in TiO<sub>2</sub>.

The ion-implantation of this transitional metal is effective in modifying the properties of TiO<sub>2</sub> thin films to make shifts in the absorption band to the visible light range. The experiments showed that if Ag is applied for longer durations, absorption increase and transparency decreases.

The refractive indices of TiO<sub>2</sub> at 550 nm, TiO<sub>2</sub>-Au, and TiO<sub>2</sub>-Ag are calculated as 2.44, 2.44 and 2.42 respectively.

### 9.1.2 Photocatalytic Properties

Photocatalytic properties of the thin films were determined through the same process of methylene blue degradation. The films displayed all of the properties shown in Figure 107, and water was used as the reference for all samples.

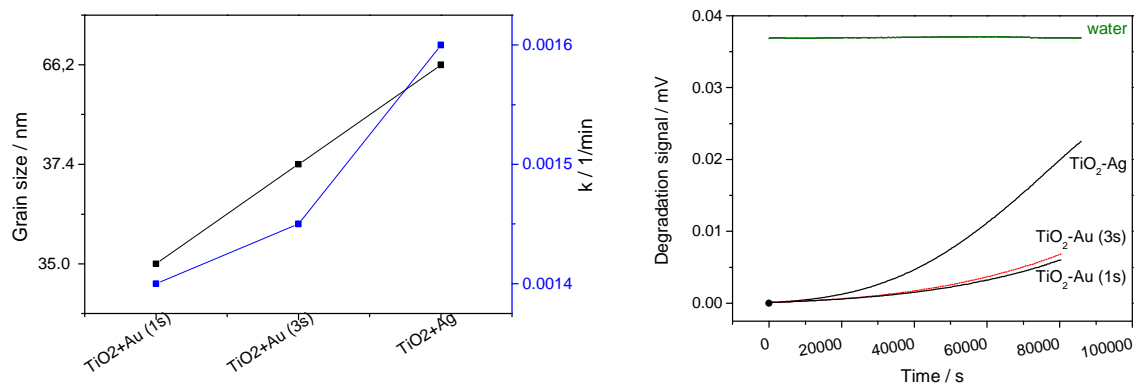


Figure 107. Grain size results and demineralization of methylene blue over 22 hours using a TL/03 lamp. This lamp emits a radiation between 380 and 480 nm.

The photocatalytic activity of the films can be compared against the degradation signal (mV) obtained from the graphs against irradiation time. It is showed that the photocatalytic decomposition carried out with visible-light source slightly depend of the Au time depositing (1 to 3s). The catalysts with silver particle are the most active. It is proposed that in the catalyst with gold particle efficiency is the responsible of the activity. Meanwhile, the plasmon surface resonance band plays an important role in the photoactivity behavior<sup>[299]</sup>. The photocatalytic reaction is highly sensitive to the catalyst surface. When looking at the electronic properties, doping will influence two factors<sup>[91]</sup>; namely (i) the charge carrier separation and mobility and (ii) the absorption edge. The first factor will affect the number of photons which can be utilized for the chemical redox- reaction while the second will change the wavelength of the light needed to activate the catalyst, mostly trying to shift the absorption edge towards visible light. Methylene blue reacts with electrons generated on the TiO<sub>2</sub> particles under near visible light. TiO<sub>2</sub>-Ag has the best photocatalytic activity, with other metals not as efficient for methylene blue degradation due to the photonic efficiency being less than pure TiO<sub>2</sub>. However, this does not mean that they are not efficient under visible light, as shown in research literature where it is possible to use different chemical components for Vis-Photocatalytic activity (such as Reactive Brilliant Red X-3B, MTBE, Nitrobenzene, methyl orange, and acetic acid)<sup>[193, 300,]</sup>.

### 9.1.3 SEM Microstructure and Grain Size Determination

SEM images of the coated IAD thin films are shown in the following Figure 108. The average grain size on each film was calculated on the basis of different values obtained from each of these images.



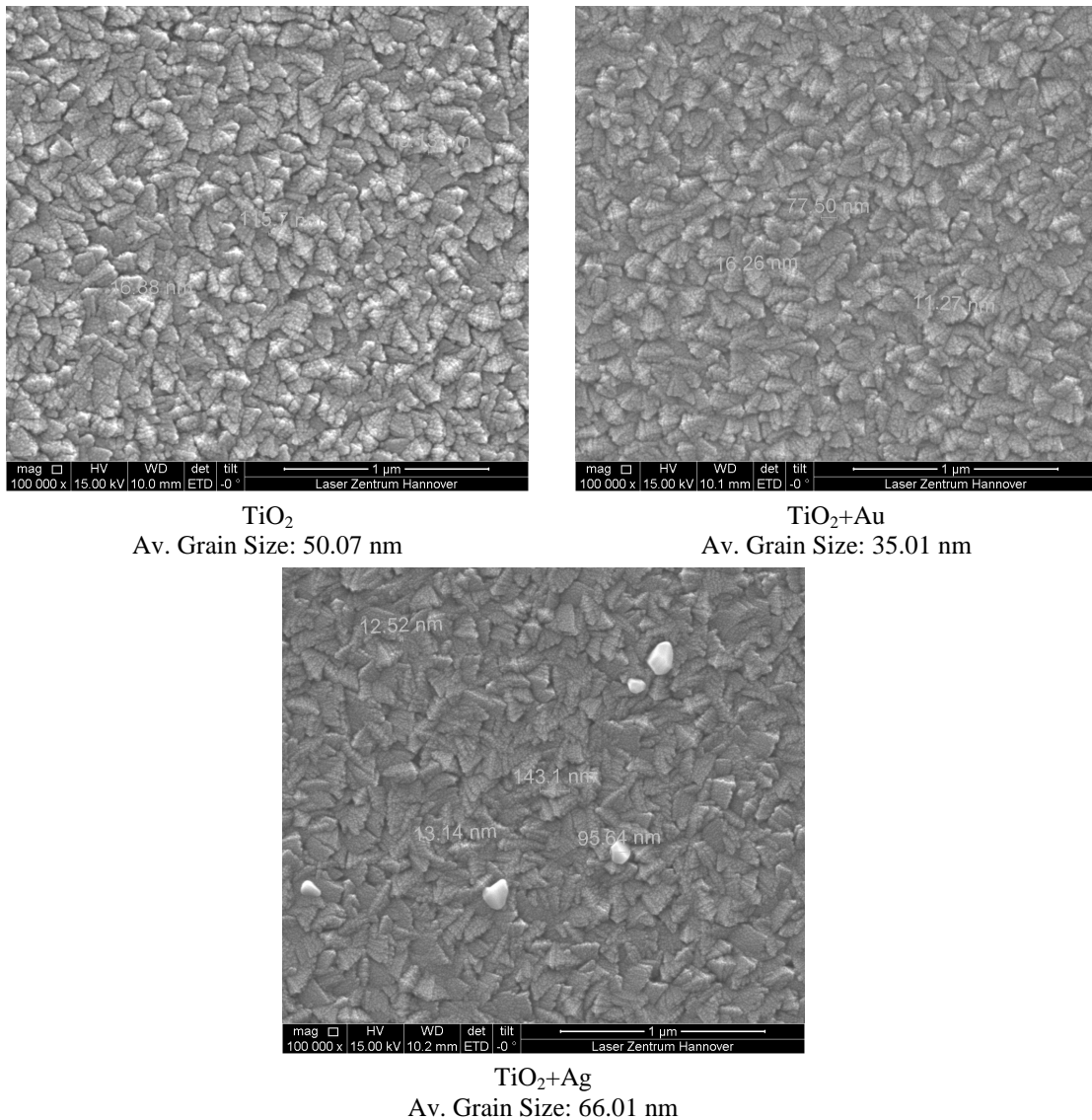


Figure 108. SEM results of different kinds of coated substrates.

The presence of silver and gold via the EDX investigations (Figure 109) are observed. Figure 108 shows that the crystallites of  $\text{TiO}_2$  are arranged in different geometric agglomerates. Two classifications can be made on the basis of these images, the first being  $\text{TiO}_2+\text{Ag}$ ,  $\text{TiO}_2+\text{Au}$  and  $\text{TiO}_2$ , which show clusters existing in irregular forms with edges.  $\text{TiO}_2$  has been used as a reference for the grouping of samples, and it is evident that  $\text{TiO}_2+\text{Au}$  and  $\text{TiO}_2+\text{Ag}$  show the average grain size of over 30 nm. The highest average grain size was observed on the  $\text{TiO}_2+\text{Ag}$  sample. When examined alongside the images in Figure 108 shows that the samples containing clusters in an irregular form and with edges have a higher grains size.

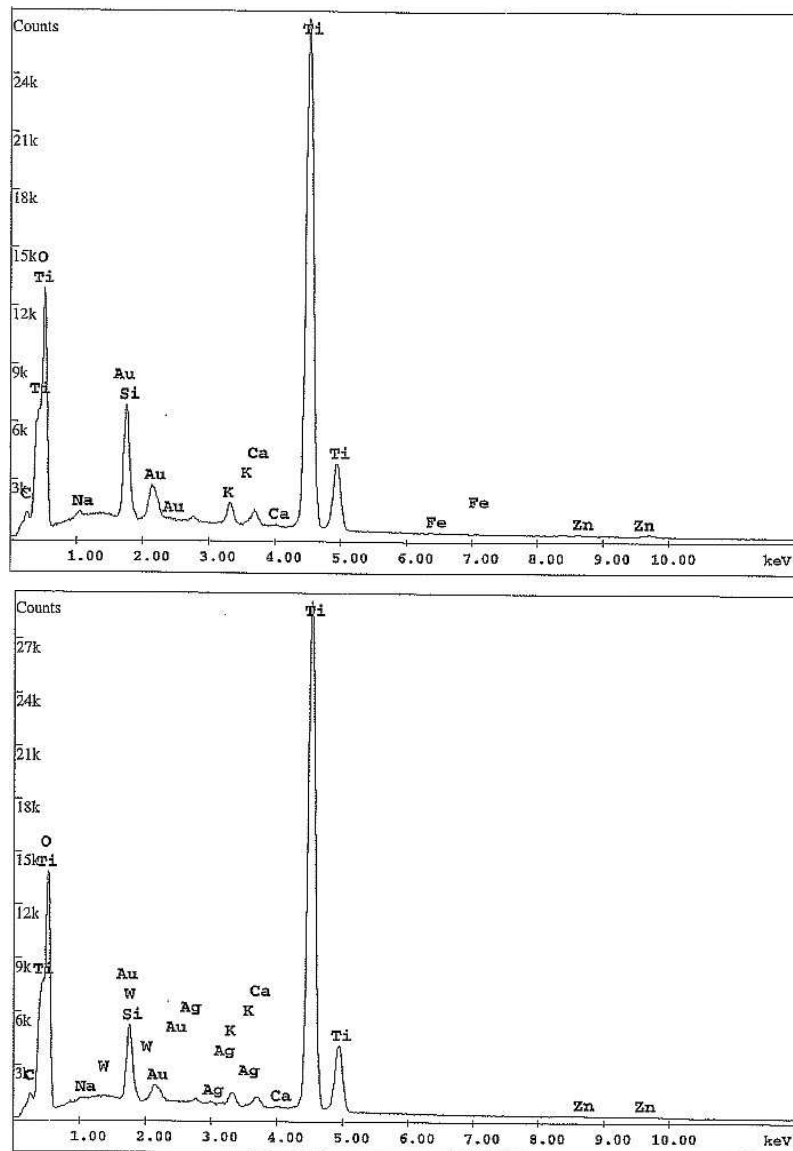


Figure 109. EDX results for a doping with Au and Ag. Left:  $\text{TiO}_2+\text{Au}$  : wt (%): O: 35.6; Ti: 54.97 at (%): O: 60,63; Ti: 31.26. Right:  $\text{TiO}_2+\text{Ag}$  wt (%): O: 35.63; Ti: 56.13; at (%): O: 62.25; Ti: 32.76.

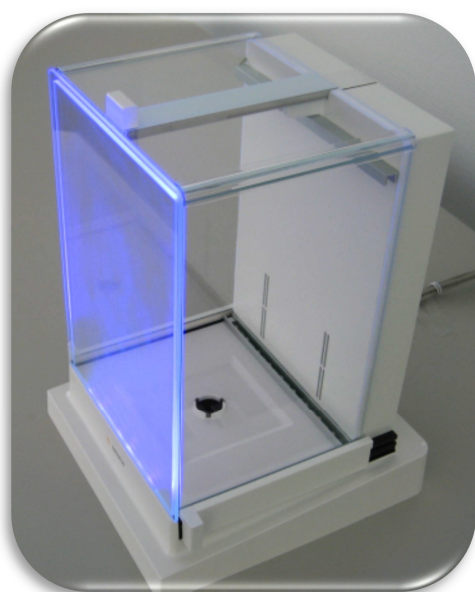
The photonic efficiency is directly proportional to the average grain size in that it improves as the average grain size increases. As the particles remain in the reactor for the entire deposition time, the grain size of these deposited multiphase particles continue their increase.

In addition, the model proposed by Edelson and Glaeser declares that the intra agglomerate densification and grain growth rate both occur more promptly than the interagglomerate densification<sup>[2]</sup>. More research is needed to investigate this process's mechanism.

## 9.2 Coating Potential on Laboratory Equipment (Scales)

During the optimization phase of this research, the results of the experiments establish the use of this technology on visible-light-exposed surfaces, shown in Chapter 8, hint at the potential use in laboratory equipment, especially scales and balances.

The presentation of the first doped coating results may be used to market this technology. The highlight of these experiments was the use of Vis-coating processes for optimized photoactivity, optical quality, and morphological analysis, such as contact angle tests. Figure 110 shows coated components of a scale used in laboratories.



Material	Component	Layer System
Standard Glass panes	Wind Screen	ITO and doped TiO <sub>2</sub>
Glass panes with ITO	Wind Screen	doped TiO <sub>2</sub>
Glass panes assemblage ITO	Wind Screen	doped TiO <sub>2</sub>
Stainless steel	Balance weight	doped TiO <sub>2</sub>
Lacquered Aluminum	Screening shield	ITO and TiO <sub>2</sub>

Figure 110. Coating a 'Future Scale' with an optimized deposition process (VI). LEDs OCU-400 UE400-X-T (Peak Wavelength 400-405 nm) was integrated as source of indoor for self-cleaning, in accordance with DIN and ISO standards. In coordination with the partner Sartorius, an IAD design concept was developed with marketing design specifications.

For the optimization of optical quality and the color impression of the coatings, done to finalize the best coating design, according to the final coating color as managed by the manufacturing procedure, are shown in Figure 111.

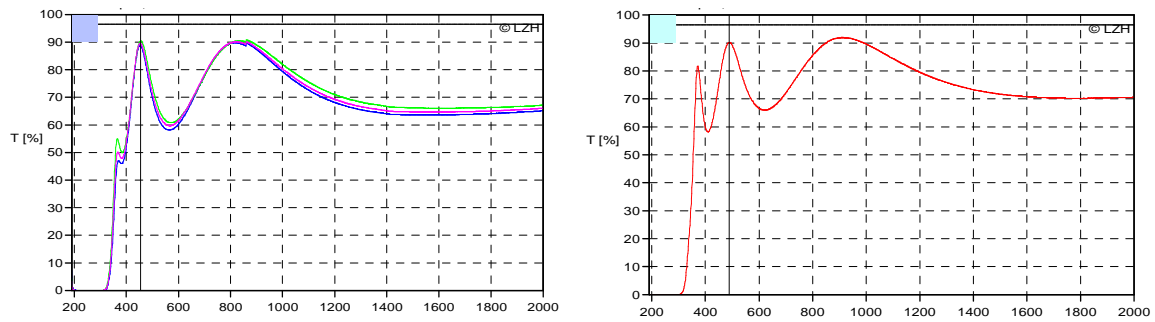


Figure 111. Optimized  $\text{TiO}_2$  spectra of different photocatalytic active coating designs. Left: blue dark for different refractive indices value. Right: blue light. The apparent color can be optically programmed.

Real industrial applications based on the IAD basic research results have already been in use since the end of 2010. The prototype of this laboratory scale application is present within the marketing division of Sartorius AG, aiming to collaborate it with the customer's suggestions and wishes.

## 10. General Conclusions

The focus of this research was to produce titania films which are as well highly optically transparent as photocatalytic active; thus the material was designed by surface and structure modification. The TiO<sub>2</sub> layers used in this thesis were deposited using the PVD method with an implemented ion assisted coating (IAD) process. The Balzers BAK 760 and SYRUSpro 1100 machines were used with Denton CC-105 and APSpro ion-sources respectively. It is possible to produce compact and homogeneous coatings of enhanced refractive index that also have reduced water adsorption and optical absorption. Different parameters were operated in the deposition and characterization stages, with the deposition process carried out with and without ion assistance, and the characterization process conducted using a UV-Vis Spectrophotometer, a photocatalytic measurement system, SEM, EDX, XRD, contact angle measurement, AFM, and TEM.

The first goal was to investigate the effect of structural properties of TiO<sub>2</sub> thin films. The XRD results of the tested samples did not show amorphous structures on the analyzed surface. A high diffraction reflex of (004) indicating a preferential crystal orientation and particle diameters of 5 to 10 nm were found for TiO<sub>2</sub> thin films that were produced using the IAD method, with the X-ray diffraction also showing a high anatase portion. The TiO<sub>2</sub> samples also showed 95% crystallinity when analyzed with TEM, and displayed a correlation between the intensities of Raman signals for anatase and rutile phases, indicating differences in the microstructure, and the deposition process. There is a strong correlation between the characteristics of the thin films and the ion-source current parameters. For example, with an increase in the ion-source current the crystallite size also increases.

The contact angle of a water droplet on the TiO<sub>2</sub> thin films under an ambient condition in air atmosphere was measured to evaluate the level of hydrophilicity, with the results showing that the contact angle increases as the ion-source current is reduced, and vice versa. An additional factor that increased the contact angle of water droplets was the annealing process, which made the surface of the thin films rougher. Additionally, the thin films became super-hydrophilic when exposed to UV light.

All the deposition processes are characterized by a layer adhesion test, a moderate abrasion test, a solubility test and a severe abrasion test. All IAD films show nearly perfect mechanical stability. It was shown in all of the abrasion tests that no scratches on coated glasses were formed on the thin films, and the solubility test confirmed that the layers were not detached from the surface. The severe abrasion test, however, shows surface scratches for PMMA. The influence of SiO<sub>2</sub> as a basic layer directly on PMMA should inhibit the presence of these deformities.

A second goal of this study was to improve the optical properties of the TiO<sub>2</sub> thin films according to their mentioned structural properties.

Thin films prepared using IAD processes possess already high refractive indexes. More energy from ion bombardment further supports the formation of even more compact structures and more uniform layers, consequently, resulting in an even higher refractive index. The tests conducted to measure the transmission spectra of the optical films within the visible and IR range indicated that a difference in oxygen flow has little-to-no impact on the optical quality of the films. This is especially true at higher temperatures. Optimized results for the refractive index at 550 nm can be gained with a value of 2.75 for a sample coated via IAD with Process V, at 350 °C, 4 A and 30 sccm. At cold, 50 °C, and hot, 350 °C, temperature levels, the refractive index goes to 2.51 and 2.55 respectively. Tests showed that the refractive index of the films coated with 25 and 30 sccm oxygen flow at 50 °C to 60 °C remains constant, and is independent as to their thickness.

A third goal of this thesis was to develop a reliable procedure for testing the photocatalytic activity of the thin films. The photocatalytic activity research carried out has provided the following points:

- Using SYRUSpro 1100 and the ion-source APSpro in the deposition process, a bias of 60 V resulted in best photoactivity.
- The films prepared using BAK 760 and Denton CC-105 showed a photodecomposition rate of methylene blue 1.8 times higher than commercially available products promising self-cleaning ability, and 36 times higher than uncoated substrates.
- A TiO<sub>2</sub> film thickness variation in the range up to 150 nm resulted in only negligible differences in the photonic or photocatalytic efficiency. However, thicknesses between 200 nm to 550 nm, and higher than 600 nm lead to a large increase and constant change in photocatalytic efficiency, respectively.

Considering the importance of microbial tests, *Sarcina Lutea* as Gram-positive has been used. The microbial evaluation was carried out by *Sarcinia Lutea* in 7 hours with a distinct 5-6-log reduction of the cell count showed high inactivation of microorganisms on titania thin films deposited with PVD-IAD proving the high antimicrobial efficiency of the obtained films. Increase of the deposition temperature to 350 °C has no influence on this efficiency.

Finally, the work carried out can be considered as a good starting point for further development of highly transparent but nevertheless photocatalytically active TiO<sub>2</sub> films due to the improvements made. The study provides the following achievements:

- The PVD-IAD method can achieve more compact and homogeneous coatings than PVD alone. The coatings provide an enhanced refractive index, high mechanical stability, reduced water adsorption, and low optical absorption in the visible range.
- PVD-IAD enables coating of polymers with TiO<sub>2</sub> films inducing a self-cleaning effect being potentially useful for countless daily and sophisticated products.
- The results of this thesis can be developed for use in lasers. The central problem is the contamination induces damage in high power UV-lasers, which decreases the laser's power. The development idea is to use a coating of aluminium laser housing via the IAD photocatalytic coating process. A silica buffer layer can be added between the metal surface and the titania layer to enhance the oxidation efficiency of the hydrocarbons on the sample surface.

The goals mentioned in the Chapter *Introduction* have been achieved, producing important results in the field of photocatalysis and coating technology. The ion-beam assisted process is an optimal candidate for many different applications involving easy-to-clean surfaces, the microelectronic industry, and in laboratory equipment, for example scales. The microstructure and optical properties of the TiO<sub>2</sub> films make them a good choice in precision optics: medical glasses, precise photo objects, touch screens for mobile phones, computers and tablets, and other potential displays. The self-cleaning and the anti-bacterial functions are based on photo-induced decomposition without the use of chemicals, demonstrating that TiO<sub>2</sub>-coated surfaces can be classified as environmentally friendly.





## 11. References

- [1] A. Fujishima and K. Honda, *Nature*, vol. 238, pp. 37-38, **1972**.
- [2] M. R. Hoffmann, S. T. Martin, W. Choi and D. W. Bahnemann, *Chem. Rev.*, vol. 95, pp. 69-96, **1995**.
- [3] K. Eufinger, 'Effect of deposition conditions and doping on the structure, optical properties and photocatalytic activity of d.c. magnetron sputtered TiO<sub>2</sub> thin films', PhD Thesis, *Ghent University*, **2007**.
- [4] C. Jayasinghe, A. G. U. Perera, H. Zhu, and Y. Zhao, *Opt. Lett.*, vol. 37, pp. 4302-4304, **2012**.
- [5] R. Wang, K. Hashimoto, A. Fujishima, M. Chikuni, E. Kojima, A. Kitamura, M. Shimohigoshi and T. Watanabe, *Nature*, vol. 388, pp. 431-432, **1997**.
- [6] N. Mellot, C. Durucan, C. Pantano and M. Guglielmi, *Thin Solid Films*, vol. 502, pp. 112-120, **2006**.
- [7] L. Peruchon, E. Puzenat, J. Hermann and C. Guillard, *Photochem. Photobiol. Sci.*, vol. 8, pp. 1040-1046, **2009**.
- [8] A. Mills and S. Le Hunte, *J. Photochem. Photobiol. A: Chem.*, vol. 108, pp. 1-35, **1997**.
- [9] R. Beydoun, R. Amal, G. Low and S. Mc Evoy, *J. Nanopart. Res.*, vol. 1, pp. 439-458, **1999**.
- [10] D. W. Bahnemann, *Isr. J. Chem.*, vol. 33, pp. 115-136, **1993**.
- [11] D. Bahnemann, D. Doeckelmann, R. Goslich, M. Hilgendorff and D. Weichgrebe, 'Photocatalytic detoxification: Novel catalysis, mechanisms and solar applications' *Elsevier*, New York, pp. 301-319. **1993**
- [12] A. Fujishima, K. Hashimoto and T. Watanabe, 'TiO<sub>2</sub> Photocatalysis: Fundamentals and Applications', *BKC. Inc.*, Tokyo, **1999**.
- [13] P. C. Hiemenz, 'Principles of Colloid and Surface Chemistry', *Dekker*, New York, **1986**.
- [14] H. Honda, A. Ishizaki, K. Hashimoto and A. Fujishima, *J. Illum. Eng. Soc.*, vol. 24, pp. 42-49, **1998**.
- [15] C. Doodeve and J. Kitchener, *Trans. Faraday Soc.*, vol. 34, pp. 570-579, **1938**.
- [16] W. Jaegermann, *Modern Aspects of Electrochemistry*, Plenum Press, New York, **1996**.

- [17] L. Peter, Applications of Kinetic Modeling, vol. 37, pp. 223-279, *Elsevier*, Amsterdam **1999**.
- [18] L. Kavan, M. Gräzel, S. E. Gilbert, C. Klemenz and H. Scheel, *J. Am. Chem. Soc.*, vol. 118, pp. 6716-6723, **1996**.
- [19] M. Fox and M. T. Dulay, *Chem. Rev.*, vol. 93, pp. 341-357, **1993**.
- [20] S. Sakthivel and H. Kisch, *Chem. Phys. Chem.*, vol. 4, pp. 487-490, **2003**.
- [21] S. Sakthivel, M. Hidalgo, D. Bahnemann, S.U. Geissen, V. Murugesan and A. Vogelpohi, *Appl. Cat. B: Environ.*, vol. 63, pp. 283-293, **2006**.
- [22] K. Hashimoto, I. Hiroshi and F. Akira, *Jpn. J. Appl. Phys.*, vol. 44, pp. 8269-8285, **2005**.
- [23] C. F. Goodeve and J. A. Kitchener, *Trans. Faraday Soc.*, vol. 34, pp. 902-908, **1938**.
- [24] X. T. Zhang, T. Taguchi, H.B. Wang, Q.B. Meng, O. Sato and A. Fujishima, *Res. Chem. Intermediat.*, vol. 33, pp. 5-11, 2007.
- [25] C. Kormann, D. W. Bahnemann and M. R. Hoffmann, *Environ. Sci. Tec.*, vol. 25, pp. 494-500, **1991**.
- [26] X. Z. Liu, Z. Huang, K. X. Li, H. Li, Chen and Q. Meng, *Chin. Phys. Lett.*, vol. 23, pp. 2606-2608, **2006**.
- [27] I. Kuyanov, D. Lacks and U. Diebold, *Phys. Rev. B.*, vol. 68, pp. 1-4, **2008**.
- [28] O. Carp, C. L. Huisman and A. Reller, *Prog. Solid State Chem.*, vol. 32, pp. 33-17, **2004**.
- [29] M. Schiavello, 'Heterogeneous photocatalysis', Wiley Series in Photoscience and Photoengineering, 3 ed., *John Wiley & Sons*, Chichester, **1997**.
- [30] A. Salinaro, A. V. Emeline, J. Zhao, H. Hikada, V. K. Rybabchuk and N. Serpone, *Pure Appl. Chem.*, vol. 71, pp. 321-335, **1999**.
- [31] B. F. Xue, H. X. Wang, Y. S. Hu, H. Li, Z. X. Wang, Q. B. Meng, X. J. Huang, L. Q. Chen, O. Sato and A. Fujishima, *C. R. Chim.*, vol. 9, pp. 627-630, **2006**.
- [32] F. Wang, R. Liu, A. Pan, L. Cao, K. Cheng, B. Xue, G. Wang, Q. Meng, J. Li, Q. Li, Y. Wang, T. Wang and B. Zou, *Mate. Lett.*, vol. 61, pp. 2000-2003, **2007**.
- [33] T. Minabe, D. A. Tryk, P. Sawunyama, Y. Kikuchi, K. Hashimoto and A. Fujishima, *J. Photochem. Photobiol. A*, vol. 137, pp. 53-62, **2000**.
- [34] A. Nakajima, K. Hashimoto, T. Watanabe, K. Takai, G. Yamauchi and A. Fujishima, *Langmuir*, vol. 16, pp. 7044-7047, **2000**.

- [35] H. K. Pulker, 'Coatings on Glass', *Elsevier*, Amsterdam, **1999**.
- [36] A. Mills, A. Lepre, N. Elliott, S. Bhopal, I. P. Parkin and S.A. O'Neill, *J. Photochem. Photobiol. A*, vol. 160, pp. 213-223, **2003**.
- [37] H. Irie, T. Ping, T. Shivata and K. Hashimoto, *Electrochem. Solid-State Lett.*, vol. 8, pp. 23-25, **2005**.
- [38] D. M. Mattox, 'Handbook of Physical Vapor Deposition (PVD) Processing: Film Formation, Adhesion, Surface Preparation and Contamination Control', *Noyes Publication*, Westwood, New Jersey, **1998**.
- [39] B. R. Appleton, 'Ion Beam Processes in Advanced Electronic Materials and Device Technology', *Materials Research Soc.*, Pittsburgh, **1985**.
- [40] Denton Vacuum LLC [Online], 'www.dentonvacuum.com', USA, [Accessed 12. 10. **2011**].
- [41] H. Ehlers, T. Groß, M. Lappschies and D. Ristau, *Vak. Forsch. Prax.*, vol. 16, pp. 284-290, **2004**.
- [42] H. Ehlers, K. Becker, R. Beckmann, N. Beermann, U. Brauneck, F. Fuhrberg, D. Gäbler, S. Jakobs, N. Kaiser, M. Kennedy, F. König, S. Laux, J. C. Müller, B. Rau, W. Riggers, D. Ristau, D. Schäfer, and O. Stenzel, *Proc. of SPIE, Advances in Optical Thin Films*, vol. 5250, pp. 646-655, **2004**.
- [43] M. Kennedy, D. Ristau and H. Niederwald, *Thin Solid Films*, vol. 333, pp. 191-195, **1998**.
- [44] Leybold Optics GmbH [Online], 'www.leyboldoptics.com', Alzenau, Germany, [Accessed 14. 03. **2012**].
- [45] A. Kaless, U. Schulz, P. Munzert and N. Kaiser, *Surf. Coat. Technol.*, vol. 200, pp. 58-61, 2004.
- [46] N. Beermann, H. Ehlers, and D. Ristau, *Proc. of SPIE, Optical Design and Engineering II*, vol. 5963, pp. 145-155, **2005**
- [47] K. Lau, 'Plasmagestützte Aufdampfprozesse für die Herstellung haftfester optischer Beschichtungen auf Bisphenol-A Polycarbonat', PhD Thesis, *ULB Sachsen Anhalt*, 2006
- [48] X. Wanga, H. Masumotoa, Y. Somenob and T. Hirai, *Thin Solid Films*, vol. 338, pp. 105-109, **1999**.

- [49] N. Kaiser, 'Laser und Optoelektronik', vol. 28, pp. 52-60, **1996**.
- [50] K. Starke, 'Übertragung von Standardmessverfahren zur Charakterisierung optischer Beschichtungen in den Bereich ultrakurzer Pulse', PhD Thesis, *LUH*, Hannover, **2004**.
- [51] D. Decker, L. Koshigoe and E. Ashley, 'Thermal properties of optical thin film materials' in *Proceedings of the Conference on Laser-Induced Damage in Optical Materials*, NBS Spec Publ, pp. 291-297, **1986**.
- [52] C. Yang, H. Fan, Y. Xi, J. Chen and Z. Li, *Appl. Surf. Sci.*, vol. 254, pp. 2685-2689, **2008**.
- [53] M. Lappschies, B. Görtz and D. Ristau, *Appl. Opt.*, vol. 45, pp. 1502-1506, **2006**.
- [54] R. Wang, K. Hashimoto, A. Fujishima, A. Chikuni, M. Kojima, E. Kitamura, M. Shimohigoshi and T. Watanabe, *Nature*, vol. 388, pp. 431-432, **1997**.
- [55] A. R. Khataee, H. Aleboeyeh and A. Aleboeyeh, *J. Exp. Nanosci.*, vol. 4, pp. 121-137, **2009**.
- [56] N. Talebian and M. R. Nilforoushhan, *Thin Solid Films*, vol. 518, pp. 2210-2215, **2010**.
- [57] Y. Li and L. Wang, 'Semiconductor Nanoclusters', *Elsevier*, P. V. Kamat, D. Meisel, pp. 391-415, Amsterdam, **1997**.
- [58] N. Serpone, D. Lawless, R. Khairutdinov and E. Pelizzetti, *J. Phys. Chem.*, vol. 99, pp. 655-661, **1995**.
- [59] R. W. Matthews, *J. Catal.*, vol. 113, pp. 549-555, **1988**.
- [60] A. Linsebigler, G. Lu and J. Yates, *Chem. Rev.*, vol. 95, pp. 735-738, **1995**.
- [61] A. Mills and J. Wang, *J. Photochem. Photobiol., A.*, vol. 127, pp. 123-124, **1999**.
- [62] H. Al-Ekabi and N. Serpone, *J. Phy. Chem.*, vol. 1, pp. 5726-5731, **1988**.
- [63] T. Watanabe, A. Nakajima, R. Wang, M. Miniabe, S. Kiozumi, A. Fujishima and H. Hashimoto, *Thin Solid Films*, vol. 351, pp. 260-263, **1999**.
- [64] S. Goldstein, D. Behar and J. Rabani, *J. Phys. Chem. C*, vol. 113 pp. 12489-12494, **2009**.
- [65] H. Kisch, N. Serpone and E. Pelizzetti, 'What is photocatalysis, Photocatalysis: Fundamentals and applications', 1-8 ed., *John Wiley & Sons, Inc.*, New York, **1989**.
- [66] M. Faisal, M. Abu Tariq and M. Muneer, *Dyes Pigm.*, vol. 72, pp. 233-239, **2007**.
- [67] J. R. Harbour and M. L. Hair, *Adv. Colloid Interf. Sci.*, vol. 24, pp. 103-141, **1986**.

- [68] H. Schmidt, M. Naumann, T. S. Muller and M. Akarsu, *Thin Solid Films*, vol. 502, pp. 132-137, **2006**.
- [69] T. Nuida, N. Kanai, K. Hashimoto, T. Watanabe and H. Ohsaki, *Vacuum*, vol. 74, pp. 729-733, **2004**.
- [70] M. Dulay and M. Fox, *Chem. Rev.*, vol. 93, pp. 341-357, **1993**.
- [71] D. Hurum, A. Agrios and K. Gray, *J. Phys. Chem. B*, vol. 107, pp. 4545-4549, **2003**.
- [72] K. Okamoto, Y. Yamamoto, H. Tanaka and A. Itaya, *Bull Chem Soc Jpn*, vol. 58, pp. 2023-2028, **1985**.
- [73] P. Maness, S. Smolinski, D. M. Blake, Z. Huang, E. J. Wolfrum and W. A. Jacoby, *Environ. Microbiol.*, vol. 65, pp. 4095-4098, **1999**.
- [74] G. Gogniat, M. Thyssen, M. Denis, C. Pulgarin and S. Dukan, *FEMS. Microbiol. Lett.*, vol. 258, pp. 18-24, **2006**.
- [75] D. Ollis and H. Al-Ekabi, 'Photocatalytic purification and treatment of water an air', pp. 301-319, *Elsevier*, Amsterdam, **1993**.
- [76] R. Fateh, A. A. Ismail, R. Dillert and D. W. Bahnemann, *J. Phys. Chem. C*, vol. 115, pp. 10405-10411, **2011**.
- [77] A. Fernhdez, G. Lassaletta, V. M. Jimeney, A. Justo, E. Gonyale, J. Herrmann and Y. Ait-Ichou, *Appl. Catal., B*, vol. 7, pp. 49-63, **1995**.
- [78] J. M. Herrmann, H. Tahiria, Y. Ait-Ichoub, G. Lassalettac, A. Gonzilez-Elipe and A. Fernbdez, *Appl. Catal., B*, vol.13, pp. 219-228, **1997**.
- [79] K. Hashimoto, H. Irie and A. Fujishima, *AAPPS Bulletin*, vol 17 pp. 12-28, **2007**.
- [80] D. Acosta, A. Martinez, C. Magan and J. Ortega, *Thin Solid Films*, vol. 490, pp. 112-117, **2005**.
- [81] J. Tschirsch, D. Bahneman, M. Wark and J. Rathousky, *J. Photochem. Photobiol., A*, vol. 194, pp. 181-188, **2008**.
- [82] A.A. Ismail, D.W. Bahnemann, J. Rathousky, V. Yarovyti and M. Wark, *J. Mater. Chem*, vol. 21, pp. 7802-7810, **2011**.
- [83] T. Graberg, P. Hartmann, A. Rein, S. Gross, B. Seelandt, C. Röger, R. Zieba, A. Traut, M. Wark and J. Janek, *Sci. Technol. Adv. Mater.* vol. 12, 025005, **2011**.
- [84] J. Rathousky, V. Kalousek, V. Yarovyti, M. Wark and J. Jirkovsky, *Photobiol. A: Chem.*,

- vol. 216, pp. 126-132, **2010**.
- [85] K. Wessels, T. Oekermann and M. Wark, *J. Adv. Oxid. Technol.*, vol. 14, pp. 158-164, **2011**.
- [86] M. Wark, J. Tschirch, O. Bartels, D. Bahnemann and J. Rathousky, *Microp. Mesop. Mater.*, vol. 84, pp. 247-253, **2005**.
- [87] J. Yu, J. Yu, W. Hoa and Z. Jianga, *New J. Chem.*, vol. 26, pp. 607-613, **2002**.
- [88] E. Kim, D. Kim and B. Ahn, *Bull. Korean Chem. Soc.*, vol. 30, pp. 193-196, **2009**.
- [89] I. Bannat, K. Wessels, T. Oekermann, J. Rathousky, D. Bahnemann and M. Wark, *Chem. Mater.*, vol. 21, pp. 1645-1653, **2009**.
- [90] K. Eufinger, D. Poelman, B. Poelman, R. De Gryse and G. Marin, *Vac. Technol. Coat.*, vol. 8, pp. 44-47, **2007**.
- [91] K. Eufinger, D. Poelman, H. Poelman, R. De Gryse and G. Marin, *J. Phys. D: Appl. Phys.*, vol. 40, pp. 5232-5238, **2007**.
- [92] H. Nam, T. Amemiya, M. Murabayashi and K. Itoh, *J. Phys. Chem. B*, vol. 108, pp. 8254-8259, **2004**.
- [93] H. Tada and M. Tanaka, *Thin Solid Films*, vol. 13, pp. 360-364, **1997**.
- [94] Y. Pihosh, *Appl. Surf. Sci.*, vol. 256, pp. 937-942, **2009**.
- [95] J. Zhang, X. Xiao and J. Nan, *J. Hazard Mater.*, vol. 176, pp. 617-622, **2010**.
- [96] M. Fernández-García, A. Martínez-Arias, J. Hanson and J. Rodríguez, *Chem. Rev.*, vol. 104, pp. 4063-4104, **2004**.
- [97] X. Han, Q. Kuang, M. Jin, Z. Xie and L. Zheng, *J. Am. Chem. Soc.*, vol. 131, pp. 3152-3153, **2009**.
- [98] A. Zöller, R. Götzelmann, H. Hagedorn, W. Klug and K. Matl, *Optical Thin Films, SPIE*, vol. 3133, pp. 196-204, **1997**.
- [99] H. Ehlers, T. Groß, M. Lappschies and D. Ristau, *Proc. SPIE*, vol. 5250, pp. 519-527, **2004**.
- [100] M. Jiang, Q. S. Li, J. N. Wang, Z. Jin, Q. Sui, Y. Ma, J. Shi, F. Zhang, L. Jia, W.G. Yao, and W. F. Dong, *Opt. Express*, vol. 21, pp. 3083-3090, 2013.
- [101] C. Hazama and S. Hachioji, 'Titanium-Oxide Photocatalyst', *Three Bond Co., LTD*, 193-

- 8533, Tokyo, **2004**.
- [102] L. Dubrovinsky, N. Dubrovinskaia, N. Swamy, J. Muscat, N. Harrison, R. Ahuja, B. Holm and B. Johansson, *Nature*, vol. 410, pp. 653-654, **2001**.
- [103] D. Cameron, T. Kääriäinen and M. Kääriäinen, *Thin Solid Films*, vol. 517, pp. 6666-6670, **2009**.
- [104] K. Guan, *Surf. Coat. Tech.*, vol. 191, pp. 155-160, **2005**.
- [105] K. P. Kühn, I. F. Chaberny, K. Massholder, M. Stickler, V. Beny, H. Sonntag and L. Erdinger, *Chemosphere*, vol. 53, pp. 71-77, **2003**.
- [106] S. Malato, J. Blanco, C. Richter and M. I. Maldonado, *Appl. Catal., B*, vol. 25, pp. 31-38, **2000**.
- [107] E. F. Duffy, F. Al Touati, S. C. Kehoe, O. A. McLoughlin, L. Gill, W. Gernjak, I. Oller, M. Maldonado, S. Malato, J. Cassidy, R. H. Reed and K. McGuigan, *Sol. Energy*, vol. 77, pp. 649-655, **2004**.
- [108] F. Chanon and M. Chanon, 'Photocatalysis- Fundamental and Applications', *Wiley-Interscience, Ed.*, N. Serpone, E. Pelizzetti, Chap. 15, **1989**.
- [109] S. Gelover, L. A. Go'mez, K. Reyes and L. Teresa, *Water Res.*, pp. 3274-3280, **2006**.
- [110] V. Vimonses, M. Chong and B. Jin, *Microporous Mesoporous Mater.*, vol. 132, pp. 201-209, **2010**.
- [111] M. V. Shankar, K. Cheralathan, B. Arabindoo, M. Palanichamy and V. Murugesan, *J. Mol. Catal. A: Chem: Chemical*, vol. 223, pp. 195-200, **2004**.
- [112] C. Nasr, K. Vinodgopal, L. Fisher, S. Hotchandani, A. Chattopadhyay and P. Kamat, *J. Phys. Chem.*, vol. 100, pp. 8436-8442, **1996**.
- [113] A. Sayari, *Chem. Mater.*, vol. 8, pp. 1840-1852, **1996**.
- [114] K. Ko, S. Park and M. J. Choi, *Bull. Korean Chem. Soc.*, vol. 21, pp. 95-961, **2000**.
- [115] V. Gerard and F. Notheisz, 'Heterogeneous Catalysis in Organic Chemistry', *Elsevier*, Amsterdam, **2000**.
- [116] M. Hassan, H. Dylla, L. Mohammad and T. Rupnow, *Construction and Building Materials*, vol. 24, pp. 1456-1461, **2010**.
- [117] S. Automative, Hygien iQ [Online], '<http://www.sigmaautomotive.com>'. [Accessed 05. 11. **2010**].

- [118] C. Trapalis, P. Keivanidis, G. Kordas, M. Zaharescu, M. Crisan, A. Szatvanyi and M. Gartner, *Thin Solid Films*, vol. 433, pp. 186-190, **2003**.
- [119] F. Gracia, F. Yubero, J. P. Holgado, J. P. Espinos, A. Gonzalez-Elipe and T. Girardeau, *Thin Solid Films*, vol. 500, pp. 19-26, **2006**.
- [120] E. Reinhold, J. Richter, H. Waydrink and E. Zschieschang, *Thin Solid Films*, vol. 377-378, pp. 14-20, **2000**.
- [121] P. Chin and D. Ollis, *Catal.Today*, vol. 123, pp. 177-188, **2007**.
- [122] L. Dobrzański and K. Luk, *Archives of Materials Science and Engineering*, vol. 28, pp. 12-18, **2007**.
- [123] R. Boughaled, S. Schlichting, H. Ehlers, D. Ristau, I. Bannat and M. Wark, *Advances in Optical Thin Films III*, vol. 7101, pp. 71010K-1 - 71010K-11, **2008**.
- [124] G. Atanassova, J. Turlob, J. Fuc and Y. Daic, *Thin Solid Films*, vol. 342, pp. 83-92, **1999**.
- [125] P. Frach, X. D. Glo , C. Modes, B. Scheffel and O. Zywitzki, *Vacuum*, vol. 80, pp. 679-683, **2006**.
- [126] B. I. Via Camozzi, italcementi, [Online], ‘ [www.italcementi.it](http://www.italcementi.it)’, [Accessed 08.12.2012].
- [127] J. Krysaa and A. Mills, *J. Photochem. Photobiol., A*, vol. 203, pp. 119-124, **2009**.
- [128] F. Dong, W. Zhao and Z. Wu, *J. Hazard Mater.*, vol. 162, pp. 763-770, **2009**.
- [129] E. Weir, A. Lawlor, A. Whelan and F. Regan, *The Analyst*, vol. 133, pp. 835-845, **2008**.
- [130] C. Chang, C. Lin and C. Chan, *Thin Solid Films*, vol. 494, pp. 274-278, **2006**.
- [131] S. Tomás, A. Luna-Resendis, L. Cortés-Cuautli and D. Jacinto, *Thin Solid Films*, vol. 518, pp. 1337-1340, **2009**.
- [132] Y. Wu, W. Jia, Q. An, Y. Liu, J. Chen and G. Li, *Nanotechnology*, vol. 20, pp. 245101-245109, **2009**.
- [133] R. Damodara, S. You and H. Chou, *J. Hazard Mater.*, vol. 172, pp. 1321-1328, **2009**.
- [134] F. Delgado, K. Go’mez and C. Morales, *Microelectron. J.*, vol. 39, pp. 1333-1335, **2008**.
- [135] W. Chen, J. Zhang and Q. Fang, *Sens. Actuators, B*, vol. 100, pp. 195-199, **2004**.
- [136] K. Naoi, Y. Ohko and T. Tatsuma, *J. Am. Chem. Soc.*, vol. 126, pp. 3664-3668, **2004**.
- [137] H. Gerischer and A. Heller, *J. Phys. Chem.*, vol. 95, pp. 5261-5267, **1991**.
- [138] M. J. Height, S. E. Pratsinis, O. Mekasuwandumrong and P. Praserthdam, *Appl. Catal., B*,



- vol. 63, pp. 305-312, **2006**.
- [139] C. A. Gouvea, F. Wypych, S. Moraes, N. Duran and P. Peralta-Zamora, *Chemosphere*, vol. 40, pp. 427-432, **2000**.
- [140] W. Y. Teoh, L. Mädler, D. Beydoun, S. Pratsinis and R. Amal, *Chem. Eng. Sci.*, vol. 60, pp. 5852-5861, **2005**.
- [141] V. Subramanian, E. Wolf and P. Kamat, *J. Phys. Chem. B*, vol. 105, pp. 11439-11446, **2001**.
- [142] T. Abe, E. Suzuki, K. Nagoshi, K. Miyashita and M. Kaneko, *J. Phys. Chem. B*, vol. 103, pp. 1119-1123, **1999**.
- [143] M. Rauf, M. Meetani, A. Khaleel and A. Ahmed, *Chem. Eng. J.*, vol. 157, pp. 373-378, **2010**.
- [144] D. Lee and I. Chol, *Microchem. J.*, vol. 68, pp. 215-223, **2001**.
- [145] J. Navio, A. Colon, M. Trillas, J. Peral, X. Domenech, J. Testa, J. Padron, D. Rodriguez and M. Litter, *Appl. Catal.*, vol. 16, pp. 187-196, **1998**.
- [146] X. Domenech and J. Peral, *Chemosphere*, vol. 38, pp. 1265-1271, **1999**.
- [147] L. Zhang, C. Yu, H. Yip, Q. Li, K. Kwong, A. Xu and P. Wong, *Langmuir*, vol. 19, pp. 10372-10380, **2003**.
- [148] H. Irie, Y. Watanabe and K. Hashimoto, *J. Phys. Chem. B*, vol. 107, pp. 5483-5486, **2003**.
- [149] T. Rungnapa and S. Kongthip, 'Effect of Silver Dispersion on Photocatalytic Activity of Silver-Loaded Titanium Oxide', Pathum Thani, **2010**.
- [150] J. Tschirch, R. Dillert, D. Bahnemann, B. Proft, A. Biedermann and B. Goer, *Res. Chem. Intermed.*, vol. 34, pp. 381-392, **2008**.
- [151] C. Wang, D. Bahnemann and J. K. Dohrman, *Water Sci. Technol.*, vol. 44, pp. 279-286, **2001**.
- [152] H. Yamashita, M. Harada, J. Misaka, H. Nakao, M. Takeuchi and M. Anpo, *Nucl. Instr. Methods Phys. Res.*, vol. B206, pp. 889-892, **2003**.
- [153] T. Yua, X. Tana and L. Zha, *J. Hazard Mater.*, vol. 176, pp. 829-835, **2010**.
- [154] M. DeRosa and R. Crutchley, *Coord. Chem. Rev.*, vol. 233, pp. 351-371, **2002**.
- [155] R. Redmond and J. Gamlin, *Photochem. Photobiol.*, vol. 70, pp. 391-475, **1999**.

- [156] C. Chung, H. I. Lin and J. L. He, *Surf. Coat. Technol.*, vol. 202, pp. 1302-1307, **2007**.
- [157] X. Wang, Y. Tang, Z. Chen and T. Lim, *J. Mater. Chem.*, vol. 43 , pp. 23149-23158, **2012**.
- [158] L. Hochmannovaa and J. Vytrasovab, *Prog. Org. Coat.*, vol. 67, pp. 1-5, **2010**.
- [159] Z. Lei and L. Jian-she, *Trans. Nonferrous Met. SOC. China*, vol. 17, pp. 772-776, **2007**.
- [160] M. F. Hossain, S. Biswas, T. Takahashi, Y. Kubota and A. Fujishima, *Thin Solid Films*, vol. 517, pp. 1091-1095, **2008**.
- [161] H. Kaufmann, *J. Vac. Sci. Technol.*, vol. 15, pp. 272-276, **1978**.
- [162] R. F. Bunshah, 'Deposition Technologies for Films and Coatings: Developments and Applications', *Noyes Publications*, New York, **1982**.
- [163] K. Seshan, 'Handbook of Thin-Films Deposition Processes and Techniques', Noyes Publications/*William Andrew Publishing*, New York, **2002**.
- [164] Thin Film Department, LZH, 'Coating methods, Power Point Presentation'. 08. 05. **2012**
- [165] C. Tien and S. Lin, 'Optimization of process parameters of titanium dioxide films by response surfaces methodology', *P. Soc. Photo-Opt. Ins.*, vol. 266, pp. 574-581, **2006**.
- [166] Udel Education, [Online], '<http://www.physics.udel.edu/~ismat/200204.pdf>', [Accessed 13.07. **2012**].
- [167] A. Anders, 'Handbook of Plasma Immersion Ion Implementation and Deposition', *Wiley-Interscience*, New York, **2000**.
- [168] D. Ristau, 'Thin Film optical coatings, Encyclopedia of Modern Optics', *Elsevier*, Oxford, **2004**.
- [169] C. Powell, J. Oxley and J. J. Blocher, 'Vapor Deposition, Electrochemical Society Series', *Wiley-Interscience*, New York, **1966**.
- [170] J. Singh, J. T. Schriempf and D. Wolfe. [Online], '[www.p2pays.org/ref/02/01161.pdf](http://www.p2pays.org/ref/02/01161.pdf).' [Accessed 15. 06. **2011**].
- [171] S. Zhenga, T. Wanga, W. Haob and R. Shena, *Vacuum*, vol. 65, pp. 155-159, **2002**.
- [172] S. Chiu, Z. Chenb, K. Yang, Y. Hsuc and D. Gana, *J. Mater. Process. Technol.*, vol. 192, pp. 60-67, **2007**.
- [173] D. Glöß, P. Frach, C. Gottfried, S. Klinkenberg and J. Liebig, *Thin Solid Films*, vol. 516, pp. 4487-4489, **2008**.

- [174] T. Wang, S. Zheng, W. Hao and C. Wang, *Surf. Coat. Technol.*, vol. 155, pp. 141-145, **2002**.
- [175] Vacuum Process Technology LLC Plymouth., [Online],  
'<http://www.vptec.com/imgs/IBS-coating-system.jpg>' [Accessed 02. 05. **2013**].
- [176] M. Yamagishia, S. Kurikib, P. Songa and Y. Shigesatoa, *Thin Solid Films*, vol. 442, pp. 227-231, **2003**.
- [177] Y. Xu and M. Shen, *J. Mater. Process. Technol.*, vol. 202, pp. 301-306, **2008**.
- [178] M. Takeuchi, Y. Onozaki, Y. Matsumura, H. Uchida and T. Kuji, *Nucl. Instrum. Methods Phys. Res.*, vol. B206, pp. 259-263, **2003**.
- [179] M. Krishna, K. Rao and S. Mohan, *J. Appl. Phys.*, vol. 73, pp. 434-438, **1993**.
- [180] J. Singh, The Applied Research Laboratory, The Pennsylvania State University, [Online],  
'[www.p2pays.org/ref/26/25287.pdf](http://www.p2pays.org/ref/26/25287.pdf).' [Accessed 10. 06. **2012**].
- [181] D. Ristau and H. Ehlers, 'Thin Film Optical Coatings, Handbook of Lasers and Optics', pp. 373-393, Springer, New York, **2007**
- [182] S. Wilbrandt, N. Kaiser and O. Stenzel, *Thin Solid Films*, vol. 502, pp. 153-157, **2006**.
- [183] J. Harhausen, R. P. Brinkmann, R. Foest, M. Hannemann, A. Ohl and B. Schröder, *Plasma Sources Sci. Technol.* vol. 21, p. 035012 (16pp), **2012**.
- [184] Waiferx, [Online], '<http://waiferx.blogspot.de/2012/01/presentation-redirecting-light.html>', [Accessed 12. 01. **2013**].
- [185] J. R. Devore, *J. Opt. Soc. Am.*, vol. 41, pp. 416-419, **1951**.
- [186] Shott, Optics Arizona Shott, [Online].  
'[http://fp.optics.arizona.edu/optomech/references/glass/Schott/tie-29\\_refractive\\_index\\_v2\\_us.pdf](http://fp.optics.arizona.edu/optomech/references/glass/Schott/tie-29_refractive_index_v2_us.pdf)'. [Accessed 4 .12. **2012**].
- [187] Z. Chenga, S. Hu, P. Zeng, T. Kuang, G. Xie and F. Gao, *Surf. Coat. Technol.*, vol. 201, pp. 5552-5555, **2007**.
- [188] H. Yamashita, H. Nakao, M. Takeuchi, Y. Nakatani and M. Anpo, *Nucl. Instrum. Methods Phys. Res.*, vol. B206, pp. 898-901, **2003**.
- [189] M. Habibi, N. Talebian and J. Choi, *Dyes Pigm.*, vol. 73, pp. 103-110, **2007**.
- [190] M. Sasase, K. Miyake, T. Yamaki, I. Takano and S. Isobe, *Thin Solid Films*, vol. 281-282, pp. 431-435, **1996**.

- [191] S. Woo and C. Hwangbo, *Surf. Coat. Technol.*, vol. 201, pp. 8250-8257, **2007**.
- [192] X. Houa and A. Liua, *Radiat. Phys. Chem.*, vol. 77, pp. 345-351, **2008**.
- [193] X. Hou, J. Maa, A. Liu, D. Li, M. Huang and X. Deng, *Nucl. Instrum. Methods Phys. Res. B*, vol. 268, pp. 550-554, **2010**.
- [194] G. Takaoka, M. Kawashita, K. Omoto and T. Terada, *Nucl. Instrum. Methods Phys. Res. B*, vol. 232, pp. 200-205, **2005**.
- [195] R. Asahi, T. Morikawa, T. Ohwaki and Y. Taga, *Science*, vol. 294, pp. 269-271, **2001**.
- [196] D. Bahnemann, *Sol. Energy*, vol. 77, pp. 445-459, **2004**.
- [197] M. Seery, [Online], '<http://photochemistryportal.net/home/index.php/2009/09/30/metal-oxide-photocatalysis/&docid=w8tkTsYgbYYNIM&imgur>', [Accessed 07. 05. **2013**].
- [198] C. Lu and W. Wu, *Mat. Sci. Eng.: B*, vol. 113, pp. 42-45, **2004**.
- [199] H. Yaghoubi, N. Taghavinia and E. Alamdari, *Surf. Coat. Technol.*, vol. 204, pp. 1562-1568, **2010**.
- [200] N. Mahdjoub, N. Allen, P. Kelly and V. Vishnyakov, *J. Photochem. Photobiol., A*, vol. 211, pp. 59-64, **2010**.
- [201] Z. Can, D. Wanyu, W. Hualin, C. Weiping and J. Dongying, *J. Env. Sci.*, vol. 21, pp. 741-744, **2009**.
- [202] P. Eiamchai, P. Chindaudom, A. Pokaipisit and P. Limsuwan, *Curr. Appl Phys.*, vol. 9, pp. 707-712, **2009**.
- [203] J. Shia, S. Shange, L. Yangd and J. Yand, *J. Alloys Compd.*, vol. 479, pp. 436-439, **2009**.
- [204] M. Fallet , S. Permpoon , J. Deschanvres and M. Langlet , *J. Mater. Sci*, vol. 41, pp. 2915-2921, **2006**.
- [205] H. Tomaszewski , K. Eufinger, D. Poelman , R. De Gryse, P. Smet and G. Marin, *Int. J. Photoenergy*, vol. 8, no. ID 95213,5 pages, **2007**.
- [206] L. Yuqionga and Y. Zhinonga, *Rare Met.*, vol. 28, pp. 559-563, **2009**.
- [207] T. Neubert, W. Sun, F. Neumann and M. Vergöhl, *OSA Technical Digest (CD), Optical Society of America, ThA10*, **2007**.
- [208] Y. Le prince Wanga, *Thin Solid Films*, vol. 359, pp. 171-176, **2000**.
- [209] S. Vilhunen, M. Vilve, M. Vepsäläinen and M. Sillanpää, *J. Hazard. Mater*, vol. 179, pp.

- 776-782, **2010**.
- [210] H. Ehlers, T. Groß, M. Lappschies, and D. Ristau, *Optics and Precision Engineering*, vol. 13, pp. 403-412, *Proceedings of the Sino-German High Level Expert Symposium on Optical Coatings*, Shanghai, **2005**
- [211] H. Ehlers, K. Becker, R. Beckmann, N. Beermann, U. Brauneck, F. Fuhrberg, D. Gäbler, S. Jakobs, N. Kaiser, M. Kennedy, F. König and D. Ristau, *Proc. SPIE*, vol. 5250, pp. 646-655, **2004**.
- [212] Balzers, 'User Manual Balzers BAK 760'. [Accessed 12. 02. **2008**].
- [213] H. Ehlers, 'Reaktive ionengestützte Prozesse für optische Hochleistungsschichten', *PhD Thesis*, LUH, Hannover, **2008**.
- [214] Kaufman & Robinson 'Broad-Beam Industrial Ion Sources', *Kaufman & Robinson Inc.*, **2003**.
- [215] P. Kadkhoda, W. Sakiew, S. Günster and D. Ristau, *Optical Measurement Systems for Industrial Inspection VI: Peter H. Lehmann, (ed.)*, *SPIE*, vol. 7389, pp. 15-18, **2009**.
- [216] L. Reimer, 'Scanning Electron Microscopy: Physics of Image Formation and Microanalysis', Springer Series in Optical Sciences, P.W. Hawkes, Berlin, **1998**.
- [217] J. Goldstein, D. Newbury, D. Joy, C. Lyman, P. Echlin, E. Lifshin, L. Sawyer and J. Michael, 'Scanning electron microscopy and x-ray microanalysis', *Plenum Publishers, 3rd Edition*, Kluwer, **2003**.
- [218] FEI Company, [Online],  
'[http://www.fei.com/uploadedfiles/documents/content/2006\\_06\\_allyouwanted\\_pb.pdf](http://www.fei.com/uploadedfiles/documents/content/2006_06_allyouwanted_pb.pdf), '  
[Accessed 13. 06. **2012**].
- [219] O. Zywitzki, T. Modes, P. Frach and D. Glöss, *Surf. Coat. Technol.* vol. 202, pp. 2488-2493, 2008.
- [220] BAM, [Online], '[ftp://ftp.bam.de/Powder\\_Cell/structure\\_files/TIO2.TXT](ftp://ftp.bam.de/Powder_Cell/structure_files/TIO2.TXT)', [Accessed 14. 09. **2011**].
- [221] F. Hansen, [Online], 'The Measurement of Surface Energy of Polymers by Means of Contact Angles of Liquids on Solid Surfaces,' [Accessed 2. 05. **2011**].
- [222] M. Greiner, C. Regal and D. Jin, *Nature*, vol. 426, pp. 537-540, **2003**.
- [223] P. Pichat, 'Photochemistry, Photocatalysis and Photoreactors', M. Schiavello, Ed., Reidel, pp. 425-455, **1985**.

- [224] J. Valladares and J. Bolton, 'Photocatalytic Purification and Treatment of Water and Air', F. Ollis, Ed., *Elsevier*, pp. 111-120, Amsterdam, **1993**,
- [225] J. Peral and D. Ollis, *J. Catal.*, vol. 136, pp. 554,- 565, **1992**.
- [226] P. Pichat, J. Hermann, J. Disdier, H. Courbon and M. Mozzanega, *Nouv. J. Chim.*, vol. 5, pp. 627, **1981**.
- [227] R. Alberci and W. Jardim, *Appl. Catal B.: Environ.*, vol. 14, pp. 55-68, **1997**.
- [228] International Organization of Standardization, 'Fine ceramics (advanced ceramics, advanced technical ceramics) -Test method for self-cleaning performance of semiconducting photocatalytic materials. PartI: Measurement of water contact angle'. Patent ISO/CD 27448-1. **2012**
- [229] Pilkington company, [Online] '<http://www.pilkingtonselfcleaningglass.co.uk>' [Accessed 8. 11 **2012**].
- [230] Faraday-cup, [Online], '<http://www.faraday-cup.com>', [Accessed 24 10 **2012**].
- [231] H. Selhofer, E. Ritter and R. Linsbod, *Appi. Opt.*, vol. 41, pp. 756, **2002**.
- [232] K.N. Rao, *Opt. Eng.*, vol. 41, pp. 2357-2364, **2002**.
- [233] C.R. Li., Z.H. Zheng, F.M. Zhang, S.Q. Yang, and X.H., *Liu Nuci. Instr. Method. Phys. Res. B*, vol. 169, pp. 21-25, **2000**.
- [234] T. R. Culver, 'Developments in Ion Assisted Multilayer Coating', *SPIE*, vol. 1848, **1992**.
- [235] N. Beermann, 'Analyse der Emissionscharakteristiken von Ionenquellen für hochwertige optische Beschichtungsprozesse', PhD Thesis, *LUH*, Hannover, **2009**.
- [236] R.W. Matthews., *J. Phys. Chem.*, vol. 91, pp. 3328-3333, **1987**.
- [237] M. Anpo, T. Shima, S. Kodama and Y. Kubokawa, *J. Phys. Chem.*, vol. 91, pp. 4305-4310, **1987**.
- [238] J. Hermann, *Catal. Today*, vol. 53, pp. 115-129, **1999**.
- [239] J. Kiwi, *J. Phys. Chem.*, vol. 89, pp. 2437-2457, **1985**.
- [240] Y. Inel and A. Okte, *J. Photochem. Photobiol. A: Chem*, vol. 96, pp. 175-180, **1996**.
- [241] J. Bandara, J. Kiwi, R. Humphry-Baker and C. Pulgarin, *J. Adv. Oxid. Technol.*, vol. 1, pp. 126-137, **1996**.
- [242] A. Assabane, Y. Ichou, H. Tahiri, C. Guillard and J. Hermann, *Appl. Catal B: Environ*,

- vol. 24, pp. 71-87, **2000**.
- [243] D. Chen and A. Ray , *Appl. Catal. B: Environ*, vol. 23, pp. 143-157, **1999**.
- [244] M. Böttger, T. Graumann, R. Boughaled, F. Neumann and W. Kowalsky, *J. Photochem. Photobiol. A: Chem.*, vol. 253, pp. 7- 15, **2013**.
- [245] H. Ichiura, T. Kitaoka and Tanaka H, *Chemosphere*, vol. 51, pp. 855-860, **2003**
- [246] T. Ibusuki and K. Takeuchi, *J. Mol. Catal.*, vol. 88, pp. 93-102, **1994**.
- [247] M. Ballari, M. Hunger, G. Husken and H. Brouwers, *Appld. Catal. B: Environ*, vol. 95, pp. 245-254, **2010**.
- [248] Y. Ohkyo, Y. Nakamura, N. Negishi, S. Matsuzawa and K. Takeuchi, *J. Photochem. Photobiol. A: Chem.*, vol. 205, pp. 28-32, **2009**.
- [249] B. Hauchercorne, D. Terrens, S. Verbruggen, J. Martens, H. Van Langenhove, K. Demeestere and S. Lenaerts, *Appld. Catal. B: Environ*, vol. 106, pp. 630-638, **2011**.
- [250] Y. Mansourpanah, S. Madaeni, A. Rahimpour, A. Farhadian and A. Taheri, *J. Membr. Sci.*, vol. 330, pp. 297-306, **2009**.
- [251] D. Kim, S. Han and S. Kwak, *J. Colloid Interface Sci*, vol. 316, pp. 85-91, 2007.
- [252] L. Miaoa, S. Tanemuraa, Y. Kondob and M. Iwatab, *Appl. Surf. Sci.*, vol. 238, pp. 125-131, **2004**.
- [253] S. Karuppuchamy, J. Jeong , D. Amalnerkar and H. Mmoura, *Vacuum*, vol. 80, pp. 494-498, **2006**.
- [254] B. Sankapal , S. Sartale , M. Lux-Steiner and A. Ennaoui, *C.R. Acad. Sci.*, vol.41, pp.155-173. **2006**.
- [255] K. Eufinger and D. Poelman, *Thin Solid Films*, vol. 531, pp.189-227, **2008**.
- [256] B. Liu, X. Zhao, Q. Zhao, C. Li and X. He, *Mater. Chem. and Phys.*, vol. 90, pp. 422-432, **2005**.
- [257] T. Asanuma, T. Matsutani, C. Liu, T. Mihara and M. Kiuchi, in *Proc. 7th Int. Symp.Sputt. Plasma Proc. (ISSP 2003)*, Kanazawa, Japan, **2003**.
- [258] P. Zeman and S. Takabayashi, *Surf. Coat. Technol.*, vol. 153, pp. 93-99, **2002**.
- [259] T. Takahashi, Takahashi, T., Prabakar, K., Nezuka, T., Yamazaki, T., Nakashima, T., Kubota, Y. and Fujishima, A., *J. Vac. Sci. Technol. A*, vol. 24, pp. 1161-1165, **2006**.

- [260] M. Bames, S. Kumar, L. Green, N. Hwang and A. Gerson, *Surf. Coat. Technol.*, vol. 190, pp. 321, **2005**.
- [261] J. Miller, S. Veeramasuneni, M. Drelich and R. Yalamanchili, *Polym. Eng. Sci.*, vol. 36, pp. 1949-1855, **1996**.
- [262] D. Kaczmarek, J. Domaradzki, D. Woicieszak and B. Gornicka, *Nanotechnology, nanomaterials and nanoelectronics*, vol. 978-1, pp. 159-162, **2008**.
- [263] Y. Hou, D. Zhuang, G. Zhang, M. Zhao and M. Wu, *Appl. Surf. Sci.*, vol. 218, pp. 97-105, **2003**.
- [264] B. Pethica, *J. Colloid Interface Sci.*, vol. 62, pp. 567-569, **1977**.
- [265] K. Tanabe, T. Sumizoshi, K. Shibata, J. Krzoura and J. Kitagawa, *Bull. Chem. Soc. Jpn.* vol. 47, pp. 1064-1066, **1974**.
- [266] H. Lin, S. Kumon, H. Kozuka and T. Yoko, *Thin Solid Films*, vol. 315, pp. 266-272, **1998**.
- [267] G. Zhao, H. Kozuka and T. Yoko, *Thin Solid Films*, vol. 277, pp. 147-154, **1996**.
- [268] D. Mardare, M. Tasca, M. Delibas and G. Rusu, *Appl. Sur. Sci.*, vol. 156, pp. 200-206, **2000**.
- [269] D. Poelman and P. Smet, *J. Phys. D: Appl. Phys.*, vol. 36, pp. 1850, **2003**.
- [270] DIN, 'Lichttransmissionsgrad nach DIN EN 410: Glas im Bauwesen -Bestimmung der lichttechnischen und strahlungsphysikalischen Kenngrößen von Verglasungen'. Germany Patent DIN EN 410. **1998**
- [271] R. Sawanepoel, *J. Phys. E: Sci. Instrum.*, vol. 16, pp. 1214-1222, **1983**.
- [272] J. Tauc and A. Menth, *J. Non-Cryst. Solids*, vol. 8, pp. 569-585, **1972**.
- [273] N. Mathews, E. Morales, M. Cortes-Jacome and J. Toledo Antonio, *Sol. Energy*, vol. 83, pp. 1499-1508, **2009**.
- [274] B. Smarsly, D. Gorosso, T. Brezesinski, N. Pinna, C. Boissire and M. Antonietti, *Chem. Mater*, vol. 16, pp. 2948-295, **2004**.
- [275] B. O'Regan and M. Grätzel, *Nature*, vol. 353, pp. 737-740, **1991**.
- [276] I. Bannat, 'Optimierung der Photokatalytischen Eigenschaften von Mesoporösen Titandioxid-Schichten durch die Modifizierung mit Gold-Nanostrukturen', PhD Thesis, *LUH*, Hannover, **2011**.



- [277] C. Vasantkumar and A. Mansingh, *Seventh IEEE International Symposium on Application of Ferroelectrics, IEEE*, pp. 713-716, New York, **1990**.
- [278] M. Lappschies, 'Rugate Filter und Mischschichten für optische Hochleistungskomponenten', PhD Thesis, *LUH*, Hannover, **2009**.
- [279] T. Sugiura, T. Yoshida and H. Minoura, *Electrochem. Solid-State Lett.* vol. 1, pp. 175-177, **1998**.
- [280] J. Kolbe, 'Entwicklung verlustarmer und strahlungsresistenter dielektrischer Spiegel für den VUV-Bereich', PhD Thesis, *LUH*, Hannover, **1991**.
- [281] PVD techniques, [Online], '<http://144.206.159.178/ft/1035/10005/192573.pdf>' [Accessed 15. 07 **2012**].
- [282] H. S. Tung, J. M. Song, S. W. Feng, C. Kuoa and I.G. Chen, *Phys. Chem. Chem. Phys.* vol.12, pp.740-744, **2010**.
- [283] P. Sudhagar, R. Sathyamoorthy and S. Chandramohan, *Appl. Surf. Sci.*, vol. 254, pp. 1919-1928, **2008**.
- [284] D. Ren, Y. Zou, C. Zhan and N. Huang, *J. Kor. Phys. Soc.*, vol. 58, no. 4, pp. 883-885, **2011**.
- [285] E. Stathatos, T. Petrova and P. Lianos, *Langmuir*, vol. 17, pp 5025-5030, **2001**.
- [286] C. Chang, J. Chen, T. Hsu, C. Lin and C. Chan, *Thin Solid Films*, vol. 516, pp. 1743-1747, **2008**.
- [287] A. Ismail, D. Bahnemann, I. Bannat and M. Wark, *J. Phys. Chem. C*, vol. 113, pp. 7429-7435, **2009**.
- [288] M. Haruta, N. Yamada, T. Kobayashi and S. Iijima, *J. Catal. 115*, vol. 301, pp 301-309, **1989**.
- [289] T. Tabakova, V. Idakiev, D. Andreeva and I. Mitov, *Appl. Catal. A*, vol. 202, pp. 91- 97, **2000**.
- [290] T. Kobayashi, M. Haruta, S. Tsubota and H. Sano, *Sens. Actuators, B*, vol. 1, pp. 222-225. **1990**.
- [291] M. Haruta, S. Tsubota, T. Kobayashi, H. Kageyama, M. Genet and B. Delmon, *J. Catal. Vol. 144*, vol. 175, pp.175-192, **1993**.
- [292] S. Tsubota, M. Haruta, T. Kobayashi, A. Ueda and Y. Nakahara, *Stud. Surf. Sci. Catal.*,

- vol. 63, pp. 695-704, **1991**.
- [293] M. Okumura, K. Tanaka, A. Ueda and M. Haruta, *Solid State Ionics*, vol. 95, pp. 143-149, **1997**.
- [294] C. M. Yang, H. S. Sheu and K. Chao, *J. Adv. Funct. Mater.*, vol. 12, pp. 143-148, **2002**.
- [295] K. L. Kelly, E. Coronado, L. L. Zhao and G. C. Schatz, *J. Phys. Chem. B*, vol. 107, pp. 668-677, **2003**.
- [296] B. Tian, J. Zhang, T. Tong and F. Chen, *Applied Catalysis B: Environmental*, vol. 79, pp. 394-401, **2008**.
- [297] I. Arabatzis, T. Stergiopoulos, D. Andreeva, S. Kitova and S. Neophytides, *J. Catal.*, vol. 127, 127-135, **2003**.
- [298] X. Li and F. Li, *Environ. Sci. Technol.*, vol. 35, pp. 2381-2387, **2001**.
- [299] V. Rodríguez-González, R. Zanella, G. del Angel and R. Gomez, *J. Mol. Catal. A-Chem*, vol. 281, pp. 93-98, **2008**.
- [300] L. Wan, J. Li, J. Feng, W. Sunb and Z. Mao, *Applied Surface Science*, vol. 253, pp. 4764-4767, **2007**.

## 12. Appendix

### 12.1 Additional information

#### 12.1.1 Additional Text

##### Info Appendix 1. Pre-deposition technical details

The actual deposition processes were conducted in the following manner. First, the cooling pump was opened to check the parameters, which were set as follows: water was held at 6 bar, volume flow meter at 50 l/min, oil valve 'in' at 7 bar, oil valve 'out' at 2 bar, coating machine 'in' between 4 to 6 bar, and plant 'out' at 2.5 bar. After that, the main apparatus, Balzers BAK 760, was switched on and left for 20 to 30 minutes to achieve suitable vacuum level. When the vacuum and water reached the appropriate level, the 'vent' button of the machine was pressed to open the apparatus. The apparatus door took 30 to 40 minutes to open, which positively affected the decrease of the substrate temperature and the particle contamination inside the chamber. During this 30 to 40 minute period, the glass substrates, in this case Suprasil and Menzel substrates were chosen and cleaned manually with acetone and isopropanol, or mechanically using an ultrasonic automatic plant. The quality of cleaning was controlled by light-microscopy. Tungsten, rolled and placed in ion-source apparatus, was used as a filament. After all the materials were placed as mentioned above, the doorframe of Balzers BAK 760 was cleaned with isopropanol and closed. After this, the vacuum and pressure were set at 0.001 mbar, and log. Lin. Ion gauge at 0.00005 mbar.

##### Info Appendix 2. Resistance of neutralizer

The ion-source neutralizer can be expressed in the following equation, considering  $R$  as its resistance:

$$R = \rho \cdot \frac{l}{A} \quad \text{Eq. App. 30}$$

In this equation,  $l$  is the length which was kept at 13 cm, density is represented by  $\rho$ . Both factors were kept constant due to which the resistance also remained constant, hence ( $U= I \cdot R$ ). If the potential, represented as  $U$ , is increased, current, represented as  $V$ , would also increase. However, if the discharge current is increased considerably, the tungsten filament will get damaged.

Info Appendix 3. Using of XTC as thin film deposition controller

With the aim of correlating the oscillation frequency of a piezoelectric crystal to the mass, the XTC controller used the Sauerbrey equation:

$$\Delta f = \frac{-2\Delta m f_0^2}{A\sqrt{\rho_q \mu_q}} = -\frac{2f_0^2}{A\sqrt{\rho_q \mu_q}} \Delta m \quad \text{Eq. App. 31}$$

where  $\Delta f$ : Frequency Change (Hz);  $\Delta m$ : Mass Change;  $f_0$  : Resonant Frequency;  $A$ : Piezoelectrically Crystal Area between electrodes (cm<sup>2</sup>);  $\rho_q$  : Density of quartz, and  $\mu_q$ : Shear Modulus of quartz.

Another factor considered in the sensor was the stability, which manages permissible increase in the frequency between the Sensor measurements taken before crystal failure and after initiation of automatic crystal switch. Additionally, three parameters were entered in the source, that of 'Control Gain', representing change in the percentage of Power for a given rate deviation, 'Density', which depended on the substrate being used, and 'Z-Ratio', which defined the correlation between mass loading on the crystal and coating thickness.

The Thin Film Deposition Controllers of XTC contain Mode-Lock, which is a measurement system of INFICON and is based on oscillator technology. It has the ability to control the thickness of the films more accurately compared with conventional methods used for this purpose. Along with precision, it also has a quicker response time. With XTC, it is possible to have closed-loop monitoring and control of different deposition layers.

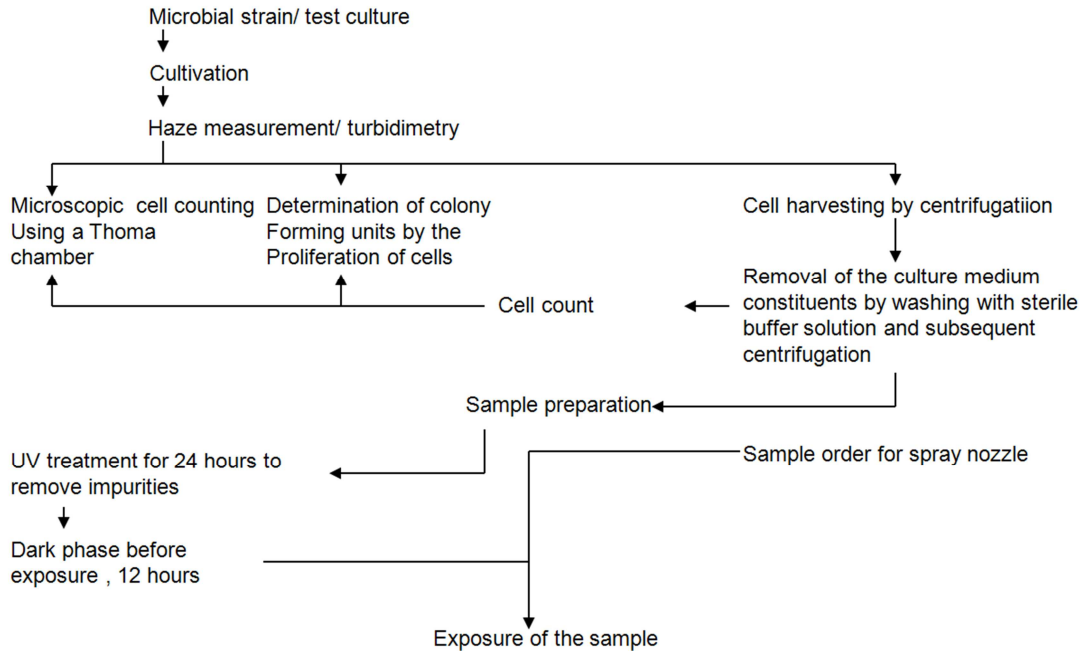
Moreover, a thickness accuracy of 1% can be achieved with a 0.06 Angstrom resolution. It is used with INFICON Rate-Watcher feature, which provides a long-term rate control for in-line or load-locked sputtering processes or for thermal evaporation from a resistive source.

Info Appendix 4. External photoactivity measurement tests

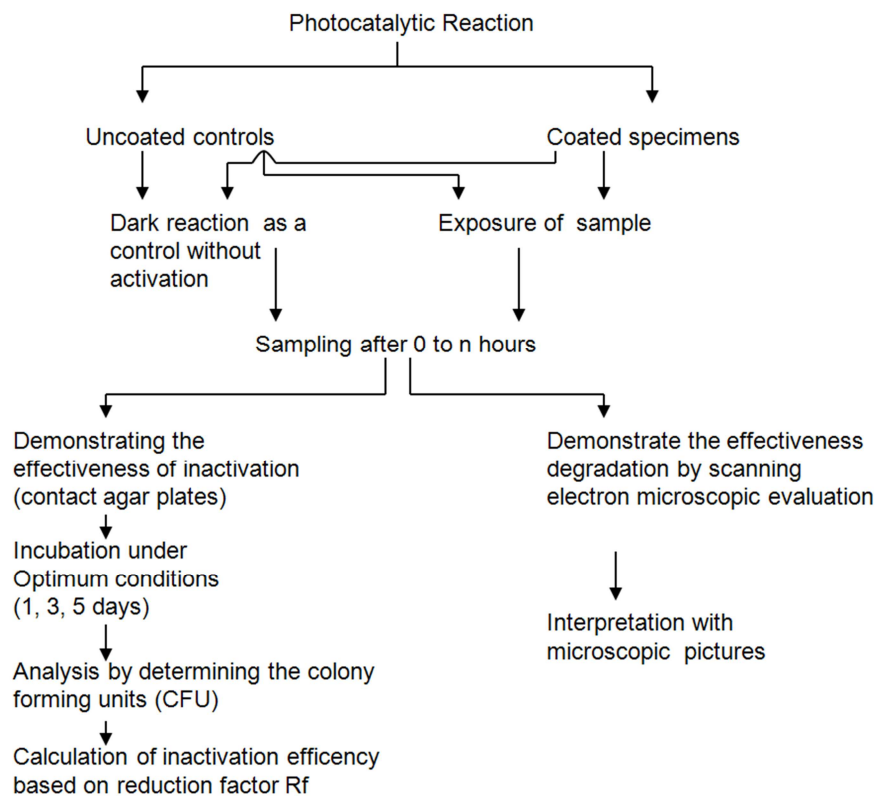
The actual processes used were presented at the DIN Group on Photocatalysis, and were approved as being compliant with the DIN 52980 standard. A presentation made was focused on a comparison between stearic acid methods used at the Institute of Surface Technology (IST) and LZH, which resulted in a possibility of new standard for 'luminescence degradation'

Info Appendix 5. Microbiological assessment in two parts: sample preparation and photocatalytic preparation (IGB, Stuttgart)

**Part One**



**Part Two**



### 12.1.2 Additional Figures

In Figure Appendix I, optimization of the automated measuring technique is symbolically illustrated to determine the photocatalytic activity on the surfaces. It clarifies that, apart from the measurement of the photocatalytic effects, additional functions can also be altered, such as temperature regulation, on-line incident lighting time, and measurement of the air humidity.

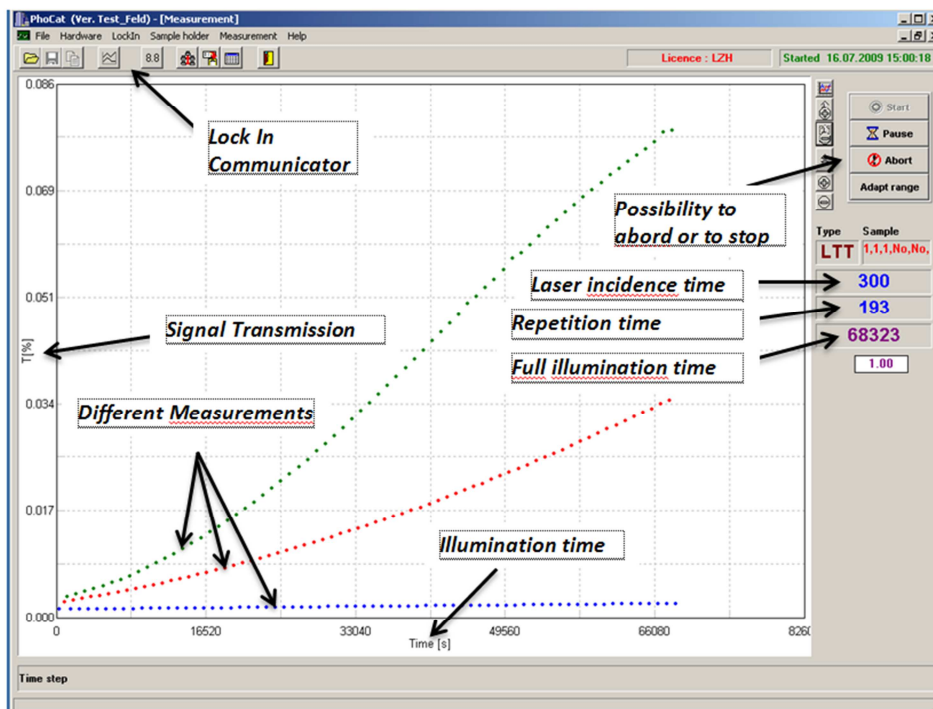


Figure Appendix I. A visualization of the C++ program used to determine the photocatalytic activity.

Figure Appendix II visualizes the surface in the context of the optimization phase of the compiled C++ software, which was based on the platform developed at the Laser Components department of LZH.

The example shows an analysis of internal and external samples in order to compare the photonic efficiency on the basis of methylene blue, the concentration of which was determined with the help of spectrophotometers.

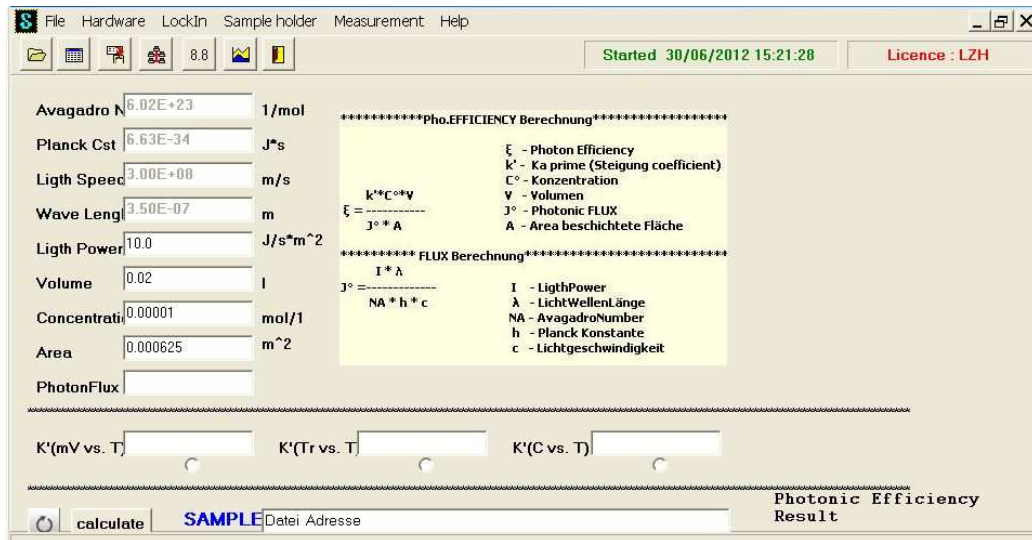


Figure Appendix II. Screen capture of the software created to calculate the photocatalytic activity.

The luminescence degradation direct method is highly sensitive and reproducible. It represents an encouraging option to be exposed in standardization exploit in photocatalysis.

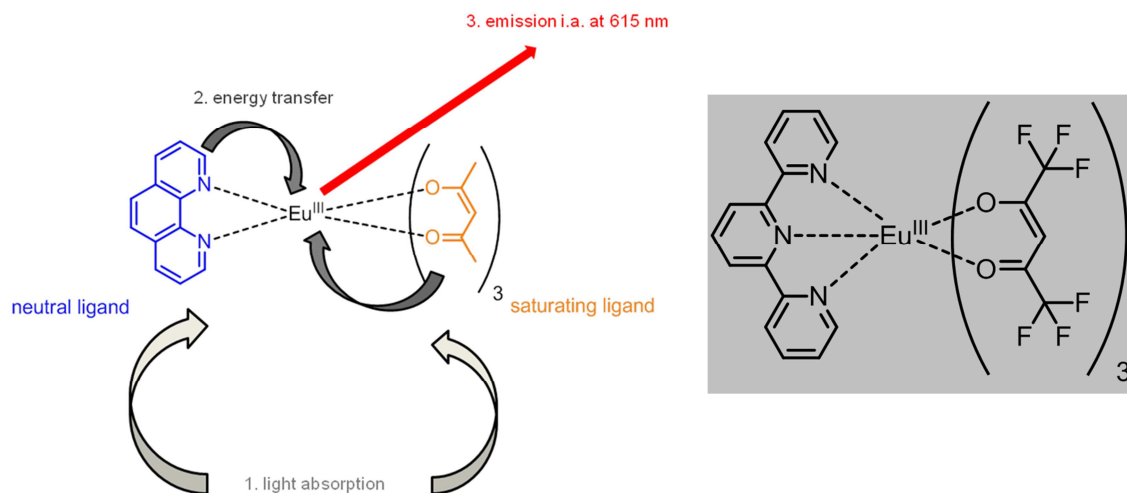


Figure Appendix III. Left: Delineation of the Weissman effect. 1.) Light absorption by the organic ligands, 2.) Energy transfer to the europium(III) cation, 3.) Main emission at 615 nm. Right: Luminescent europium (III) complex (terpy)Eu(hfac)<sub>3</sub><sup>[244]</sup>.

The XRD results of samples of different process variants show that the samples in Figure Appendix IV exhibited different textures.

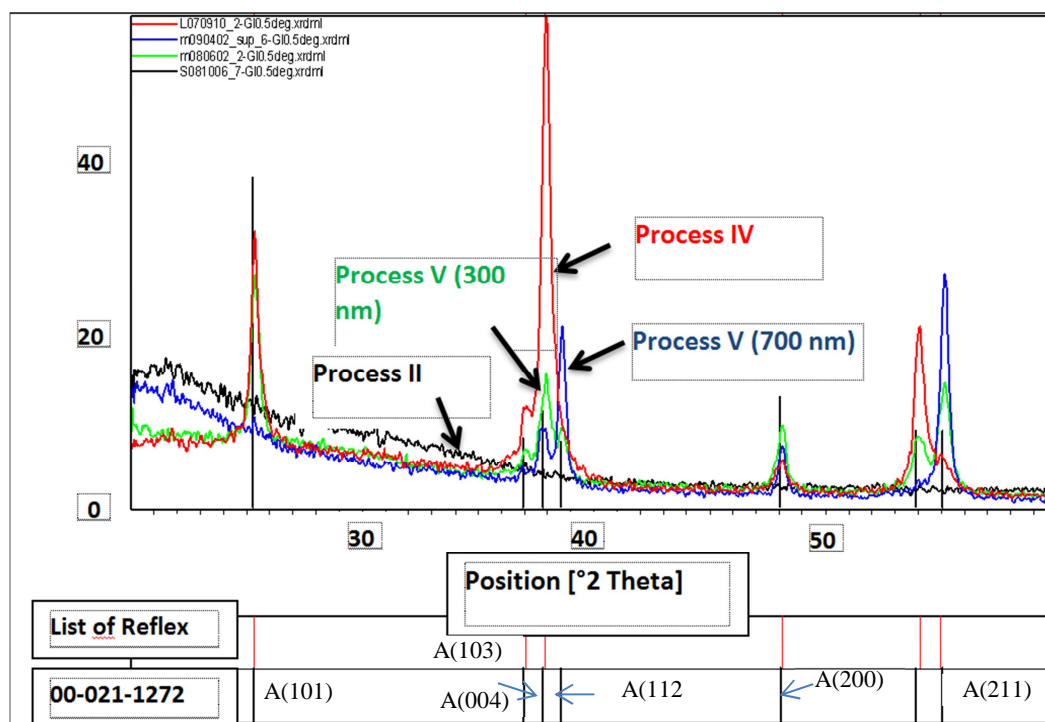


Figure Appendix IV. Additional XRD results of the photocatalytically coated thin films (measurements Fraunhofer IST).

The results of the thin film's microstructure are shown in the graph of Figure Appendix IV and, with the red, blue, green and black curves representing (1) IAD using CC-104, (2) IAD using CC-105 at high temperature, (3) IAD using CC-105 at a cold temperature, 50 °C to 60 °C, and (4) simple IAD using APS, respectively. These different process results show that IAD using CC-104 has a high anatase reflection on the reflex at 2 Theta ( $2\theta$ ) 25° and 38°, and a lower reflex on anatase (110) at  $2\theta$  55°. The IAD process with CC-105 at cold process temperature leads to a medium level of photoactivity, and is represented in Figure Appendix IV by reflexes at 38°, 54° and 55°.

Deposition of films using SYRUSpro 1100 with APS resulted in an absence of anatase and rutile phases, but with an amorphous microstructure, and a lower level of photoactivity when compared to the above processes. The highest intensity of anatase reflexes, represented in the graph with reflexes at  $2\theta$  25 (001), and 55° (411), were observed on films deposited using the IAD process at approximately 250 °C with CC-105. It is only in the case of IAD that the reflex point reaches 39°, which represents high photoactivity.

It was revealed that using the vacuum evaporation method with Denton CC-105 resulted in the effective controlling of the structural characteristics of TiO<sub>2</sub> layers, and also that different crystal modifications influenced certain coating parameters.



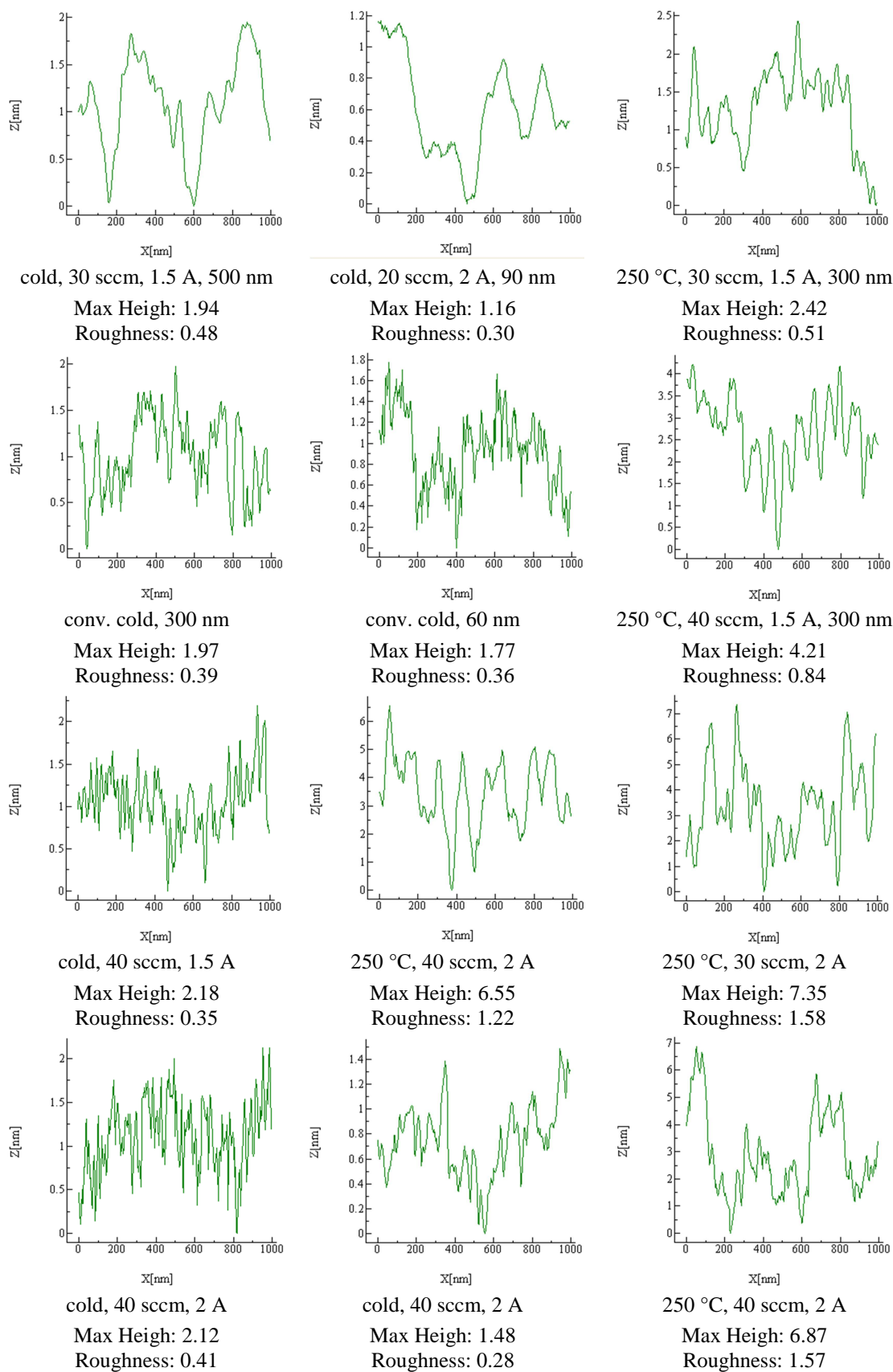


Figure Appendix V (a). 'Section analysis' study on the titania AFM images.

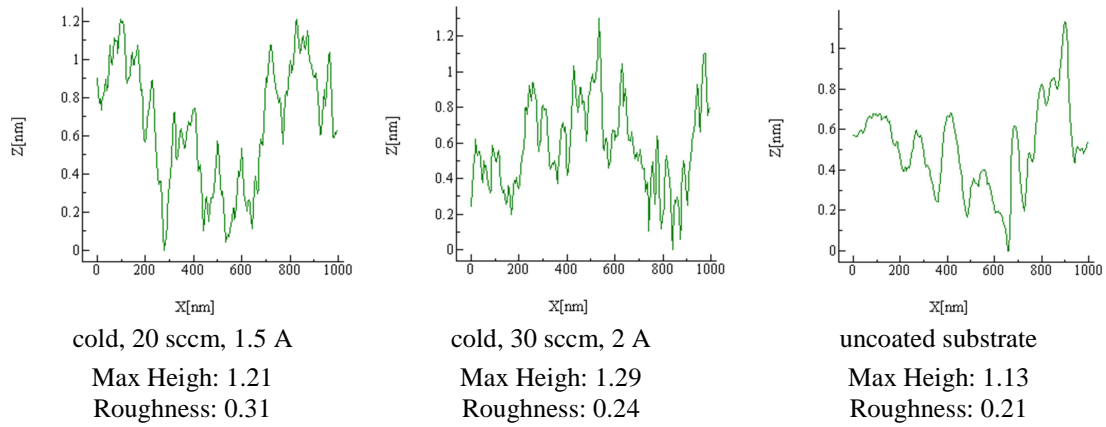
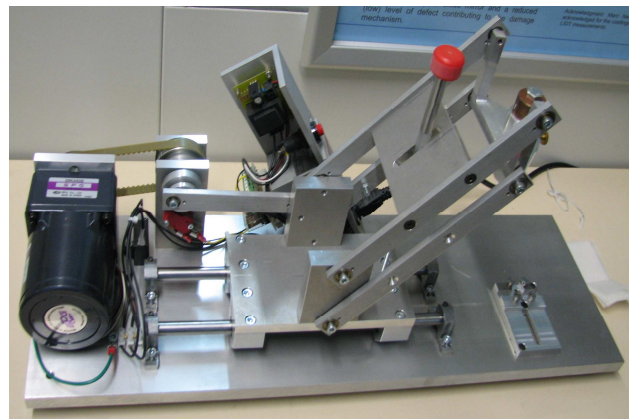


Figure Appendix V (b). 'Section analysis' study on the titania AFM images.



Sand erosion test



Moderate abrasion



Severe abrasion resistance test.

Figure Appendix VI. Durability tests: mechanical and environmental stability. Ref. MIL (MIL-C-48497) and DIN Standards (DIN 52348, DIN ISO 9211-4).



Figure Appendix VII. Solubility Test result. Left: before test, right: after test.

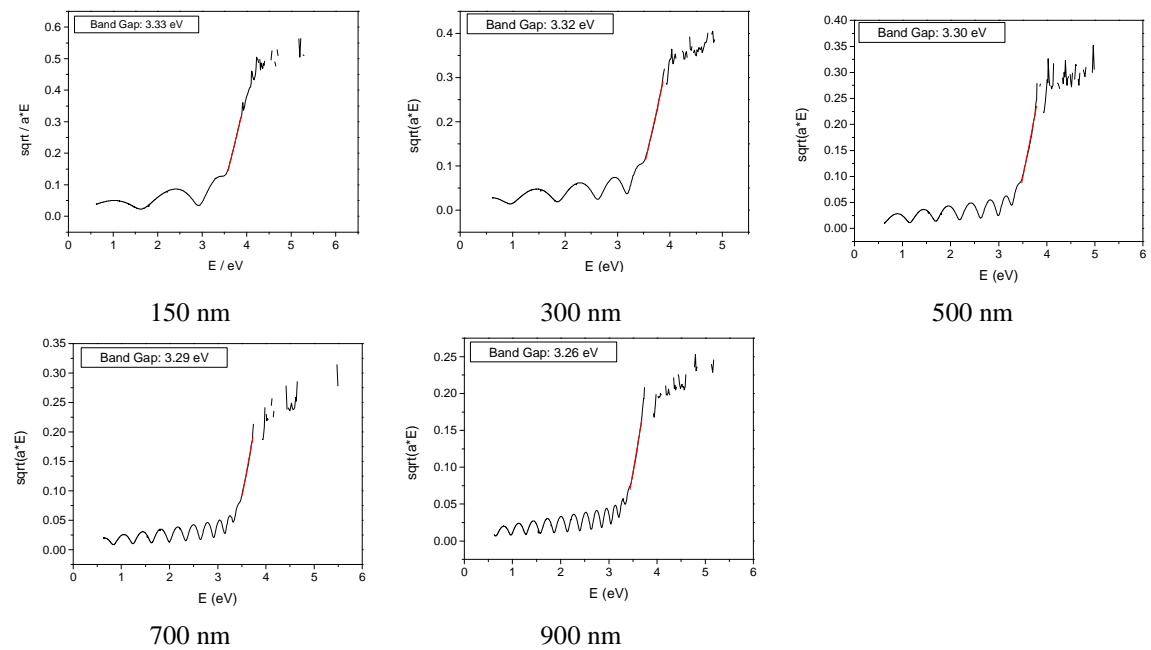


Figure Appendix VIII. Band gap for different coating thicknesses.

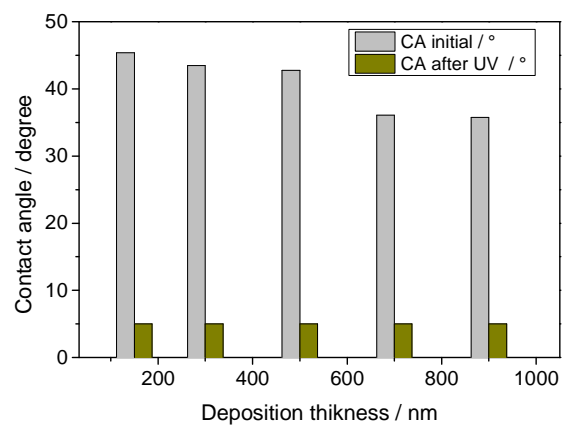


Figure Appendix IX. Hydrophilicity results for different deposition thicknesses using IAD.

### 12.1.3 Additional Tables

Table Appendix 1. Technical parameters of e-beam deposition using Balzers BAK 760.

Plant & Coating Process Properties					
Voltage	8 - 10 kV		Rotary Cage Control		40 rpm
Current	0.3 - 0.5 A		XTC Controller-Tooling Factor		80 - 120 %
Calotte Heater (=Process temperature)	Cold - 350 °C		Crucible Control Speed		6 rpm
High Vacuum	0.001 mbar		TiO <sub>2</sub> Ion-Beam Focus		0 - 0.8 A
Log-linear Ion Gauge	0.00005 mbar		Emission Current	Plant	0.1 - 0.50 A
				Ion-Beam	22-30 A
O <sub>2</sub> Valve Control Unit	0.0003 mbar		Plasma Etching	O <sub>2</sub> gas	20-40 sccm*
				Heater	Cold – 350 °C
				Time	5 - 30 min
Coating Thickness	10 - 1000 nm		Electrical Connections		130 - 260 V
Coating Rate	TiO <sub>2</sub>	0.15 nm/s	Cleaning, Preconditioning		Chemical
	SiO <sub>2</sub>	0.35 nm/s			Mechanical
Ion-Source Properties					
Neutralizer Wire	Tungsten		O <sub>2</sub> Ion-Source Flow		20 - 40 sccm*
Neutralizer Power	Voltage	8 - 15 V	Filament	Voltage	9 - 13 V
	Current	25 - 33 A		Current	22 - 30 A
Energy of gaseous ions	up to 300 eV	Single phase: 50 Hz	Ion-Source Process	Bias Voltage	160 - 280 V
Filament	Diameter	0.020"		Current	1 - 5 A
Magnets	Hicorex Cobalt	0.5" d. x 0.19"	Size	Diameter: 9 cm Length: 17.5 cm	
Cathode	Body of the Ion-Source		Water-Cooling	15 - 26 °C	
			Discharge Voltage	Power Supply Unit	50 - 800 V DC

\*[1sccm= 0.01646 mbar-l/s]

Table Appendix 2. Result of the TS measurements mapping at 633nm

Background sample		Thin Film coated at 1.5 A, 30 sccm, 300 °C		Thin Film coated at 5 A, 30 sccm, 300 °C	
Mean:	0.00431	Mean:	0.0478	Mean:	0.356
Std. Dev.:	0.207	Std. Dev.:	0.687	Std. Dev.:	1.85
Opti. Mean:	<u>1.00 e-08</u>	Opti. Mean:	<u>1.81 e-04</u>	Opti. Mean:	<u>3.04 e-04</u>
Opti. std. Dev.:	8.59e-12	Opti. std. Dev.:	2.17e-05	Opti. std. Dev.:	3.72e-05
Opti. Median:	1.00e-08	Opti. Median:	1.80e-04	Opti. Median:	3.08e-04
Iterations:	38.0	Iterations:	33.0	Iterations:	9.00

## 12.2 Symbols and Abbreviations

<b>Abbreviation</b>	<b>Meaning</b>
AFM	atomic force microscopy
Ar	argon
AC	alternative current
CAM	contact angle measurement
CB	conduction band
CVD	chemical vapor deposition
DC	direct current
DIN	Deutsches Institut für Normung e.V.
$e^-$	electron formed upon illumination of a semiconductor
E	energy
$E^0$	standard redox potential
$E_g$	band gap energy
<i>et al.</i>	Latin: <i>et alii</i> (English: <i>and others</i> )
$E_{bg}$	band gap energy
$E_c$	conduction band edge
EDX	energy-dispersive analysis by x-rays
EF	Fermi level
eV	electron volts
h	hour
$h^+$	hole formed upon illumination of a semiconductor
$h\nu$	incident photon energy: energy of light
I	intensity of light
IAD	ion assisted deposition
IBICVD	ion-beam induced chemical vapor deposition
IBS	ion-beam sputtering
IR	infrared
ISO	International Organization for Standardization
k	reaction rate constant
MB	methylene blue
mL	milliliter
mol	mole
nm	nanometer
$O_2^{\cdot-}$	superoxide ion radical
$OH^{\cdot}$	hydroxyl radical
PECVD	plasma-enhanced chemical vapor deposition
ppm	part per million
PVD	physical vapor deposition
sccm	standard cubic centimeters per minute
SEM	scanning electron microscopy
T	temperature
TEM	transmission electron microscopy
UV	ultraviolet light
VB	valence band
Vis	visible light
XRD	X-ray diffraction analysis
$\lambda$	wavelength
$\xi$	photonic efficiency
$\mu\text{L}/\mu\text{mol}$	microliter/ micromol

## 12.3 Table of Figures

### Figure Appendix

Figure Appendix I. A visualization of the C++ program used to determine the photocatalytic activity. ....	198
Figure Appendix II. Screen capture of the software created to calculate the photocatalytic activity. ....	199
Figure Appendix III. Left: Delineation of the Weissman effect. 1.) Light absorption by the organic ligands, 2.) Energy transfer to the europium(III) cation, 3.) Main emission at 615 nm. Right: Luminescent europium (III) complex (terpy)Eu(hfac) <sub>3</sub> <sup>[244]</sup> .....	199
Figure Appendix IV. Additional XRD results of the photocatalytically coated thin films (measurements Fraunhofer IST). ....	200
Figure Appendix V (a). 'Section analysis' study on the titania AFM images.....	201
Figure Appendix VI. Durability tests: mechanical and environmental stability. Ref. MIL (MIL-C-48497) and DIN Standards (DIN 52348, DIN ISO 9211-4). ....	202
Figure Appendix VII. Solubility Test result. Left: before test, right: after test.....	203
Figure Appendix VIII. Band gap for different coating thicknesses. ....	203
Figure Appendix IX. Hydrophilicity results for different deposition thicknesses using IAD. ....	203

### Info Appendix

Info Appendix 1. Pre-deposition technical details.....	195
Info Appendix 2. Resistance of neutralizer.....	195
Info Appendix 3. Using of XTC as thin film deposition controller .....	196
Info Appendix 4. External photoactivity measurement tests.....	196
Info Appendix 5. Microbiological assessment in two parts: sample preparation and photocatalytic preparation (IGB, Stuttgart) .....	197

## 12.4 Tables

### Text

Table 1. Cell parameters and density of TiO <sub>2</sub> forms, $\rho_s$ is the selection density <sup>[102]</sup> .....	20
Table 2. Technical data of the coating process from Balzers BAK760 using CC-105. ....	50
Table 3. Comparison of the photonic efficiencies between stearic acid (IST) and methylene blue (LZH) .....	68
Table 4. Parameterization of processes.....	70
Table 5. New Developed Stearic acid and luminescent investigation results acquired by Fraunhofer IST. ...	81
Table 6. Antibacterial study of IAD optimized process (VI).....	85
Table 7. Comparisons of the contact angular measurement.....	106
Table 8. Results of the accomplished contact angle.....	109

---

<i>Table 9. Fixed deposition coating parameters.....</i>	<i>120</i>
<i>Table 10. Fixed deposition coating parameters.....</i>	<i>129</i>
<i>Table 11. Fixed deposition coating parameters.....</i>	<i>134</i>
<i>Table 12. Result of the photocatalytic activities of the coated samples using different deposition parameters. ....</i>	<i>157</i>
<i>Table 13. Estimation of porosity using an IAD and conventional examples.....</i>	<i>162</i>

### ***Appendix***

<i>Table Appendix 1. Technical parameters of e-beam deposition using Balzers BAK 760.....</i>	<i>204</i>
<i>Table Appendix 2. Result of the TS measurements mapping at 633nm .....</i>	<i>204</i>

## 12.5 Scientific publications

### 12.5.1 Journal publications

R. Boughaled, S. Schlichting, H. Ehlers, D. Ristau, I. Bannat, M. Wark

*'Optimization and characterization of transparency photocatalytic TiO<sub>2</sub> thin film prepared by ion assisted deposition'*

Proc. of SPIE, vol. 7101, pp. 71010K-71010K-11, **2008**.

M. Böttger, T. Graumann, R. Boughaled, F. Neumann, W. Kowalsky, H.H. Johannes

*'Development of a new qualification method for photocatalytically active surfaces based on a solid state luminescent dye'*

J. of Photochemistry and Photobiology A: Chemistry. vol. 253, pp. 7-15, **2013**.

### 12.5.2 Papers in Progress

R. Boughaled, O. Merka, M. Wark, H. Ehlers, A.M. Welsch, D. Ristau

*'Surface Morphology and Microstructure of Photocatalytic TiO<sub>2</sub> Optical Thin Films Deposited Prepared by Ion Assisted Deposition'*

J. Surface and Coatings Technology, in progress, **2013**.

J. Kurz, R. Boughaled, L. Robben, L. Erdinger

*'Photocatalytic properties of commercial sunscreens'*

in progress, **2013**.

### 12.5.3 Conference Talks

R. Boughaled, H. Ehlers, D. Ristau, M. Wark

*'Optimization and characterization of transparency photocatalytic TiO<sub>2</sub> thin film prepared by ion assisted deposition'*

SPIE symposium on Optical of system Design 1-5 Septembers **2008**, Glasgow, Schotland.

R. Boughaled, H. Ehlers, D. Ristau, M. Wark

*'Self-cleaning and anti- microbial transparency photocatalytic thin film prepared by ion assisted deposition'*

Twelfth internationally Conference on plasma Surface Engineering, Paper nmbr. 3j1556-OR, PSE **2010**, Garmisch-Partenkirchen, Germany.



R. Boughaled, H. Ehlers, D. Ristau, M. Wark

*'Influence of Temperature, Oxygen Flow, and Thickness on the Structural and Optical Properties of Photocatalytical TiO<sub>2</sub> of Film Prepared by Ion Assisted Deposition'*

15th International Conference on TiO<sub>2</sub> Photocatalysis, **2010**, San Diego, United States of America.

R. Boughaled, H. Ehlers, M. Wark, D. Ristau

*'Photokatalytisch wirksame dünne Schichten mit hoher optischer Qualität hergestellt mit ionengestützten Verfahren'*, in German

Deutsche Physikalische Gesellschaft e.V.(DPG), Stuttgart, **2012**, Germany.

#### 12.5.4 Seminar Talks

R. Boughaled

*'Optimization and characterization of TiO<sub>2</sub> thin films prepared by ion assisted deposition'*

Solid State Seminar, 06.02.**2008**, PCI Institute, Leibniz University. Germany.

#### 12.5.5 Press Release

R. Boughaled

*'Ionengestützte Verfahren zur Herstellung photokatalytischer Schichten'*, in German

J. Photonik, Fachzeitschrift für die Optischen Technologien, p.12, 1/**2009**.

#### 12.5.6 Final Project Reports

R. Boughaled, H. Ehlers, D. Ristau

*'Photokatalytische Oberflächenveredelungen für die Medizin, Fertigungstechnik und Konsumgüter'*, in German

BMBF Project 'Photokat': 01RI0637H, LZH e.V. **2010**.

R. Boughaled, H. Ehlers, D. Ristau

*'Entwicklung von antimikrobiellen Beschichtungen im Wägeraum von Laborwaagen'*, in German

BMWi- ZIM Projekt 'Future Scales': VP2186405MK9, LZH e.V. **2011**.

GEFÖRDERT VOM



Bundesministerium  
für Bildung  
und Forschung



### **12.5.7 Conference Posters**

R. Boughaled, H. Ehlers, D. Ristau, M. Wark

*'Self-Cleaning and anti- Microbial transparency Photocatalytic thin film Prepared by ion Assisted deposition'*

PSE **2010**, Twelfth internationally Conference on plasma Surface Engineering Garmisch-Partenkirchen, Germany.

R. Boughaled, H. Ehlers, D. Ristau, M. Wark

*'Transparent Photocatalytic PVD Thin Films'*

NanoDay **2011**, Laboratory of Nano and Quantum Engineering, Leibniz University, Hannover, Germany.

## 12.6 Curriculum Vitae

### *Personal Data*

Full Name Redouan, Boughaled El Lakhmissi  
 Birthday 26/03/1972 in Tissouka (Chaouen), Morocco (ma)  
 Family status Single  
 Nationality German

### *School Education*

07/1977 – 06/1982 Primary school and High school in Kenitra, (ma)  
 07/1982 – 06/1989 BIRD Lycée, Kenitra, (ma); S Baccalauréat 'Sciences Expérimentales'  
 10/1990– 07/1991 BIRD Lycée, Kenitra, (ma); L Baccalauréat 'Littérature Moderne'

### *University Education*

10/1990 – 07/1997 Ibn Tofail University, Kenitra, (ma); Bachelor of Science in Chemistry  
 First professional qualifying degree; Licence National Code: 97/1402  
 10/1993 – 07/1997 Bachelor of Arts in Linguistics; Licence National Code: 97/3745  
 11/1997 – 01/2000 Diploma study in Applied Chemistry 'Diplôme d' Etudes Supérieures  
 Approfondies' (D.E.S.A.). Kenitra University, (ma). Note: 16/20  
 Title of D.E.S.A. thesis: 'Infrared and Raman spectroscopy of  $ALnP_2O_7$   
 diphosphates: A = Na, K, Rb;  $Ln^{3+}$  = Lanthanides'. Defended: 02/2000,  
 Second academic completion of university studies. Diploma  
 Code: C40/97/DESA/K  
 01/2000 – 03/2001 Research project participant: Associated to Diploma Research, (de)  
 Infrared and Raman: High Performances Institute, Frankfurt (O)  
 Organic Chemistry, UV photochemistry: Leipzig University  
 Electrochemistry and Raman: Technical University, Chemnitz

### *Professional Experience; Research Associate*

04/2001 – 12/2002  $TiO_2$  photocatalysis and active surfaces: ISFH, Hameln  
 02/2003 – 07/2005 Analytical techniques in trace element analysis: University of Hannover.  
 10/2005 – 09/2006 Nanosphere lithography, crystallography, CMAT Inst., Univ. of Halle .

### *Industrial Qualifications Management*

07/2006 – 04/2007 Certified Professional in Project Management, German association  
 (GPM), Project Management International (PMI), Lausanne, (ch)  
 Certified Quality Management Representative (QMB)  
 Internal Auditor (IA): Deutsche Gesellschaft für Qualität (DGQ)

### *Professional Experience and PhD Research*

06/2007 – 05/2013 Research Associate, Laser Zentrum Hannover, e.V. (de): Department of  
 Thin Film Technology, Group: Process Development:  
 BMBF Project: 'Photokat': 01RI0637H  
 BMWi, ZIM Project: 'Future Scales': VP2186405MK9  
 PhD student at the PCI Institute at Leibniz University of Hannover, (de)  
 Member 'Photokatalyse' Institute for Standardization DIN (de).